OLIGO(*p*-PHENYLENEVINYLENE) DERIVED ORGANOGELS: A NOVEL CLASS OF FUNCTIONAL SUPRAMOLECULAR MATERIALS

THESIS SUBMITTED TO

COCHIN UNIVERSITY OF SCIENCE AND TECHNOLOGY

IN PARTIAL FULFILMENT OF THE REQUIREMENTS FOR THE

DEGREE OF DOCTOR OF PHILOSOPHY

IN CHEMISTRY UNDER THE FACULTY OF SCIENCE

BY

SUBI JACOB GEORGE

UNDER THE SUPERVISION OF

Dr. A. AJAYAGHOSH

PHOTOSCIENCES AND PHOTONICS DIVISION
REGIONAL RESEARCH LABORATORY (CSIR)
THIRUVANANTHAPURAM-695 019
KERALA, INDIA

OCTOBER 2004

Dedicated To My Beloved Parents

DECLARATION

I hereby declare that the matter embodied in the thesis entitled: *"***Oligo(*p*-phenylenevinylene) Derived Organogels: A Novel Class of Functional Supramolecular Materials***"* is the result of the investigations carried out by me at the Photosciences and Photonics Division of the Regional Research Laboratory (CSIR), Trivandrum, under the supervision of Dr. A. Ajayaghosh and the same has not been submitted elsewhere for any other degree.

In keeping with the general practice of reporting scientific observations, due acknowledgement has been made wherever the work described is based on the findings of other investigators.

Subi

Subi Jacob George

PHOTOSCIENCES AND PHOTONICS DIVISION
REGIONAL RESEARCH LABORATORY (CSIR)
TRIVANDRUM-695 019, INDIA

Phone: 91-471-2515306
Fax : 91-471-2490186, 91-471-2491712
E. mail: aajayaghosh@rediffmail.com

Dr. A. AJAYAGHOSH
SCIENTIST-EII

October 01, 2004

CERTIFICATE

This is to certify that the work embodied in the thesis entitled: **"Oligo(*p*-phenylenevinylene) Derived Organogels: A Novel Class of Functional Supramolecular Materials"** has been carried out by Mr. Subi Jacob George under my supervision at the Photosciences and Photonics Division of the Regional Research Laboratory (CSIR), Trivandrum and the same has not been submitted elsewhere for any other degree.

A. Ajayaghosh
(Thesis Supervisor)

ACKNOWLEDGEMENTS

It is with great pleasure I extend my deep sense of gratitude to Dr. A. Ajayaghosh, my thesis supervisor, for suggesting the research problem, for his constant guidance, support and encouragement, leading to the successful completion of this work.

I would like to express my sincere gratitude to Professor M. V. George for his constant encouragement, inspiration and useful discussions throughout the tenure of this work.

I wish to thank Professor T. K. Chandrashekar, Director and Dr. G. Vijay Nair, Dr. B. C. Pai and Professor Javed Iqbal, former Directors, of the Regional Research Laboratory, Trivandrum for providing me the necessary facilities for carrying out the work.

I have great pleasure in thanking Dr. Suresh Das, Dr. K. R. Gopidas, Dr. D. Ramaiah, and Dr. K. George Thomas, Scientists of the Photosciences and Photonics Division, for their help and valuable suggestions at different stages of my work.

I express my sincere gratitude to Professor Bert Meijer, Professor Rene Janssen, Dr. Albert Schenning and Mr. Pascal Jonkheim, Eindhoven University of Technology, The Netherlands for their valuable advices and whole hearted cooperation during my stay at TU/e.

I gratefully acknowledge the encouragements and support given by Dr. Joby Eldo and Dr. E. Arunkumar, former associates of the Photosciences and Photonics Division, RRL, Trivandrum throughout my work.

I thank all the members of the Photosciences and Photonics Division, particularly Ms. Priya Carol, Mr. V. K. Praveen, Mr. Reji Varghese, Mr. C. Vijayakumar and Ms. P. Chitra. I would also like to remember the help rendered by Mr. Robert Philip and Ms. Sarada Nair.

I also thank all the members of Organic Chemistry Division and other Divisions of the Regional Research Laboratory, Trivandrum for their help. I would like to thank Ms. Saumini Shoji and Ms. S. Viji (NMR spectra), Dr. Peter Koshy and Mr. P. Prabhakar Rao (SEM analyses), Dr. U. Shyamaprasad and Mr. P. Guruswamy (XRD analyses) and Dr. C. K. S. Pillai and Dr. C. Arumughan (DSC analyses) for extending analytical facilities described in the work.

I express my sincere thanks to all my teachers for their encouragement at different stages of my academic career.

I am deeply grateful to my parents and sister for their support, love and prayers throughout my life.

Financial assistance from Council of Scientific and Industrial Research (CSIR) and the Department of Science and Technology (DST), Government of India is gratefully acknowledged.

Subi Jacob George

CONTENTS

PREFACE

Control of the mesoscopic ordering of synthetic molecules for the creation of nanosized, complex architectures, by exploiting the principles of supramolecular chemistry and noncovalent synthesis is a topic of considerable importance. The cooperative effect of noncovalent forces such as H-bonding, π-stacking, dipolar and van der Waals interactions are the driving force behind the self-assembly of molecules leading to novel architectures with reversible functional properties. In the domain of molecular assemblies, utilization of π-conjugated systems have attracted considerable interest as active supramolecular organic materials for various electronic devices such as solar cells, field effect transistors and light emitting diodes. In addition, supramolecular ordering of conjugated molecules allows the tuning of the optoelectronic properties for controlling the energy and electron transfer process in artificial light harvesting assemblies. Recently, considerable research activities are focused to realize the concept of supramolecular electronics, where novel supramolecular assemblies of π-conjugated systems are targeted as active materials for the design of optoelectronic devices.

Among the various classes of π-conjugated systems, oligo(phenylene-vinylene)s (OPVs) are one of the well studied class of compounds due to their interesting optical and electronic properties. A challenging problem towards this end is the control on the self-assembly of π-conjugated oligomers to form supramolecular architectures of nanometer dimensions. In this context, gelation of low molecular weight organic molecules has attracted the widespread attention of supramolecular chemists, because these systems exhibit striking self-assembling properties leading to a variety of novel supramolecular architectures. Organogels prevent the flow of entrapped solvents by the formation of a continuous, three dimensional, entangled network held together by noncovalent forces such as dipole-dipole, van der Waals and hydrogen bonding interactions. Several examples of organic gels based on cholesterol derivatives, amides, ureas, carbohydrates, peptides and amphiphilic systems are known in the literature. However, organogels based on π-conjugated

systems are relatively few despite the fact that gelation can significantly influence the optical properties of such systems. The present thesis entitled "**Oligo(*p*-phenylenevinylene) Derived Organogels: A Novel Class of Functional Supramolecular Materials**" embodies the results of our attempt to create functional chromophoric assemblies of π-conjugated oligomers through the formation of organogels, with the objective of crafting nanoscopic assemblies of different size and shape, thereby modulating their optical and electronic properties.

The thesis is comprised of four chapters. In the first chapter, a review on functional supramolecular assemblies with special emphasis on functional H-bonded chromophoric assemblies and low molecular weight organogels is presented. Attention has been paid to discuss various chromophore derived self-assemblies and organogelators reported in the literature, which is relevant to the objective of the present study. At the end of the first chapter, the aim and the outline of the thesis are also presented.

The second chapter of the thesis describes the design, synthesis and properties of a novel class of oligo(*p*-phenylenevinylene) (OPV) derived π-conjugated gels.[1] The design strategy involves the functionalization of the rigid OPV backbone with H-bonding end groups and long hydrocarbon side chains. This strategy allowed a cooperative interaction of H-bonding, π-π stacking and van der Waals forces to form a three-dimensional supramolecular entangled nanoscopic network which are able to hold large amount of appropriate solvent molecules within the self-assembly, thereby forming the gel. In order to gain insight into the structure property relationship on gelation and morphology of the resultant gels, a variety of OPV derivatives having different end functional groups and hydrocarbon side chains have been synthesized. The length and position of the hydrocarbon side chains and the presence of the hydrogen bonding groups are crucial for the efficient gelation. Among the different OPV derivatives investigated, **BH-OPV1a** with hexadecyl side chains and two hydroxymethyl end groups showed maximum efficiency of gelation in dodecane. The gelation properties and the morphology of the gels are established from the DSC, ^{1}H NMR, XRD, OPM, SEM, TEM and AFM analyses of the gels from

different solvents. XRD analysis revealed a lamellar type packing of the molecules whereas the OPM showed the growth of birefringent fibers. Electron microscopic studies revealed the formation of twisted and entangled supramolecular tapes of an average of 50-200 nm in width and several micrometers in length. These fluorescent organogelators described in this chapter are examples of π-conjugated chromophore based gels and may find application as light harvesting and hybrid electroluminescent materials and in the emerging field of supramolecular electronics by virtue of the strong absorption and emission properties.

The third chapter of the thesis deals with the self-assembly induced changes in the absorption and emission properties of a variety of tailor made OPV derivatives and their use as light harvesting gels.[2] Gelation of OPVs is marked by significant thermoreversible changes in optical properties, characteristic of the π-electronic coupling between OPV molecules, which can be used as a probe for studying the self-assembly phenomena. Detailed photophysical studies revealed the co-existence of unassembled and self-assembled molecules, the ratio of which varies as a function of concentration, temperature, solvent and the structure of the OPV derivatives. In the presence of Rhodamine B as an acceptor, strong fluorescence resonance energy transfer quenching (FRET) of the emission, exclusively from the self-assembled species could be observed. The efficiency of FRET is considerably influenced by the ability of the OPV to form the self-assembled species and hence could be controlled by temperature. Amplification of the dye emission through energy transfer from OPV xerogel when compared to that by direct excitation is characteristic of through-space Förster type light harvesting. Interestingly, energy transfer was marginal in the case of OPVs, which failed to form gels. Detailed studies revealed that FRET occurs only to the dye molecules, which are entrapped between the polar channels of the OPV gel. This is a unique example for the remarkable changes in the emission properties as a result of self-assembly induced gelation where selective energy transfer is possible exclusively from the self-assembled donor scaffold and not from the isotropic solution.

In the fourth chapter, crafting of helical coiled-coil gel nanostructures via the self-assembly of structurally modified oligo(*p*-phenylenevinylene)s having remote

chiral handles is described.[3] Among the three derivatives, **COPV1**, **COPV2** and **COPV3**, only **COPV2** forms gel in apolar hydrocarbon solvents, revealing the crucial role of the nature of the side chains in the gelation of chiral OPVs. FE-SEM and AFM analyses of **COPV2** dodecane gels revealed concentration dependent hierarchical self-assembly leading to the formation of left-handed helical fibers of 20-50 nm and coiled-coil ropes of ca. 100 nm in width. Solvent, concentration and temperature dependent UV/Vis, emission and CD measurements of **COPV2** provided insight into the hierarchical self-assembly and helix formation during the gelation. In the initial levels, the molecules organize to form left-handed chiral aggregates, which are helical as indicated by the weak bisignated CD signal. At higher concentrations, these initial chiral assemblies grow further into helical fibers and coiled-coil ropes resulting in a strong exciton coupled CD signal. Moreover, using the 'sergeants and soldiers' experiments, with a mixture of chiral (**COPV2-3**) and achiral (**BH-OPV1a-b**) OPVs, it has been shown that the chirality of the molecules could be expressed as supramolecular helicity in the resulting co-assembled gel network.

In summary, we have uncovered a novel property of OPVs, a class of π-conjugated molecules, which are extensively studied in the literature, due to their novel optical properties and importance in electroluminescent display devices. This is the first extensive investigation on the gelation behavior of OPVs and the consequent changes in the physical and morphological properties. The remarkable control of morphologies, optical and chiroptical properties and the selective energy transfer derived as a result of gelation of the different OPVs described in this work highlight the power of noncovalent interactions in molecules, to the design of new and novel materials.

References

1. Ajayaghosh, A.; George, S. J. *J. Am. Chem. Soc.* **2001,** *123*, 5148.
2. Ajayaghosh, A.; George, S. J.; Praveen, V. K. *Angew. Chem. Int. Ed.* **2003**, *42*, 332.
3. George, S. J.; Ajayaghosh, A.; Jonkheijm, P.; Schenning, A. P. H. J.; Meijer, E. W. *Angew. Chem. Int. Ed.* **2004**, *43*, 3421.

Chapter 1

Functional Supramolecular Assemblies: On the Way to Novel Organic Materials

Abstract

Supramolecular chemistry is one of the most fascinating fields of chemistry, which is defined as the 'chemistry beyond the molecule' or 'chemistry of noncovalent interactions'. Inspired by the unrivalled imagination of nature, supramolecular chemists are pursuing the translation of the principles of supramolecular self-assembly into novel organic materials with specific functions. In this chapter, a review of functional supramolecular assemblies is presented with special emphasis on H-bonded chromophore assemblies and low molecular weight organogels. Finally, the aim and the outline of the thesis are presented.

1.1. Supramolecular Chemistry

In nature, large and complex biological systems such as the lipid bilayers, the DNA double helix, the collagen triple helix and the tertiary and quaternary structures of proteins are formed by defined supramolecular organization of natural building blocks with the help of various noncovalent interactions. This unrivalled complexity and elegance of natural assemblies through molecular recognition and the desire to understand and mimic the structure and functions of such architectures were the inspiration to chemists to the development of supramolecular chemistry. It is generally defined as the 'chemistry beyond the molecule' and deals with the design and

synthesis of novel supramolecular architectures via spontaneous self-assembly of molecules, governed by various noncovalent interactions between or within molecules.[1] The concept and terms of supramolecular chemistry were coined by Lehn in 1978. According to him supramolecular chemistry may be divided into two broad and partially overlapping areas as supermolecules and supramolecular assemblies. Supermolecules are well-defined, discrete oligomolecular species formed by the intermolecular association of a few components based on the principles of molecular recognition. Supramolecular assemblies are polynuclear entities that result from the spontaneous self-assembly of a large undefined number of components into a specific phase having more or less well-defined microscopic organization and macroscopic characteristics depending upon its nature, as in the case of membranes, vesicles, micelles etc.

Started only as a scientific curiosity nearly 30 years ago by the pioneers in this field Donald Cram, Jean-Marie Lehn and Charles Pedersen (Figure 1.1), supramolecular chemistry has emerged into one of the most fascinating and active fields of research of modern chemistry. The contributions of Cram, Lehn and Pedersen were recognized by conferring the Nobel prize for chemistry in the year 1987. The roots of the supramolecular chemistry lie on molecular recognition and host-guest interaction. However, the modern supramolecular chemistry stretches from molecular recognition in natural and artificial complexes to the design of functional supramolecular materials for applications in biology, medicine and material science. Therefore, supramolecular chemistry is an interdisciplinary area of research and plays a crucial role to the development of the emerging area of nanoscience and technology.

Figure 1.1. The pioneers of supramolecular Chemistry: Donald Cram (left), Jean-Marie Lehn (middle) and Charles Pedersen (right).

1.2. Noncovalent Interactions and Noncovalent Synthesis

One of the most important aspects of supramolecular chemistry is its ability to utilize noncovalent interactions for the controlled, reversible assemblies of functional building blocks. Noncovalent interactions can be of attractive and repulsive intermolecular forces, with interaction energies ranging from 4-400 $kJmol^{-1}$, as can be observed from Table 1.1. These are in the order of decreasing strength (a) electrostatic interactions (ion-ion, ion-dipole and dipole-dipole interactions) (b) hydrogen bonding (c) π-π stacking (d) solvent effects and (e) van der Waals interactions.

Ion-ion, ion-dipole and dipole-dipole interactions are basically electrostatic (coulombic) interactions, which arise due to the delocalization of charges on organic ions. Ion-ion interactions are the strongest noncovalent interaction, having strength comparable to the covalent bonding and are resulted from the attraction between opposite charges (Table 1.1-entry 1). The bonding of an ion, such as Na^+, with a polar molecule, such as water, due to the attraction of oxygen lone pairs to the cation positive charge is known as ion-dipole interactions. A typical example is the binding of cations by crown ethers (Table 1.1-entry 2). Dipole-dipole interactions are resulted from the opposite alignment of two adjacent dipoles leading to an electrostatic attraction between the opposite poles (Table 1.1-entry 4).

Table 1.1. Average interaction energies of various noncovalent interactions frequently used in supramolecular chemistry[a]

Entry	Interaction	Energy/ kJmol^{-1}	Illustration/Example
1.	Ion-ion	50-400	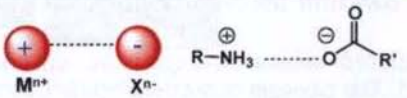
2.	Ion-dipole	50-200	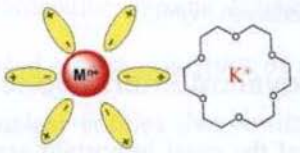
3.	Hydrogen bond	4-120	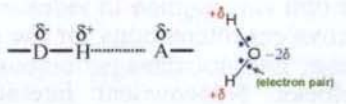
4.	Dipole-dipole	4-40	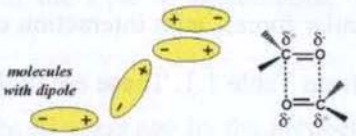
5.	π-π stacking	4-20	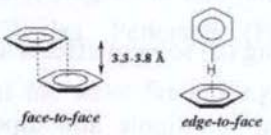
6.	Solvent effects	4-40	
7.	van der Waals forces	<5	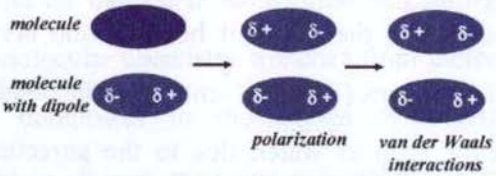

[a]Cations (M), anions (X), electronegative element (D), elements with lone pair of electrons (A), host (H) and guest (G).

A hydrogen bond, D—H···A, is formed between a hydrogen atom attached to an electronegative donor atom (D) and a neighboring acceptor atom with lone pair of electrons (A), which will be discussed in detail in section 1.3 (Table 1.1-entry 3).

π-π Stacking interactions are the weak electrostatic interactions between aromatic rings. There are two general types of π-stacking interactions: face-to-face and edge-to-face. A well known example is the stacking of nucleobases to stabilize the DNA double helix (Table 1.1-entry 5). Solvent effects in supramolecular chemistry mainly consist of hydrophilic and hydrophobic interactions. Hydrophobic interactions are generally the exclusion of large molecules or those that are weakly solvated from polar solvents, particularly from water. This can produce attraction between organic molecules and play a crucial role in the binding of organic guest molecules by cyclodextrin or cyclophane host molecules in water (Table 1.1-entry 6). Hydrophilic interactions are the interaction between water and organic molecules so that the molecules are attracted to water. This is an important reason for the good solvent properties of water. van der Waals interactions arise from the temporary polarization of an electron cloud by the proximity of an adjacent nucleus, resulting in a weak electrostatic interaction. They are usually non-directional and can be of attractive or repulsive in nature (Table 1.1-entry 7).

Despite the weakness of noncovalent interactions, the cooperative action of several such interactions may lead to thermodynamically and kinetically stable supramolecular assemblies under a variety of conditions. Moreover, the reversibility of these noncovalent interactions will allow self-correction during the organization process leading to well-defined supramolecular architectures. The term 'noncovalent synthesis' refers to the use of noncovalent interactions to design macromolecular architectures of reversibility and complexity.[2] Noncovalent synthesis enables one to

synthesize supramolecular entities having molecular mass of several kDa, that are extremely difficult to prepare by covalent synthesis.

1.3. Hydrogen Bond – *The Favorite in Supramolecular Chemistry*

Among different noncovalent interactions, hydrogen bonds are the most crucial and favorite glue to stick molecules together. The advantage of H-bonds is their tunable strength, directionality and specificity. Hydrogen bonds are attractive electrostatic interaction between a positively charged hydrogen atom bonded to an electronegative element (the donor: $D^{\delta-}$ - $H^{\delta+}$), and a negatively charged atom with a lone pair of electrons (the acceptor: $A^{\delta-}$). The strength of a single H-bond is related to the acidity of the hydrogen bonding donor group and the basicity of the hydrogen bonding acceptor group involved, which ranges from 10-65 $kJmol^{-1}$ for neutral molecules, to 40-190 $kJmol^{-1}$ for an ionic acid-base hydrogen bond. H-Bonds are responsible for the existence of H_2O as a liquid and DNA as a double helix which means that they are vital for the existence of life. Apart from this fundamental significance of H-bonds, they in cooperation with other noncovalent forces can lead molecules to organize in different ways to form stable supramolecular architectures of definite shape and properties. Therefore, the study of H-bonds and its use in the creation of supramolecular architectures are of fundamental and technological importance, particularly in the area of advanced materials science.

1.4. Hydrogen Bonded Chromophoric Assemblies – *The Door to Functional Materials*

Highly organized arrays of π-conjugated chromophore and organic dyes are of great interest as mimics of natural photosynthetic systems. The beautiful examples found in nature, for example the photosynthetic light harvesting antenna complexes

and reaction centers in bacteria and green plants, contain highly organized self-assemblies of chlorophyll molecules held together by protein scaffolds. The natural photosynthesis begins with the capture of sun light by light harvesting antenna complexes, which then excite the reaction centers indirectly via energy transfer. This is followed by a series of electron transfer events within the photoreaction centers. Inspired by these naturally occurring architectures, much attention is currently focused on the design of supramolecular chromophoric model systems and nanosized chromophoric assemblies which may find application in solar energy conversion devices. In addition chromophoric assemblies are also considered to be the key to introduce novel optical and electronic properties to organic materials for potential applications in molecular and supramolecular electronic devices.[3]

Learning lessons from the nature's self-assembly process, supramolecular chemists have succeeded to a small extent to create a variety of artificial nanoarchitectures of chromophoric molecules using noncovalent interactions such as H-bonding, π-π stacking, electrostatic and van der Waals associations. These studies have generated a wealth of knowledge to the design of a variety of materials with intriguing properties. Among various noncovalent interactions, H-bonding plays a crucial role in controlling the supramolecular organization of the individual building blocks. In this section, an overview is given on H-bonded chromophoric and dye assemblies such as porphyrin, phthalocyanine, perylene and cyanine based assemblies and π-conjugated oligomeric assemblies.

1.4.1. Porphyrin Assemblies

Porphyrins represent an important class of dyes with promising application in many areas such as optoelectronics, chemosensors and catalysis. These dyes exhibit

strong absorption and emission in the visible region and show electrochemical activity. The self-assembly of porphyrins is mainly inspired by the photosynthetic systems in nature and is not only important to the better understanding of natural processes, but also valuable towards application in optoelectronic devices.[4]

A variety of energy and electron donor or acceptor molecules have been used to create H-bonded complexes with porphyrins as mimics of photosynthetic systems. In a pioneering work, Hamilton and coworkers have designed porphyrin based multichromophoric hydrogen bonded dyads and triads comprised of various fluorescent or redox active naphthalene, ferrocene and dansyl chromophores and studied the energy and electron transfer processes.[5] The self-complementary interactions were based on the hexa-hydrogen bonding complementarity between barbiturate derivatives and two 2,6-diaminopyridine units linked through an isophthalate unit (K_a = 1.1 x 10^{-6} M^{-1}) as shown in Figure 1.2.

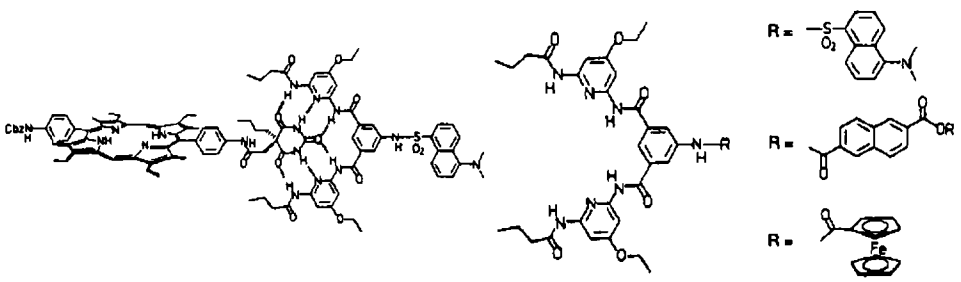

Figure 1.2. Porphyrin derived H-bonded donor-acceptor dyads developed by Hamilton.

Later Sessler *et al.* exploited the Watson-Crick nucleobase pairing H-bonding interactions between guanosine and cytidine to design a trimeric array 1 of two zinc porphyrins and one free base porphyrin in CD_2Cl_2.[6] The protected ribosyl sugar groups present on the nucleobase act as solubilizing groups. The Zinc(II) and free base porphyrins act as the donor and acceptor molecules respectively and both singlet and

triplet energy transfer occurred within these porphyrin H-bonded arrays. More recently, many hydrogen bonded assemblies, where porphyrins are complexed with naphthalene bisimides[7] and phenoxynaphthacenequinones[8] are reported. In the 1:1 triple H-bonded supramolecular dimer **2** composed of a diacyl aminopyridine bearing zinc porphyrin and naphthalene tetracarboxylic acid diimide, Osuka and Okada have studied in detail the electron transfer dynamics within the self-assembly.[7] Photoinduced electron transfer in the H-bonded assembly occurs in benzene with rates of charge separation and recombination of $k_{CS} = 4.1 \times 10^{10}\ s^{-1}$ and $k_R = 3.7 \times 10^{9}\ s^{-1}$, respectively.

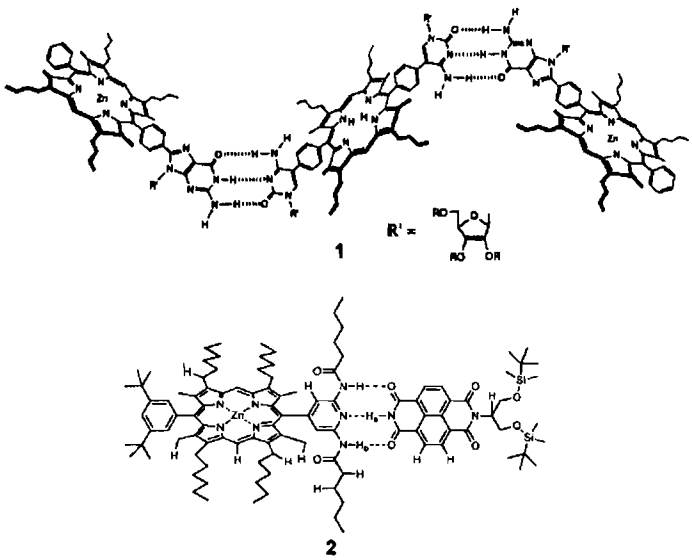

Chart 1.1

An interesting one-dimensional H-bonded porphyrin assembly in nonpolar solvents such as cyclohexane and chloroform, based on bis(imidazol-4-yl)porphyrin (**3**) to mimic natural light harvesting antennae function was reported by Kobuke and coworkers.[9] Even though the H-bond interactions are very weak, the cooperative effect of multiple H-bonding, hydrophobic and π-π interactions stabilize the one-

dimensional assembly of **3** (Figure 1.3b). The resultant assembly showed an efficient excited state energy transfer followed by electron transfer to quenchers like chloranil. However, the bis(imidazoyl) porphyrin **4**, in which alkoxy phenyl substituents of **3** is modified with carboxyl groups, was found to self-assemble in water to form liposomes, as a result of cooperative H-bond, π-stack and solvophobic forces (Figure 1.3c).[10] Detailed AFM and TEM studies revealed liposomes of an average diameter 20-30 nm.

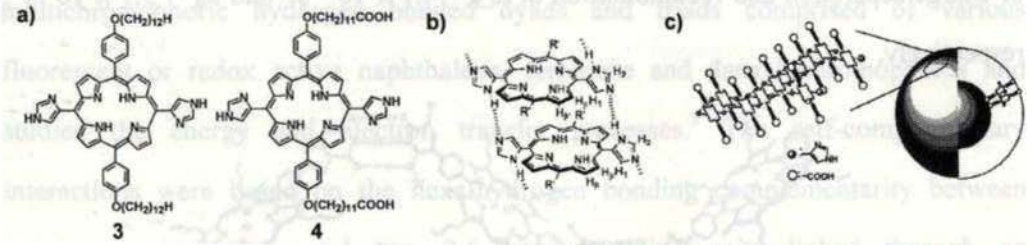

Figure 1.3. a) Structures of bis(imidazoyl) porphyrins, b) self-assembly of **3** to one-dimensional assemblies and c) self-assembly of **4** in water to form liposomes.

The self-assembly of monopyrazolylporphyrins (**5**) to form a dimer and tetramer in chloroform due to the intermolecular H-bonding interactions between pyrazole units have been reported (Figure 1.4a).[11] The association constants of the dimer $[\mathbf{5}]_2$ and the tetramer $[\mathbf{5}]_4$ were found to be 39 M^{-1} and 9.3 x 10^3 M^{-3} respectively, which are relatively low. However, more stable and interesting cyclic porphyrin H-bonded architectures have been reported by functionalizing the porphyrin with multiple H-bonding motifs. A cyclic porphyrin rosette (**6**) composed of three triaminotriazine units bearing two appended tetraphenyl porphyrins or their zinc complexes and three complementary dialkylbarbituric acid derivatives (BBA) was reported by Lehn, which closely resembles B850 chlorophylls architectures present in the light harvesting complexes of photosynthetic bacteria (Figure 1.4b).[12]

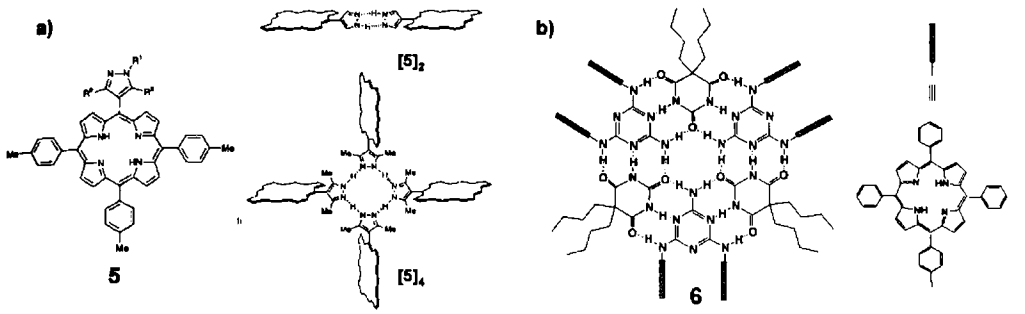

Figure 1.4. a) Self-assembly of monopyrazolylporphyrins and b) Lehn's cyclic porphyrin rosette.

A large variety of multiporphyrin H-bonded arrays with different spatial relationships in predefined geometries, such as discrete squares and linear tapes, have been reported. When two porphyrins substituted with complementary H-bonding groups of uracil and diacetamido pyridyl in a 90° topology, are mixed in a 1:1 stoichiometry, a tetrameric supramolecular square (**7**) was formed by triple H-bonding hetero-complementary interactions.[13] On the other hand 180° topology of the complementary H-bonding groups, each on a different porphyrin, results in the self-assembly of linear porphyrin tapes in toluene. Another series of self-assembled discrete squares of porphyrins (**8**) are formed by the self-complementary quadruple H-bonding interactions between diacetamido pyridyl groups rigidly linked to the chromophores.[14] K_a values of the order 10^9 and 10^{12} have been reported for the tetrameric squares **7** and **8**, respectively.

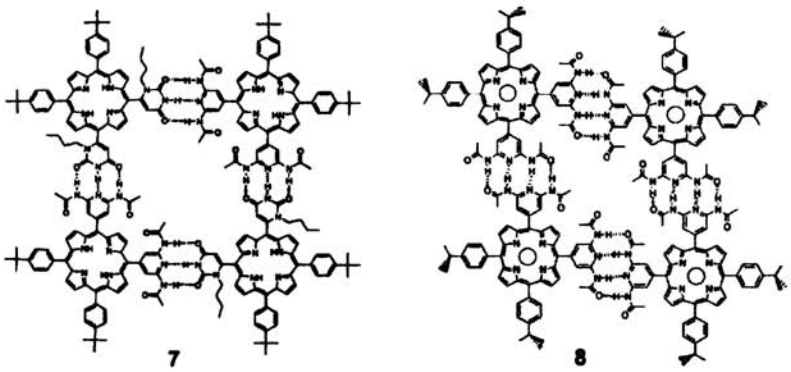

Chart 1.2

Recently, Aida and coworkers have reported the fullerene triggered unidirectional supramolecular association of acyclic zinc porphyrin dimer (**9**) having six carboxylic acid functionality, resulting in the so-called 'supramolecular peapods', with high aspect ratio and good thermal stability (Figure 1.5).[15] The porphyrin derivative **9** also bears large (G4)-poly(benzyl ether) dendritic wedges, which provide solubility to the zinc porphyrin.

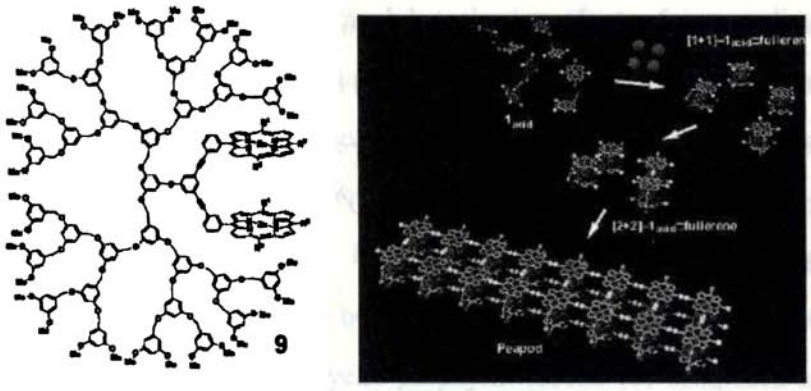

Figure 1.5. Self-assembly in porphyrin derived supramolecular peapods.

Recently, Shinkai *et al.* have reported the one-dimensional self-assembly of sugar, urea or amide-appended porphyrins leading to the gelation of solvents. These studies will be discussed in detail under the section of porphyrin derived organogels (section 1.7.3).

1.4.2. Phthalocyanine Assemblies

H-Bonded self-organization of amphiphilic copper phthalocyanine molecules substituted with eight diol groups into nanoscale fibrous assemblies, have been reported by Kimura *et al.*[16] Both the racemic (**10**) and the optically active (**11**) phthalocyanine complexes produce fibrous assemblies from aqueous solution through two noncovalent interactions, π-π interaction among phthalocyanine rings and hydrogen bonding among diol units. However the detailed CD, XRD and TEM studies have revealed different types of long range ordering of molecules for the two phthalocyanine derivatives within the fibrous assemblies as shown in Figure 1.6. The racemic copper phthalocyanine **10** forms columnar stacks, which then self-assembles spontaneously to the two-dimensional hexagonal lattice. On the other hand, the chiral phthalocyanine molecules (**11**) are arranged in a left-handed helical sense within the column, which then self-assembles into a lamellar structure as the chirality of the side chains affect the intercolumnar structure.

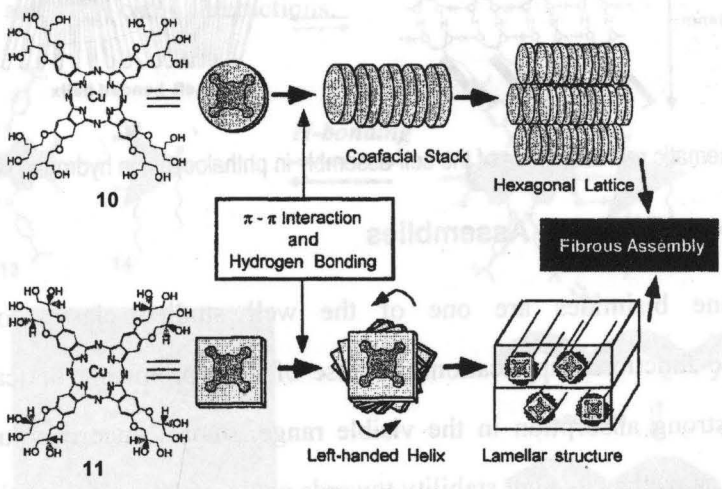

Figure 1.6. Schematic representation of the self-assembly in Kimura's phthalocyanine molecules.

Temperature dependent self-organization of hydrogen bonded dimers of Zinc(II) phthalocyanines (**12**) decorated with six optically active side chains and one chiral diol groups resulted in the formation of two different supramolecular structures.[17] At room temperature, the polymeric H-bond among the diol groups allowed the construction of a lamellar sheet. However, the cleavage of the H-bond network at 130 °C caused the structure to change to a hexagonal columnar phase, in which zinc phthalocyanine molecules are arranged in a left-handed helical manner (Figure 1.7).

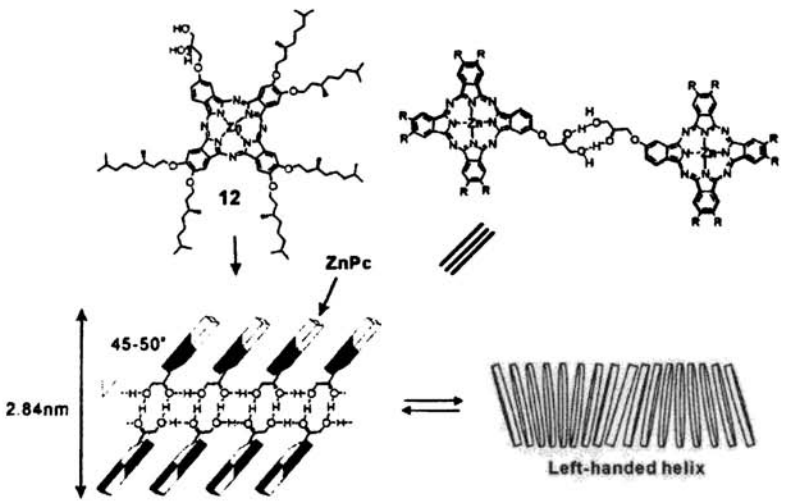

Figure 1.7. Schematic representation of the self-assembly in phthalocyanine hydrogen bonded dimers.

1.4.3. Perylene Bisimide Assemblies

Perylene bisimides are one of the well studied classes of dyes for optoelectronic functional applications because of their promising optical properties such as the strong absorption in the visible range, fluorescence quantum yields of almost 100% as well as its high stability towards photooxidation. In addition, perylene bisimides feature a relatively low reduction potential, which enables them to act as an electron acceptor in photoinduced charge transfer reactions. Because of their striking

properties, they have been extensively used in various optoelectronic applications such as field effect transistors, photovoltaic devices and light emitting devices. A variety of H-bonded functional supramolecular architectures, incorporating perylene imides as the functional building blocks, have been reported. This section focuses on some of these interesting examples.

Würthner *et al.* have extensively studied the hierarchical self-organization of perylene based complementary building blocks to nano- and mesoscopic superstructures, which are expected to show supramolecular functional properties such as light harvesting and long range vectorial transport of excitation energy within the superstructures.[18] Hierarchical self-organization of the perylene bisimide (**13**) and the melamine (**14**) by multiple orthogonal intermolecular interactions lead to fluorescent mesoscopic structures as shown in Figure 1.8.[19] The complementary H-bonding between perylene bisimides and melamines initially form linear polymeric chains that subsequently aggregate to extended supramolecular systems as a result of cooperative π-π stacking and alkyl chain interactions.

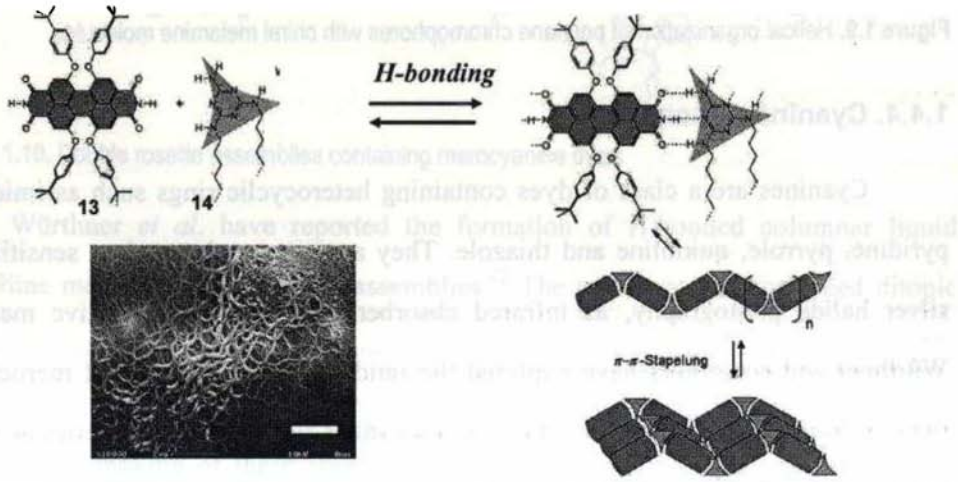

Figure 1.8. Formation of functional perylene superstructures by hierarchical self-organization.

The chiral molecule **15**, having long side chains consisting of octadecyl esters of alanine and phenylalanine, when mixed with the ditopic perylene bisimides (**13**), gave extended superstructures.[20] The perylene chromophores are arranged in a helical manner, whose helicity is determined by the stereoisomerism of the corresponding melamines (Figure 1.9). Circular dichroism (CD) experiments, which showed an exciton coupled CD signal for perylene absorption, characteristic of its helical arrangement, revealed that (*S,S*) melamines lead to a left-handed helical and (*R,R*) enantiomers lead to a right-handed helical arrangement of the chromophores.

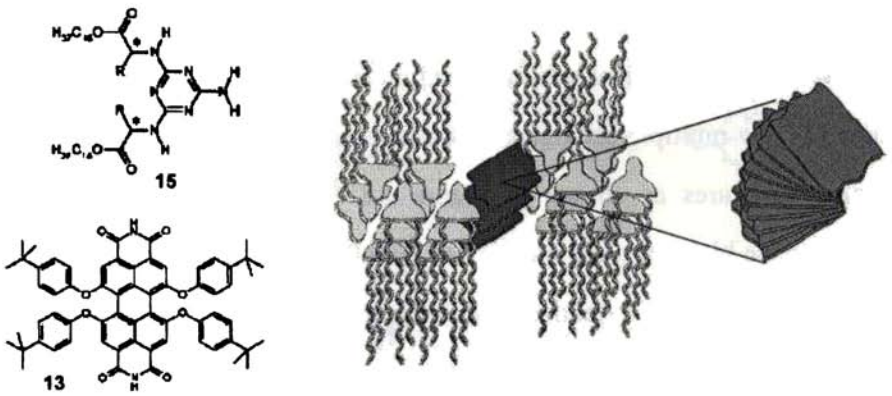

Figure 1.9. Helical organization of perylene chromophores with chiral melamine molecules.

1.4.4. Cyanine Assemblies

Cyanines are a class of dyes containing heterocyclic rings such as imidazole, pyridine, pyrrole, quinoline and thiazole. They are commonly used as sensitizers in silver halide photography, as infrared absorbers and as photorefractive materials. Würthner and coworkers have explored the imide functional groups of merocyanine dyes, to form a variety of supramolecular assemblies such as double rosettes as well as mesoscopic and liquid crystalline materials by complementary triple hydrogen bonding interactions with a variety of melamine derivatives.[21-23] Reinhoudt and

Würthner have shown that six merocyanine chromophores can be arranged in a helical sense by incorporating them into well-defined double rosette assemblies (Figure 1.10).[21] These cyclic rosette assemblies, consist of two stacked rosettes, are formed by the self-assembly of three calixarene dimelamine **(16)** and six merocyanine **(17)** (a chromogenic barbiturate derivative) chromophores via 36 H-bonds. The two stacked rosettes are held together by the calixarene molecules. The helical arrangement of the merocyanine dye molecules into double rosette is controlled by the chiral configuration of the calixarene dimelamines. In addition, as a result of the strong dipole-dipole interactions between the chromophores, exciton coupling is observed giving rise to strong Cotton effects whose sign depends on its helical packing.

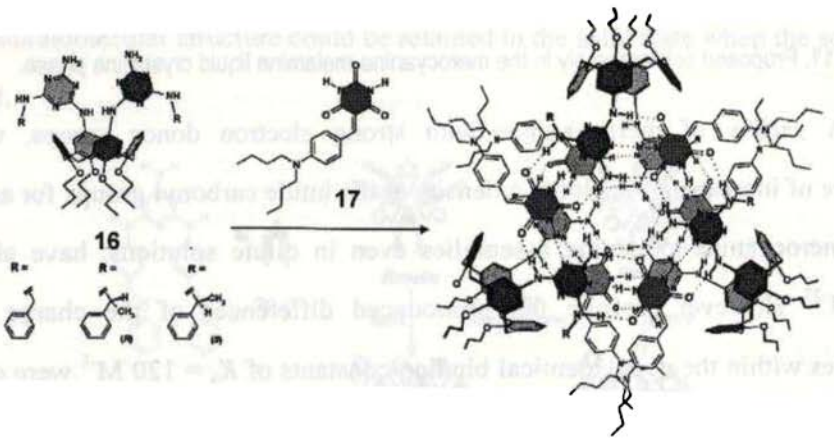

Figure 1.10. Double rosette assemblies containing merocyanine dyes.

Würthner *et al.* have reported the formation of H-bonded columnar liquid crystalline merocyanine-melamine assemblies.[22] The trialkoxy functionalized ditopic melamine derivative **18**, bearing long alkyl chains, and the merocyanine dye **(19)** together form linear extended tapes through triple H-bonding interactions. Dipole assisted π-π stacking of these tapes leads to ribbons which finally assemble into a

columnar structure by microphase segregation and steric effects as shown in Figure 1.11. The columnar mesophase is characterized by OPM, XRD and DSC.

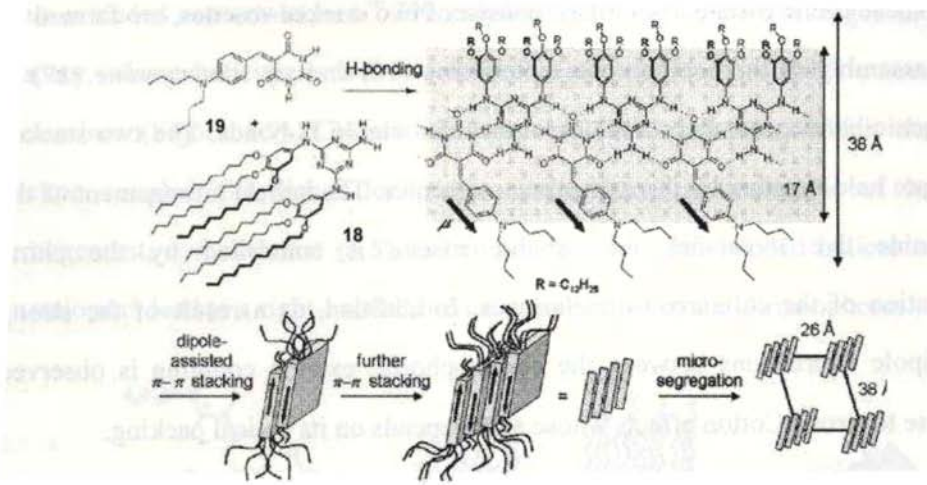

Figure 1.11. Proposed self-assembly in the merocyanine-melamine liquid crystalline phase.

A variety of merocyanines with strong electron donor groups, with the objective of increasing the electron density at the imide carbonyl groups for achieving stable merocyanine-melamine assemblies even in dilute solutions, have also been reported.[23] However, despite the pronounced differences of the charge transfer properties within the dyes, identical binding constants of K_a = 120 M^{-1} were observed for the H-bonding interactions with the melamine derivatives in chloroform. UV/Vis spectral changes observed in methylcyclohexane indicate the formation of colloidal assemblies through a cooperative effect of H-bonding and dipolar aggregation between merocyanine dyes.

1.4.5. Azo Dye Derived Assemblies

Azo dyes contain at least one azo group that can be in the *trans* or *cis* form, the switching between these two isomeric forms is possible with light. Surprisingly, hydrogen bond interactions have been rarely applied in tuning the properties of these

dyes. Ammonium head group-appended azobenzene cyanuric acids and glutamate derivatized melamines have been organized in water[24,25] and at the air water interface[26] by complementary hydrogen bonding. In water, helical superstructures were formed and the aggregation process could be controlled by photoisomerization of the azobenzene dye resulting in segregation of the two components.

Recently, Yagai and Kitamura *et al.* reported the photoswitching properties of *trans*-azobenzene incorporated melamine **20** and barbiturate **21** H-bonded assemblies (Figure 1.12).[27] Photoisomerization of azobenzene units on melamine enhances the thermodynamic stability of the rosette assembly in chloroform solution and suppress its transformation into insoluble tape-like polymers. Interestingly, the resulting stable rosette supramolecular structure could be retained in the solid state when the solvent is removed.

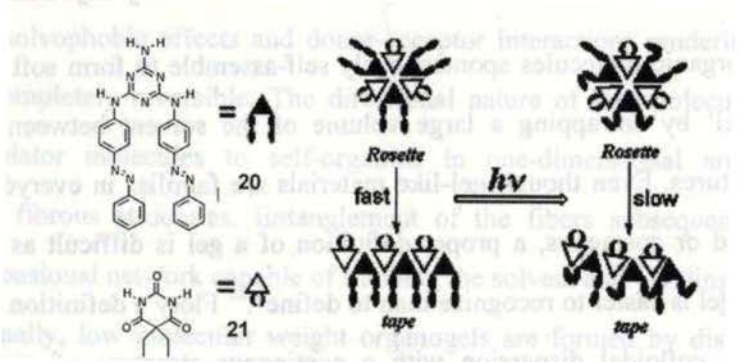

Figure 1.12. Schematic representation of the photoswitchable aggregation process of melamine-barbiturate H-bonded assembly.

In another report, carboxylic acids have been used to self-assemble azo dyes, which could be controlled by photoisomerization of the azo moiety.[28] The *trans*-azobenzene isomer **22** of this dye associates into infinitely hydrogen bonded linear tapes, while the *cis*-azobenzene **23** yields hydrogen bonded self-assembled tetramers that form rod-like aggregates by additional π-π stacking interactions (Figure 1.13).

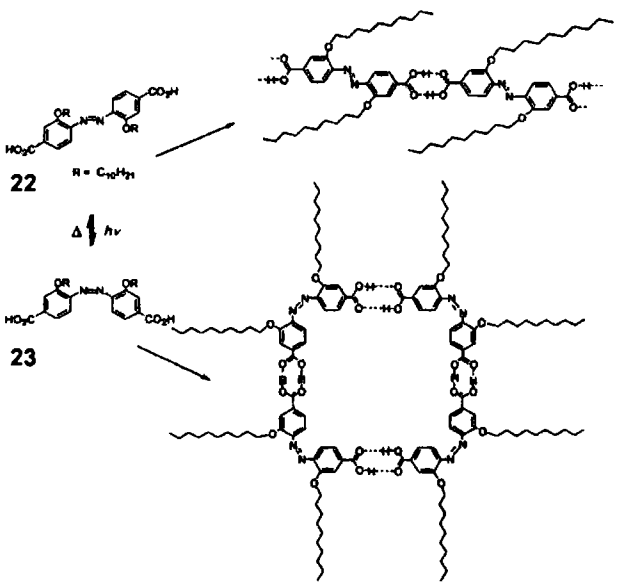

Figure 1.13. Control of organization of hydrogen bonded azo dyes by photoirradiation.

1.5. Low Molecular Weight Organogels – *The World of Soft Materials*

Certain organic molecules spontaneously self-assemble to form soft solid-like mass called 'gel' by entrapping a large volume of the solvent between the self-assembled structures. Even though gel-like materials are familiar in everyday life in the form of food or cosmetics, a proper definition of a gel is difficult as stated by Jordan Lloyd, "gel is easier to recognize than to define".[29] Flory's definition of gels as two component, colloidal dispersion with a continuous structure of macroscopic dimensions that is permanent on the time scale of the experiment and is solid-like in its rheological behavior, is the most accepted one, despite the difficulty of applying it on a routine basis.[30] However, it seems more appropriate to define gels as pervasive materials that are composed of a fibrous three-dimensional network whose interstitial spaces are filled with solvents and hence behave like soft solids. Historically, most gels are composed of covalently crosslinked polymers having very high molecular

weights.[31] These gels can be swollen or shrunk by the addition or removal of the solvent, and by temperature. However, the formation of these gels is irreversible. More recently there has been an enormous increase of interest in the design of low molecular weight organogelators, which immobilize various organic fluids as a result of three-dimensional supramolecular network formation.[32] This novel class of supramolecular materials exhibit striking properties with respect to self-assembly phenomena leading to diverse supramolecular architectures. The diversity of nanostructures provided by organogels makes them promising candidates for several potential applications ranging from cosmetics, photography, food, petroleum industries and catalysis to optoelectronics and related areas.

In contrast to the macromolecular gels, low molecular weight organogel network is held together solely by noncovalent interactions such as H-bonding, π-stacking, solvophobic effects and donor-acceptor interactions rendering the gelation process completely reversible. The directional nature of intermolecular interactions allows gelator molecules to self-organize in one-dimensional arrays producing elongated fibrous structures. Entanglement of the fibers subsequently produces a three-dimensional network capable of trapping the solvent and yielding the gel (Figure 1.14). Usually, low molecular weight organogels are formed by dissolving a small amount of the gelator in hot solvents and the subsequent cooling below gel transition temperature (T_{gel}). The gelation of organic molecules can be visualized by the formation of a thick non-flowing mass, even when turned upside down. Organogels are usually characterized by a variety of analytical techniques, particularly spectroscopic and microscopic techniques.

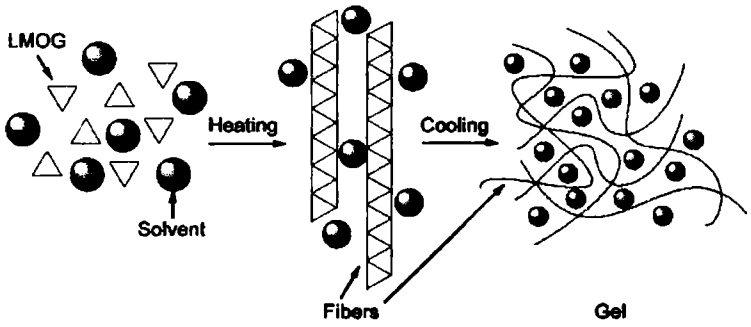

Figure 1.14. Schematic representation of the self-assembly of low molecular weight organogelators (LMOG) into one-dimensional stacks and the subsequent formation of an entangled network.

Even though there are numerous approaches towards the design of organogelators, most gelators are found rather by serendipity than by design. However, the following features are considered to be of importance in the design of organogelators: (1) formation of one-dimensional aggregates via anisotropic growth process, (2) intertwining of these one-dimensional aggregates to form three-dimensional network and (3) the prevention of crystallization or precipitation of the self-assembled aggregate through a delicate balance between order and disorder. Therefore, the designing of new gelling agents have to account for all these aspects and hence continues to be a challenging task.

The huge library of low molecular weight organogelators known to date can be classified into two broad categories according to the difference in the mode of self-organization, namely, non-hydrogen bonded gelators and hydrogen bonded gelators. Organogels formed by van der Waals, π-π stacking, dipole-dipole and donor-acceptor interactions are classified in to the first category. Cholesterol based gelators are typical examples of this category. Hydrogen bonding interactions are well exploited for the designing of gels, which mainly include amide, urea, sugar, amino acid and nucleobase derivatives constituting the second category of gels.

Among various non-hydrogen bonded gelators cholesterol based gelators are the most extensively studied molecules.[32,33] In cholesterol based gelators, the C-3 hydroxyl group of the steroid molecule is appropriately functionalized with a variety of aromatic moieties through linkers. The driving force for the self-assembly of such molecules is the aggregation of the cholesterol skeleton, as a result of dipole-dipole and van der Waals interactions, which is assisted by the π-π interactions between the aromatic moieties. A schematic representation of the cholesterol based gel assemblies are shown in Figure 1.15, in which the cholesterol groups are stacked in a helical manner to form the central core thereby directing the aromatic groups outwards to form a spiral staircase assembly. A large variety of functional aromatic groups such as anthracene, azobenzene, squaraine, porphyrin and stilbene, have been appended to the cholesterol for designing new gelator molecules, which will be discussed in detail in the following section on chromophore derived organogels.

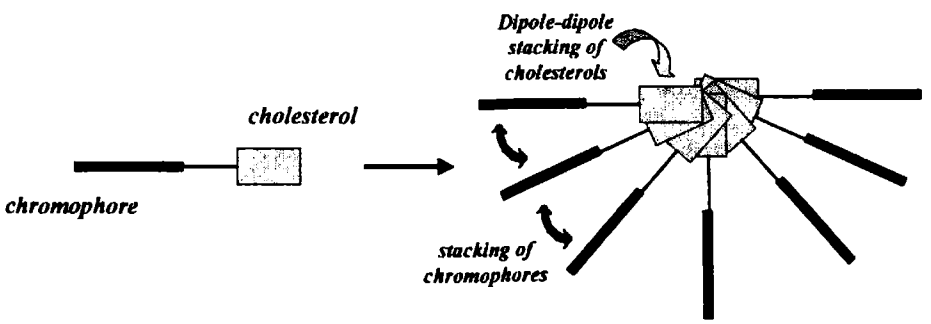

Figure 1.15. Schematic representation of the self-assembly of cholesterol derived organogelators.

Other non-hydrogen bonded gelators include anthracene[34] (**24**) and anthraquinone[35] (**25**) derivatives, the self-assembly of which is directed by the dipolar and π-π stacking interactions. Surprisingly, simple organogelators such as long linear hydrocarbons (C24, C26, C32 and C38) are known to form organogels through

London dispersion forces, which are the weakest of all noncovalent interactions.[36] In addition, simple gelators such as semifluorinated alkanes[37] (**26**) and alkanes containing one heteroatom,[38] including quaternary ammonium salts with long aliphatic chains[39] (**27-30**) are also known. Charge transfer interactions have also been exploited by Maitra[40] and Shinkai,[41] for the creation of donor-acceptor two component organogels.

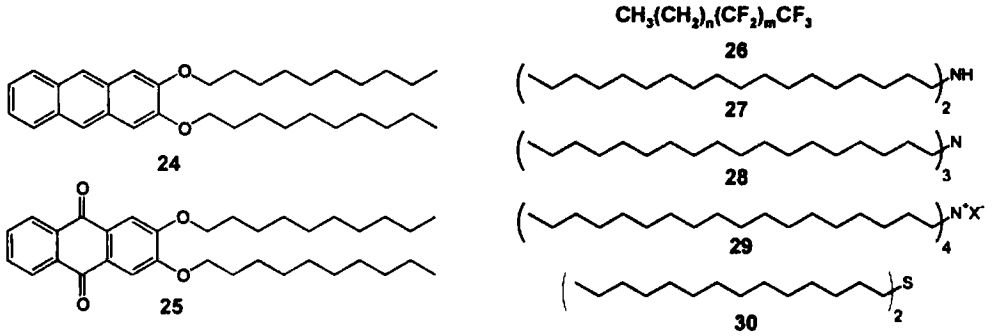

Chart 1.3

Many of the H-bonded organogelators reported in literature contain functional groups such as urea and amide. It was established that multiple urea and amide groups are essential to drive the self-assembly to a completion. The urea-urea H-bonding interactions, which are known to have high directionality and less conformational flexibility, have been extensively exploited in the laboratories of Feringa[42] and Hanabusa[43] to design one-dimensional gel assemblies (Figure 1.16). It has been shown that two urea groups in one molecule are sufficient enough to enforce aggregation in dilute solutions of a range of organic solvents. Organogelators comprised of acyclic[42a,42c,43] (**31**), cyclic[42d] (**32, 33**), geminal[42e] (**34**) and tripodal urea[44] (**35**) groups have been reported. Hamilton and coworkers have reported the gelation behavior of bisurea-dicarboxylic acid[45] (**36**) and monourea serine[46] (**37**) derivatives.

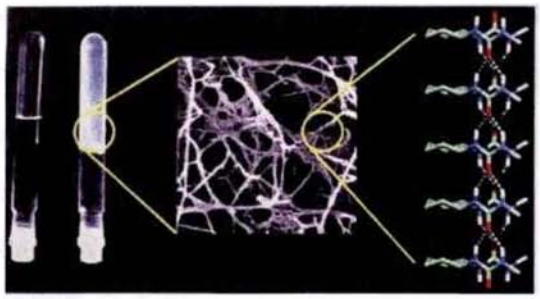

Figure 1.16. Schematic representation of the self-assembly of cyclohexyl urea derivative **33**, by directional urea-urea interactions, to one-dimensional fibers and entangled network, which causes the gelation.

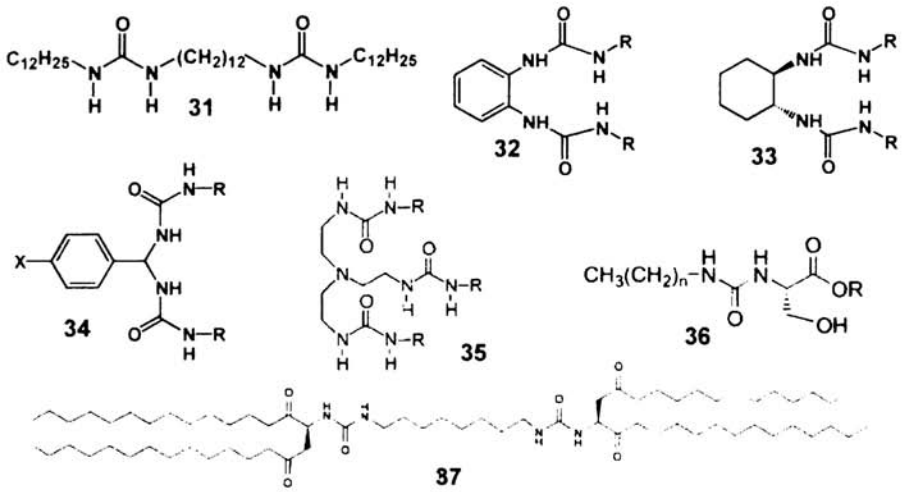

Chart 1.4

Hanabusa and coworkers have shown that amide-amide H-bonding interactions can also be used to design a variety of gelators such as *trans*-1,2-diaminocyclohexane[47] (**38**), 1,3,5-benzenetricarboxylic acid[48] (**39**) and *cis*-1,3,5-cyclohexanetricarboxylic acid[49] (**40**) derivatives. More recently, gelation of a series of C_3-symmetrical trisamide (**41**, **42**) and corresponding trisurea substituted disc-shaped molecules have been studied by Meijer and coworkers.[50] The gelation of a series of oligoamides (**43**) was also reported from Mésini's group.[51]

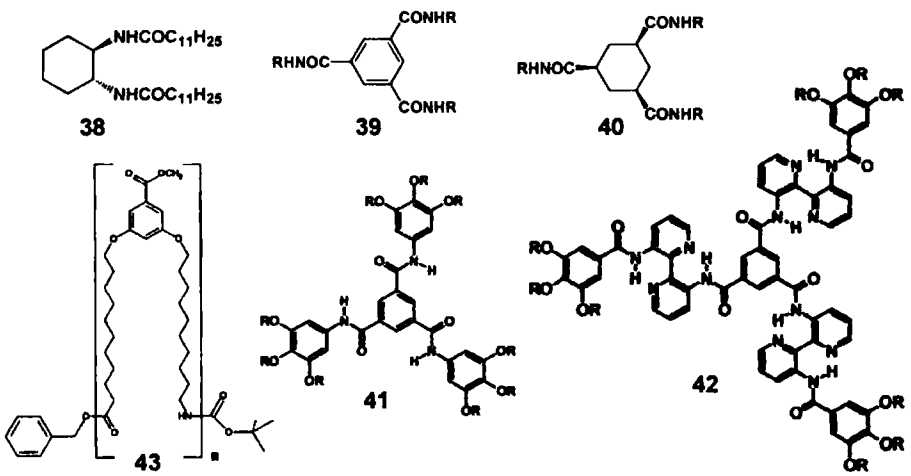

Chart 1.5

Reinhoudt and Shinkai have synthesized a library of methyl-4,6-*O*-benzylidine monosaccharide derived organogelators (**44-47**) and carried out their detailed structural studies.[52] Aldopyranoside amphiphilic hydrogelators (**48**) from Shimizu's group[53] and gluconamide based aminosugars (**49**) from Nolte's group[54] are also present in the literature. More recently, Shinkai and coworkers reported a series of sugar-appended porphyrin and azobenzene based gelators which will be reviewed later in this chapter.

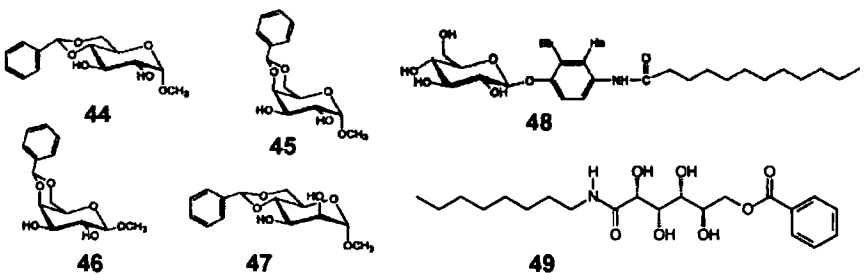

Chart 1.6

In addition, a large variety of amino acid[55] and nucleobase[56] based H-bonded gelators are also present in literature. However, detailed discussion of all classes of organogels is not the objective of the present review. Instead a short description on some of the applications of organogels is given followed by a detailed discussion on functional dyes and chromophore based organogels.

1.6. Application of Organogels – *As Templates in Materials Synthesis*

In recent years, there has been considerable interests in the design of organogels for specific application in the field of advanced materials, apart from their well known traditional applications in industry, food and cosmetics, which rely mainly on polymeric gels. Thus, various organogel derivatives have been successfully used in molecular imprinting,[57] lasing,[58] electrolytes for solar cells[59] and electrochemical cells,[60] drug delivery,[61] humidity sensing[62] and enantioselective separation.[63] For example, organogelators **50** and **51** have been used to gel the electrolytic solutions of solar cells and electrochemical cells, respectively, thereby avoiding the potential danger of leakage of electrolyte solution.[59,60] Measurements have shown that, for the gel electrolytes, virtually the same ion mobility and conductivity are obtained as in the normal liquid phase. Organogelators, **52** and **53**, that gel supercritical CO_2 have been used to construct pressure and thermoreversible aerogels.[64] Molecular imprinting of organogels has been reported, by gelling methyl methacrylate or styrenes with **29**, **49** and **54**, followed by polymerization and removal of the gelator molecules.[57] This will give a rigid polymer matrix whose pores are one order of magnitude larger than the cross sections of the gel nanostructures. Kato *et al.* have gelled liquid crystalline molecules such as 4'-octyl-4-biphenylcarbonitrile, by a variety of organogelators such as **24**, **38**, **49** and **51**, to give anisotropic gels, which are a novel class of functional

materials.[65] These liquid crystalline gels are proved to be potential candidates for electrooptical switching devices.

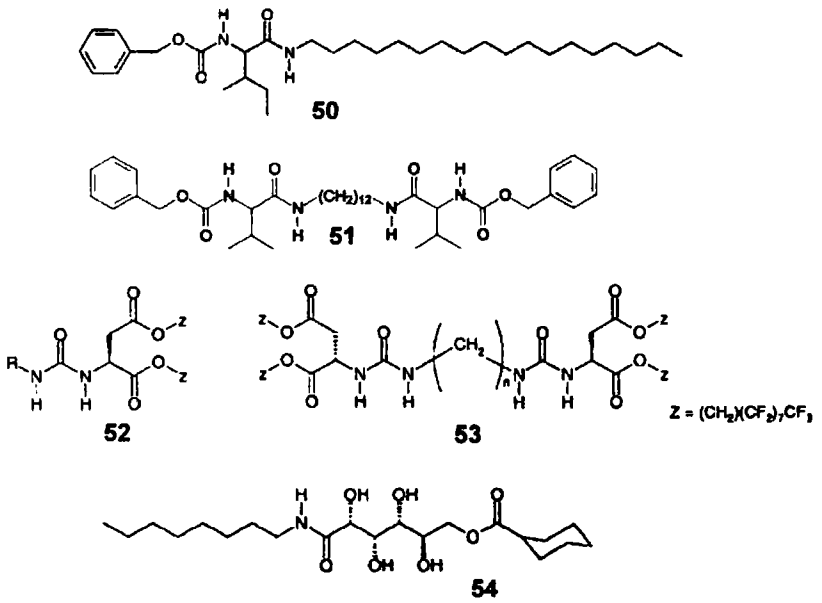

Chart 1.7

Shinkai and coworkers have succeeded in using organogels as templates for the growth of a variety of inorganic nanostructures. This was achieved by the gelation of liquid tetraethyl orthosilicate (TEOS), with cholesterol derived gelators and the subsequent sol-gel polymerization of TEOS.[66] During the polymerization, the gel fibrils transcribe its nanostructures to the polymerized silica, which will retain the 'imprint' even after the removal of the gelator by calcination. Strong electrostatic attraction or H-bonding interactions between gelator functional groups and TEOS is required for the silica transcription. Most remarkably, even the chirality of the gelator component could be transferred successfully to the resulting silica superstructures. Using this approach, a variety of novel silica architectures such as multilayered

vesicular silica, chiral spiral silica, multilayered rolled paper-like silica, and helical ribbons could be obtained (Figure 1.17).

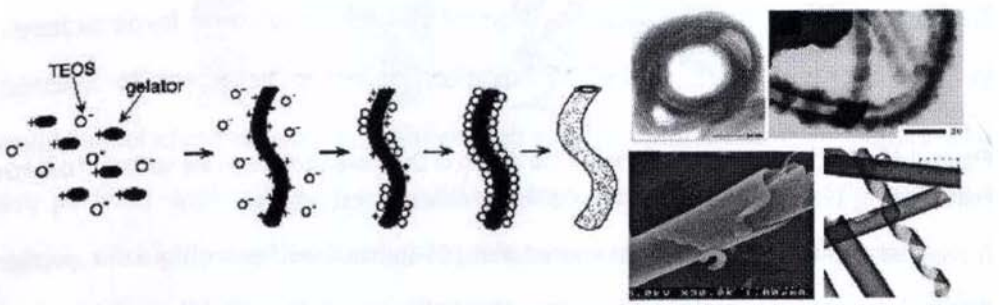

Figure 1.17. Schematic representation of the mechanism of silica transcription from organogel fibrils and TEM images of various transcribed silica nanostructures.

There are several exciting reports from the group of Stupp at the Northwestern University on the use of gel forming rod-coil and peptide molecules as templates for the synthesis of inorganic nanostructured materials.[67-69] They have shown that, 'dendron rod-coil' triblock molecule (**55**) can self-assemble through hydrogen bonds between the hydroxyl and carbonyl groups of the hydrophilic dendron segments and the π-π stacking interactions of the aromatic rod segment resulting in supramolecular twisted nanoribbons, causing the gelation of organic solvents.[67] The rod-coil dendron nanoribbons have been further used as templates for the mineralization of CdS to form coiled-coil helices, as a result of preferential growth of CdS along one face of the twisted ribbon template (Figure 1.18).[68]

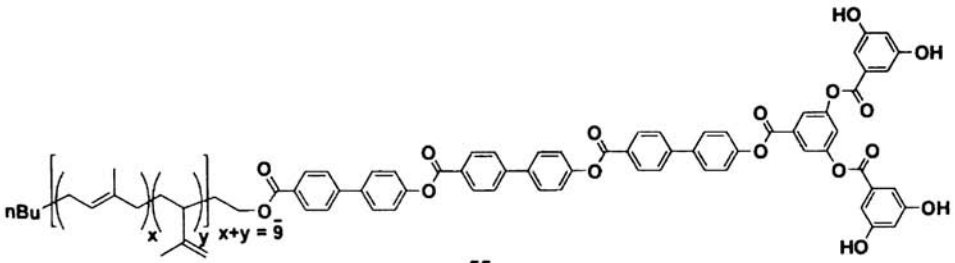

55

Chart 1.8

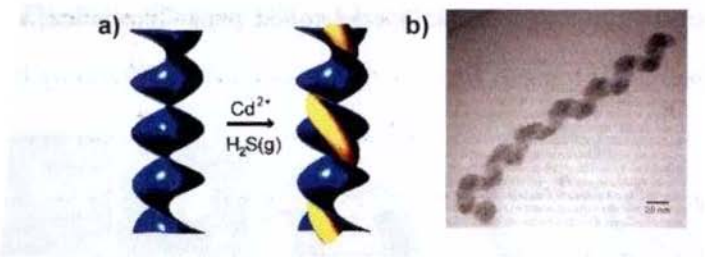

Figure 1.18. a) Schematic representation of the growth of CdS coiled helices on the surface of dendron ribbons and b) TEM image of the resultant CdS coiled helical nanostructures.

Stupp and coworkers have used the pH-induced self-assembly of a peptide amphiphile (**56**) to make a nanostructured fibrous gel scaffold reminiscent of extracellular matrix (Figure 1.19).[69] The design of this peptide amphiphile facilitates the direct mineralization of hydroxy appetite to form a composite material which is aligned the same way as collagen fibrils and hydroxy appetite crystals in bone.

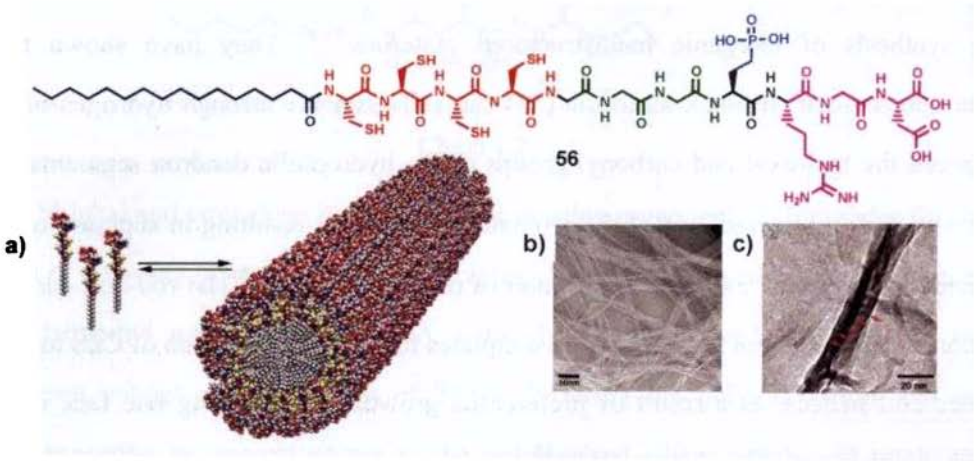

Figure 1.19. a) Self-assembly of the peptide amphiphile **56** into nanofibers, b) TEM image of the nanofiber and c) TEM image of the mineralized hydroxy appetite crystals on the surface of peptide nanofibers.

In addition to the above mentioned applications, in recent years there has been considerable interest in the supramolecular organization of chromophores (see section 1.7) through gelation which has potential optical and electronic applications.

1.7. Organogels Based on Functional Dyes and Chromophores

Gels based on functional chromophores and dyes have attracted immense interest as novel functional materials for optoelectronic applications. Supramolecular alignment of functional molecules constructed through the gelation process, can provide novel chromophoric assemblies with tunable optoelectronic properties which have potential applications in molecular and supramolecular electronic devices. In addition, the highly organized arrays of electron conducting molecules can be used for the formation of conducting supramolecular wires. This section presents a detailed review on the chromophore and dye based gels reported in literature so far.

1.7.1. Anthracene Derived Organogels

Control of the molecular organization of [n]acenes such as anthracene, tetracene and pentacene has attracted much attention, because of their significant charge mobility, intense absorption and emission, and photochromism which have potential applications in the fields of organic electronics and photovoltaic devices.[70] Keeping this in mind, the groups of Weiss and Desvergne have contributed extensively to the self-assembly and gelation of anthracene derivatives.

The serendipitical observation of the gel formation of 3-β-cholesteyl-4-(2-anthryloxy)butanoate (**57**, CAB) in a variety of organic liquids has led to a novel class of steroid based gelators.[71] They consist of an aromatic group (A), connected to a steroidal moiety (S) via a linking group (L) and hence are called ALS gelators (Figure 1.20). The kinetics of gel formation and the gel melting temperature (T_{gel}) have been determined from the fluorescence and CD spectral changes. Detailed studies indicated a helical face-to-face stacked arrangement of CAB molecules within the gel aggregates. Electron microscopic studies of the CAB gels revealed that they consist of

molecular domains of helically twisted fibrous bundles having several micrometers in length. A series of ALS gelators have been synthesized by modifying the structural features of each part of the ALS molecules.[72] In the case of the 2-substituted-9,10-anthraquinone (**58**, CAQ) the gelation ability is favored by a (*S*)-chirality at the C-3 position of the steroidal part, while changes at C-17 does not have much influence.

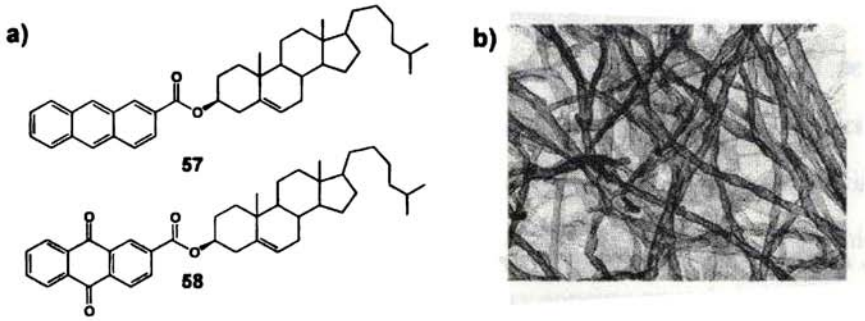

Figure 1.20. a) Structures of CAB (**57**) and CAQ (**58**) ALS gelators and b) TEM image of the helical fibers of the propanol gels of CAB.

Desvergne and coworkers have reported that 2,3-bis-*n*-decyloxyanthracene (**24**, DDOA) can form fluorescent gels in various alkanes, alcohols, aliphatic amines and nitriles, through dipole-dipole interactions, van der Waals forces and π-π stacking.[34] DDOA showed a ground state dipole moment of 1.9 Debye showing the presence of dipolar forces in the resulting gels. Gel formation is accompanied by significant changes in the absorption and emission properties of the anthracene chromophores, which suggested an anti-parallel head-tail arrangement for the aromatic rings with partial overlap between them. Furthermore, freeze-fracture electron micrographs of DDOA gels showed a dense three-dimensional random network of fibrous rigid bundles (Figure 1.21b). Detailed studies have shown that slight structural variations on DDOA, such as shortening the length of the alkyl side chains, removing the oxygen atom, mismatching the alkyl side chains or truncating the aromatic part to naphthyl

chromophores considerably reduce the gelation properties. However, hydrogenation of one of the anthryl rings[73] (**59** and **60**) or replacement of it by a phenazine[74] (**61**) or an anthraquinone[35] (**25**) produced efficient organogelators and are studied in detail. 2,3-Di-*n*-alkoxyphenazine organogels (**61**) showed reversible acid sensitive properties, at ambient temperatures in acetonitrile. Terech *et al.* synthesized a new class of 2,3-di-*n*-decyloxy-6,7-dichloroanthracene derivatives (**62**) with a higher dipole moment (3.4 D).[75] Recently, Pozzo and coworkers have shown that highly oriented DDOA gel fibers showing strong anisotropic features can be obtained by applying a mechanical stress during the cooling of hot isotropic solutions, which is evident from the optical polarizing microscopy (OPM) and TEM images (Figures 1.21c and d).[76] These anisotropic organic materials are expected to show enhanced mechanical, photonic, magnetic and electronic properties along a given direction.

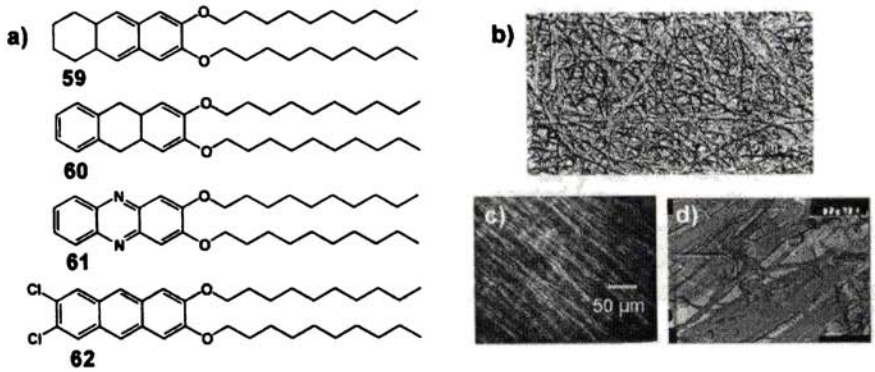

Figure 1.21. a) Structures of various anthracene gelators, b) TEM image of the gel fibers of DDOA, c) OPM and d) TEM images of aligned DDOA gel fibers.

1.7.2. Azobenzene Derived Organogels

A new class of gelators containing substituted azobenzenes as the aromatic part has been studied extensively by Shinkai and coworkers. In their first report, two types of gelators, with either a natural (*S*)-configuration (**63**) or the inverted (*R*)-

configuration (**64**) at the C-3 position of the steroidal part have been reported.[77] Among them, the gelators bearing a *p*-alkoxyazobenzene moiety are found to be the most efficient and they can specifically gel either nonpolar solvents (*S* derivatives, **63**) or polar solvents (*R* derivatives, **64**). Interestingly, it is possible to 'read-out' the sol-gel phase transition as well as the chirality of the supramolecular stacks using CD spectroscopy. For example, **63** showed a positive exciton coupling and **64** showed a negative exciton coupled band characteristic of the clockwise and anticlockwise orientation of the azobenzene dipoles in the gel state, respectively. This is supported by the observation of right- and left-handed helical fibers through SEM pictures. In this case, the sol-gel transition could be controlled by the *cis*-to-*trans* isomerization of azobenzene, leading to photoresponsive organogels (Figure 1.22b)

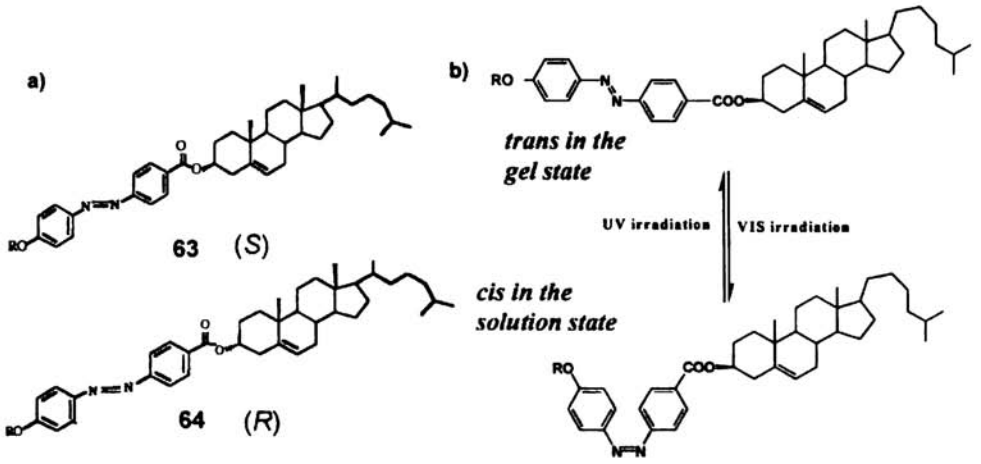

Figure 1.22. a) Structures of azobenzene-appended gelators and b) *trans*-to-*cis* isomeriztation of **63**.

Detailed studies of a variety of azacrown substituted azobenzene-cholesterol gelators, have revealed the formation of different supramolecular architectures such as vesicles[78] (**65**, Figure 1.23a) layered tubules[78] (**66**, Figure 1.23b), curved lamellas[79] (**67**, Figure 1.23c), cylindrical tubules[79] (**68**, Figure 1.23d) and helical ribbons[80] (**69**, Figure 1.23e).

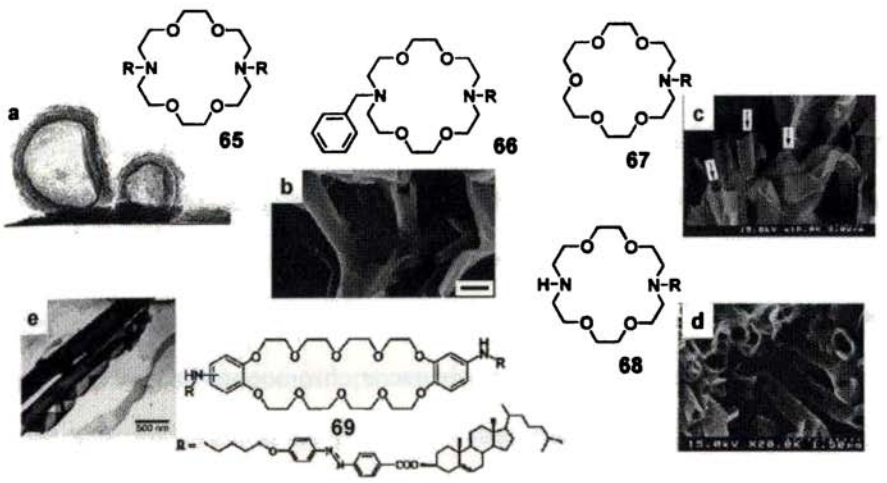

Figure 1.23. Azobenzene-appended organogelators and TEM images of resultant gel nanostructures.

The chiral azobenzene (**70**) containing a cyclic *syn*-carbonate moiety, reported by Kato and coworkers self-assembles via dipole-dipole interactions to form a photoswitchable organogelator (Figure 1.24).[81]

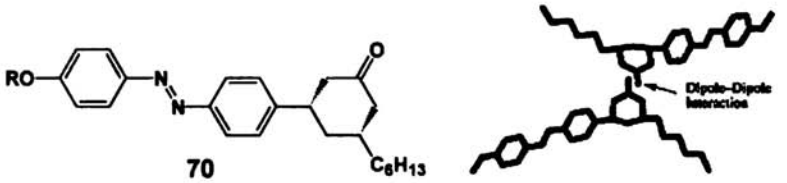

Figure 1.24. Structure and dipole-dipole assisted self-assembly of an azo containing organogelator **70**.

A new family of hydrogelators based on azobenzene-appended sugar bolaamphiphiles (**71-74**) has been reported jointly by Shinkai and Reinhoudt.[82] These bolaamphiphiles consist of two solvophilic aminophenyl sugar skeleton, such as β-D-glucopyranoside (**71**), α-D-glucopyranoside (**72**), α-D-galactopyranoside (**73**) or α-D-mannopyranoside (**74**), as chiral-aggregate forming site and one solvophobic azobenzene moiety as a π-π stacking site. Compound **71** is found to be a 'super' hydrogelator, as it can form gels even at concentrations as low as 0.05 wt%, whereas

compound **72** could gelate only 1:1 (v/v) DMSO-water solvent mixtures. On the other hand, **73** and **74** could not gelate any of the solvents investigated. The chiral sugar derivatives **71** and **72** are found to form right-handed helical aggregates in 50 vol% DMSO, whereas **73** and **74** form left-handed helical aggregates as evident from the corresponding exciton coupled CD spectra. TEM studies revealed right-handed helical fibrillar structures for the aggregates of **71** and **72**, reflecting the microscopic one-dimensional columnar orientation of azobenzene chromophores. However **73** and **74** tend to aggregate into vesicular structures as a result of their two-dimensional aggregation mode, which prevent them from gelation (Figure 1.25).

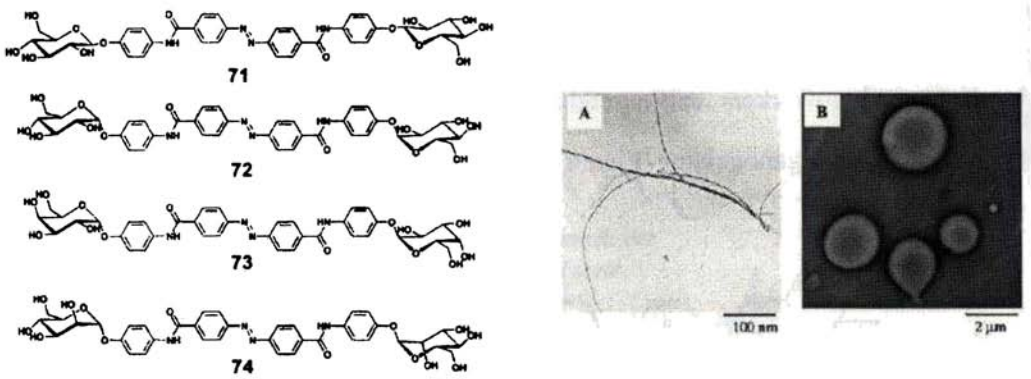

Figure 1.25. Structures of sugar-appended azobenzene organogelators and the TEM images of **72** (A) and **73** (B) in 1:1 (v/v) DMSO-water mixtures.

Feringa and coworkers reported chiral recognition in hybrid gel assemblies of 1,2-bis(uriedocyclohexane) derivative **75** and the azobenzene incorporated derivative **76**. Both (*R*)-**76** and (*S*)-**76** isomers showed concentration independent exciton coupled CD spectra corresponding to the azobenzene absorption as a result of the intramolecular stacking of the azobenzene chromophores, the sign of which depends on the absolute configuration of the molecule.[42g] Incorporation of (*R*)-**76** into a gel of (*S*)-**75** or (*R*)-**75** resulted in distinctly different chiral gels, in which azobenzene

chromophores are stacked in different orientations depending on the chirality of **75** (Figure 1.26). The CD spectra of (*R*)-**76** in 1-butanol gel of (*S*)-**75** showed a slightly more intense bisignated CD signal at room temperature, indicating that the environment of (*R*)-**76** is less polar when it is incorporated into the (*S*)-**75** gel than in 1-butanol itself as shown in Figure 1.26b. However, incorporation of (*R*)-**76** in a gel of (*R*)-**75** results in a strong positive Cotton effect, which is not exciton coupled, indicating that the azobenzene groups are no longer stacked but incorporated between the closely packed alkyl chains of (*R*)-**75** as shown in Figure 1.26a. In both the cases intramolecular exciton coupled CD signal of (*R*)-**76** reappears upon the melting of the gel. In addition, the more exposed "solvent like' environment of (*R*)-**76** in the (*S*)-**75** gel results in its slow isomerization when incorporated into the former gel.

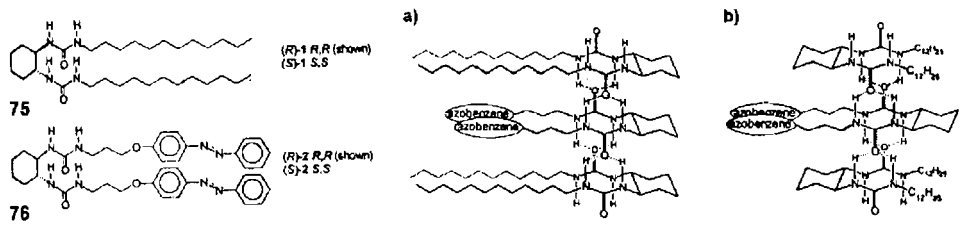

Figure 1.26. Structures of the 1,2-bis(uriedocyclohexane) derivatives. Schematic representation for the incorporation of (*R*)-**76** in a) an aggregate of (*R*)- **75** or b) an aggregate of (*S*)- **75** showing the different environments for the azobenzene groups.

van Esch and coworkers have studied the gelation behavior of the bisurea-appended azobenzene derived organogelators **77** and **78**.[83] 4,4'-Disubstituted derivative (**77**) is found to be a poor gelator, whereas the 2, 2'-disubstituted derivative (**78**) is an excellent gelator of a variety of organic solvents at concentrations as low as 0.2 mM. Interestingly, **78** showed remarkable polymorphism in their gel state leading to two different types of supramolecular aggregates, which differ in the stacking of chromophore moiety as well as in their H-bonding patterns, as evident from the

differences in the UV/Vis absorption and IR spectra. This novel observation of polymorphism in organogels was found to depend on the solvent polarity and kinetic factors.

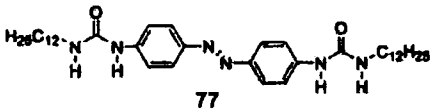

77

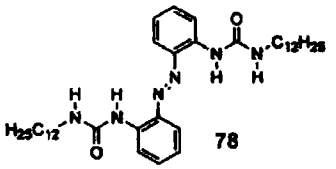

78

Chart 1.9

1.7.3. Porphyrin Derived Organogels

Terech *et al.* have shown that a long chained ester of *meso*-tetrakis(*p*-carboxyphenyl)porphyrin (**79**), can form thixotropic gel-like materials in hydrocarbon solvents.[84] The presence of both metal ion and acidic group is found to be crucial for gelation. The gelator network consists of molecular rods with moderate length with one molecule per cross section as repeating unit. Later Shinkai and coworkers have reported a novel gelator by linking the porphyrin part to the cholesterol moiety (**80**).[85] Both cyclohexane and methylcyclohexane are gelled by **80**, but not by its structural epimer with (*R*)-configuration at the C-3 of the cholesterol group. Subsequently, the gelation ability of Zinc(II) porphyrin-appended cholesterol gelators could be enhanced by intermolecular interactions with fullerenes through the formation of a 2:1 Zinc(II) porphyrin/C_{60} sandwich complex (Figure 1.27).[86] The direct bathochromic shift of the Soret absorption band and the enhancement in the negative exciton coupled CD signal in the presence of C_{60} established that intermolecular interactions do exist between Zinc(II) porphyrin and the fullerenes in the gel phase.

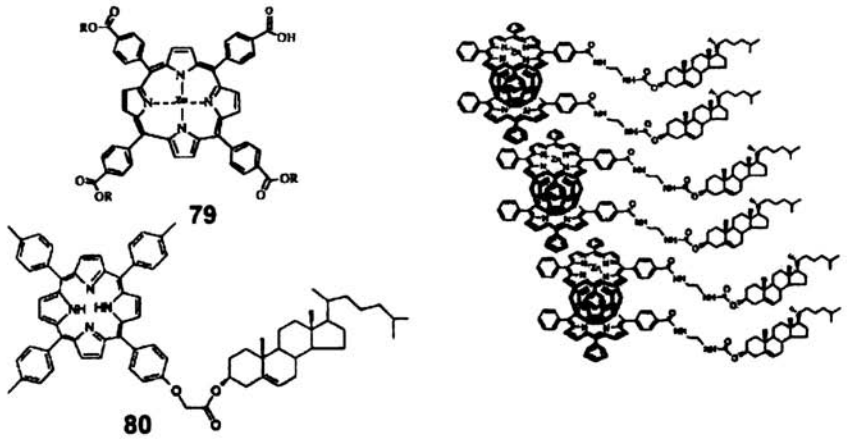

Figure 1.27. Structures of the porphyrin-appended organogelators and the schematic representation of the sandwich complex between porphyrin and fullerene in the gel network.

A variety of H-bonded one-dimensional gel assemblies, by substituting the periphery of the porphyrin chromophores with sugar, urea or amide hydrogen bonding groups, have been reported by Shinkai and coworkers.[87-90] An amphiphilic porphyrin bearing four β-D-galactopyranoside groups (**81**) was shown to form left-handed helical coiled-coil gel nanostructures in DMF/alcohol solvent mixtures.[87] One-dimensional assemblies of porphyrin chromophores are stabilized by the synergistic effect of the π-π stacking interaction among the porphyrin aromatic cores and the H-bonding interactions between sugar moieties, as shown in Figure 1.28.

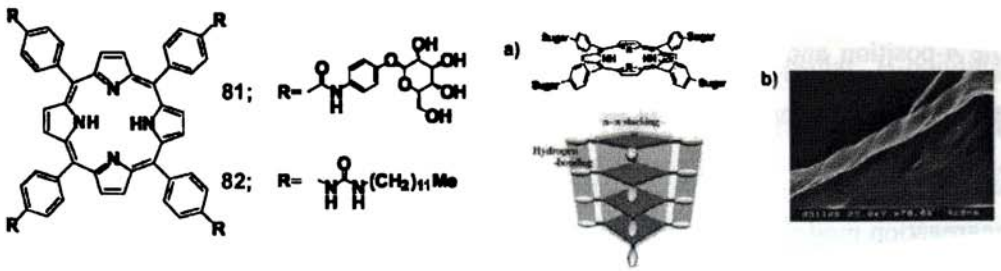

Figure 1.28. a) Schematic picture of the one-dimensional stacking of sugar-appended porphyrin organogelators and b) the SEM image of the helical gel nanostructures of **81**.

The stability of the porphyrin based gel assemblies has been significantly increased when the peripheral sugar moieties are replaced with urea groups.[88] The urea-appended porphyrin (**82**) can form stable organogels in anisole with sol-gel phase transition temperature greater than 140 °C, even at 0.125 wt/vol%. Interestingly, chiral urea derivatives such as (*R*)- and (*S*)-enantiomers of *N*-(1-phenylethyl)-*N'*-dodecyl urea (*R*)-**83** and (*S*)-**83**, respectively could bound to the one-dimensional porphyrin stacks to twist them in a helical sense, which is evident from the resultant exciton coupled CD spectra (Figure 1.29).

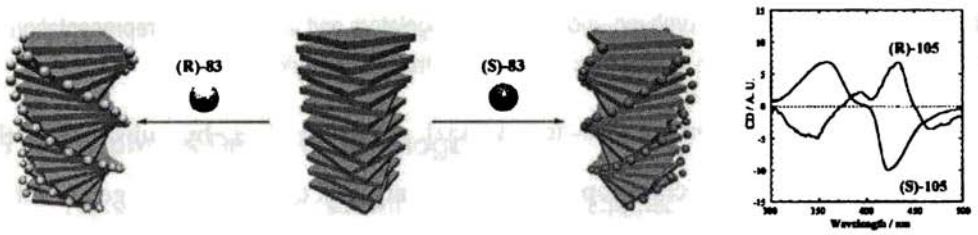

Figure 1.29. Schematic picture of the helical twisting of one-dimensional stacking of sugar-appended porphyrin organogelators upon addition of chiral urea guests and the corresponding CD spectra.

Shinkai and coworkers have synthesized the amide-appended porphyrin organogelators **84** and **85** which showed competition between 'H' *vs.* 'J' aggregation mode of the porphyrin in the gel assemblies.[89] Appropriate positioning of the peripheral H-bonding amide motifs could facilitate the formation of one of the aggregates preferentially. The gelators **84** and **85** are substituted with amide groups at the 4-position and the 3,5 positions of the *meso*-phenyl groups, respectively. X-ray analysis of the single crystals established that the porphyrins in **84** adopt the 'H'-aggregation mode resulting in columnar stacks, whereas those in **85** adopt the 'J'-aggregation mode resulting in two-dimensional planar assemblies. UV/Vis absorption, XRD and SEM measurements established that the organization modes of porphyrins in the gel state of **84** and **85** are similar to that in the corresponding single crystals.

SEM analysis of the cyclohexane gels of **84** and **85** revealed one-dimensional fibrillar and two-dimensional sheet like structures, respectively indicating that the difference in the microscopic H-bonded organization of the porphyrin chromophores are expressed even at the macroscopic morphology (Figure 1.30).

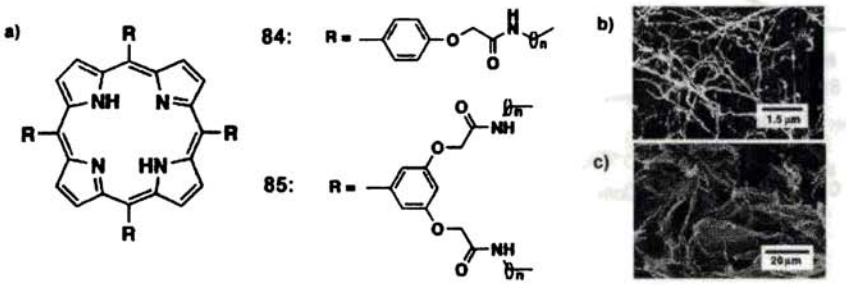

Figure 1.30. a) Structures of amide-appended porphyrin gelators and the SEM images of the xerogels of b) **84** and c) **85** from cyclohexane.

The porphyrin derivative **85** can self-assemble to one-dimensional multicapsular structures in the presence of C_{60} as a cooperative effect of strong C_{60}-porphyrin interactions and 'inter- and intracapsular' H-bonding interactions between the amide groups, which is entirely different from that of the two dimensional 'J'-type aggregates in the absence of C_{60} (Figure 1.31).[90] Detailed UV/Vis absorption, elemental analysis, XRD, ATR-IR and computer modeling studies have shown that four amide groups from two adjacent porphyrins form a circular H-bonding array, which can easily encapsulate a C_{60} molecule to give a 1:2 complex. These 'capsules' will further grow into a one-dimensional assembly through 'intercapsular' H-bonding interactions between amide groups on the other side of the complex. SEM and TEM analysis showed a gradual change from the sheet like morphology to a fibrous network on increasing the concentration of the C_{60} from 0-0.5 equivalents, which clearly support the one-dimensional aggregation mode. The complete quenching of

the fluorescence of one-dimensional multicapsular structure indicated a novel electron transfer phenomena between porphyrin 'walls' and encapsulated C_{60}.

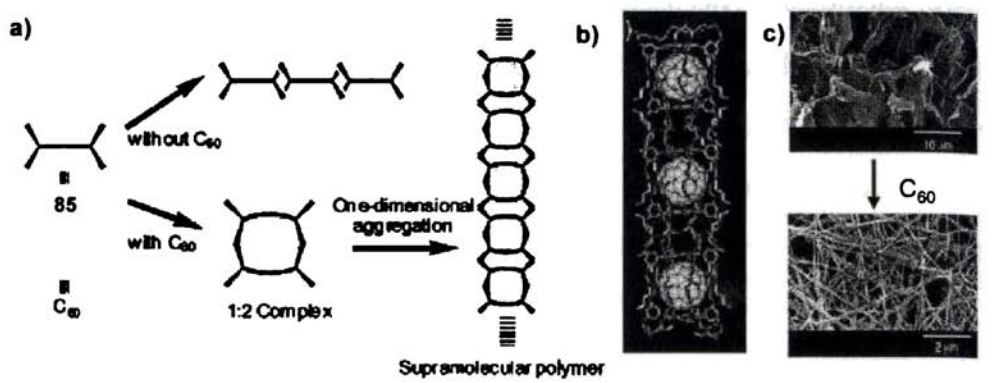

Figure 1.31. a) Aggregation modes of **85**, b) side view of the energy minimized structure of $(C_{60})_3$.$(\mathbf{85})_6$ and c) the SEM images showing the morphological changes in the benzene gels of **85** on adding the fullerenes.

1.7.4. Pyrene Derived Organogels

Pyrene, due to its strong fluorescence and excimer formation is a useful probe for photophysical and photobiological studies. Pyrene can also be used as a probe to study the self-assembly properties of organic molecules. In this context, the two component system consisting of bile acid based molecular tweezers (**86** and **87**) and 2,4,7-trinitrofluorenone (TNF, **88**) acceptor molecules are shown to form organogels in a variety of hydroxyl and hydrocarbon solvents through charge transfer interactions (Chart 1.10).[40] Recently, a new class of pyrene derived organogelators in which the bile acid part is replaced by alkyl chains connecting to pyrene chromophores through a variety of linkers have been reported.[91] Compounds with ester (**89**) or ether (**90**) linkages are shown to form gels only in the presence of TNF through charge-transfer interactions, which can be monitored by a substantial color change and the appearance of the charge transfer band (Chart 1.10). However, the compounds with amide (**91**),

urea (**92**) an ureathane (**93**) linkers can self-assemble into one-dimensional gels through H-bond and π-stack interactions (Chart 1.11).[91,92] The chiral pyrene organogelator (**94**), substituted with a (*R*)-(-)-2-octyl urethane group self-assemble into *P*-helical aggregates.

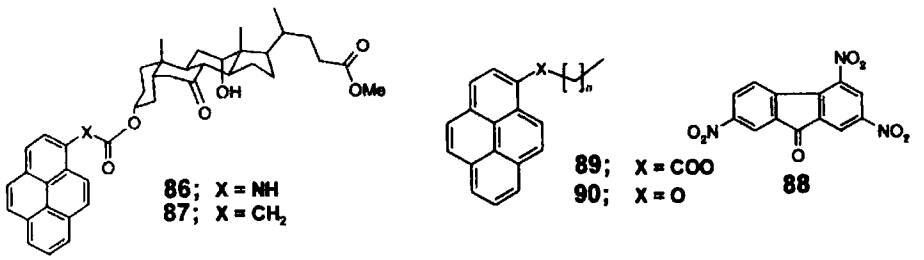

Chart 1.10

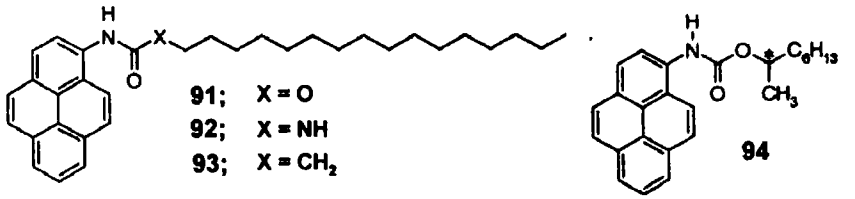

Chart 1.11

The groups of Ihara and Sagawa have prepared fibrous gel assemblies of porphyrin **95** and pyrene **96** substituted by L-glutamic acid.[93] By amide hydrogen bonding, both chromophores self-assemble co-facially into chiral fibers of several micrometers in length which can be controlled by temperature. The porphyrin **95** forms a physical gel and optical studies confirm the presence of highly ordered aggregates even below the critical gel forming concentration. Though the pyrene **96** did not produce a gel state at room temperature, it does form aggregate in solution. Preliminary results indicate energy transfer within mixed assemblies in solution from pyrene excimers to porphyrin traps. Moreover, the L-glutamic acid induces helicity into the fibers, as can

be concluded from the observed Cotton effects for both the porphyrin and the pyrene systems.

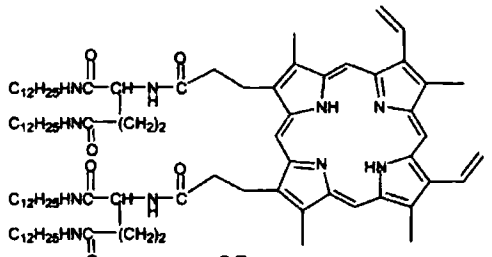

95

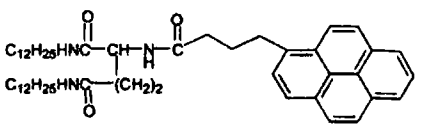

96

Chart 1.12

1.7.5. Miscellaneous Chromophore Based Gelators

The stilbene-appended cholesterol derivative **97**, is reported to form organogels in appropriate solvents.[94] Time dependent evolution of the gel nanostructures of **97** has been studied using AFM technique, in order to get a direct observation on the role of solvent during the gel formation (Figure 1.32).[95] Detailed ^{1}H NMR investigation on the composition, structure and dynamics of the stilbene-cholesterol gels were also reported.[96] The cholesterol-appended squaraine derivative **98**, form a gel in butanol, which is marked by the blue shift in the absorption spectra, loss of fluorescence and the appearance of exciton coupled CD spectra, indicating that the dye molecules are arranged in a helical 'H'-aggregate fashion.[94] However, detailed studies of **98** at the air-water interface and in Langmuir-Blodgett films showed an unusual folded type conformation in which there are attractive noncovalent interactions between the squaraine chromophores and cholesterol.[97]

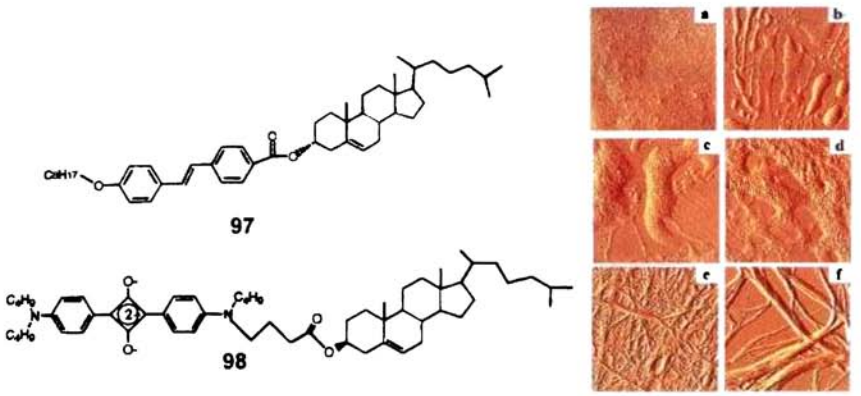

Figure 1.32. Structures of stilbene- and squaraine-appended cholesterol gelators and time dependent AFM images of the formation of gel fibers of **97**.

Shinkai and coworkers have designed proton sensitive, highly fluorescent 1,10-phenanthroline-appended cholesterol based gelator (**99**), which acts as an efficient energy transfer system (Figure 1.33).[98] Even in the presence of two equivalents of TFA, the purple emission (360 nm) of the gel phase of **99** is quenched completely, with the appearance of the yellow emission (530 nm) corresponding to the protonated form of **99**, due to an efficient energy transfer from the neutral to the protonated form of **99**. However, when the gel was converted into the solution phase at 90 °C in the presence of TFA, a blue emission with bimodal emission maxima was obtained indicating the absence of energy transfer.

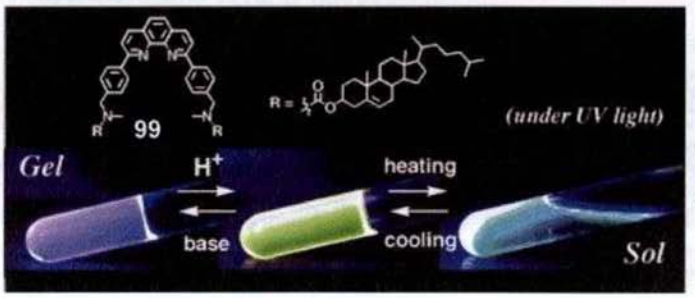

Figure 1.33. Emission changes in the phenanthroline-appended cholesterol based gelator **99** upon protonation.

In an attempt to design self-assembling molecular wires, tetrathiafulvalene (TTF) molecules were attached to bis-arborols, to provide the compound **100**, which is found to be an efficient organogelator.[99] Phase contrast microscopy revealed string like superstructures of several micrometers in length and diameter ranging from about 30 to several hundred nanometers (Figure 1.34). Absorption spectroscopy indicated the presence of stacked TTF molecules in the gel phase, which could act as a conducting supramolecular wire.

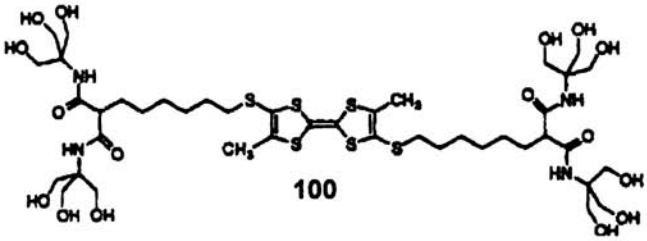

100

Figure 1.34. Phase contrast microscopic picture of the TTF gels.

The triphenylene derivatives (**101** and **102**) substituted with six amide groups and six hydrocarbon side chains are found to form fluorescent organogels with unusual emission properties in nonpolar solvents as a result of highly directional columnar self-assemblies through a cooperative effect of π-π, H-bonding and van der Waals interactions.[100] Detailed fluorescence measurements have shown that the triphenylenes in the gel of **102** are arranged in a staggered manner, similar to the packing in triphenylene based LCs. However, in **101** the aromatic cores are arranged in an eclipsed manner leading to an unusual observation of excimer emission in triphenylene based assemblies, at 525 nm (Figure 1.35). Furthermore, XRD analysis of the xerogels revealed a lateral rectangular and hexagonal columnar arrangement for **101** and **102**, respectively indicating the crucial role of alkyl chains in controlling the packing mode.

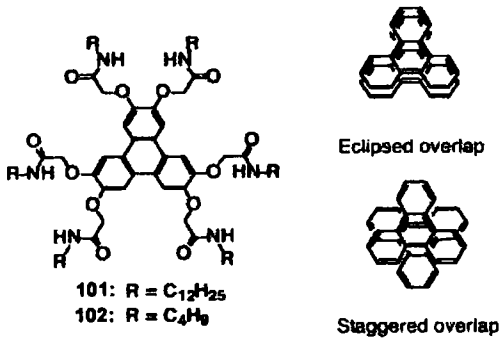

Figure 1.35. Structure of triphenylene derived organogelators. Eclipsed and staggered modes of packing of triphenylene chromophore in the gels of **101** and **102**, respectively are also shown.

Recently, novel photoresponsive chiral organogels, based on the dithienylethene photochromic unit functionalized with (*R*)-1-phenylethylamine derived amides, have been reported from Feringa's group.[101] The dithienylethene **103** exists as two antiparallel interconvertible open forms with *P*- and *M*-helicity, which cyclize in a fully reversible manner upon irradiation with UV light to form two diastereomers of the ring closed product **104** (Figure 1.36). The open form **103** is found to be an efficient organogelator of nonpolar solvents such as toluene, benzene and hexane. CD and TEM studies of the toluene gels revealed that the molecule **103** self-assemble to helical fibers, owing to the expression of the *M*- or *P*-chirality of the open form at the supramolecular level (Figure1.37).

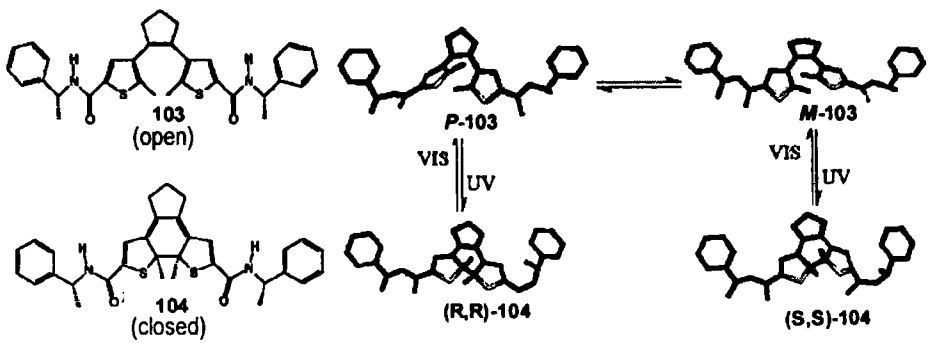

Figure 1.36. Open and closed forms of dithienylethene organogelators.

Interestingly, the photocyclization of **103** in the gel state showed nearly absolute stereocontrol though there is no stereoselectivity in the non-gelled solution. Both the open **103** and closed **104** forms can exist in two different chiral gel states, denoted as α and β, leading to a four-state chiroptical supramolecular switch, since these four states can be cycled by a sequence of photochemical reactions as shown in Figure 1.37. A stable gel of (α)-**103** (*P*-helicity) is obtained on cooling the isotropic solution of the open form **103**. Photocyclization results in the formation of the metastable gel (α)-**104** which will convert into the thermodynamically stable gel (β)-**104** (M-helicity) upon the heating-cooling cycles. Irradiation of the gel (β)-**104** with visible light results in the metastable gel (β)-**103**, which will then change into the original stable gel (α)-**103** via an isotropic solution of **103**, after a heating-cooling cycle. The optical switching between different supramolecular chiral aggregates and the interplay of molecular and supramolecular chirality in these systems is attractive for designing molecular memory systems and smart functional materials.

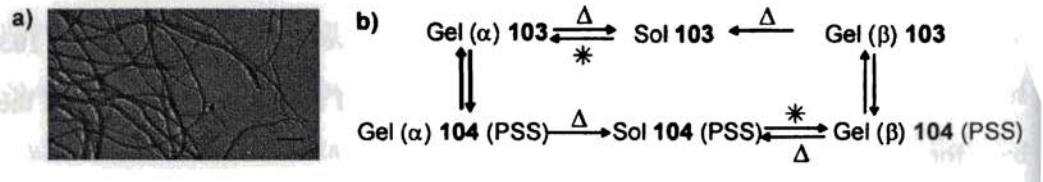

Figure 1.37. a) TEM image of the helical fibers of a toluene gel of **103**. b) Four different chiral aggregated states and the switching processes of the chiroptical supramolecular switch consisting of the open form **103** and the closed form of **104**.

Recently, a highly fluorescent organogel was reported by the intermolecular H-bonding interactions between the non-emissive oxadiazole based benzene-1,3,5-tricarboxamide molecule (**105**, Figure 1.38).[102] Detailed studies have shown that the intermolecular face-to-face H-bonding interactions in the columnar gel aggregates

play a key role in the enhancement of fluorescence upon gelation, by providing significant singlet-triplet splitting to reduce the rate of ISC.

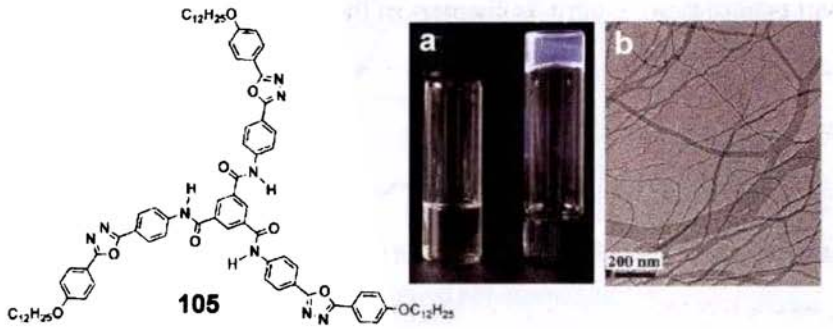

Figure 1.38. a) An oxadiazole based gel under UV irradiation and b) the TEM image.

Würthner and coworkers have reported the hierarchical self-organization of the merocyanine dye molecules (**106-107**), which are tethered to tris(*n*-dodecyloxy)xylene unit to form supramolecular polymers and organogels, through dipolar aggregation.[103] AFM and *cryo*-TEM studies of the gels revealed long and stiff rod-type assemblies, whereas, the X-ray diffraction studies revealed columnar mesomorphism. Based on these observations, a structural model is proposed in which six helically preorganized strands of the initially formed supramolecular polymer intertwined to form a rod with a diameter of about 5 nm (Figure 1.39).

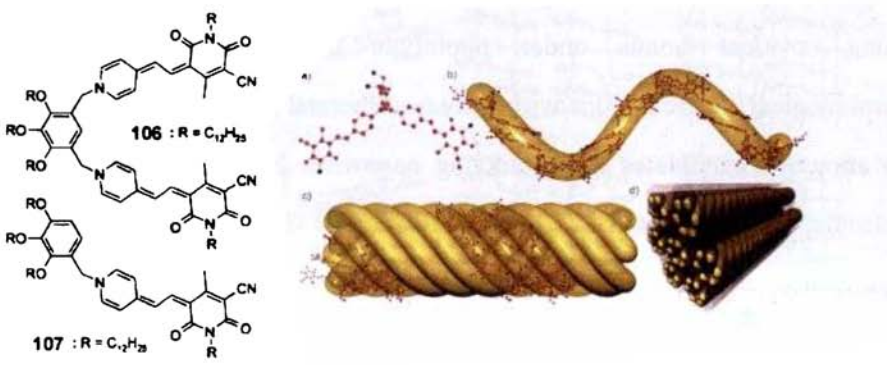

Figure 1.39. Structural model for the hierarchical self-organization of merocyanine gelators.

In addition, organogelators based on the cholesterol-appended perylene[104] (**108**) and phthalocyanine[105] (**109**) chromophores have also been reported, the details of which will be discussed in various chapters of the thesis.

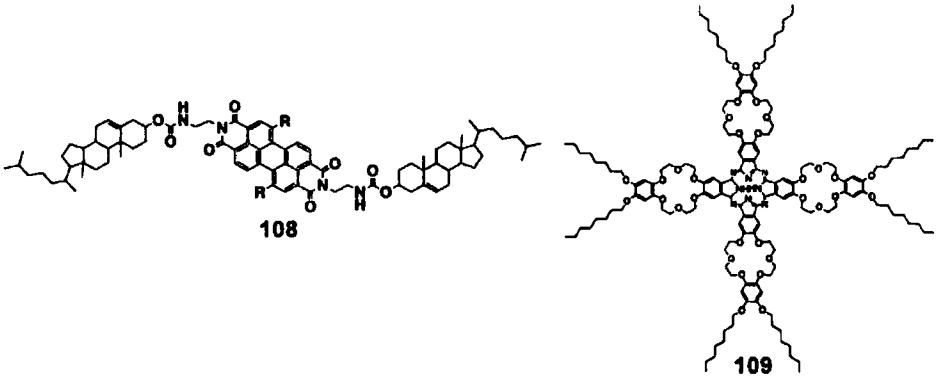

Chart 1.13

1.7.6. Diacetylene Derived Organogels

In recent years there has been considerable interest in the self-assembly of diacetylene derivatives as they allow the covalent fixation of supramolecular assemblies through photopolymerization reactions to give polydiacetylenes (Figure 1.40). Gel forming diacetylenes are particularly interesting because the gel network which is stabilized by the noncovalent interaction can be permanently supported by strong covalent bonds under photolytic conditions, thereby retaining the morphological characteristics with increased thermal stability. Since polydiacetylenes are attractive candidates as conducting nanowires having potential applications in molecular electronic devices, covalent fixation of the organized assembly has great significance.

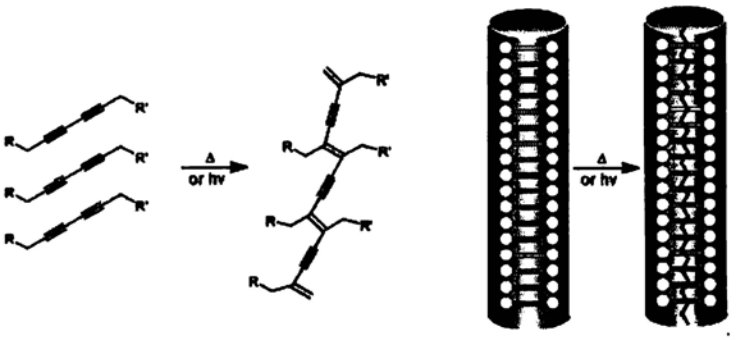

Figure 1.40. Photopolymerization of diacetylenes to polydiacetylenes and the schematic representation of the concept of covalent fixation of diacetylene derived self-assemblies.

Masuda *et al.* reported diacetylene-1-glucosamide bolaamphiphiles **110** and **111**, which self-assemble to form nanofibers leading to the gelation of organic solvents.[106] The self-assembly of **110** is directed by the linear amide H-bonding interactions, whereas in **111**, the self-assembly is supported by the H-bonding interactions among the sugar groups (Figure 1.41). Photopolymerization of the nanofibers of **110** form a relatively low molecular weight soluble polymer (13-mer), whereas **111** produced relatively higher molecular weight polymer (64-mer), due to the higher molecular packing order in the latter.

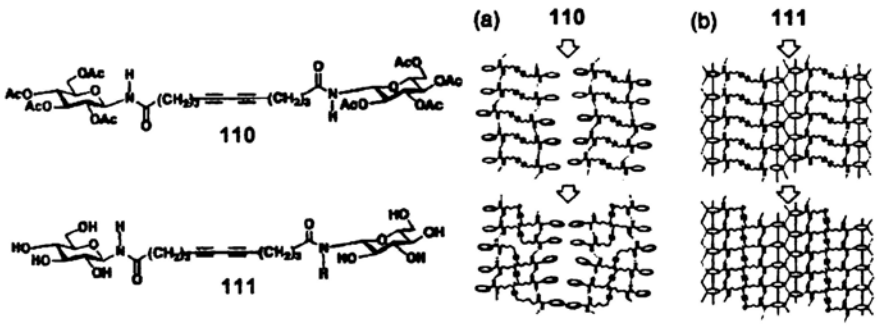

Figure 1.41. Schematic representation of the photopolymerization of **110** and **111** gels.

Diacetylene dicholesteryl ester derivatives having urethane linkages (**112**) have been polymerized in the organogel state to form colored gels containing

polydiacetylene nanowires.[107] Gels before irradiation was stabilized by H-bonding interactions between the urethane groups which are further stabilized by van der Waals interaction between the cholesterol groups. The polymerization is accompanied by a color change from white to blue. Electron microscopy revealed that the fibrillar gel morphology was not basically changed after polymerization. A series of 10,12-pentacosadiynoic acid derived organogelators with conjugated diyene units (**113**) and their photopolymerization was reported by Weiss and coworkers.[108] 1, 2-Aminocyclohexyl derivatives have also been polymerized in the gel network, by incorporating diacetylene linkages to the alkyl side chains (**114**).[42b]

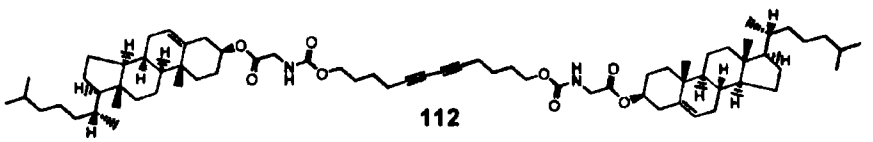

112

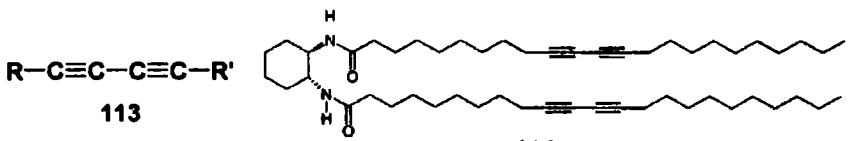

113 **114**

Chart 1.14

1.7.7. Organogels Derived from Extended Aromatic π-Conjugated Systems

The bisurea-appended oligo(thiophene)s (**115-116**) have been reported to self-assemble into elongated fibers resulting in the formation of organogels in solvents such as tetralin and 1,2-dichloroethane.[109] Electron microscopy and X-ray diffraction studies revealed that the fibers have a lamellar structure, in which the molecules are arranged as one-dimensional ribbons with their long molecular axis parallel to each other (Figure 1.42). Moreover, it was shown by pulse-radiolysis time resolved microwave conductivity (PR-TRMC) experiments that the good electronic overlap

between the thiophene rings due to the H-bond assisted π-stacking of adjacent oligomers results in high charge carrier mobility of at least 0.001 cm^2/Vs for **115** and 0.005 cm^2/Vs for **116**. These values are relatively high when compared to that of simple thiophene oligomers.

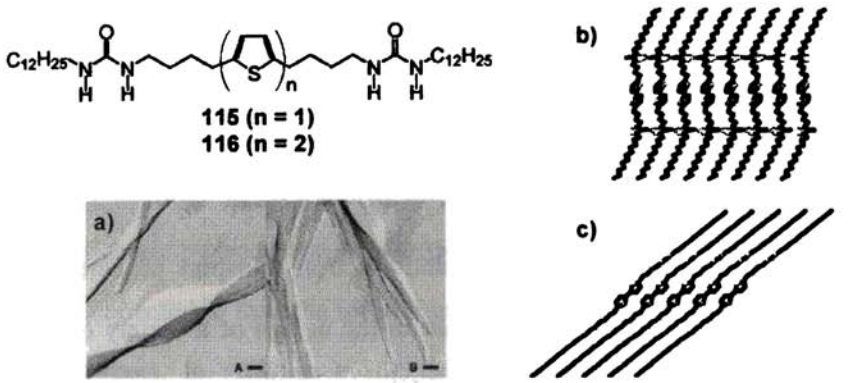

Figure 1.42. Structure of bisurea-appended thiophene oligomers. a) Electron micrographs of the lamellar fibers of **115** (A) and **116** (B). Possible arrangement of **116** in the lamella: b) view of a hydrogen bonded ribbon, and c) a tilted stack of ribbons that form a lamella.

Tour and coworkers reported that the well known π-stacking forces between shape persistent cyclophanes could be enhanced through hydrogen bonding interactions by incorporating multiple H-bonding sites at the periphery of the cyclophane ring.[110] The H-bond assisted stacking interaction in **117** results in the formation of cyclophane dimers and gels at moderate concentrations in solvents such as CH_2Cl_2 and $CHCl_3$. Very recently, a strong fluorescent gel comprising fibrillar self-assembly of a trifluoromethyl-based cyanostilbene derivative **(118)** has been reported.[111] The gelation of **118** is attributed to the cooperative effect of the strong π-π stacking interactions of the rigid rod-like aromatic segments and supplementary intermolecular interactions induced by the four CF_3 units.

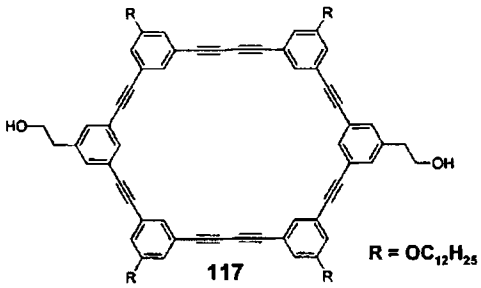

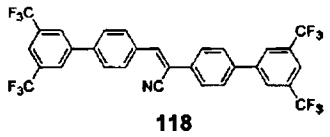

118

Chart 1.15

1.8. Origin, Objectives and Approach to the Thesis

Despite the interesting optical and electron transport properties of linear π-conjugated systems, which are important in the design of a variety of molecular and supramolecular devices, not much attention is given to the self-assembly induced gelation and the resultant modulation of the optical properties except in a very few recent reports (Section 1.7.7).[109-112] Gel formation in the case of certain π-conjugated polymers as a result of the unwanted crosslinking and chain branching reactions, as in the case of a few phenyleneethynylenes has been noticed earlier.[112] Later, gelation is observed in the case of oligo(thiophene),[109] cyanostilbene[111] and phenylacetylene[110] based cyclophane derivatives. However, the importance of π-conjugated molecules in advanced applications demands self-assembly induced gelation and the consequent changes in the morphology and optical properties. Therefore, the main objective of the present study is to have a detailed investigation on the gelation properties, morphology and optical properties of small π-conjugated oligomers. For this purpose we have chosen oligo(*p*-phenylenevinylene)s (OPVs), a class of molecules which have received considerable attention due to their unique optical and electronic properties. Though a large number of reports are available in the literature on the self-

assembly properties of tailor made OPVs, none of them pertain to the design of nanostructures based on organogels. In view of this, we aimed at the creation of functional chromophoric assemblies of π-conjugated OPVs through the formation of organogels, with the objective of crafting nanoscopic assemblies of different size and shape thereby modulating their optical and electronic properties.

In order to fulfill the above objectives, the design and synthesis of a variety of OPVs with appropriate structural variations were planned. The design principle involves the derivatization of OPVs with weak H-bonding hydroxymethyl end groups and with long aliphatic hydrocarbon side chains. The noncovalent interactions in these molecules were expected to lead the formation of supramolecular assembly and gels in hydrocarbon solvents. In such an event, detailed study of gelation and extensive analysis of the morphology of the gel structures were planned using advanced microscopic techniques. Since OPVs are strongly fluorescent molecules, gelation is expected to perturb the optical properties. Therefore, detailed study on the gelation induced optical properties as a way to probe the nature and stability of the self-assembly was planned. Apart from this, the potential use of the modulation of the optical properties for the purpose of light harvesting was aimed. The approach to this problem was to entrap an appropriate energy trap to the OPV gel matrix which may lead to the efficient energy transfer from the OPV gel based donor to the entrapped acceptor. The final question that we wanted to address in this investigation was the creation of helical nanostructures through proper modification of the OPV backbone with chiral handles. The present thesis is a detailed and systematic approach to the realization of the above objectives which are presented in different chapters of the thesis.

1.9. References

1. (a) Lehn, J.-M. *Supramolecular Chemistry*; VCH: Winheim, Germany, 1995. (b) Schneider, H.-J.; Yatsimirsky, A. *Principles and Methods in Supramolecular Chemistry*; Wiley: Chichester, 2000. (c) Steed, J. W.; Atwood, J. L. *Supramolecular Chemistry*; Wiley: Chichester, 2000.
2. Prins, L. J.; Reinhoudt, D. N.; Timmerman, P. *Angew. Chem. Int. Ed.* **2001**, *40*, 2382.
3. (a) Percec, V.; Glodde, M.; Bera, T. K.; Miura, Y.; Shiyanovskaya, I.; Singer, K. D.; Balagurusamy, V. S. K.; Heiney, P. A.; Schnell, I.; Rapp, A.; Spiess, H.-W.; Hudson, S. D.; Duan, H. *Nature* **2002**, *419*, 384. (b) Meijer, E. W.; Schenning, A. P. H. J. *Nature* **2002**, *419*, 353.
4. Burrell, A. K.; Officer, D. L.; Plieger, P. G.; Reid, D. C. W. *Chem. Rev.* **2001**, *101*, 2751.
5. Tecilla, P.; Dixon, R. P.; Slobodkin, G.; Alavi, D. S.; Waldeck, D. H.; Hamilton, A. D. *J. Am. Chem. Soc.* **1990**, *112*, 9408.
6. Sessler, J. L.; Wang, B.; Harriman, A. *J. Am. Chem. Soc.* **1995**, *117*, 704.
7. Osuka, A.; Yoneshima, R.; Shiratori, H.; Okada, T.; Taniguchi, S.; Mataga, N . *Chem. Commun.* **1998**, 1567.
8. Myles, A. J.; Branda, N. R. *J. Am. Chem. Soc.* **2001**, *123*, 177.
9. Nagata, N.; Kugimiya, S-i.; Kobuke, Y. *Chem. Commun.* **2000**, 1389.
10. Nagata, N.; Kugimiya, S-i.; Kobuke, Y. *Chem. Commun.* **2001**, 689.
11. Ikeda, C.; Nagahara, N.; Motegi, E.; Yoshioka, N.; Inoue, H. *Chem. Commun.* **1999**, 1759.
12. Drain, C. M.; Russel, K. C.; Lehn, J.-M. *Chem. Commun.* **1996**, 337.
13. Shi, X.; Barkigia, K. M.; Fajer, J.; Drain, C. M. *J. Org. Chem.* **2001**, *66*, 6513.
14. Drain, C. M.; Shi, X.; Milic, T.; Nifiatis, F. *Chem. Commun.* **2001**, 287.
15. Yamaguchi, T.; Ishii, N.; Tashiro, K.; Aida, T. *J. Am. Chem. Soc.* **2003**, *125*, 13934.

16. Kimura, M.; Muto, T.; Takimoto, H.; Wada, K.; Ohta, K.; Hanabusa, K.; Shirai, H.; Kobayashi, N. *Langmuir* **2000**, *16*, 2078.

17. Kimura, M.; Kuroda, T.; Ohta, K.; Hanabusa, K.; Shirai, H.; Kobayashi, N. *Langmuir* **2003**, *19*, 4825.

18. Würthner, F. *Chem. Commun.* **2004**, 1564.

19. (a) Würthner, F.; Thalacker, C.; Sautter, A. *Adv. Mater.* **1999**, *11*, 754. (b) Würthner, F.; Thalacker, C.; Sautter, A.; Schärtl, W.; Ibach, W.; Hollricher, O. *Chem. Eur. J.* **2000**, *6*, 3871.

20. Thalacker, C.; Würthner, F. *Adv. Funct. Mater.* **2002**, *12*, 209.

21. Prins, L. J.; Thalacker, C.; Würthner, F.; Timmerman, P.; Reinhoudt, D. N. *Proc. Natl. Acad. Sci. U.S.A.* **2001**, *98*, 10042.

22. Würthner, F.; Yao, S.; Heise, B.; Tschierske, C. *Chem. Commun.* **2001**, 2260.

23. Würthner, F.; Yao, S. *J. Org. Chem.* **2003**, *68*, 8943.

24. Kimizuka, N.; Kawasaki, T.; Hirata, K.; Kunitake, T. *J. Am. Chem. Soc.* **1998**, *120*, 4094.

25. Kawasaki, T.; Tokuhiro, M.; Kimizuka, N.; Kunitake, T. *J. Am. Chem. Soc.* **2001**, *123*, 6792.

26. Ariga, K.; Kunitake, T. *Acc. Chem. Res.* **1998**, *31*, 371.

27. Yagai, S.; Karatsu, T.; Kitamura, A. *Chem. Commun.* **2003**, 1844.

28. Radotondradany, F.; Whitehead, M.; Lebuis, A.; Slieman, H. *Chem. Eur. J.* **2003**, *9*, 4771.

29. Jordon Lloyd, D. *Colloid Chemistry*; Alexander, J., Ed.; The Chemical Catalog Co.: New York, 1926; Vol. 1, p 767.

30. Flory, P. J. *Discuss Faraday Soc.* **1974**, *57*, 7.

31. (a) Guenet, J.-M. *Thermoreversible Gelation of Polymers and Biopolymers*; Academic Press, London, 1992. (b) Saiani, A.; Guenet, J.-M. *Macromolecules* **1997**, *30*, 967. (c) Saiani, A.; Guenet, J.-M. *Macromolecules* **1999**, *32*, 657.

32. Reviews on low molecular weight organogels: (a) Terech, P.; Weiss, R. G. *Chem. Rev.* **1997**, *97*, 3133. (b) van Esch, J. H.; Feringa, B. L. *Angew. Chem. Int. Ed.* **2000**, *39*, 2263. (c) Abdallah, D. J.; Weiss, R. G. *Adv. Mater.* **2000**, *12*, 1237. (d) Estorff, L. A.; Hamilton, A. D. *Chem. Rev.* **2004**, *104*, 1201.

33. Shinkai, S.; Murata, M. *J. Mater. Chem.* **1998**, *8*, 485.

34. Brotin, T.; Utermöhlen, R.; Fages, F.; Bouas-Laurent, H.; Desvergne, J.-P. *J. Chem. Soc., Chem. Commun.* **1991**, 416.

35. Clavier, G. M.; Brugger, J.-F.; Bouas-Laurent, H.; Pozzo, J.-L. *J. Chem. Soc., Perkin Trans. 2*, **1998**, 2527.

36. Abdallah, D. J.; Weiss, R. G. *Langmuir* **2000**, *16*, 352.

37. Twieg, R. J.; Russell, T. P.; Siemens, R. L.; Rabolt, J. F. *Macromolecules* **1985**, *18*, 1361.

38. Abdallah, D. J.; Lu, L.; Weiss, R. G. *Chem. Mater.* **1999**, *11*, 2907.

39. Lu, L.; Weiss, R. G. *Chem. Commun.* **1996**, 2029.

40. Maitra, U.; Kumar, P. V.; Chandra, N.; D'Souza, L. J.; Prasanna, M. D.; Raju, A. R. *Chem. Commun.* **1999**, 595.

41. Friggeri, A.; Gronwald, O.; van Bommel, K. J. C.; Shinkai, S.; Reinhoudt, D. N. *J. Am. Chem. Soc.* **2002**, *124*, 10754.

42. (a) Van Esch, J.; Kellogg, R. M.; Feringa, B. L. *Tetrahedron Lett.* **1997**, *38*, 281. (b) De Loos, M.; Van Esch, J.; Stokroos, I.; Kellogg, R. M.; Feringa, B. L. *J. Am. Chem. Soc.* **1997**, *119*, 12675. (c) Van Esch, J.; De Feyter, S.; Kellogg, R. M.; De Schryver, F.; Feringa, B. L. *Chem. Eur. J.* **1997**, *3*, 1238. (d) Van Esch, J. H.; Schoonbeek, F. S.; De Loos, M.; Spek, A. L.; Kellogg, R. M.; Feringa, B. L. *Chem. Eur. J.* **1999**, *5*, 937. (e) Schoonbeek, F. S.; Van Esch, J. H.; Hulst, R. H.; Kellogg, R. M.; Feringa, B. L. *Chem. Eur. J.* **2000**, *6*, 2633. (f) Brinksma, J.; Feringa, B. L.; Kellogg, R. M.; Vreeker, R.; van Esch, J. *Langmuir* **2000**, *16*, 9249. (g) de Loos, M.; van Esch, J.; Kellogg, R. M.; Feringa, B. L. *Angew. Chem. Int. Ed.* **2001**, *40*, 613.

43. Hanabusa, K.; Shimura, K.; Hirose, K.; Kimura, M.; Shirai, H. *Chem. Lett.* **1996**, 885.

44. De Loos, M.; Ligtenbarg, A. G. J.; van Esch, J.; Kooijman, H.; Spek, A. L.; Hage, R.; Kellogg, R. M.; Feringa, B. L. *Eur. J. Org. Chem.* **2000**, 3675.

45. Estroff, L. A.; Hamilton, A. D. *Angew. Chem. Int. Ed.* **2000**, *39*, 3447.

46. Wang, G.; Hamilton, A. D. *Chem. Commun.* **2003**, 310.

47. Hanabusa, K.; Yamada, M.; Kimura, M.; Shirai, H. *Angew. Chem. Int. Ed.* **1996**, *35*, 1949.

48. (a) Lightfoot, M. P.; Mair, F. S.; Pritchard, R. G.; Warren, J. E. *Chem. Commun.* **1999**, 1945. (b) Hanabusa, K.; Okui, K.; Karaki, K.; Kimura, M.; Shirai, H. *J. Coll. Int. Sci.* **1997**, 86. (c) Yasuda, Y.; Iishi, E.; Inada, H.; Shirota, Y. *Chem. Lett.* **1996**, 575.

49. Hanabusa, K.; Kawakami, A.; Kimura, M.; Shirai, H. *Chem. Lett.* **1997**, 191.

50. van Gorp, J. J.; Vekemans, J. A. J. M.; Meijer, E. W. *J. Am. Chem. Soc.* **2002**, *124*, 14759.

51. (a) Schmidt, R.; Schmutz, M.; Michel, M.; Decher, G.; Mésini, P. J. *Langmuir* **2002**, *18*, 5688. (b) Schmidt, R.; Schmutz, M.; Mathis, A.; Decher, G.; Rawiso, M.; Mésini, P. J. *Langmuir* **2002**, *18*, 7167.

52. (a) Yoza, K.; Amanokura, N.; Ono, Y.; Akao, T.; Shinmori, H.; Takeuchi, M.; Shinkai, S.; Reinhoudt, D. N. *Chem. Eur. J.* **1999**, *5*, 2722. (b) Amanokura, N.; Kanekiyo, Y.; Shinkai, S.; Reinhoudt, D. N. *J. Chem. Soc., Perkin Trans. 2*, **1999**, 1995. (c) Luboradzki, R.; Gronwald, O.; Ikeda, M.; Shinkai, S.; Reinhoudt, D. N. *Tetrahedron* **2000**, *56*, 9595. (d) Gronwald, O.; Shinkai, S. *Chem. Eur. J.* **2001**, *7*, 4329.

53. (a) John, G.; Masuda, M.; Okada, Y.; Yase, K.; Shimizu, T. *Adv. Mater.* **2001**, *13*, 715. (b) Jung, J. H.; John, G.; Masuda, M.; Yoshida, K.; Shinkai, S.; Shimizu, T. *Langmuir* **2001**, *17*, 7229. (c) John, G.; Jung, J. H.; Minamikawa, H.; Yoshida, K.;

Shimizu, T. *Chem. Eur. J.* **2002**, *8*, 5494. (d) Jung, J. H.; Shinkai, S.; Shimizu, T. *Chem. Eur. J.* **2002**, *8*, 2684.

54. Hafkamp, R. J. H.; Feiters, M. C.; Nolte, R. J. M. *J. Org. Chem.* **1999**, *64*, 412.

55. (a) Bhattacharya, S.; Acharya, S. N. G. *Chem. Mater.* **1999**, *11*, 3121. (b) Menger, F. M.; Caran, K. L. *J. Am. Chem. Soc.* **2000**, *122*, 11679. (c) Hanabusa, K.; Matsumoto, M.; Kimura, M.; Kakehi, A.; Shirai, H. *J. Coll. Int. Sci.* **2000**, *224*, 231. (d) Bhattacharya, S.; Krishnan-Ghosh, Y. *Chem. Commun.* **2001**, 185. (e) Mieden-Gundert, G.; Klein, L.; Fischer, M.; Vögtle, F.; Heuzé, K.; Pozzo, J.-L.; Vallier, M.; Fages, F. *Angew. Chem. Int. Ed.* **2001**, *40*, 3164. (f) Suzuki, M.; Yumoto, M.; Kimura, M.; Shirai, H.; Hanabusa, K. *Chem. Commun.* **2002**, 884. (g) Frkanec, L.; Jokić, M.; Makarević, J.; Wolsperger, K.; Žinić, M. *J. Am. Chem. Soc.* **2002**, *124*, 9716. (h) Wang, G.; Hamilton, A. D. *Chem. Eur. J.* **2002**, *8*, 1954.

56. (a) Snip, E.; Shinkai, S.; Reinhoudt, D. N. *Tetrahedron Lett.* **2001**, *42*, 2153. (b) Iwaura, R.; Yoshida, K.; Masuda, M.; Yase, K.; Shimizu, T. *Chem. Mater.* **2002**, *14*, 3047. (c) Giorgi, T.; Grepioni, F.; Manet, I.; Mariani, P.; Masiero, S.; Mezzina, E.; Pieraccini, S.; Saturni, L.; Spada, G. P.; Gottarelli, G. *Chem. Eur. J.* **2002**, *8*, 2143. (d) Yun, Y. J.; Park, S. M.; Kim, B. H. *Chem. Commun.* **2003**, 254.

57. (a) Hafkamp, R. J. H.; Kokke, B. P. A.; Danke, I. M.; Geurts, P. M.; Rowan, A. E.; Feiters, M. C.; Nolte, R. J. M. *Chem. Commun.* **1997**, 545. (b) Gu, W.; Lu, L.; Chapman, G. B.; Weiss, R. G. *Chem. Commun.* **1997**, 543.

58. Lal, M.; Pakatchi, S.; He, G. S.; Kim, K. S.; Prasad, P. N. *Chem. Mater.* **1999**, *11*, 3012.

59. Kubo, W.; Murakoshi, K.; Kitamura, T.; Wada, Y.; Hanabusa, K.; Shirai, H.; Yanagida, S. *Chem. Lett.* **1998**, 1241.

60. Hanabusa, K.; Hiratsuka, K.; Kimura, M.; Shirai, H. *Chem. Mater.* **1999**, *11*, 649.

61. Murdan, S.; Gregoriadis, G.; Florence, A. T. *Eur. J. Pharm. Sci.* **1999**, *8*, 177.

62. Choi, M. F.; Shaung, S. *Analyst* **2000**, *125*, 301.

63. Ihara, H.; Shudo, K.; Hirayama, C.; Hachisako, H.; Yamada, K. *Liq. Cryst.* **1996**, *20*, 807.

64. Shi, C.; Huang, Z.; Kilic, S.; Xu, J.; Enick, R. M.; Beckman, E. J.; Carr, A. J.; Melendez, R. E.; Hamilton, A. D. *Science* **1999**, *286*, 1540.

65. (a) Kato, T.; Kutsuna, T.; Hanabusa, K.; Ukon, M. *Adv. Mater.* **1998**, *10*, 606. (b) Mizoshita, N.; Hanabusa, K.; Kato, T. *Adv. Mater.* **1999**, *11*, 392. (c) Yabuuchi, K.; Rowan, A. E.; Nolte, R. J. M.; Kato, T. *Chem. Mater.* **2000**, *12*, 440. (d) Kato, T.; Kutsuna, T.; Yabuuchi, K.; Mizoshita, N. *Chem. Mater.* **2002**, *18*, 7086.

66. van Bommel, K. J. C.; Friggeri, A.; Shinkai, S. *Angew. Chem, Int. Ed.* **2003**, *42*, 980 and the references cited therein.

67. Zubarev, E. R.; Pralle, M. U.; Sone, E. D.; Stupp, S. I. *J. Am. Chem. Soc.* **2001**, *123*, 4105.

68. Sone, E. D.; Zubarev, E. R.; Stupp, S. I. *Angew. Chem. Int. Ed.* **2002**, *41*, 1705.

69. Hartgerink, J. D.; Beniash, E.; Stupp, S. I. *Science* **2001**, *294*, 1684.

70. Herwig, P. T.; Müllen, K. *Adv. Mater.* **1999**, *11*, 480.

71. Lin, Y.-C.; Weiss, R. G. *Macromolecules* **1987**, *20*, 414.

72. (a) Lin, Y.-C.; Kachar, B.; Weiss, R. G. *J. Am. Chem. Soc.* **1989**, *111*, 5542. (b) Mukkamala, R.; Weiss, R. G. *Chem. Commun.* **1995**, 375. (c) Mukkamala, R.; Weiss, R. G. *Langmuir* **1996**, *12*, 1474. (d) Ostuni, E.; Kamaras, P.; Weiss, R. G. *Angew. Chem. Int. Ed.* **1996**, *35*, 1324.

73. Placin, F.; Colomes, M.; Desvergne, J.-P. *Tetrahedron Lett.* **1997**, *38*, 2665.

74. Pozzo, J.-L.; Clavier, G. M.; Desvergne, J.-P. *J. Mater. Chem.* **1998**, *8*, 2575.

75. Terech, P.; Meerschaut, D.; Desvergne, J.-P.; Colome, M.; Bouas-Laurent, H. *J. Coll. Int. Sci.* **2003**, *261*, 441.

76. Lescanne, M.; Colin, A.; Mondain-Monval, O.; Heuzé, K.; Fages, F.; Pozzo, J.-L. *Langmuir* **2002**, *18*, 7151.

77. Murata, K.; Aoki, M.; Suzuki, T.; Harada, T.; Kawabata, H.; Komori, T.; Ohseto, F.; Ueda, K.; Shinkai, S. *J. Am. Chem. Soc.* **1994**, *116*, 6664.

78. (a) Jung, J. H.; Ono, Y.; Sakurai, K.; Sano, M.; Shinkai, S. *J. Am. Chem. Soc.* **2000**, *122*, 8648. (b) Jung, J. H.; Ono, Y.; Shinkai, S. *Angew. Chem. Int. Ed.* **2000**, *39*, 1862.

79. (a) Jung, J. H.; Ono, Y.; Shinkai, S. *J. Chem. Soc., Perkin Trans. 2*, **1999**, 1289. (b) Jung, J. H.; Ono, Y.; Shinkai, S. *Langmuir* **2000**, *16*, 1643.

80. Jung, J. H.; Kobayashi, H.; Masuda, M.; Shimizu, T.; Shinkai, S. *J. Am. Chem. Soc.* **2001**, *123*, 8785.

81. Mamiya, J.-i.; Kanie, K.; Hiyama, T.; Ikeda, T.; Kato, T. *Chem. Commun.* **2002**, 1870.

82. (a) Kobayashi, H.; Friggeri, A.; Koumoto, K.; Amaike, M.; Shinkai, S.; Reinhoudt, D. N. *Org. Lett.* **2002**, *4*, 1423. (b) Kobayashi, H.; Koumoto, K.; Jung J. H.; Shinkai, S. *J. Chem. Soc., Perkin Trans. 2*, **2000**, 1930.

83. van der Laan, S.; Feringa, B.; Kellogg, R.; van Esch, J. *Langmuir* **2002**, *18*, 7136.

84. Terech, P.; Gebel, G.; Ramasseul, R. *Langmuir* **1996**, *12*, 4321.

85. Tian, H. J.; Inoue, K.; Yoza, K.; Ishi-i, T.; Shinkai, S. *Chem. Lett.* **1998**, 871.

86. (a) Ishi-i, T.; Jung, J. H.; Shinkai, S. *J. Mater. Chem.* **2000**, *10*, 2238. (b) Ishi-i, T.; Iguchi, R.; Snip, E.; Ikeda, M.; Shinkai, S. *Langmuir* **2001**, *17*, 5825.

87. Tamaru, S.-i.; Nakamura, M.; Takeuchi, M.; Shinkai, S. *Org. Lett.* **2001**, *3*, 3631.

88. Tamaru, S.-i.; Uchino, S.-y.; Takeuchi, M.; Ikeda, M.; Hatano, T.; Shinkai, S. *Tetrahedron Lett.* **2002**, *43*, 3751.

89. Shirakawa, M.; Kawano, S.-i.; Fujita, N.; Sada, K.; Shinkai, S. *J. Org. Chem.* **2003**, *68*, 5037.

90. Shirakawa, M.; Fujita, N.; Shinkai, S. *J. Am. Chem. Soc.* **2004**, *125*, 9902.

91. Babu, P.; Sangeetha, N. M.; Vijaykumar, P.; Maitra, U.; Rissanen, K.; Raju, A. R. *Chem. Eur. J.* **2003**, *9*, 1922.

92. Maitra, U.; Potluri, V. K.; Sangeetha, N. M.; Babu, P.; Raju, A. R. *Tetrahedron: Asymmetry* **2001**, *12*, 477.

93. Sagawa, T.; Fukugawa, S.; Yamada, T.; Ihara, H. *Langmuir* **2002**, *18*, 7223.

94. Geiger, C.; Stanescu, M.; Chen, L.; Whitten, D. G. *Langmuir* **1999**, *15*, 2241.

95. Wang, R.; Geiger, C.; Chen, L.; Swanson, B.; Whitten, D. G. *J. Am. Chem. Soc.* **2000**, *122*, 2399.

96. Duncan, D. C.; Whitten, D. G. *Langmuir* **2000**, *16*, 6445.

97. Stanescu, M.; Samha, H.; Perlstein, J.; Whitten, D. G. *Langmuir* **2000**, *16*, 275.

98. Sugiyasu, K.; Fujita, N.; Takeuchi, M.; Yamada, S.; Shinkai, S. *Org. Biomol. Chem.* **2003**, *1*, 895.

99. Jorgensen, M.; Bechgaard, K. *J. Org. Chem.* **1994**, *59*, 5877.

100. Ikeda, M.; Takeuchi, M.; Shinkai, S. *Chem. Commun.* **2003**, 1354.

101. de Jong, J. J. D.; Lucas, L. N.; Kellog, R. M.; van Esch, J. H.; Feringa, B. L. *Science* **2004**, *304*, 278.

102. Ryu, S. Y.; Kim, S.; Seo, J.; Kim, Y.-W.; Kwon, O.-H.; Jang, D.-J.; Park, S. Y. *Chem. Commun.* **2004**, 70.

103. (a) Würthner, F.; Yao, S.; Beginn, U. *Angew. Chem. Int. Ed.* **2003**, *42*, 3247. (b) Yao, S.; Beginn, U.; Gress, T.; Lysetska, M.; Würthner, F. *J. Am. Chem. Soc.* **2004**, *126*, 8336.

104. Sugiyasu, K.; Fujita, N.; Shinkai, S. *Angew. Chem. Int. Ed.* **2004**, *43*, 1229.

105. Engelkamp, H.; Middelbeek, S.; Nolte, R. J. M. *Science* **1999**, *284*, 785.

106. (a) Masuda, M.; Hanada, T.; Yase, K.; Shimizu, T. *Macromolecules* **1998**, *31*, 9408. (b) Masuda, M.; Hanada, T.; Okada, Y.; Yase, K.; Shimizu, T. *Macromolecules* **2000**, *331*, 9233.

107. Tamaoki, N.; Shimada, S.; Okada, Y.; Belaissaoui, K.; Kruk, G.; Yase, K.; Matsuda, H. *Langmuir* **2000**, *16*, 7545.

108. George, M.; Weiss, R. G. *Chem. Mater.* **2003**, *15*, 2879.

109. Schoonbeek, F. S.; van Esch, J. H.; Wegewijs, B.; Rep, D. B. A.; de Haas, M. P.; Klapwijk, T. M.; Kellogg, R. M.; Feringa, B. L. *Angew. Chem. Int. Ed.* **1999**, *38*, 1393.

110. Lin, C.-H.; Tour, J. *J. Org. Chem.* **2002**, *67*, 7761.

111. An, B.-K.; Lee, D.-S.; Lee, J.-S.; Park, Y.-S.; Song, H.-S.; Park, S. Y. *J. Am. Chem. Soc.* **2004**, *126*, 10232.

112. Swager, T. M.; Gil, C. J.; Wrighton, M. S. *J. Phys. Chem.* **1995**, *99*, 4886.

Chapter 2

π-Conjugated Organogels: A Novel Class of Supramolecular Materials Derived from Self-Assembled Oligo(*p*-phenylenevinylene)s

Abstract

A new class of π-conjugated organogels based on oligo(p-phenylenevinylene) (OPV) derivatives are reported. A variety of all-trans OPVs containing hydroxymethyl groups and hydrocarbon side chains were prepared and shown to form organogels in apolar hydrocarbon solvents. A cooperative interaction between H-bonding, π-stacking and van der Waals forces leads to the self-assembly and gelation which are strongly influenced by the structure of the gelator and the nature of the solvent. The length and position of the hydrocarbon side chains and the presence of the hydrogen bonding groups are crucial for the efficient gelation. The gelation properties and the morphology of the gels are established from the DSC, ^1H NMR, XRD, OPM, SEM, TEM and AFM analyses of the gels from different solvents. Variable temperature ^1H NMR spectral studies revealed the thermoreversible self-assembly of the molecules in the gel state. DSC analysis provided the gel melting temperatures and gel stability under different conditions. XRD analysis revealed a lamellar type packing of the molecules whereas the OPM showed the growth of birefringent fibers. Electron microscopic studies revealed the formation of twisted and entangled supramolecular tapes of an average of 50-200 nm in width and several micrometers in length which are in agreement with

the AFM analysis. The organogels reported herein are the first examples of OPV based organogels derived from extended π-conjugated aromatic molecules.

2.1. Introduction

Control of the self-assembly of synthetic molecules in the creation of nanosized architectures, using the principles of supramolecular chemistry is a topic of considerable importance.[1] The cooperative effect of noncovalent forces such as H-bonding, π-stacking, dipolar and van der Waals interactions are the driving force behind the self-assembly of molecules, leading to a variety of novel supramolecular architectures with reversible functional properties. Nature has the ability to control the architecture and function of supramolecular assemblies such as DNA double helix, collagen triple helix, ion channels and photosynthetic reaction centers which has been the major source of inspiration to scientists to mimic natural systems with the help of synthetic molecules.[2-6] In the domain of functional molecular assemblies and nanoarchitectures, supramolecular control of chromophore-linked molecular systems is a challenging task, particularly in the fabrication of nanoscale devices since chromophore orientation has tremendous influence on the optoelectronic properties.[7] Organic π-conjugated systems play a crucial role as an integral component of supramolecular devices due to their interesting optical and electronic properties that are associated with the delocalized π-electrons, which can be modulated by intermolecular interactions.[3,8] Therefore, self-organization of such systems with the aid of weak noncovalent associations are of extreme importance.

Even though the conjugated polymers are easy to synthesize and process into a device structure, the energetic and positional disorder of its chromophores induced by

the structural defects and entanglement of extended side chains affect the device performance. A solution to this problem is to build well-defined supramolecular structures through the self-assembly of π-conjugated oligomers, thus combining the high molecular order with ease of processing. Hence in recent years, considerable efforts are being focused to realize the concept of 'supramolecular electronics', where supramolecular assemblies of 10-100 nm lengths, from functional π-conjugated oligomers are targeted as active organic materials for the electrooptical devices.[9]

Among various π-conjugated systems, phenylenevinylenes (PVs) are one of the well studied class of molecules due to their importance in various electrooptical devices such as LEDs,[10] photovoltaic cells[11] and FETs.[12] Control of the HOMO-LUMO gap by donor-acceptor interaction and by varying the conjugation length of oligomers provide materials with well-defined functional properties.[13] In this context, extensive studies have been reported in the literature, pertaining to the optical and electronic properties of oligo(*p*-phenylenevinylene)s (OPVs).[14-17] Apart from these studies, there are several reports related to the liquid crystalline behavior,[18] solid-state packing[19] and self-assembly[20] of phenylenevinylene derivatives. The main objective of these studies is the control of the optical and related electronic properties as a function of the self-assembly to form supramolecular architectures of nanometer dimensions. Combining the advantages of H-bond directed supramolecular interactions with the optical properties of PVs could provide an elegant way of creating functional nanoscopic as well as macroscopic assemblies of desired properties.

Recently, Meijer and coworkers have made significant contributions to the understanding of the supramolecular organization of OPVs.[20b-g] They have

synthesized OPVs, which are functionalized with uriedo-*s*-triazine quadruple H-bonding units.[20c] These OPV derivatives are further equipped with tridodecyloxy end groups and enantiomerically pure (*S*)-2-methylbutoxy side chains. In chloroform, monofunctional OPV derivatives (**1**) dimerizes through quadruple H-bonding motifs with an association constant of K_{dim} = (2.1 ± 0.3) x 10^4 $Lmol^{-1}$. In nonpolar solvents like dodecane, the H-bonded dimers self-assemble into left-handed helical stacks (Figure 2.1). Temperature and concentration dependent measurements have shown that the stability of the self-assembled stacks increases with conjugation length, due to favorable π-π interactions.[20e] Most importantly, the self-assembled fibers could be successfully transferred on to solid surfaces, which is essential for the fabrication of future supramolecular electronic devices. Detailed AFM studies have shown that, single fibers could be transferred only to inert substrates like graphite and silicium oxide. In the case of repulsive surfaces (mica and glass) clustering of the stacks occurs, while at attractive surfaces (gold) the stacks are destroyed. This systematic AFM study shows the importance of inert substances for the fabrication of nanodevices. However, the bifunctional OPV derivative (**2**) could only form less organized frustrated polymeric stacks, due to the competition between favorable π-π interactions and restricted conformational freedom, due to the hexyl spacer (Figure 2.2). The length of these supramolecular polymers and its chirality could be controlled by the addition of the monofunctional OPV derivatives as chain stoppers.

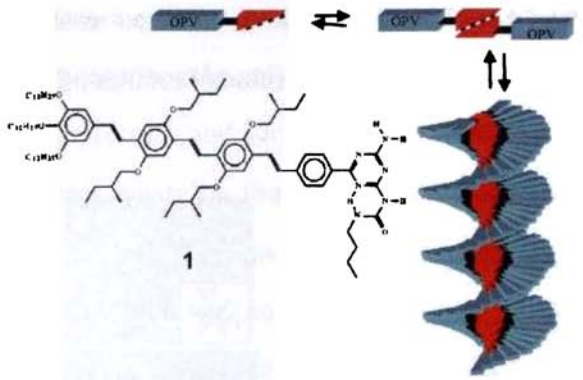

Figure 2.1. Schematic representation of the self-organization of **1** into helical stacks.

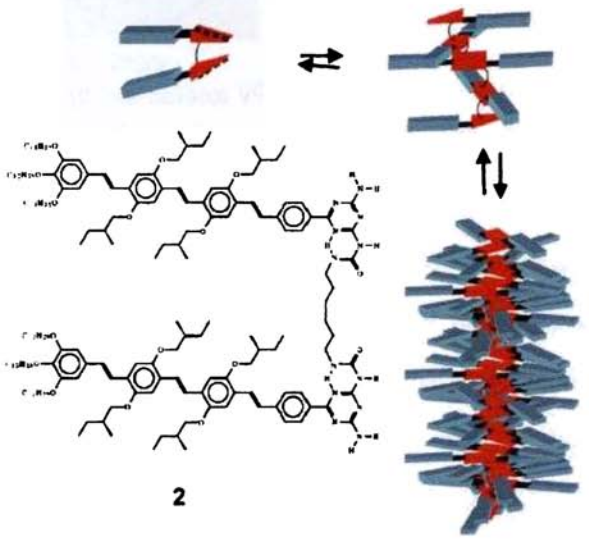

Figure 2.2. Schematic representation of the self-organization of **2** into frustrated polymeric stacks.

Recently, the self-assembly of diaminotriazine substituted OPV molecules (**3-4**) to hexameric π-conjugated rosette structures and the subsequent growth into chiral tubular objects have been reported.[20f] STM images have shown that chiral hexameric rosette structures lying flat on the surface with the diaminotriazine moieties pointing towards the center forming hydrogen bonds (Figure 2.3a). AFM and CD studies have shown that in nonpolar solvents these hexameric rosette assemblies stack on each

other using π-π interactions to form tubular self-assemblies as shown in Figure 2.3b. Detailed SANS experiments revealed the formation of tubules of 7 nm in diameter and 180 nm in length.

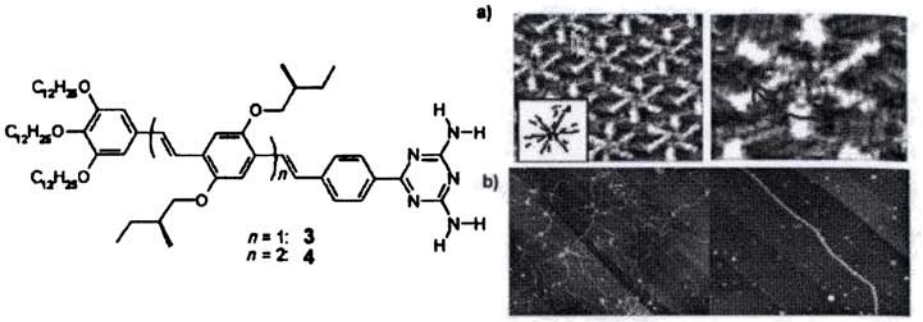

Figure 2.3. a) STM images of the chiral hexameric OPV rosettes and b) AFM images of the OPV rosette nanotubes derived from the self-assembly of **3.**

An important aspect of supramolecular assembly of certain organic molecules is their ability to entrap a large volume of the solvent within the self-assembly to form a non-flowing soft mass called 'gel'.[21] Though a large number of non-chromophore and chromophore containing organogels are known, extended π-conjugated systems are the least exploited class of molecules in gel chemistry.[22] An early report on gelation of π-conjugated systems pertains to urea functionalized oligo(thiophene)s (**5**) (Figure 2.4).

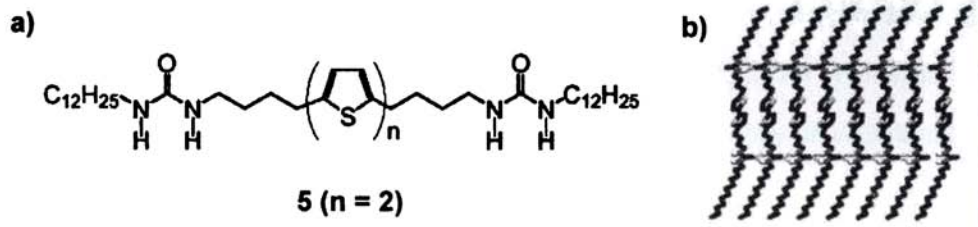

Figure 2.4. a) Bisurea-appended thiophene oligomer **5** and b) possible supramolecular arrangement of **5** through urea-urea H-bonding interactions.

Though there are a number of reports on the self-assembly of OPV based systems, none of them describes the gelation properties of these molecules. Therefore, it is of considerable importance and curiosity to design OPVs which self-assemble to form organogels, to investigate on the properties and morphology of the resultant supramolecular assemblies. In the present chapter, we describe the detailed studies of the synthesis, gelation behavior and morphological analysis of OPV based organogelators which belong to a new class of supramolecular materials.

2.2. Results and Discussion

2.2.1. The Design Strategy

The actual cause of gelation of organic molecules is still a matter of debate though it is known that supramolecular noncovalent organization to form entangled structures, which are different from the simple molecular aggregates, are mainly responsible. Therefore, gelation can be considered as a delicate balance between crystallization, precipitation and solubility of noncovalently interacting molecules in a suitable solvent. Keeping this view in mind, we set to design π-conjugated molecules in such a way that they satisfy most of the conditions necessary for the formation of an extended self-assembly required for gelation (Figure 2.5). In this design, an appropriate π-conjugated system is equipped with two weak H-bonding end groups and sufficient number of long hydrocarbon side chains. Thus, a variety of tailor-made OPV derivatives were synthesized, the structures of which are shown in Figure 2.6. The presence of the two hydroxymethyl end groups will allow the molecules to self-assemble via weak nondirectional 2-point H-bonding, which will give sufficient freedom to the molecules to organize themselves. The presence of long hydrocarbon side chains facilitates the packing of the molecules, assisted by the weak van der

Waals interaction. These interactions will be reinforced by π-stacking of the rigid aromatic OPV backbone. A cooperative interaction of all these forces will eventually lead the molecules to form ordered assembly, resulting in the formation of entangled nanoscopic structures which are able to hold large amount of appropriate solvent molecules within the self-assembly, thereby forming a gel.

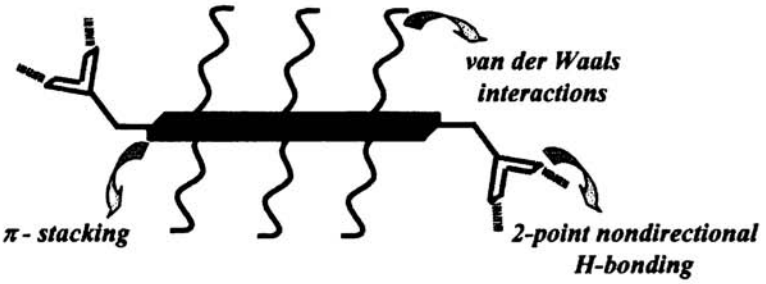

Figure 2.5. Design features of the OPV based organogelators showing various noncovalent interactions.

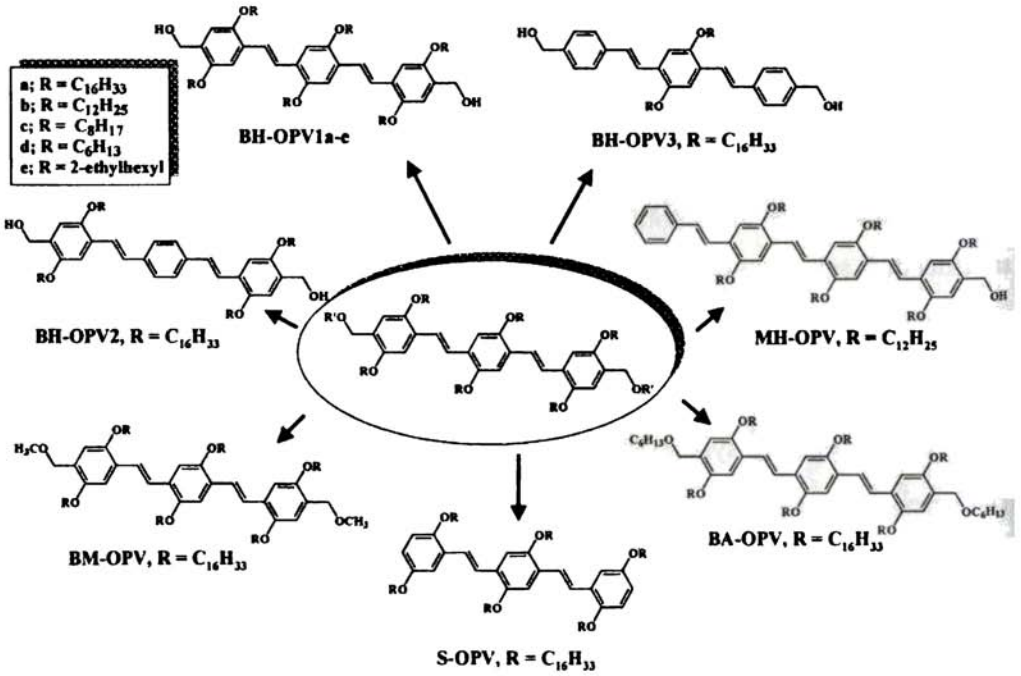

Figure 2.6. Library of OPV organogelators under investigation.

2.2.2. Synthesis of OPVs

The bisalcohols, **BH-OPV1a-e**, **BH-OPV2** and **BH-OPV3** were synthesized by the controlled Wittig reaction of the appropriate bisaldehydes and bisphosphonium salts, followed by the reduction of the resulted OPV bisaldehydes with $NaBH_4$ (Scheme 2.1). Controlled Wittig-Horner reaction between the bisaldehyde (**6**) and the benzyl phosphonate (**7**) afforded the OPV monoaldehyde **8** in 35% yield, which in turn was reduced to **MH-OPV** by $NaBH_4$ in 95% yield (Scheme 2.1). Synthesis of **S-OPV** was based on a literature procedure (90% yield).[23] Preparation of the hydroxyl protected derivatives **BM-OPV** and **BA-OPV** were accomplished by the alkylation of **BH-OPV1a** with the corresponding alkyl halides in 95% and 60% yields, respectively (Scheme 2.2). All the OPV derivatives under investigation were characterized by spectral analyses. The all-*trans* configurations of the OPVs are confirmed by the *J* values (16.5 Hz) of the vinylic protons in their respective ^1H NMR spectra.

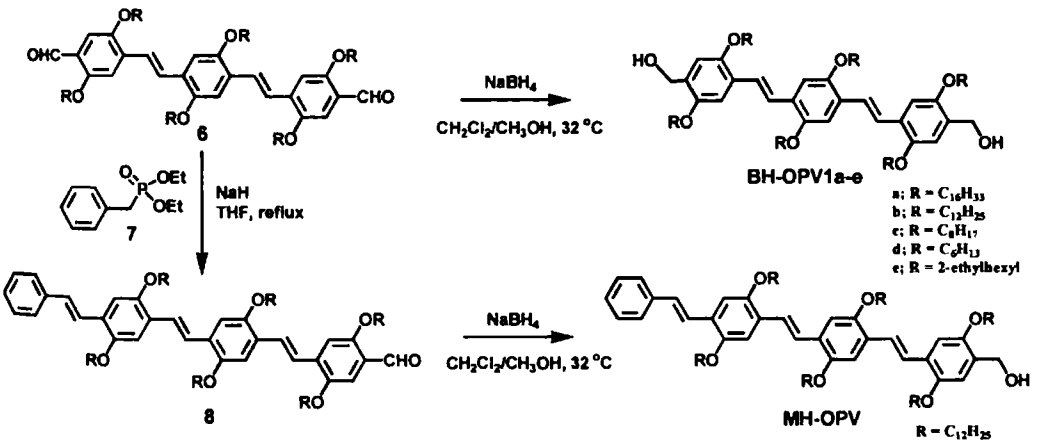

Scheme 2.1. Synthesis of the mono- and bishydroxymethyl OPV derivatives.

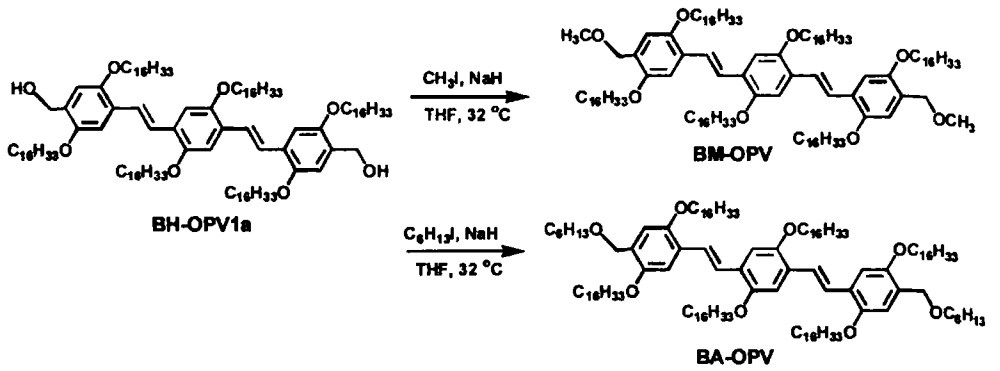

Scheme 2.2. Synthesis of the hydroxyl protected OPVs.

2.2.3. Gelation Studies

Gelation behavior of the newly synthesized OPV derivatives was examined in a range of organic solvents by dissolving different amounts in a specific volume (1 mL) of the solvent under heating and cooling. It has been observed that either gelation, precipitation or a clear solution could be obtained depending upon the solvent and structure of the compound. Gel formation could be detected readily by the failure of the resultant mass to flow when the vial was tilted upside down and also from the soft and transparent appearance. The results of the gelation experiments are presented in Table 2.1, which reveal that the bishydroxy compounds **BH-OPV1a-c**, having long linear hydrocarbon chains are efficient gelators of nonpolar hydrocarbon solvents such as hexane, decane, dodecane, cyclohexane, benzene and toluene. They could also gelate hydrocarbon fuels such as diesel and petrol. The maximum gelation efficiency is obtained for **BH-OPV1a** with a hexadecyloxy side chains and the critical gelator concentrations (CGC) in dodecane, decane and cyclohexane were 0.8, 0.9 and 1.1 mM, respectively. This means that **BH-OPV1a** can entrap approximately 10,000 molecules of dodecane per gelator molecules and falls under the category of supergelators.[24]

Table 2.1. Critical gelator concentrations (mM)[a] of the OPV derived organogelators **BH-OPV1a-e, BH-OPV2** and **BH-OPV3** in different solvents

Gelator	Dodecane	Decane	Cyclohexane	Hexane	Toluene	Benzene	Chloroform
BH-OPV1a	0.8	0.9	1.1	1.7	2.8	3.0	5.6
	(s,tr)	(s,tr)	(s,tr)	(s,tr)	(s, tr)	(s, tr)	(th,o)
BH-OPV1b	1.0	1.1	1.4	2.1	4.2	4.1	17.3
	(s,tr)	(s,tr)	(s,tr)	(s,tr)	(s,tr)	(s,tr)	(th,o)
BH-OPV1c	4.5 (PG)	4.8 (PG)	6.3	I	12.6	11.6	S
			(s,tr)		(s,tr)	(s,tr)	
BH-OPV1d	I	I	10.6	I	15.9	16.0	S
			(s,tr)		(s,tr)	(s,tr)	
BH-OPV1e	S	S	S	S	S	S	S
BH-OPV2	P	P	15.4	11.5	23.0	P	P
			(s,o)	(s,o)	(s,o)		
BH-OPV3	P	P	P	I	P	P	S

[a]CGC = Critical gelator concentration, which is the minimum concentration required for the formation of a stable gel at room temperature. In parenthesis, s = stable, tr = transparent, th = thixotropic, o = opaque. S = soluble, I = insoluble, P = precipitation, PG = partial gelation at room temperature.

The gelation was selective for hydrocarbon solvents even from an emulsion with water. Photographs of the gels prepared under different conditions are shown in Figure 2.7. The gels obtained were transparent and stable so that the glass vial could be turned upside down without damaging the structure (Figures 2.7b and 2.7c). This is clear from Figure 2.7e where a gel of **BH-OPV1a** in diesel could hold an equal amount of water without falling (water is stained to distinguish from the diesel). The gelation ability of **BH-OPV1d**, carrying hexyloxy side chains is relatively poor (CGC is 10 mM in cyclohexane) whereas **BH-OPV1e** having branched 2-ethylhexyloxy side chain gave a homogeneous solution in all the solvents investigated. Nature of the solvents has considerable influence on the gelation behavior of **BH-OPV1a-d**

(Table 2.1). For example, the CGC of **BH-OPV1a** in chloroform is 5.6 mM and the resulting gels are unstable upon shaking (thixotropic). However, in a slightly less polar solvent like toluene, **BH-OPV1a** forms a reasonably stable gel with a CGC of 2.8 mM. Another factor, which influences the gelation ability of OPV derivatives, is the number of the hydrocarbon side chains present on the conjugated backbone (Table 2.1). For example, the CGC of **BH-OPV2** having side chains only at the terminal phenyl rings is 15.6 mM in cyclohexane resulting in a turbid gel, whereas **BH-OPV3**, with side chains only at the central phenyl ring, does not gelate any of the solvents investigated. Hence, it is clear that for an OPV derivative to form a gel, it is necessary to maintain a balance between crystallization, solubility and precipitation where the length and position of the hydrocarbon side chains play an important role.

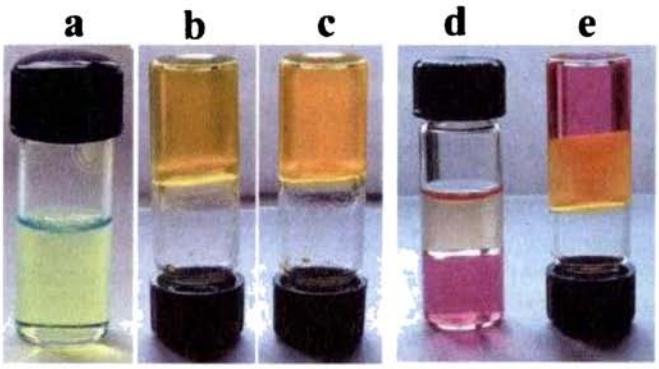

Figure 2.7. **BH-OPV1a** in decane a) before and b) after gelation. c) A toluene gel of **BH-OPV1a**. d) and e) **BH-OPV1a** in a mixture of water and diesel before and after gelation respectively. Water is stained with a dye to distinguish the two layers.

In order to investigate on the role of H-bond assisted π-stacking in the gelation process, we extended our studies to other OPV derivatives where the H-bonding groups are either protected or replaced by other functional groups. The results of the gelation studies of **BM-OPV**, **BA-OPV**, **S-OPV** and **MH-OPV** are summarized in Table 2.2. Interestingly, in the case of **BM-OPV** and **BA-OPV**, gelation occurred only

at high concentrations when compared to the corresponding bisalcohol derivative **BH-OPV1a**. The critical gelator concentration of **BM-OPV** is 3.3 mM in cyclohexane, and the resulting gels are thixotropic. **BM-OPV** failed to fully gelate solvents such as chloroform and THF, which may be due to the absence of H-bond donor groups that are necessary for the positional locking of the molecules within the π-stacked assembly. Compound **BA-OPV**, having the hexyloxy end groups, could gelate only nonpolar solvents such as dodecane and decane. In the case of **MH-OPV** with only one hydroxymethyl group, gel formation was observed in nonpolar solvents though it is not as efficient as in the case of **BH-OPV1a** and **BH-OPV1b**. However, **S-OPV**, without any end functional groups, could not gelate any of the solvents investigated, instead aggregate formation was observed which are not able to trap the solvents. These studies indicate the crucial role of H-bonding in assisting the weak interactions such as π-stacking and van der Waals associations in the process of self-assembly and gelation.

Table 2.2. Critical gelator concentrations (mM) of the OPV derived organogelators **S-OPV**, **BM-OPV**, **BA-OPV** and **MH-OPV** in different solvents

Gelator	Dodecane	Decane	Cyclohexane	Hexane	Toluene	Benzene	Chloroform
S-OPV	P	P	P	P	P	P	P
BM-OPV	1.6	1.8	3.3	4.4	7.2	6.8	16.5
	(th,tr)	(th,tr)	(th,tr)	(th,tr)	(th,tr)	(th,tr)	PG
BA-OPV	4.9	5.2	10.4	10.4	S	S	S
	(th,tr)	(th,tr)	(th,o)	(th,o)			
MH-OPV	1.4	1.5	2.3	4.6	4.6	4.2	S
	(s,tr)	(s,tr)	(s,tr)	(th,o)	(s,tr)	(s,tr)	

In parenthesis, s = stable, tr = transparent, th = thixotropic, o = opaque. S = soluble, I = insoluble, P = precipitation, PG = partial gelation at room temperature.

2.2.4. Thermotropic Behavior

The thermotropic behavior of the gels formed by **BH-OPV1a-c**, **BM-OPV** and **MH-OPV** were investigated by dropping ball method[25] and by differential scanning calorimetry to understand the impact of the structure of the OPVs and the nature of the solvents on the gel stability. In the case of **BH-OPV1a-c**, a regular increase in the gel melting temperature (T_{gel}) with increasing concentration of the gelator molecules was observed (Figure 2.8). Phase diagrams of the gels of **BH-OPV1a-c** in cyclohexane were obtained by plotting the T_{gel} at different concentrations (Figure 2.8a). The phase above each curve is a solution, whereas the phase below is a gel. The increase in T_{gel} with increase in alkyl chain length shows increased stability of the gels, which could be due to the solvation assisted intermolecular packing of the long alkyl chains. Phase diagrams of **BH-OPV1a** gels from dodecane, cyclohexane, toluene and chloroform are shown in Figure 2.8b, which indicate that **BH-OPV1a** form strong gels in dodecane and cyclohexane, which showed higher melting temperatures even at very low concentrations. This observation is in accordance with the gelation studies presented in Table 2.1. Figure 2.8c shows the plots of the gel melting temperatures of the cyclohexane gels of **BH-OPV1a**, **BM-OPV** and **MH-OPV**, at different concentrations. These plots show remarkable stability for **BH-OPV1a** gel, due to H-bonding between the hydroxymethyl groups. For example, a cyclohexane gel of the methoxy derivative **BM-OPV** at a concentration of 10 $mgmL^{-1}$ melts at 47 °C, which is 15 °C lower than the corresponding **BH-OPV1a** gel. It is also clear that the gels of the monohydroxy derivative **MH-OPV** is more stable than that of the hydroxyl protected **BM-OPV** gel, however less stable than the **BH-OPV1a** gel. These results clearly indicate that the stability of the gels strongly depends upon the length and position of the side chains, polarity of the solvents and the presence of H-bonding

groups. Thermodynamic parameters calculated from the plots of the T_{gel} *vs.* concentration using equation 1, which is derived from the Schrader's relation,[26] showed ΔH values of 258 $kJmol^{-1}$, 196.32 $kJmol^{-1}$ and 110.4 $kJmol^{-1}$ for the cyclohexane gels of **BH-OPV1a**, **BH-OPV1b** and **BH-OPV1c**, respectively.

$$\ln C = -\frac{\Delta H}{R}\frac{1}{T_{gel}} + \text{constant} \qquad \ldots\ldots\ (1)$$

In this equation C, ΔH, T_{gel} and R are molar concentration, melting enthalpy, gel melting temperature and gas constant, respectively. The ΔH values of **BH-OPV1a** in cyclohexane, toluene and in chloroform were 258 $kJmol^{-1}$, 143 $kJmol^{-1}$ and 114 $kJmol^{-1}$, respectively. These values show a maximum stability for **BH-OPV1a** in cyclohexane. Though this equation is often used to determine the ΔH values in polymeric and low molecular mass gels,[26] ambiguity exists in the validity of equation 1 in the case of the sol-gel process of small molecules. Therefore, we have presented these values only for the purpose of comparison.

Differential Scanning Calorimetric (DSC) studies of the methylcyclohexane gels of **BH-OPV1a-c**, **BM-OPV** and **MH-OPV** are shown in Figure 2.9. These studies showed a similar trend in the stability of the gels as observed by the dropping ball methods. A broad exothermic transition was observed during the heating process, which is characteristic of a noncovalently associated supramolecular assembly. In the case of **BH-OPV1a-c**, the transition temperatures of the heating exotherms and the cooling endotherms increase in the order **BH-OPV1a > BH-OPV1b > BH-OPV1c** (Figure 2.9a). As in the case of the dropping ball experiment, the DSC analysis showed increased stability for the gels in hydrocarbon solvents of higher chain length. For example, among the three solvents used, the dodecane gel showed maximum

thermal stability (Figure 2.9b). The role of H-bonding is also evident from the DSC thermograms where **BH-OPV1a** showed a melting temperature of 63.5 °C which is 12.5 °C and 14 °C higher than that of the **MH-OPV** and **BM-OPV**, respectively (Figure 2.9c). In all these cases, it is interesting to note that the cooling transitions are sharper and occurred approximately 15-16 °C lower than the heating transition curves, indicating a better cooperativity in the formation of the self-assembly in the cooling process, leading to the gelation.

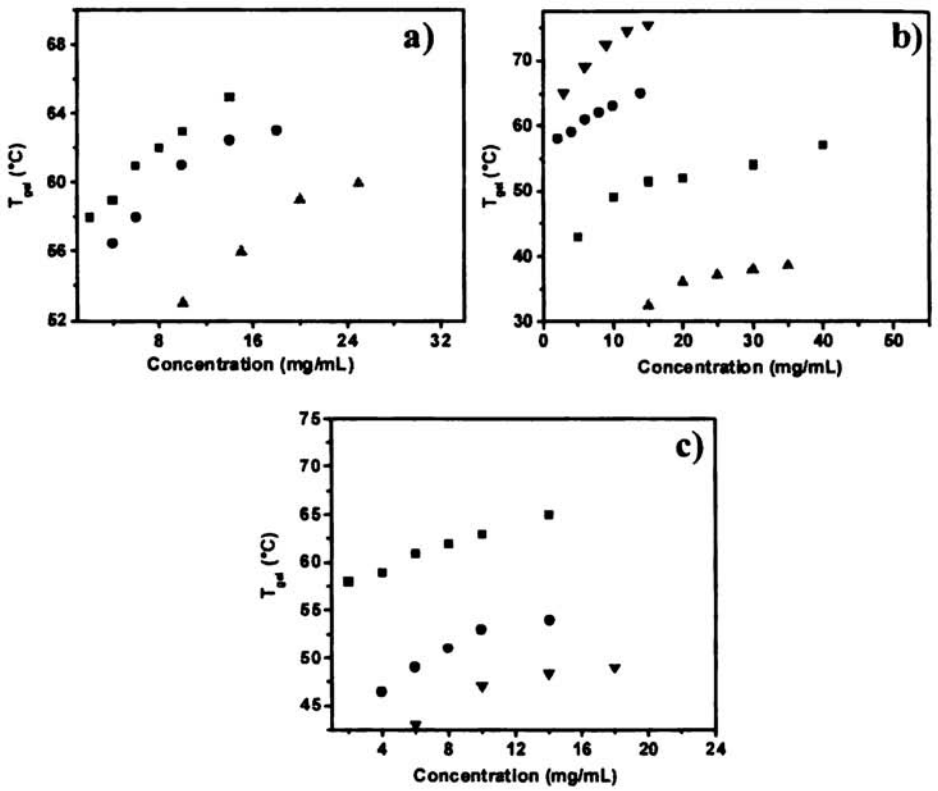

Figure 2.8. Binary phase diagrams of the OPV organogels showing the effect of side chains, solvents and H-bonding on stability. a) cyclohexane gels of **BH-OPV1a** (■), **BH-OPV1b** (•) and **BH-OPV1c** (▲), b) **BH-OPV1a** gels in dodecane (▼), in cyclohexane (•), in toluene (■) and in chloroform (▲) and c) cyclohexane gels of **BH-OPV1a** (■), **MH-OPV** (•) and **BM-OPV** (▼).

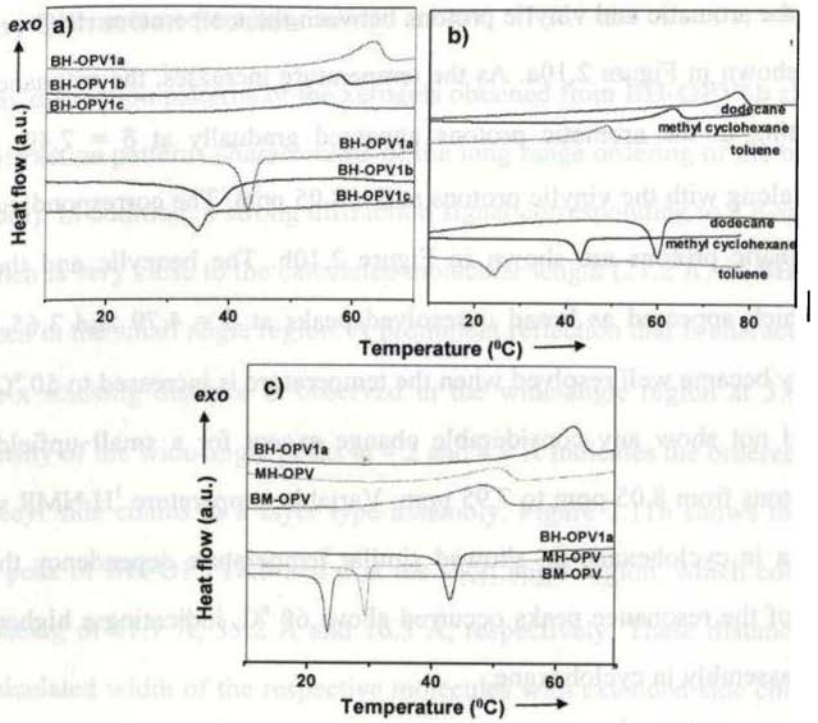

Figure 2.9. DSC thermograms of a) **BH-OPV1a-c** in methylcyclohexane, b) **BH-OPV1a** in different solvents and c) **BH-OPV1a**, **MH-OPV** and **BM-OPV** in methylcyclohexane (8 mgmL^{-1}). The heating and cooling rates are 5 °C/min in all experiments.

2.2.5. Variable Temperature ^{1}H NMR Studies

The ^{1}H NMR spectra of **BH-OPV1a-b** in $CDCl_3$ and benzene-d_6 (5 mM) showed distinctly different features when recorded at room temperature. For example, the ^{1}H NMR spectrum of **BH-OPV1a** in $CDCl_3$ gave well resolved resonance signals in accordance with the structure of the molecule, whereas in benzene-d_6, the spectrum did not show any of the characteristic resonance signals corresponding to the aromatic and vinylic protons. These observations point towards the strong intermolecular interaction due to the aggregation of the OPV units through noncovalent self-assembly of the molecules in benzene-d_6. In such cases, the ^{1}H NMR signals are too broad and weak to be distinguished due to the long correlation time. Changes in the resonance

signals of the aromatic and vinylic protons between the temperature ranges of 10 °C - 70 °C are shown in Figure 2.10a. As the temperature increases, the resonance signals corresponding to the aromatic protons appeared gradually at δ = 7.49, 7.37 and 7.05 ppm, along with the vinylic protons at δ = 8.05 ppm. The corresponding changes to the aliphatic protons are shown in Figure 2.10b. The benzylic and the $-OCH_2$ protons which appeared as broad unresolved peaks at δ = 4.79 and 3.65-3.9 ppm, respectively became well resolved when the temperature is increased to 50 °C. Further heating did not show any considerable change except for a small upfield shift of vinylic protons from 8.05 ppm to 7.95 ppm. Variable temperature ^1H NMR spectra of **BH-OPV1a** in cyclohexane-d_{12} showed similar temperature dependency though the resolution of the resonance peaks occurred above 60 °C, indicating a higher stability of the self-assembly in cyclohexane.

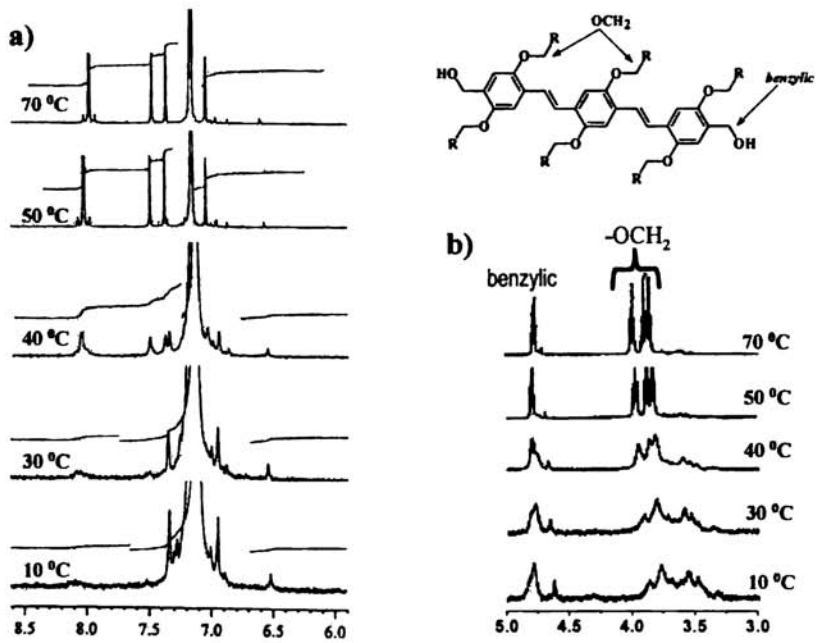

Figure 2.10. Temperature dependent ^1H NMR spectra of **BH-OPV1a** in benzene-d_6 (5 mM) on the heating cycle.

2.2.6. X-ray Diffraction Studies

X-ray diffraction patterns of the xerogels obtained from **BH-OPV1b** show well resolved diffraction patterns characteristic of the long range ordering of the molecules (Figure 2.11a). In addition, a strong diffraction signal corresponding to a d-spacing of 23.2 Å, which is very close to the calculated molecular length (21.2 Å) of **BH-OPV1b** could be seen in the small angle region. A prominent reflection that is characteristic of a typical π-π stacking distance is observed in the wide-angle region at 3.8 Å. The strong intensity of the wide-angle peaks at 4.2 and 4.9 Å indicates the ordered packing of the dodecyl side chains in a layer type assembly. Figure 2.11b shows the intense diffraction peak of **BH-OPV1a,b** and **d** at the short angle region, which corresponds to the d-spacing of 41.7 Å, 35.2 Å and 16.5 Å, respectively. These distances match with the calculated width of the respective molecules with extended side chains. This is an indication of the lamellar packing distance that should vary with the length of the side chains. This argument is clear from the comparison of the observed d-spacing. Based on these data, it appears that the xerogel of **BH-OPV1b** most likely consists of a lamellar type packing through a cooperative H-bonding, π-stacking and van der Waals interactions as shown in Figure 2.12. In the lamellar packing, **BH-OPV1b** adopts a planar structure, in which the aryl units are coplanar and the alkyl side chains are laterally extended with a complete stretching of the side chains within the same plane of the conjugated backbone. The diffraction patterns of **BM-OPV** carrying hexadecyl side chains, where the H-bonding of the two hydroxymethyl groups were blocked, showed relatively broad reflections (Figure 2.11a). The absence of higher order reflections and the presence of broad reflections in the wide-angle region point toward a low degree of ordering in this case. The wide-angle region showed broad diffraction at 3.8 and 4.8 Å corresponding to a weak π-π stacking. These observations

are in agreement with the observed gelation behavior of **BH-OPV1a** and **BM-OPV** as indicated in Table 2.1 and Table 2.2.

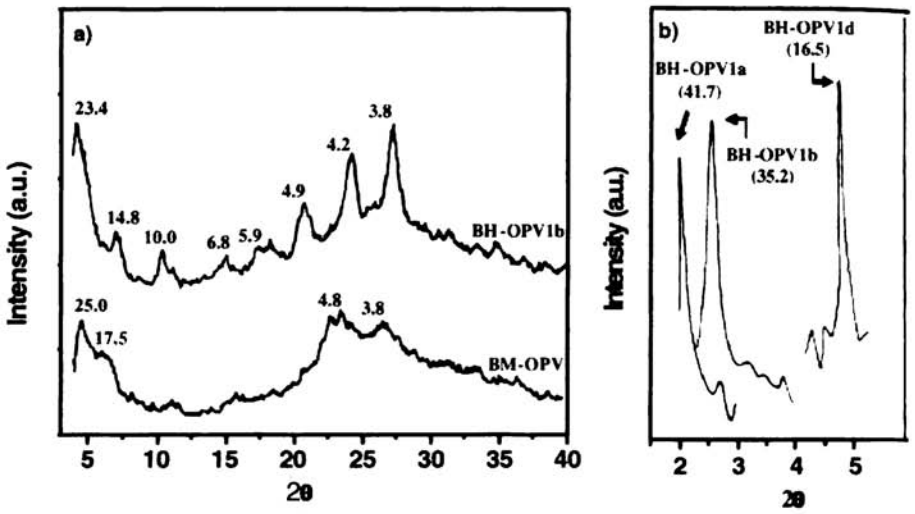

Figure 2.11. a) X-ray diffraction patterns (room temperature) of the xerogels of **BH-OPV1b** and **BM-OPV**. b) Diffraction patterns in the short angle region corresponding to the lamellar packing distance of **BH-OPV1a**, **BH-OPV1b** and **BH-OPV1d**.

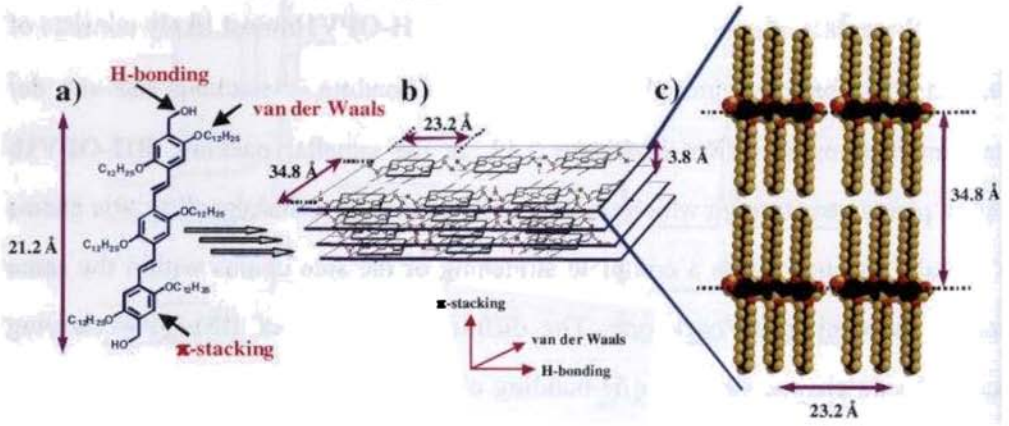

Figure 2.12. Schematic view of the lamellar packing of **BH-OPV1b** in the gel state. a) Structure of **BH-OPV1b**, b) side view and c) molecular model of the top view of the lamellar packing.

2.2.7. Optical Polarizing Microscopy

When viewed through crossed polarizers, the neat bishydroxy derivatives **BH-OPV1a-c** showed birefringent textures below the isotropic melting temperature. For example, when the neat **BH-OPV1a** is allowed to cool from the isotropic melt, spontaneous growth of long birefringent tape like textures could be observed at 114 °C as shown in Figures 2.13a and b. Presence of these textures indicates the linear growth of anisotropic H-bonded assemblies of the OPV molecules. Interestingly, it is observed that the length of the hydrocarbon side chains strongly influences the evolution of the textures. For example, the OPM picture of **BH-OPV1d** with hexyl side chains showed characteristic of crystalline textures when compared to the long fibrous textures of **BH-OPV1a** (Figure 2.13c). The role of H-bonded supramolecular assemblies in the growth of the tape-like structures is justified by comparing the OPM textures of the neat **S-OPV** (Figure 2.13d) with that of the **BH-OPV1a** (Figure 2.13a). Cooled melt of **S-OPV** at 106 °C showed the presence of crystallites due to the lack of H-bond assisted self-assembly. The birefringent tape-like textures obtained for the neat **BH-OPV1a** is very similar to that reported in the case of some helicenes and such textures are rare in the literature.[27]

Figures 2.14a and 2.14b represent the optical micrographs of a **BH-OPV1b** gel in decane under different magnification, which are obtained under a moderate cooling rate of 5 °Cmin^{-1}. When cooled from the isotropic solution, birefringent fibrous aggregates emanating from random nucleation centers could be seen. The individual strands are difficult to discern within the bundles of fibers. The strong birefringence of the fibers indicates a well-defined molecular arrangement during the gelation as noticed in the case of the neat gelators, which is the result of the three-dimensional

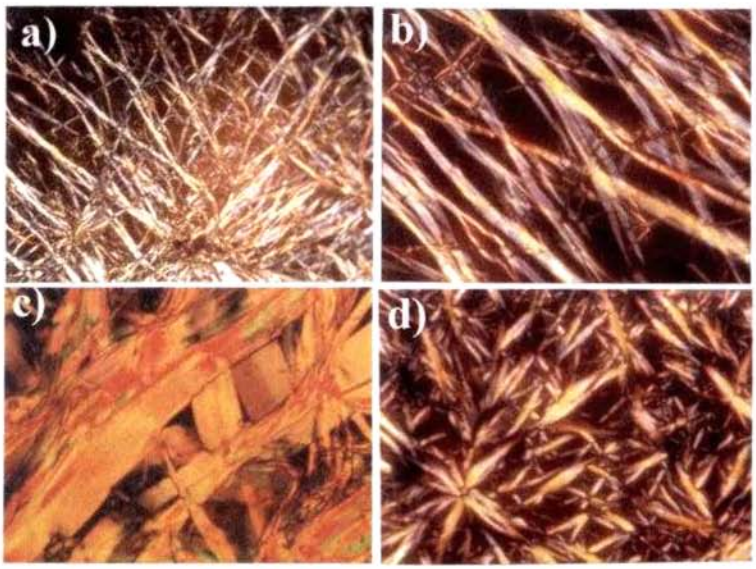

Figure 2.13. Optical polarizing microscopic image of neat OPVs. a) **BH-OPV1a** (100 x), b) **BH-OPV1a** (400 x), c) **BH-OPV1d** (400 x) and d) **S-OPV** (400 x), when cooled from the corresponding isotropic melt.

organization of the ordered aggregates. When the same experiment was performed at a very low cooling rate of 0.5 °Cmin^{-1}, slow growth of elongated, birefringent fibers were observed which is evident from Figures 2.14c and 2.14d, indicating that the cooling rate is critical in the directional growth of the fibrous assembly. Fast cooling induces large number of nucleation sites leading to the radial growth of aggregates whereas slow cooling produces fewer nucleation centers leading to the directional linear growth of long fibers. Similar textures were observed for the decane gels of other bisalcohols, although the aggregate size varies with the structure and concentration of the OPVs. Decane gels of **MH-OPV** also showed birefringent fibers, even though they are short, thin and less directional (Figure 2.14e). Interestingly, the decane gels of the methyl ether derivative **BM-OPV** upon slow cooling form microcrystallites from several nucleation centers as shown in Figure 2.14f which

failed to form long fibrous aggregates in contrast to **BH-OPV1b**. The difference in the morphology of the structures obtained from the gels of **BH-OPV1b** and **BM-OPV** reveals that hydroxymethyl groups are essential for the formation of the extended supramolecular assemblies with long range ordering, leading to fiber growth and efficient gelation.

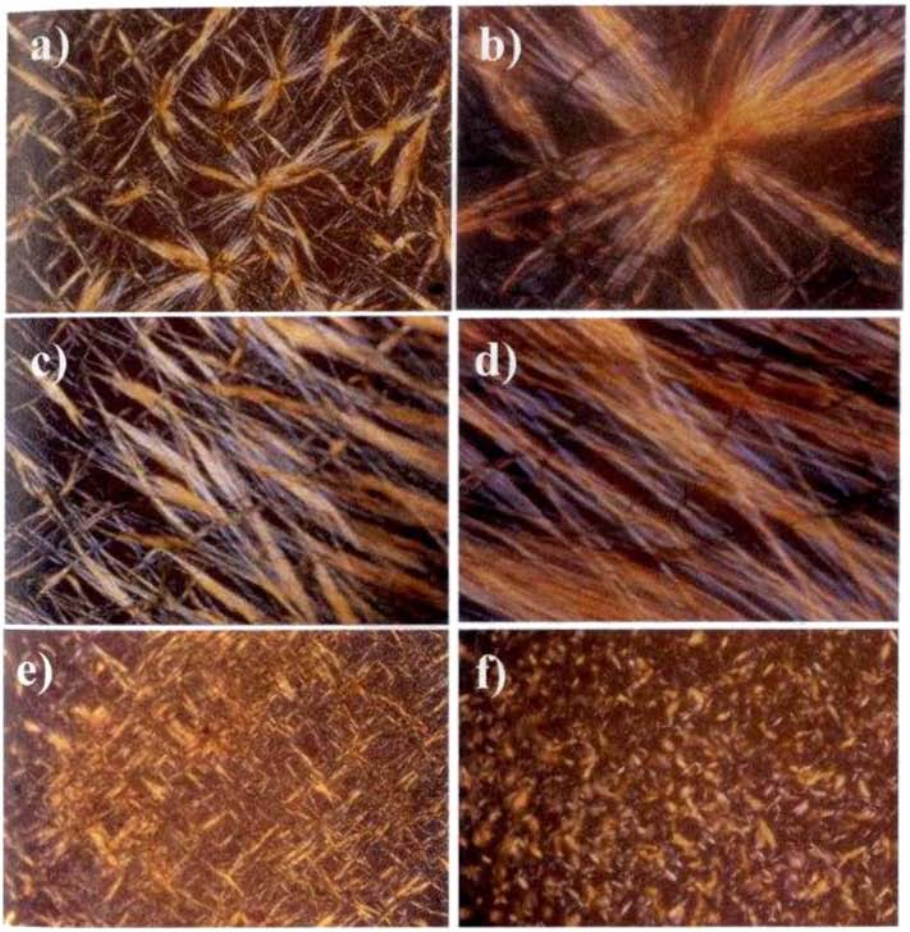

Figure 2.14. Optical micrographs of the decane gels of **BH-OPV1b** under moderate cooling a) 100x and b) 400x and by slow cooling c) 100x and d) 400x. Optical micrographs of the decane gels of e) **MH-OPV** and f) **BM-OPV** observed under moderate cooling (100 x).

2.2.8. Electron Microscopic and Atomic Force Microscopic Studies

Representative Scanning Electron Microscopic (SEM) images of the dried **BH-OPV1a** gels from toluene are shown in Figures 2.15a and b. These micrographs show the presence of entangled network of twisted supramolecular tapes formed by the self-assembly of **BH-OPV1a**. Careful analysis showed that these twisted tapes are approximately 50-100 nm in width and several micrometers in length. SEM pictures indicate that the fibers split and fuse with other fiber bundles, leading to the formation of junction zones, which stabilize the three-dimensional entangled network structures. Figures 2.15c and d are the SEM pictures of the dried gels of **BH-OPV1a** from decane. In this case the fibers are more dense, entangled and twisted. A magnified image indicates that entangled textures have the morphology of twisted tapes. The width of the tapes obtained from the decane gel is larger than that of the toluene gel, which indicates that intermolecular interaction is much stronger in the former case. In addition, the solvent-gelator interaction and as a result, the interactions between individual tapes are much strong in decane thereby leading to the formation of longer twisted tapes. Thus the observed gelation efficiency and the stability of the OPV gels are in agreement with the observed morphology.

Figure 2.16 represents the SEM pictures of a drop casted film of the bisalcohol **BH-OPV1a**, which showed fibrous morphology irrespective of the solvent used for the preparation of the film. In this case, large bundles of fibers with diameters varying from 0.2-0.8 μm are obtained which might be formed from small tapes and fibers. Figure 2.16b shows the SEM image of such a large bundle of fibers comprising of several coiled and entangled small fibers.

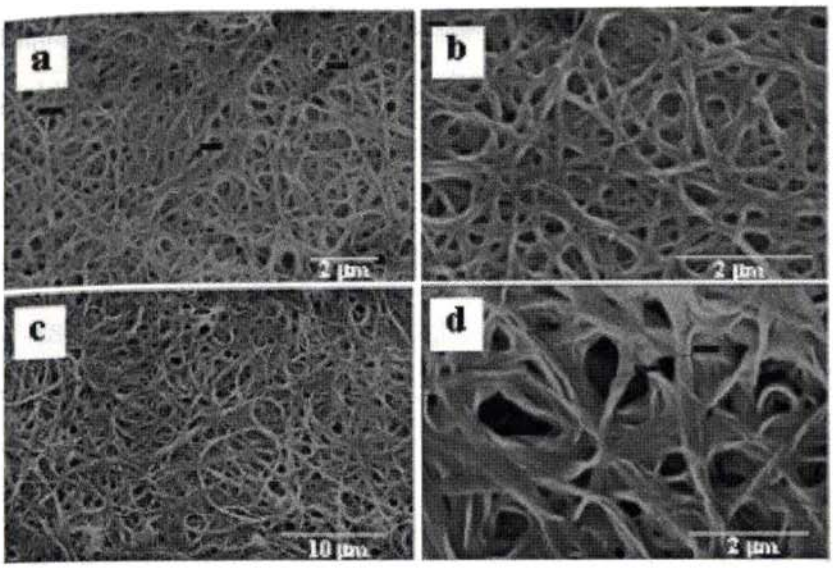

Figure 2.15. Scanning electron microscopic pictures of **BH-OPV1a** gels from toluene (a, b) and decane (c, d).

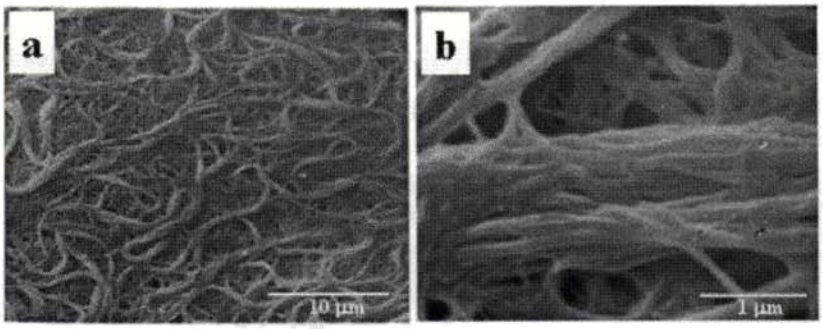

Figure 2.16. Scanning electron microscopic pictures of the **BH-OPV1a** drop casted from chloroform solution. a) magnification 5,000 and b) magnification 20, 000.

A comparative study of the SEM pictures of the different OPV derivatives provided insight to the role of the H-bonding functionality on the morphology of the self-assembled structures. In the case of the methyl ether derivative **BM-OPV**, short 'feather-like' aggregates are obtained which are in contrast to the several micrometers long fibers of the bisalcohol derivatives (Figure 2.17a). This observation is in agreement with the OPM studies of **BM-OPV**, which showed the presence of short

fibers resulting from the lack of cooperative interactions of an anisotropic growth. However, the gelation of **BM-OPV** in hydrocarbon solvents reveals that long fibrous morphology is not a crucial factor in the formation of organogels, particularly in long hydrocarbon solvents, although this may affect the efficiency of gelation and the stability of the gels to a considerable extent. A SEM picture of a film of **S-OPV** having no end substituents showed a completely different morphology, in which randomly clustered aggregates of 0.5-1.0 μm in size are present (Figure 2.17b). These aggregates failed to trap organic solvents and hence **S-OPV** was not able to form gels. Interestingly, the SEM picture of **BH-OPV1b** showed the formation of fibrous aggregates in chloroform-methanol solvent mixtures, the morphology of which is entirely different from the gel fibers obtained from toluene or cyclohexane (Figure 2.17c). The above observations indicate that H-bond formation between the terminal hydroxymethyl groups is a key factor for the efficient gelation of OPVs, leading to the formation of supramolecular textures of definite shape and size.

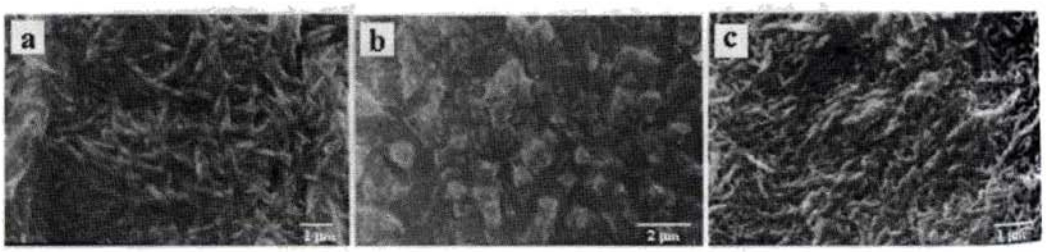

Figure 2.17. Scanning electron microscopic pictures of a) cyclohexane gel of **BM-OPV**, b) **S-OPV** as a casted film and c) aggregates of **BH-OPV1b** from chloroform-methanol solvent mixture.

The transmission electron micrograph (TEM) of **BH-OPV1a** from a dilute toluene solution provided more information on the morphology of the self-assembled textures. The TEM picture in this case shows the presence of isolated twisted tapes of 50-100 nm in diameter and several micrometers in length (Figure 2.18). In a

magnified image (Figure 2.18b) the presence of several thin fiber-like structures of 10-20 nm in diameter could also be seen in addition to the large twisted structures. The alternate dark and bright regions observed are the indication of the twisted morphology of the fibers.

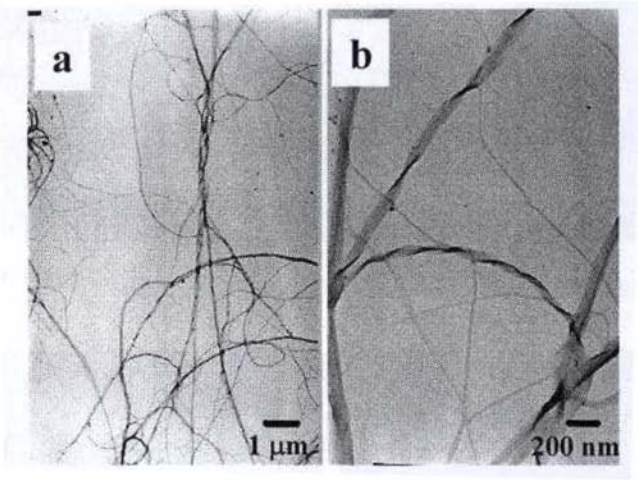

Figure 2.18. TEM pictures of the twisted fibers of **BH-OPV1a** gels from toluene.

AFM images of the **BH-OPV1a** self-assembly from toluene shows the presence of supramolecular tapes which consists of intertwined bundles of 50-150 nm in width and several micrometers in length (Figures 2.19a and 2.19b). It is also clear that the fiber bundles are built up from thinner fibers of 10-20 nm width. The width of the smallest fiber bundle that can be distinguished is 50-70 nm. Several isolated fibers could be observed under the AFM, when a dilute solution of the **BH-OPV1a** is deposited by drop casting. The morphology of such a single fiber is shown in Figure 2.19c. The presence of an array of the dark and bright areas of approximately 2 nm in width shows the molecular level lamellar organization of the individual OPV units. AFM analysis of the toluene gels **MH-OPV** (Figure 2.20a) and **BM-OPV**

(Figure 2.20b) showed the presence of fibrous and plate-like morphologies, respectively which are in agreement with the SEM results.

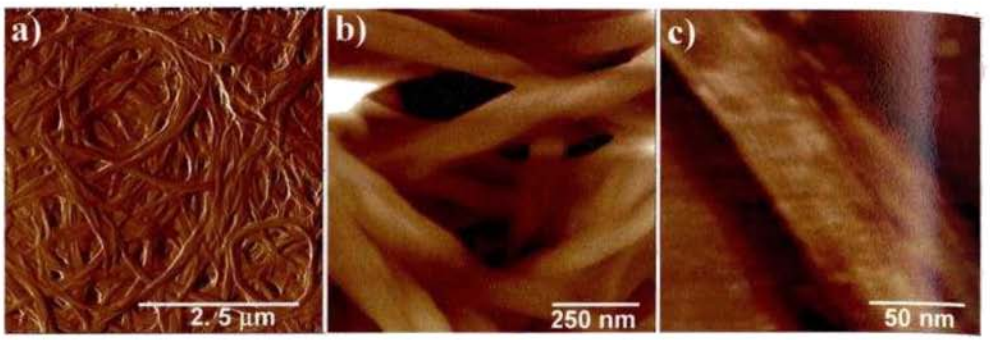

Figure 2.19. AFM of **BH-OPV1a** from toluene under different magnification.

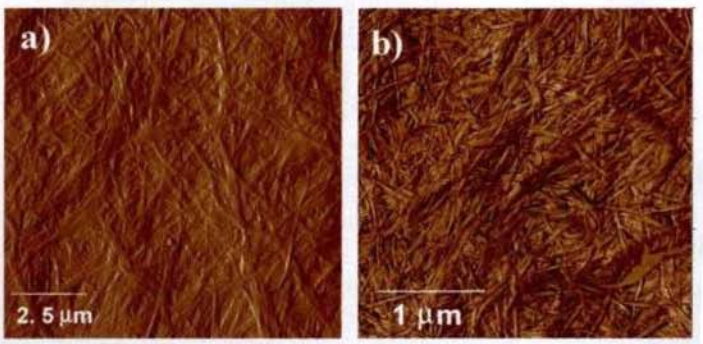

Figure 2.20. AFM of a) **MH-OPV** and b) **BM-OPV** from toluene.

Based on the results obtained by the ^{1}H NMR, DSC, X-ray, OPM, SEM, TEM and AFM studies, it is clear that the gelation of the **BH-OPV1a-d** is due to the cooperative supramolecular organization of the OPV units which is assisted by H-bonding, π-stacking and van der Waals interactions. The weak nondirectional H-bonding interaction of the hydroxymethyl end groups allows the formation of linear H-bonded assemblies as shown in Figure 2.12. These linear H-bonded assemblies will form supramolecular layer-like assemblies through the lamellar packing. The layered assemblies will be reinforced by π-stacking and van der Waals interactions leading to

the formation of supramolecular tapes. H-bonding may also be possible between the stacked layers which may act as reversible noncovalent crosslinking, resulting in a three-dimensional network. Further growth will result in the twisting of the tapes thereby forming elongated fibrous network leading to the immobilization of large volume of solvents within and between the networks, resulting in the gelation. The morphological analysis of the self-assemblies obtained from other OPV derivatives under investigation clearly established the role of the H-bonding motifs and the length and position of the side chains in the gelation process.

2.3. Conclusions

The OPV based organogelators reported here is a novel class of hydrocarbon gelators derived from rigid aromatic π-conjugated molecules. The presence of weak H-bonding hydroxymethyl groups and long hydrocarbon side chains are crucial for the gelation. Formation of strong gels even at a concentration below 1 mM shows that OPVs are efficient gelators of hydrocarbon solvents. The gelation properties and the morphology of the resultant supramolecular systems can be controlled by suitable modification of the OPV structures. Detailed morphological studies using OPM, SEM, TEM and AFM techniques revealed the formation of birefringent, entangled nanostructures of 50-100 nm in width and several micrometers in length. Evolution of the self-assembled fibrous network and the consequent gel formation is attributed to a cooperative interaction of H-bonding, π-stacking and van der Waals association of the individual OPV units leading to linear arrays of molecular stacks. The present study illustrates the importance of weak nondirectional H-bonding motifs for the design of strong gelators of hydrocarbon solvents. The different morphologies induced by the

gelation and the consequent reversible changes in the macroscopic properties endow these OPV organogels as a novel class of materials with tunable properties.

2.4. Experimental Section

2.4.1. Synthesis and Characterization

Unless otherwise stated, all starting materials and reagents were purchased from commercial suppliers and used without further purification. The solvents used were purified and dried by standard methods prior to use. Melting points were determined with a Mel-Temp-II melting point apparatus and are uncorrected. ^{1}H and ^{13}C NMR spectra were measured on a 300 MHz Bruker Avance DPX spectrometer using TMS as internal standard. FT-IR spectra were recorded on a Nicolet Impact 400D infrared spectrophotometer. Matrix-assisted laser desorption ionization time-of-flight (MALDI-TOF) mass spectra were obtained on a Perseptive Biosystems Voyager DE-Pro MALDI-TOF mass spectrometer. High-resolution mass spectra were recorded on a JEOL JM AX 505 HA mass spectrometer. The OPV bisaldehydes **6**, were prepared using a reported procedure.[28]

General Procedure for the Preparation of the Bisalcohols BH-OPV1a-e, BH-OPV2 and BH-OPV3. The appropriate precursor bisaldehyde[28] (**6**, 0.2 mmol) was dissolved in a mixture of methanol (10 mL) and dichloromethane (35 mL). To this solution, sodium borohydride (0.4 mmol) was added and stirred at room temperature for 45 minutes. The reaction mixture was poured into water and extracted with dichloromethane. The organic layer was dried and concentrated to give the corresponding alcohols. Yields, melting points, and spectral details of each product are given below.

BH-OPV1a. Yield: 92%. mp 113-114 °C. FT-IR (KBr) ν_{max} = 851, 965, 1011, 1068, 1202, 1259, 1341, 1388, 1418, 1460, 1511, 2845, 2918, 3381 cm^{-1}. ^1H NMR (300 MHz, $CDCl_3$, TMS): δ 0.85-0.87 (m, 18H, $-CH_3$), 1.25-1.83 (m, 168H, $-CH_2$), 2.3 (s, br., 2H, –OH), 3.97-4.04 (m, 12H, $-OCH_2$), 4.68 (s, 4H, $-CH_2OH$), 6.86 (s, 2H, aromatic), 7.12 (s, 2H, aromatic), 7.14 (s, 2H, aromatic), 7.45 (s, 4H, vinylic) ppm. ^{13}C NMR (75 MHz, $CDCl_3$) δ 14.10, 22.69, 26.21, 26.26, 28.70, 28.95, 29.37, 29.57, 29.58, 29.72, 31.93, 62.31, 68.57, 69.49, 69.70, 109.10, 110.73, 114.00, 122.69, 123.33, 127.25, 127.35, 129.29, 150.64, 151.05 ppm. MALDI-TOF MS (MW = 1785.12): *m/z* = 1785.55 $[M]^+$.

BH-OPV1b. Yield: 93%. mp 115-116 °C. FT-IR (KBr) ν_{max} = 851, 963, 1072, 1207, 1258, 1344, 1389, 1421, 1466, 1510, 2847, 2920, 3056, 3349 cm^{-1}. ^1H NMR (300 MHz, $CDCl_3$, TMS): δ 0.87 (m, 18H, $-CH_3$), 1.25-1.83 (m, 120H, $-CH_2$), 2.4 (s, br., 2H, –OH), 3.98-4.04 (m, 12H, $-OCH_2$), 4.67 (s, 4H, $-CH_2OH$), 6.86 (s, 2H, aromatic), 7.12 (s, 2H, aromatic), 7.14 (s, 2H, aromatic), 7.45 (s, 4H, vinylic) ppm. ^{13}C NMR (75 MHz, $CDCl_3$) δ 14.09, 22.67, 26.20, 26.25, 26.31, 29.36, 29.46, 29.59, 29.68, 31.91, 62.28, 68.58, 69.50, 69.70, 109.08, 110.67, 114.00, 122.64, 123.34, 127.21, 127.36, 129.32, 150.65, 151.07 ppm. HRMS-ES$^+$: $[M+Na]^+$ calcd for $C_{96}H_{166}O_8Na$, 1470.2480; found, 1470.2490.

BH-OPV1c. Yield: 95%. mp 126-127 °C. FT-IR (KBr) ν_{max} = 851, 964, 1026, 1073, 1207, 1253, 1340, 1392, 1423, 1474, 1515, 2850, 2922, 3339 cm^{-1}. ^1H NMR (300 MHz, $CDCl_3$, TMS): δ 0.87-0.89 (m, 18H, $-CH_3$), 1.27-1.85 (m, 72H, $-CH_2$), 2.6 (s, br., 2H, –OH), 3.97-4.06 (m, 12H, $-OCH_2$), 4.68 (s, 4H, $-CH_2OH$), 6.87 (s, 2H, aromatic), 7.12 (s, 2H, aromatic), 7.15 (s, 2H, aromatic), 7.45 (s, 4H, vinylic) ppm.

^{13}C NMR (75 MHz, $CDCl_3$) δ 14.09, 22.67, 26.31, 29.36, 29.42, 29.49, 31. 89, 62.32, 68.59, 69.53, 69.72, 109.12, 110.71, 114.03, 123.38, 123.56, 127.24, 127.39, 129.34, 150.66, 151.09 ppm. HRMS-FAB: $[M]^+$ calcd for $C_{72}H_{118}O_8$, 1110.8827; found, 1110.8842.

BH-OPV1d. Yield: 96%. mp 134-135 °C. FT-IR (KBr) ν_{max} = 854, 965, 1053, 1208, 1259, 1344, 1391, 1425, 1466, 1511, 2859, 2930, 3416 cm^{-1}. ^{1}H NMR (300 MHz, $CDCl_3$, TMS): δ 0.90-0.91 (m, 18H, $-CH_3$), 1.26-1.85 (m, 48H, $-CH_2$), 3.89-4.06 (m, 12H, $-OCH_2$), 4.68 (s, 4H, $-CH_2OH$), 6.87 (s, 2H, aromatic), 7.13 (s, 2H, aromatic), 7.15 (s, 2H, aromatic), 7.45 (s, 4H, vinylic) ppm. ^{13}C NMR (75 MHz, $CDCl_3$) δ 14.04, 22.64, 25.93, 29.48, 31.64, 62.31, 68.55, 69.47, 69.66, 109.06, 110.56, 113.93, 118.91, 123.27, 123.38, 125.5, 127.15, 150.65, 151.05 ppm. HRMS-FAB: $[M]^+$ calcd for $C_{60}H_{94}O_8$, 942.6949; found, 942.6921.

BH-OPV1e. Yield: 85%. mp 74-75 °C. FT-IR (KBr) ν_{max} = 852, 965, 1077, 1201, 1259, 1341, 1385, 1424, 1465, 1511, 2845, 2920, 3367 cm^{-1}. ^{1}H NMR (300 MHz, $CDCl_3$, TMS): δ 0.87-0.89 (m, 18H, $-CH_3$), 1.27-1.85 (m, 72H, $-CH_2$ and –CH), 2.4 (s, br., 2H, –OH), 3.97-4.06 (m, 12H, $-OCH_2$), 4.67 (s, 4H, $-CH_2OH$), 6.86 (s, 2H, aromatic), 7.12 (s, 2H, aromatic), 7.14 (s, 2H, aromatic), 7.44 (s, 4H, vinylic) ppm. ^{13}C NMR (75 MHz, $CDCl_3$) δ 11.32, 14.06, 23.08, 24.27, 29.15, 30.81, 39.74, 62.19, 70.63, 71.50, 71.89, 108.10, 109.44, 113.65, 112.39, 122.54, 127.05, 127.23, 129.35, 150.67, 151.13 ppm. MALDI-TOF MS (MW = 1110.88): *m/z* = 1110.82 $[M]^+$.

BH-OPV2. Yield: 93%. mp 95-96 °C. FT-IR (KBr) ν_{max} = 852, 960, 1017, 1073, 1104, 1212, 1269, 1337, 1393, 1424, 1470, 1511, 2856, 2928, 3381 cm^{-1}. ^{1}H NMR (300 MHz, $CDCl_3$, TMS): δ 0.85-0.87 (m, 12H, $-CH_3$), 1.25-1.85 (m, 112H, $-CH_2$),

3.47 (s, br., 2H, –OH), 4.03-4.06 (m, 8H, $-OCH_2$), 4.71 (s, 4H, $-CH_2OH$), 6.80 (s, 2H, aromatic), 7.10 (s, 2H, aromatic), 7.34-7.39 (d, J = 16.5 Hz, 2H, vinylic), 7.46-7.51 (d, J = 16.5 Hz, 2H, vinylic), 7.56 (s, 4H, aromatic) ppm. ^{13}C NMR (75 MHz, $CDCl_3$) δ 14.10, 22.68, 26.21, 29.36, 29.42, 29.69, 62.24, 68.67, 69.68, 107.60, 113.90, 123.31, 126.45, 126.79, 128.41, 129.61, 137.09, 150.77, 151.04 ppm. MALDI-TOF MS (MW = 1303.13): m/z = 1303.03 $[M]^+$.

BH-OPV3. Yield: 95%. mp 96-97 °C. FT-IR (KBr) ν_{max} = 847, 965, 1017, 1104, 1207, 1264, 1336, 1393, 1424, 1475, 1516, 2850, 2918, 3283 cm^{-1}. ^1H NMR (300 MHz, $CDCl_3$, TMS): δ 0.85-0.87 (m, 6H, $-CH_3$), 1.25-1.86 (m, 56H, $-CH_2$), 3.49 (s, br., 2H, –OH), 4.03-4.07 (t, J = 6.39 Hz, 4H, $-OCH_2$), 4.70 (s, 4H, $-CH_2OH$), 7.10-7.15 (d, J = 16.4 Hz, 2H, vinylic), 7.12 (s, 2H, aromatic), 7.34-7.37 (d, J = 7.8 Hz, 4H, aromatic), 7.45-7.50 (d, J = 16.5 Hz, 2H, vinylic), 7.51-7.54 (d, J = 7.7 Hz, 4H, aromatic) ppm. ^{13}C NMR (75 MHz, $CDCl_3$) δ 14.11, 22.68, 26.21, 26.62, 29.37, 29.57, 29.65, 29.69, 31.92, 65.21, 69.61, 105.47, 110.72, 123.61, 126.69, 126.88, 127.39, 137.49, 139.99, 151.13 ppm. MALDI-TOF MS (MW = 822.65): m/z = 822.60 $[M]^+$.

Preparation of MH-OPV. **MH-OPV** was prepared by the reduction of the monoaldehyde derivative **8** as described above for the syntheses of **BH-OPVs**. Yield: 95%. mp 112-113 °C. FT-IR (KBr) ν_{max} = 852, 964, 1071, 1206, 1259, 1343, 1387, 1420, 1462, 1511, 2842, 2922, 3322 cm^{-1}. ^1H NMR (300 MHz, $CDCl_3$, TMS): δ 0.86-0.87 (m, 18H, $-CH_3$), 1.18-1.95 (m, 120H, $-CH_2$), 2.4 (s, br., 2H, –OH), 3.97-4.04 (m, 12H, $-OCH_2$), 4.67-4.69 (d, J = 6.3 Hz, 4H, $-CH_2OH$), 6.87 (s, 1H, aromatic), 7.12 (s, 2H, aromatic), 7.16 (s, 4H, vinylic), 7.33-7.38 (m, 3H, aromatic), 7.45 (s, 2H,

vinylic), 7.48 (s, 3H, aromatic), 7.52-7.54 (d, J = 7.8 Hz, 2H, aromatic) ppm. ^{13}C NMR (75 MHz, $CDCl_3$) δ 14.09, 22.62, 25.62, 28.95, 29.37, 29.49, 29.62, 29.82, 31.68, 60.65, 68.21, 69.51, 69.73, 109.11, 114.37, 114.65, 115.90, 122.34, 126.0, 127.11, 128.36, 129.32, 131.24, 150.65, 151.07, 155.11 ppm MALDI-TOF MS (MW = 1520.45): m/z = 1520.27 $[M]^+$.

Preparation of BM-OPV. The bisalcohol **BH-OPV1a** (0.1 mmol) was dissolved in dry THF and NaH (0.3 mmol) in dry THF was added in portions. Methyl iodide (0.3 mmol) was added to this solution while cooling. The reaction mixture was stirred for 12 h and poured into water and then extracted with dichloromethane. Concentration of the organic layer followed by the column chromatography (hexane/chloroform, 3:1) over silica gel (100-200 mesh) gave the pure product **BM-OPV**. Yield 95 %. mp 99-100 °C. FT-IR (KBr) ν_{max} = 846, 955, 1011, 1068, 1094, 1125, 1202, 1248, 1336, 1382, 1418, 1465, 1511, 2850, 2923 cm^{-1}. ^1H NMR (300 MHz, $CDCl_3$, TMS): δ 0.85-0.89 (m, 18H, $-CH_3$), 1.25-1.85 (m, 168H, $-CH_2$), 3.45 (s, 6H, $-OCH_3$), 3.97-4.05 (m, 12H, $-OCH_2$), 4.51 (s, 4H, $-CH_2OCH_3$), 6.96 (s, 2H, aromatic), 7.11 (s, 2H, aromatic), 7.14 (s, 2H, aromatic), 7.45 (m, 4H, vinylic) ppm. ^{13}C NMR (75 MHz, $CDCl_3$) δ 14.04, 22.68, 26.20, 26.62, 28.70, 28.95, 29.34, 29.71, 29.69, 31.91, 58.4, 68.32, 69.27, 69.52, 109.46, 110.68, 113.63, 123.29, 126.92, 127.28, 127.42, 150.70, 151.05 ppm. MALDI-TOF MS (MW = 1813.03): m/z = 1813.55 $[M]^+$.

Preparation of BA-OPV. Reaction of the bisalcohol **BH-OPV1a** (0.1 mmol) and 1-bromohexane (0.3 mmol) as per the procedure described for the preparation of **BM-OPV** provided the **BA-OPV** in 60% yield after purification. mp 88-89 °C. FT-IR (KBr) ν_{max} = 855, 965, 1032, 1078, 1207, 1264, 1346, 1387, 1428, 1416, 1516, 2855, 2922 cm^{-1}. ^1H NMR (300 MHz, $CDCl_3$, TMS): δ 0.85-0.90 (m, 24H, $-CH_3$), 1.24-1.85

(m, 184H, $-CH_2$), 3.50-3.55 (t, J = 6.63 Hz, 4H, $-OCH_2C_5H_{11}$), 3.98-4.05 (m, 12H, $-OCH_2$), 4.55 (s, 4H, $-CH_2OC_6H13$), 6.99 (s, 2H, aromatic), 7.10 (s, 2H, aromatic), 7.14 (s, 2H, aromatic), 7.45 (m, 4H, vinylic) ppm. ^{13}C NMR (75 MHz, $CDCl_3$) δ 14.06, 14.11, 22.69, 26.01, 26.24, 26.32, 29.37, 29.50, 29.53, 29.58, 29.68, 29.72, 29.83, 31.77, 31.93, 67.30, 68.84, 69.51, 69.56, 70.83, 109.37, 110.63, 113.58, 123.15, 123.46, 126.70, 127.38, 127.87, 150.65, 151.02 ppm. MALDI-TOF MS (MW = 1953.30): m/z = 1952.84 $[M]^+$.

Preparation of S-OPV. **S-OPV** was prepared by Wittig-Horner reaction according to a reported procedure.[23] Yield 90%. mp 106-107 °C. FT-IR (KBr) ν_{max} = 847, 965, 1074, 1223, 1254, 1347, 1398, 1429, 1465, 1506, 2840, 2923 cm^{-1}. ^1H NMR (300 MHz, $CDCl_3$, TMS): δ 0.85-0.87 (m, 18H, $-CH_3$), 1.25-1.84 (m, 168H, $-CH_2$), 3.97-4.01 (m, 12H, $-OCH_2$), 6.7s (s, 2H, aromatic), 6.82 (d, J = 8.7 Hz, 2H, aromatic), 7.14 (s, 2H, aromatic), 7.18 (d, J = 8.5 Hz, 2H, aromatic), 7.47 (s, 4H, vinylic) ppm. ^{13}C NMR (75 MHz, $CDCl_3$) δ 14.09, 22.68, 26.12, 26.22, 26.28, 29.36, 29.48, 29.58, 29.63, 29.71, 31.92, 68.63, 69.54, 69.61, 110.79, 112.24, 114.00, 1223.44, 123.87, 127.41, 128.32, 129.29, 150.93, 153.34 ppm. MALDI-TOF MS (MW = 1724.93): m/z = 1724.58 $[M]^+$.

2.4.2. General Procedure for Gelation Studies

A weighed amount of the compound in an appropriate solvent was placed in a glass vial, which was sealed and heated until the compound was dissolved. The solution was allowed to cool to room temperature and the gel formation was confirmed by the failure of the transparent soft mass to flow by inverting the glass vial. The reversibility of the gelation was confirmed by repeated heating and cooling.

2.4.3. Description on Experimental Techniques

Differential Scanning Calorimetry. An accurately weighed amount of the gel from appropriate solvents was analyzed on a Mettler Toledo Star DSC instrument under nitrogen atmosphere at the heating and cooling rates of 5 °C per minute.

X-ray Diffraction. Gels of the different OPVs from hexane or toluene were coated on glass plates and the solvents were slowly evaporated. X-ray diffractograms of the dried films were recorded on a Phillips diffractometer using Ni filtered Cu Kα radiation.

Optical Polarizing Microscopy. The gel texture was observed on a polarizing light microscope (Nikon HFX 35 A Optiphot equipped with a Linkan THMS 600 heating and freezing stage connected to Linkan TP 92 temperature programmer).

Scanning Electron Microscopy. Sheared gels from decane, cyclohexane or toluene were placed on sample studs and coated with gold by ion sputtering. SEM pictures were obtained either on a JEOL 5600 LV scanning electron microscope with an accelerating voltage of 10 kV, or a Hitachi S 2004 at an accelerating voltage of 15 kV.

Transmission Electron Microscopy. Transmission Electron Microscopy was performed on a Hitachi H-7100 microscope. Samples were prepared by drop casting the OPV solution from toluene on carbon coated copper grids and the TEM pictures were obtained without staining.

Atomic Force Microscopy. Atomic Force Microscopy images were recorded under ambient conditions using a Digital Instrument Multimode Nanoscope IV operating in the tapping mode regime. Micro-fabricated silicon cantilever tips (NSG01/Pt) with a

resonance frequency of approximately 150 kHz and a spring constant of about 5.5 Nm^{-1} were used. The scan rate varied from 0.5 to 1.5 Hz. The set-point amplitude ratio ($r_{sp} = A_{sp}/A_o$, where A_{sp} is the amplitude setpoint, and A_o is the amplitude of the free oscillation) was adjusted to 0.9. All AFM images shown here were subjected to a first-order plane-fitting procedure to compensate for sample tilt. AFM analysis was done offline. AFM samples were prepared by drop casting the OPV solution on freshly cleaved muscovite mica.

2.5. References

1. (a) Lehn, J.-M. *Supramolecular Chemistry*; VCH: Winheim, Germany, 1995. (b) Schneider, H.-J.; Yatsimirsky, A. *Principles and Methods in Supramolecular Chemistry*; Wiley: Chichester, 2000. (c) Steed, J. W.; Atwood, J. L. *Supramolecular Chemistry*; Wiley: Chichester, 2000.
2. (a) Engelkamp, H.; Middelbeek, S.; Nolte, R. J. M. *Science* **1999**, *284*, 785. (b) Oda, R.; Huc, I.; Schmutz, M.; Candau, S. J.; MacKintosh, F. C. *Nature* **1999**, *399*, 566. (c) Prins, L. J.; Huskens, J.; de Jong, F.; Timmerman, P.; Reinhoudt, D. N. *Nature* **1999**, *398*, 498. (d) Hirschberg, J. H. K. K.; Brunsveld, L.; Ramzi, A.; Vekemans, J. A. J. M.; Sijbesma, R. P.; Meijer, E. W. *Nature* **2000**, *407*, 167. (e) Berl, V.; Huc, I.; Khoury, R. G.; Krische, M. J.; Lehn, J.-M. *Nature* **2000**, *407*, 720.
3. (a) Nelson, J. C.; Saven, J. G.; Moore, J. S.; Wolynes, P. G. *Science* **1997**, *277*, 1793. (b) Moore, J. S. *Acc. Chem. Res.* **1997**, *30*, 402. (c) Prince, R. B.; Brunsveld, L.; Meijer, E. W.; Moore, J. S. *Angew. Chem. Int. Ed.* **2000**, *39, 228*. (d) Brunsveld, L.; Meijer, E. W.; Prince, R. B.; Moore, J. S. *J. Am. Chem. Soc.* **2001**, *123*, 7978.
4. (a) Bong, D. T.; Clark, T. D.; Granja, J. R.; Ghadiri, M. R. *Angew. Chem. Int. Ed.* **2001**, *40*, 988 and the references cited therein. (b) Sakai, N.; Matile, S. *Chem. Commun.* **2003**, 2514 and the references cited therein.

5. (a) Stupp, S. I.; LeBonheur, V.; Walker, K.; Li, L. S.; Huggins, K. E.; Keser, M.; Amstutz, A. *Science* **1997**, *276*, 384. (b) Zubarev, E. R.; Pralle, M. U.; Li, L.; Stupp, S. I. *Science* **1999**, *283*, 523. (c) Hartgerink, J. D.; Beniash, E.; Stupp, S. I. *Science* **2001**, *294*, 1684. (d) Zubarev, E. R.; Pralle, M. U.; Sone, E. D.; Stupp, S. I. *J. Am. Chem. Soc.* **2001**, *123*, 4105.

6. (a) Würthner, F.; Sautter, A.; Schmid, D.; Weber, P. J. A. *Chem. Eur. J.* **2001**, *7*, 894. (b) Sautter, A.; Schmid, D. G.; Jung, G.; Würthner, F. *J. Am. Chem. Soc.* **2001**, *123*, 5424. (c) Prins, L. J.; Thalacker, C.; Würthner, F.; Timmerman, P.; Reinhoudt, D. N. *Proc. Natl. Acad. Sci. U. S. A.* **2001**, *98*, 10042. (d) Würthner, F.; Sautter, A. *Org. Biomol. Chem.* **2003**, *1*, 240.

7. See the references 4-28 cited in Chapter 1 of the thesis.

8. (a) McQuade, D. T.; Kim, J.; Swager, T. M. *J. Am. Chem. Soc.* **2000**, *122*, 5885. (b) McQuade, D. T.; Hegedus, A. H.; Swager, T. M. *J. Am. Chem. Soc.* **2000**, *122*, 12389. (c) Bunz, U. H. F. *Chem. Rev.* **2000**, *100*, 1605. (d) Bunz, U. H. F. *Acc. Chem. Res.* **2001**, *34*, 998. (e) Levitus, M.; Schmieder, K.; Ricks, H.; Shimizu, K. D.; Bunz, U. H. F.; Garcia-Garibay, M. A. *J. Am. Chem. Soc.* **2001**, *123*, 4259. (f) Kim, J.; Swager, T. M. *Nature* **2001**, *411*, 1030. (g) Arnt, L.; Tew, G. N. *J. Am. Chem. Soc.* **2002**, *124*, 7664. (h) Breitenkamp, R. B.; Tew, G. N. *Macromolecules* **2004**, *37*, 1163.

9. (a) Percec, V.; Glodde, M.; Bera, T. K.; Miura, Y.; Shiyanovskaya, I.; Singer, K. D.; Balagurusamy, V. S. K.; Heiney, P. A.; Schnell, I.; Rapp, A.; Spiess, H.-W.; Hudson, S. D.; Duan, H. *Nature* **2002**, *419*, 384. (b) Meijer, E. W.; Schenning, A. P. H. J. *Nature* **2002**, *419*, 353.

10. (a) Burroughes, J. H.; Bradley, D. D. C.; Brown, A. R.; Marks, R. N.; MacKay, K.; Friend, R. H.; Burns, P. L.; Holmes, A. B. *Nature* **1990**, *347*, 539. (b) Kraft, A.; Grimsdale, A. C.; Holmes, A. B. *Angew. Chem. Int. Ed.* **1998**, *37*, 402.

11. (a) Yu, G.; Gao, J.; Hummelen, J. C.; Wudl, F.; Heeger, A. J. *Science* **1995**, *270*, 1789. (b) Halls, J. J. M.; Walsh, C. A.; Greenham, N. C.; Marseglia, E. A.; Friend, R. H.;

Moratti, S. C.; Holmes, A. B. *Nature* **1995**, *376*, 498. (c) Brabec, C. J.; Sariciftci, N. S.; Hummelen, J. C. *Adv. Funct. Mater.* **2001**, *11*, 15. (d) El-ghayoury, A.; Schenning, A. P. H. J.; van Hal, P. A.; van Duren, J. K. J.; Janssen, R. A. J.; Meijer, E. W. *Angew. Chem. Int. Ed.* **2001**, *40*, 3660. (e) Ramos, A. M.; Rispens, M. T.; van Duren, J. K. J.; Hummelen, J. C.; Janssen, R. A. J. *J. Am. Chem. Soc.* **2001**, *123*, 6714.

12. (a) Horowitz, G. *Adv. Mater.* **1998**, *10*, 365. (b) Sirringhaus, H.; Brown, P. J.; Friend, R. H.; Nielsen, M. M.; Bechgaard, K.; Langeveld-Voss, B. M. W.; Spiering, A. J. H.; Janssen, R. A. J.; Meijer, E. W.; Herwig, P.; de Leeuw, D. M. *Nature* **1999**, *401*, 685. (c) Cornil, J.; Beljonne, D.; Calbert, J.-P.; Bréads, J.-L. *Adv. Mater.* **2001**, *13*, 1053.

13. (a) Martin, R. E.; Diederich, F. *Angew. Chem. Int. Ed.* **1999**, *38*, 1350. (b) Tour, J. M. *Chem. Rev.* **1996**, *96*, 537. (c) Müllen, K.; Wegner, G. *Electronic Materials*; *The Oligomer Approach*; VCH: Weinheim, Germany, 1998.

14. (a) Schenk, R.; Gregorius, H.; Meerholz, K.; Heinze, J.; Müllen, K. *J. Am. Chem. Soc.* **1991**, *113*, 2634. (b) Tian, B.; Zerbi, G.; Schenk, R.; Müllen, K. *J. Chem. Phys.* **1991**, *95*, 3191. (c) Cornil, J.; Beljonne, D.; Shuai, Z.; Hagler, T. W.; Campbell, I.; Bradley, D. D. C.; Brèdas, J. L.; Spangler, C. W.; Müllen, K. *Chem. Phys. Lett.* **1995**, *247*, 425.

15. Stalmach, U.; Kolshorn, H.; Brehm, I.; Meier, H. *Liebigs Ann.* **1996**, 1449. (b) Gebhardt, V.; Bacher, A.; Thelakkat, M.; Stalmach, U.; Meier, H.; Schmidt, H.-W.; Haarer, D. *Adv. Mater.* **1999**, *11*, 119. (c) Meier, H.; Gerold, J.; Kolshorn, H.; Baumann, W.; Bletz, M. *Angew. Chem. Int. Ed.* **2002**, *41*, 292.

16. (a) Gaylord, B. S.; Wang, S.; Heeger, A. J.; Bazan, G. C. *J. Am. Chem. Soc.* **2001**, *123*, 6417. (b) Robinson, M. R.; Wang, S.; Heeger, A. J.; Bazan, G. C. *Adv. Funct. Mater.* **2001**, *11*, 413. (c) Liu, B.; Gaylord, B. S.; Wang, S.; Bazan, G. C. *J. Am. Chem. Soc.* **2003**, *125*, 6705.

17. (a) Peeters, E.; Ramos, A. M.; Meskers, S. C. J.; Janssen, R. A. J. *J. Chem. Phys.* **2000**, *112*, 9445. (b) Peeters, E.; van Hal, P. A.; Knol, J.; Brabec, C. J.; Sacriciftci, N. S.; Hummelen, J. C.; Janssen, R. A. J. *J. Phys. Chem. B* **2000**, *104*, 10174.

18. (a) Maddux, T.; Li, W.; Yu, L. *J. Am. Chem. Soc.* **1997**, *119*, 844. (b) Bao, Z.; Amundson, K. R.; Lovinger, A. J. *Macromolecules* **1998**, *31*, 8647. (c) Hoag, B. P.; Gin, D. L. *Adv. Mater.* **1998**, *10*, 1546. (d) Eckert, J.-F.; Maciejczuk, U.; Guillon, D.; Nierengarten, J.-F. *Chem. Commun.* **2001**, 1278.

19. (a) Strehmel, B.; Sarker, A. M.; Malpert, J. H.; Strehmel, V.; Seifert, H.; Neckers, D. C. *J. Am. Chem. Soc.* **1999**, *121*, 1226. (b) van Hutten, P. F.; Wildeman, J.; Meetsma, A.; Hadziioannou, G. *J. Am. Chem. Soc.* **1999**, *121*, 5910. (c) Renak, M. L.; Bartholomew, G. P.; Wang, S.; Ricatto, P. J.; Lachicotte, R. J.; Bazan, G. C. *J. Am. Chem. Soc.* **1999**, *121*, 7787.

20. For hydrogen bonded self-assembly in phenylenevinylenes: (a) Eckert, J.-F.; Nicoud, J.-F.; Guillon, D.; Nierengarten, J.-F. *Tetrahedron Lett.* **2000**, *41*, 6411. (b) El-ghayoury, A.; Peeters, E.; Schenning, A. P. H. J.; Meijer, E. W. *Chem. Commun.* **2000**, 1969. (c) Schenning, A. P. H. J.; Jonkheijm, P.; Peeters, E.; Meijer, E. W. *J. Am. Chem. Soc.* **2001**, *123*, 409. (d) Schenning, A. P. H. J.; van Herrikhuyzen, J.; Jonkheijm, P.; Chen, Z.; Würthner, F.; Meijer, E. W. *J. Am. Chem. Soc.* **2002**, *124*, 10252. (e) Jonkheijm, P.; Hoeben, F. J. M.; Kleppinger, R.; van Herrikhuyzen, J.; Schenning, A. P. H. J.; Meijer, E. W. *J. Am. Chem. Soc.* **2003**, *125*, 15941. (f) Jonkheijm, P.; Miura, A.; Zdanowska, M.; Hoeben, F. J. M.; De Feyter, S.; Schenning, A. P. H. J.; De Schryver, F. C.; Meijer, E. W. *Angew. Chem. Int. Ed.* **2004**, *43*, 74. (g) Würthner, F.; Chen, Z.; Hoeben, F. J. M.; Osswald, P.; You, C.-C.; Jonkheijm, P.; van Herrikhuyzen, J.; Schenning, A. P. H. J.; van der Scoot, P. P. A. M.; Meijer, E. W.; Beckers, E. H. A.; Meskers, S. C. J.; Janssen, R. A. J. *J. Am. Chem. Soc.* **2004**, *126*, 10611.

21. See the references 29-108 cited in Chapter 1 of the thesis.

22. Schoonbeek, F. S.; van Esch, J. H.; Wegewijs, B.; Rep, D. B. A.; de Haas, M. P.; Klapwijk, T. M.; Kellogg, R. M.; Feringa, B. L. *Angew. Chem. Int. Ed.* **1999**, *38*, 1393.

23. Chen, S.-A.; Chang, E.-C. *Macromolecules* **1998**, *31*, 4889.

24. Luboradzki, R.; Gronwald, O.; Ikeda, A.; Shinkai, S. *Chem. Lett.* **2000**, 1148.

25. In a dropping ball method, a steel ball (150 mg) was placed on the top of a 1 mL volume gel in a sealed glass vial. Then the gels are slowly heated, while the position of the ball on the top of gel is continuously observed, until the gel no longer bears the ball. The temperature at which the ball reaches the bottom of vial is taken as the sol-gel phase transition temperature (T_{gel}).

26. (a) Murata, K.; Aoki, M.; Suzuki, T.; Harada, T.; Kawabata, H.; Komori, T.; Ohseto, F.; Ueda, K.; Shinkai, S. *J. Am. Chem. Soc.* **1994**, *116*, 6664. (b) Yoza, K.; Amanokura, N.; Ono, Y.; Akao, T.; Shinmori, H.; Takeuchi, M.; Shinkai, S.; Reinhoudt, D. N. *Chem. Eur. J.* **1999**, *5*, 2722. (c) Clavier, G. M.; Brugger, J.-F.; Bouas-Laurent, H.; Pozzo, J.-L. *J. Chem. Soc., Perkin Trans. 2*, **1998**, 2527.

27. (a) Philips, K. E. S.; Katz, T. J.; Jockusch, S.; Lovinger, A. J.; Turro, N. J. *J. Am. Chem. Soc.* **2001**, *123*, 11899. (b) Chen, D.; Wan, L.; Fang, J.; Yu, X. *Chem. Lett.* **2001**, 1156.

28. Wang, B.; Wasielewski, M. R. *J. Am. Chem. Soc.* **1997**, *119*, 12.

Chapter 3

Supramolecular Control of Optical Properties and Energy Transfer in π-Conjugated Light Harvesting Gels

Abstract

Self-assembly induced changes in the absorption and emission properties of a variety of tailor made fluorescent OPV based organogels and their use in light harvesting are described. Detailed photophysical studies revealed the co-existence of the unassembled and self-assembled molecules, the ratio of which varies as a function of concentration, temperature, solvent and the structure of the OPV derivatives. The length and position of the hydrocarbon side chains and the presence of the hydrogen bonding groups on the OPV backbone are crucial for the efficient modulation of the optical properties. The gelation induced changes in the absorption and emission properties are used as a tool to probe the self-assembly of OPVs. In the presence of Rhodamine B as an acceptor, strong fluorescence resonance energy transfer (FRET) quenching of the emission, exclusively from the self-assembled species could be observed. The efficiency of FRET is considerably influenced by the ability of the OPV to form the self-assembled species and hence could be controlled by temperature. Energy transfer from a xerogel film was more efficient than from a decane gel. FRET efficiencies of the OPVs, which could not form gels, were significantly low. FRET occurs only to the dye molecules, which are entrapped between the polar channels of the OPV gel. This is a unique example for the remarkable

changes in the emission properties as a result of self-assembly induced gelation where selective energy transfer is possible exclusively from the self-assembled donor and not from the isotropic solution. The present study highlights the importance of chromophore organization in the design of supramolecular light harvesting assemblies.

3.1. Introduction

In recent years there has been considerable interest in the design of extended π-conjugated systems[1] as active components of various organic semiconductor devices such as photovoltaic cells,[2] FETs[3] and light emitting diodes.[4] Among different conjugated systems, oligo(phenylenevinylene)s (OPVs) have received significant attention, mainly due to the well-defined molecular structures and novel optical properties.[5-8] Therefore, tuning of the optical properties of OPVs is extremely important for specific applications, which is usually achieved by structural modifications. An alternate approach towards the modulation of optical and electronic properties of π-conjugated systems utilizes supramolecular self-assembly of molecules with the help of directional noncovalent interactions.[9,10] Supramolecular chemistry of OPVs has been at the center stage of research in recent years by virtue of their novel optical and electronic properties which are sensitive to intermolecular interactions and molecular organization.[11] Therefore, mesoscopic ordering of π-conjugated systems and the consequent changes in the optical properties are gaining importance in the emerging area of supramolecular electronics.[12]

Control of supramolecular organization of chromophores[13] plays a key role in facilitating electron and energy transfer process, which are extremely important in light harvesting systems. There are several strategies such as, the use of H-bonded supramolecular complexes,[14] dendrimers,[15] chromophore-linked polymers,[16]

Langmuir-Blodgett films[17] and self-assembled monolayers[18] for the organization of chromophore assemblies. However, the current interest is to develop highly organized nanoscale supramolecular donor-acceptor arrays, which have advantages in view of device fabrication. Energy transfer from OPVs and PPVs to different acceptors has been reported in several cases.[19-21] More recently, Meijer and coworkers have successfully demonstrated energy transfer in H-bonded helical co-assembly of the OPVs **1** and **2** of different conjugation length bearing identical ureido-*s*-triazine hydrogen bonding motif.[22] A fast and efficient energy transfer from the shorter to the longer oligomers inside the supramolecular helical stacks as illustrated by the loss of the donor fluorescence signal was observed on increasing the concentration of the acceptor molecules (Figure 3.1). Up to about 2 mol%, the acceptor molecules exist only as isolated energy traps, but at higher concentrations clustering of acceptor molecules occur as evident from its quenched and red shifted fluorescence after energy transfer.

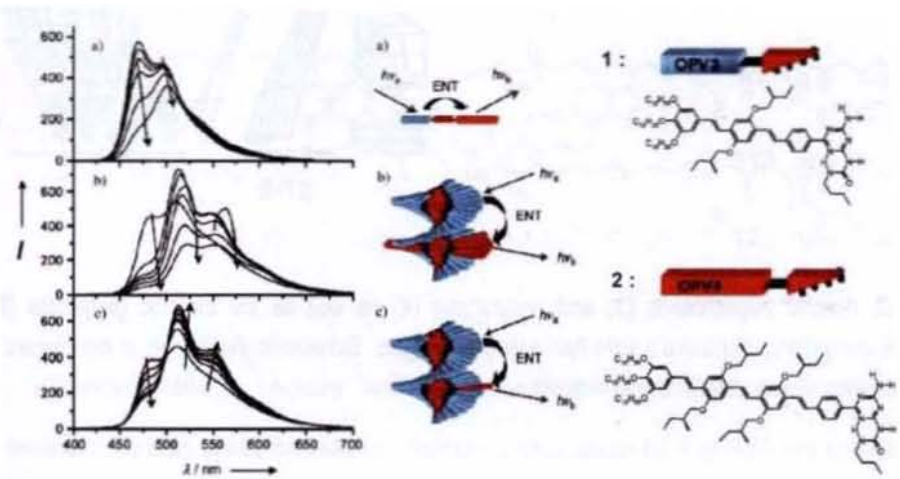

Figure 3.1. Photoluminescence spectra for mixtures of **1** and **2** in dodecane solution a) 0-30 mol% **2** at 80 °C b) 0-30 mol% **2** at 10 °C c) 0-1.2 mol% **2** at 10 °C. The self-complementary hydrogen bonding motif of OPVs **1** and **2** enables the formation of hetero-dimers and mixed helical stacks, in which efficient energy transfer is observed from **1** to **2**.

Though there are several reports pertaining to FRET in organized assemblies, organogels are rarely used as scaffold for efficient energy transfer between donor-acceptor chromophores.[23] Recently, Nakashima and Kimizuka have demonstrated energy transfer between anionic naphthalene (**3**, donor) and anthracene (**4**, acceptor) derivatives in the hydrogel fibrous assemblies of the cationic glutamate derivatives (**5** and **6**) through electrostatic interactions.[23a] The regular packing of the glutamate chains into bilayers ensures highly ordered chromophoric assembly and consequently, efficient energy transfer from the naphthalene donors to the anthracene acceptors has been observed (Figure 3.2). In a similar way, co-assembled gel networks of glutamate substituted pyrene (**7**) and porphyrin (**8**) chromophores and the resultant energy transfer from pyrene excimers to porphyrins have been reported (Figure 3.3).[23b]

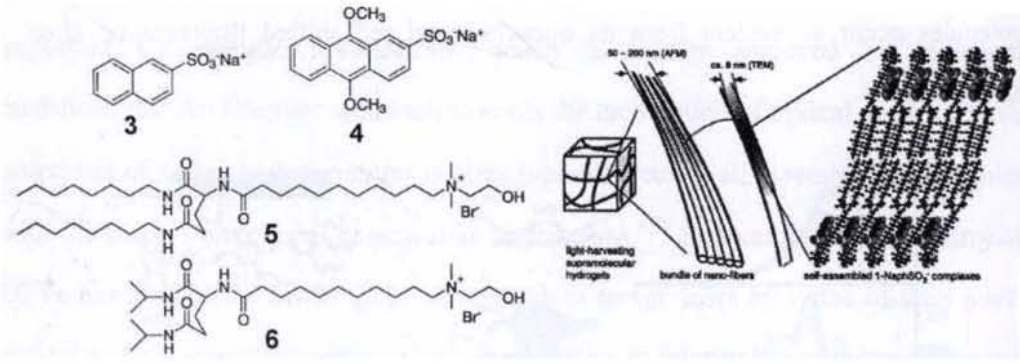

Figure 3.2. Anionic naphthalene (**3**) and anthracene (**4**) as well as the cationic glutamate (**5, 6**) derivatives comprising Kimizuka's light harvesting hydrogels. Schematic illustration is the hierarchical self-organization of supramolecular hydrogels.

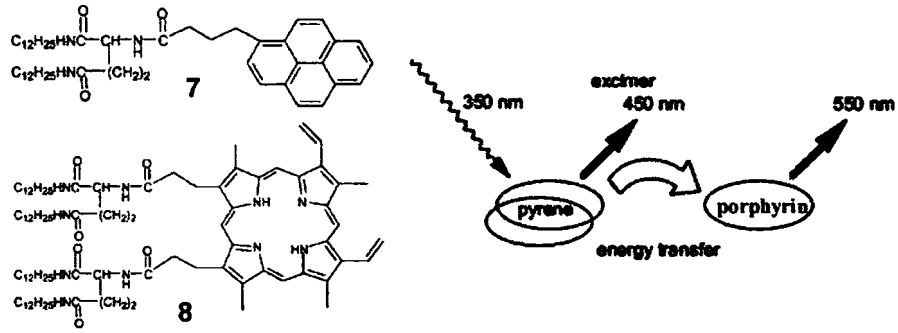

Figure 3.3. Didodecyl L-glutamic acid substituted porphyrin (**8**) and pyrene (**7**) form mixed assemblies in benzene. The energy transfer process in the assemblies is schematically depicted.

Recently, Shinkai and coworkers have described a visible light harvesting energy transfer cascade in co-assembled organogels of perylene bisimide functionalized cholesterol-based gelators **9-12**.[23d] For this purpose, the absorption spectra of the four perylene bisimides were tuned across the visible spectrum by attaching different substituents at the bay positions of the chromophores.

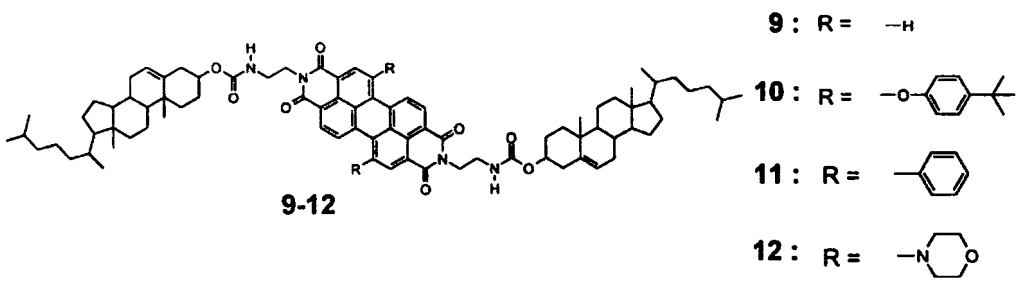

Chart 3.1

Various binary, ternary and quaternary perylene gels were prepared and subjected to energy transfer studies. Selective excitation of **9** at 457 nm resulted in the quenching of its emission at λ_{em} = 544 nm with efficiencies of 68% for **10**, 53% for **11** and 34% for **12**, consistent with decreasing donor-acceptor spectral overlap (Figure 3.4). In the quaternary system, perylene bisimide **12** effectively acts as an energy sink

as a consequence of its twisted intramolecular charge-transfer character. It is interesting to note that the supramolecular organization of the chromophores in the gel state guarantees the success of this cascade transfer process, since in solution the mentioned effects are not observed.

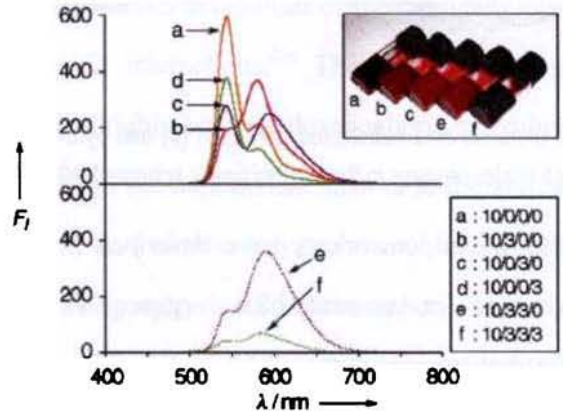

Figure 3.4. Fluorescence spectra of mixed perylene gels. The numbers in inset denote the molar ratios for **9/10/11/12**. The corresponding photographs of the mixed gels are also shown in the inset.

With the help of various analytical and microscopic techniques, we have established the structure-property relationship of the gelation process and the morphological characteristics of a variety of OPV based organogelators (see Chapter 2). For example, the bishydroxymethyl OPV derivatives (**BH-OPV1a-d**) showed very efficient gelation, which is strongly enhanced by long hydrocarbon side chains. However, if the hydroxymethyl groups are protected, the gelation efficiency drastically decreases, still forming weak gels at higher concentrations or lower temperature in long hydrocarbon solvents such as in decane, dodecane etc. It is observed that gelation of OPVs are accompanied by strong change in the color of the emission when the gels are irradiated (Figure 3.5). In order to shed further insight, we thought of using the strong absorption and emission properties of OPVs as a tool for

probing self-assembly and gelation. With this objective, we investigated on the change in the optical and photophysical properties of a variety of OPV derivatives as a function of gelation in different hydrocarbon solvents. In addition, we have carried out a detailed study on the potential use of the OPV based gelators as donors for selective energy transfer from the self-assembled chromophores to a suitable acceptor. The structures of the different OPV based organogelators used for the studies are shown in Figure 3.6.

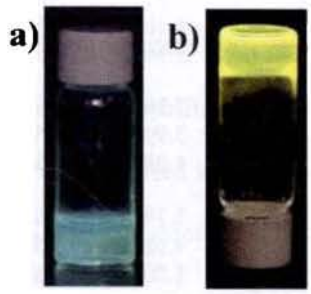

Figure 3.5. BH-OPV1a decane gels a) before and b) after gelation under irradiation.

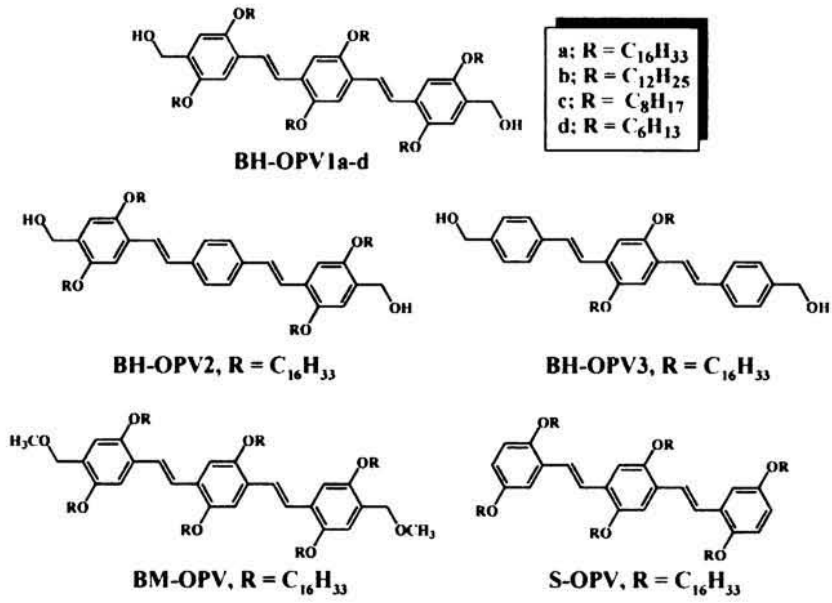

Figure 3.6. Molecular structure of OPV derivatives under investigation.

3.2. Results and Discussion

3.2.1. Absorption and Emission Properties

Table 3.1. Optical Properties of OPV Derivatives in Different Solvents

compound	solvent	absorption		emission		
		λ_{max} (nm)	$\varepsilon \times 10^4$ ($M^{-1}cm^{-1}$)	λ_{max} (nm)	Φ_f[a]	Φ_f[b]
BH-OPV1a	chloroform	407	3.91	463, 490	0.73	-
	cyclohexane	401, 468	4.48	454, 476, 527, 561	-	0.20
	dodecane	404, 467	1.86	537, 567	-	0.23
BH-OPV1b	chloroform	408	3.26	464, 492, 533	0.72	-
	cyclohexane	404, 468	3.99	452, 478, 520	0.62	0.25
	dodecane	406, 467	1.08	539, 574	-	0.16
BH-OPV1c	chloroform	408	3.19	465, 491, 533	0.69	-
	cyclohexane	401, 469	4.68	452, 480, 518	0.66	0.11
	dodecane	405, 469	1.00	454, 484, 528, 565	0.60	0.19
BH-OPV1d	chloroform	409	3.13	465, 491, 533	0.73	-
	cyclohexane	405, 468	3.72	451, 481, 518	0.65	0.01
	dodecane	417, 468	1.10	454, 483, 526	0.45	0.09
BH-OPV2	chloroform	390, 450	3.23	435, 461, 491	0.79	-
	cyclohexane	384, 445	3.31	423, 445, 480, 520	0.61	-
	dodecane	386, 434	1.26	424, 446, 480, 524	0.60	0.20
BH-OPV3	chloroform	389, 460	3.93	437, 489	0.82	-
	cyclohexane	386, 460	3.40	425, 443, 478, 538	0.69	-
	dodecane	391, 460	0.64	436, 464, 497, 528	0.67	0.14
BM-OPV	chloroform	408	4.21	464, 496, 533	0.71	0.17
	cyclohexane	401, 468	3.71	452, 480, 520	0.66	0.34
	dodecane	394, 465	3.53	517, 552	-	
S-OPV	chloroform	394	2.40	458, 488	0.71	-
	cyclohexane	385, 467	1.81	446, 479, 508, 544	0.39	0.17
	dodecane	389, 465	0.86	449, 511, 548, 602	0.39	0.20

[a] Fluorescence quantum yields of the monomeric species as determined using quinine sulphate as the standard (Φ_f = 0.546 in 0.1 N H_2SO_4) on excitation at 380 nm. [b] Fluorescence quantum yields of the self-assembled molecules as determined using Rhodamine 6G (Φ_f = 0.9 in ethanol) on selective excitation at 470 nm, error limit ± 5%. [c] Minor contribution from the self-assembled species cannot be ruled out.

The photophysical data of the OPVs under investigation are presented in Table 3.1. All of them showed strong absorption corresponding to the π-π* transition and strong emission with high quantum yields. As a representative case, the absorption and emission spectra of **BH-OPV1a** under different experimental conditions are shown in Figures 3.7a and 3.7b, respectively. In chloroform (1 x 10^{-5} M), the absorption maximum of **BH-OPV1a** is observed at 407 nm (ε = 3.91 x 10^4 $M^{-1}cm^{-1}$) and emission maxima are at 463 and 490 nm (Φ_f = 0.73). In cyclohexane (λ_{max} = 401 nm, ε = 4.48 x 10^4 $M^{-1}cm^{-1}$) and in dodecane (λ_{max} = 404 nm, ε = 1.86 x 10^4 $M^{-1}cm^{-1}$) the absorption maxima are slightly blue shifted and the intensity of the π-π* band is decreased with the formation of a red shifted shoulder band at 467 nm. When the same solution was heated to 65 °C, the shoulder band at 467 nm disappeared and the original intensity of the π-π* transition is regained as in the case of chloroform except for a slight red shift of the absorption maximum which could be due to the change in the solvent polarity. However, absorption spectrum of a film of **BH-OPV1a** showed close resemblance to the spectrum in dodecane. The emission spectra of **BH-OPV1a** in chloroform showed an intense band with maxima around 463 nm and 490 nm whereas in dodecane the emission was completely shifted towards the long wavelength region with maxima around 537 and 567 nm. However in cyclohexane at room temperature a broad emission with several maxima at 454, 476, 527 and 561 nm (Φ_f = 0.20) were obtained, the relative intensities of which are dependent upon the temperature and concentration (Figure 3.7b). Upon heating, the emission spectrum became similar as in chloroform except for a slight red shift. Interestingly, as noticed in the case of absorption, the emission of the **BH-OPV1a** film was matching with that in dodecane. These observations reveal that in chloroform **BH-OPV1a** prefers to be in

the molecularly dissolved monomeric forms whereas in dodecane or in film form it exists almost completely as self-assembled species. However, in cyclohexane at room temperature, **BH-OPV1a** molecules are present in more than one co-existing species, the composition of which varies as a function of concentration and temperature. The resemblance of the emission spectra of **BH-OPV1a** in dodecane at 25 °C and as a drop casted film, indicate a similar kind of chromophore packing in both cases. Since the long wavelength emission bands at 537 and 567 nm in dodecane, occur at the same spectral position as that of the solid films, it is clear that these bands correspond to the self-assembled OPV molecules.

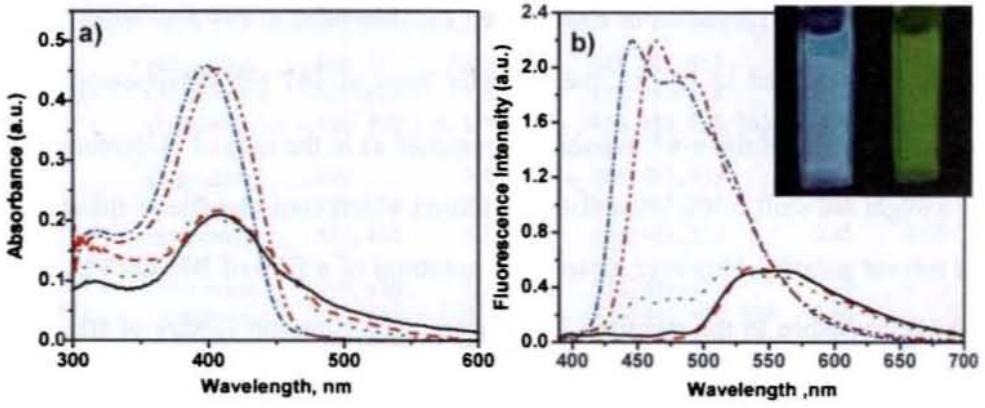

Figure 3.7. a) Absorption and b) emission spectra of **BH-OPV1a** in chloroform (– · – · –), cyclohexane (·····), and dodecane (—) at 25 °C, dodecane at 65 °C (– · – · –), and in the solid state (– – –) as a coated film (λ_{exc} = 380 nm). Inset of Figure 3.7b shows the visual emission from molecularly dissolved (left) and self-assembled (right) **BH-OPV1a** molecules in dodecane.

Variable temperature UV/Vis and fluorescence spectra of **BH-OPV1a** in dodecane showed a transition from the self-assembled species to the molecularly dissolved species as the temperature is increased from 15 °C to 65 °C (Figure 3.8). In the UV/Vis spectra, an increase in the intensity of the absorption maximum at 404 nm was observed upon increasing the temperature. This is accompanied by a concomitant

decrease in the intensity of the shoulder band at 467 nm through an isosbestic point at 428 nm (Figure 3.8a). Similarly, in the fluorescence spectra (λ_{ex} = 380 nm), the intensity of the long wavelength maxima at 537 and 567 nm decreases with the simultaneous increase in the intensity of the emission bands at 452 nm and 459 nm (Figure 3.8b) when the temperature is increased from 20-65 °C. These observations clearly show the existence of atleast two different species of **BH-OPV1a** in dodecane, the self-assembled species at room temperature and the non-assembled species at elevated temperatures. Gradual decrease of the emission from the self-assembled species with increase in temperature could be observed more clearly when they were selectively excited at 470 nm (Figure 3.8c). Further proof for the existence of the two different phases for **BH-OPV1a** comes from the plots of the fraction of aggregated species[24] (α) versus the temperature, as obtained from the temperature dependent UV/Vis and fluorescence experiments. In both cases, a good correlation was obtained for the melting temperatures (53 °C by UV/Vis and 51 °C by fluorescence) of the self-assembled species (Figure 3.8d).

Detailed analysis of the UV/Vis spectra of **BH-OPV1a** in dodecane when cooled from the isotropic solution, revealed a slight linear red shift of the absorption maximum at the initial stages, indicating a probable planarization of the OPV units as a result of the H-bonded self-assembly. On further cooling, a non-linear red shift is observed, indicating a three-dimensional growth of the self-assembled OPV molecules as a result of H-bonding and π-π stacking. This is in accordance with the earlier observation by Schenning *et al.* as in the case of the self-assembly of ureido-*s*-triazine attached OPVs.[11a] However, in our case, the decrease in the intensity of the π-π^* transition and the growth of the shoulder band at 470 nm are very predominant

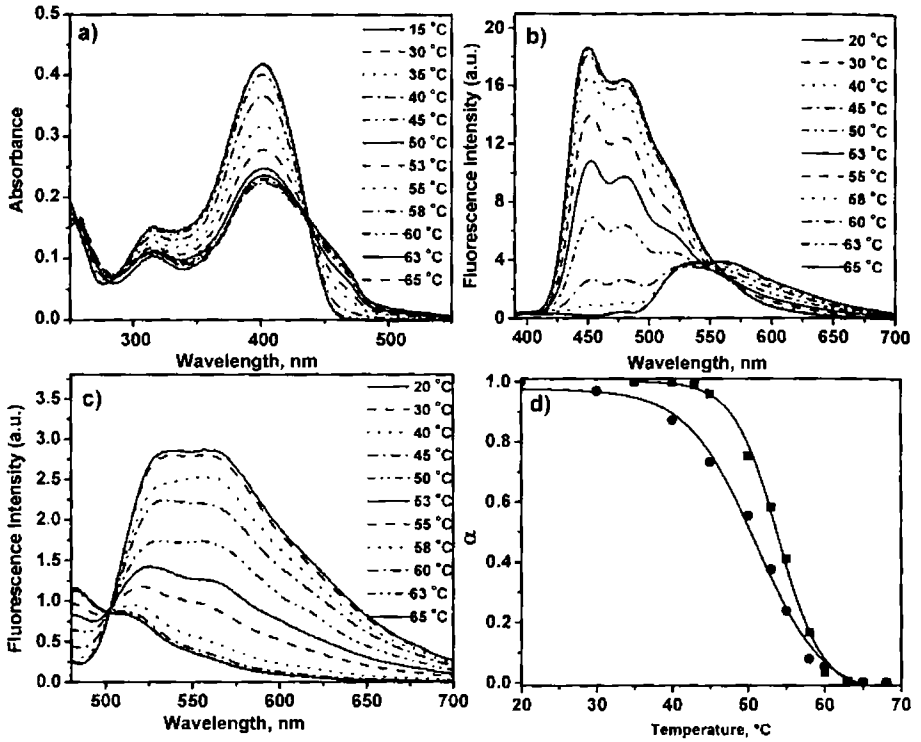

Figure 3.8. a) Temperature dependent absorption spectra and fluorescence spectra b) at λ_{ex} = 380 nm and c) at λ_{ex} = 470 nm, respectively of **BH-OPV1a** in dodecane (1 x 10^{-5} M). d) Plots of the fraction of aggregate versus temperature obtained from the absorption (■) and fluorescence (•) changes at 470 nm and 450 nm, respectively.

indicating a strong hierarchical supramolecular assembly. This is also clear from the remarkable shift of the emission spectrum upon cooling from the isotropic solution. The melting transition curves for the self-assembly of **BH-OPV1a** in dodecane (1 x 10^{-5} M) obtained by plotting absorbance at 400 nm versus temperature for the heating and cooling cycle is shown in Figure 3.9a. Upon cooling, the aggregation starts at around 40 °C, which is 15 °C lower than the melting temperature of the self-assembled species. The hysteresis noticed in the heating and cooling cycles indicates that the self-assembly is a time dependent process. This is clear from the time dependent fluorescence spectral studies of **BH-OPV1a**, which reveal that the

fluorescence maxima at 452 and 479 nm decrease with a concomitant increase in the emission at 537 and 567 nm, with time (Figure 3.9b). The inset of Figure 3.9b shows that the monomer emission is almost quenched within 10 minutes while keeping the solution at room temperature and becomes fast as we go further down with temperature.

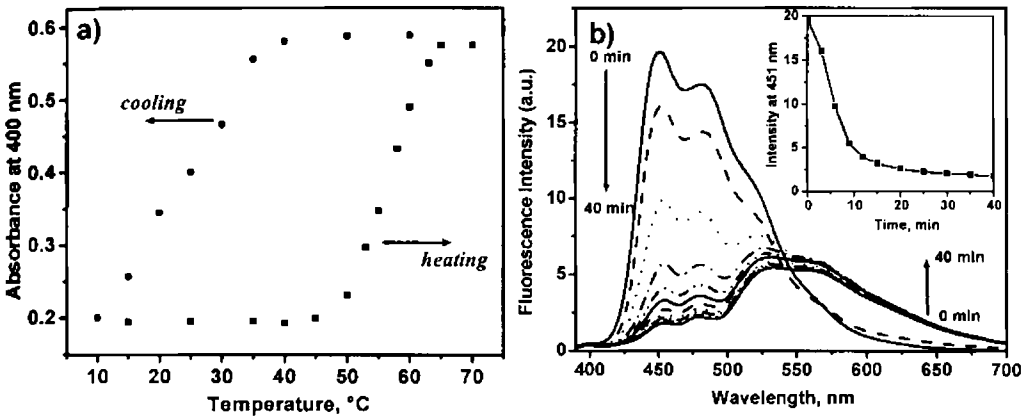

Figure 3.9. a) Heating (■) and cooling (•) transition curves for **BH-OPV1a** in dodecane (1 x 10^{-5} M) on plotting absorbance at 400 nm with temperature. b) The time dependent recovery of emission of the self-assembled molecules of **BH-OPV1a** in dodecane (1 x 10^{-5} M) on keeping the preheated isotropic solution at 25 °C. Inset of Figure 3.9b shows the decrease in the fluorescence intensity at 450 nm with time at 25 °C.

Attribution of the red shifted emission and its dependence on temperature and concentration, to the self-assembled species and not due to the formation of an excimer is established from the excitation and emission spectra of **BH-OPV1a** in dodecane and cyclohexane (Figure 3.10). The first argument against the excimer formation is the solvent and temperature dependent growth of the long wavelength absorption shoulder in the UV/Vis spectrum indicating ground state interactions between molecules. Secondly, when the emission of **BH-OPV1a** in dodecane at room temperature was monitored at 520 nm, an excitation spectrum having maximum at

400 nm with a shoulder at 470 nm was obtained, which corresponds in shape and position to the absorption spectrum in dodecane at room temperature (Figure 3.10a). Interestingly, the excitation spectrum (dashed line) at higher temperatures (monitored at 520 nm) in dodecane does not have a vibronic shoulder and are similar to the corresponding absorption spectrum. In addition, the excitation spectra of **BH-OPV1a** in cyclohexane at 20 °C collected at 450 and 620 nm matches with the absorption spectra of the free and self-assembled **BH-OPV1a** molecules, respectively (Inset of Figure 3.10a). The presence of self-assembled molecules is further justified by the formation of a red shifted emission spectrum (λ_{em} = 527 and 561 nm) of **BH-OPV1a** in cyclohexane when selectively excited at the shoulder band at 470 nm, in contrast to the broad spectrum observed on excitation at 380 nm (Figure 3.10b). These studies strongly support the fact that the solvent, temperature and concentration dependent changes in the emission spectra of **BH-OPV1a** in dodecane are due to the existence of the self-assembled molecules and not due to the formation of an excimer.

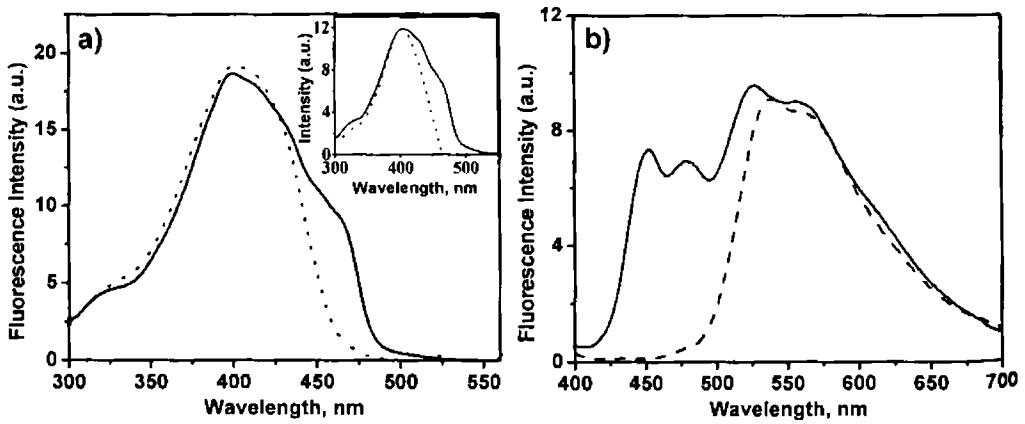

Figure 3.10. a) Excitation spectra of **BH-OPV1a** in dodecane at 20 °C (——) and at 60 °C (·····) (λ_{em} = 520 nm). b) Emission spectra of **BH-OPV1a** in cyclohexane at an excitation wavelength of 380 nm (——) and 470 nm (-----). Inset of Figure 3.10a shows the excitation spectra of **BH-OPV1a** in cyclohexane when collected at 450 (·····) and 620 nm (——).

The excited state lifetimes of the self-assembled and molecularly dissolved phases of **BH-OPV1a** under different conditions were obtained by the time resolved fluorescence experiments at different excitation and emission wavelengths (Figure 3.11). The excited state decay dynamics and lifetimes of the monomeric and self-assembled species are expected to be distinctly different from each other. The fluorescence decay of the molecularly dissolved **BH-OPV1a** in chloroform is monoexponential with an excited state lifetime of 1.64 ns (100%) at room temperature (Figure 3.11a). However, the fluorescence decay of **BH-OPV1a** in cyclohexane showed biexponential decay with time constants of 2.09 (57.85%) and 0.82 ns (42.2%), when analyzed at 520 nm. The decay of the emission corresponding to the free molecules at 450 nm in cyclohexane gave a monoexponential fit with a time constant of 1.46 ns, which is close to the lifetime in chloroform in its magnitude (Figure 3.11a). In cyclohexane at 50 °C, a monoexponential decay with a lifetime of 1.58 ns was observed irrespective of the monitoring wavelength indicating the presence of only one species, which is the molecularly dissolved **BH-OPV1a** (Figure 3.11b).

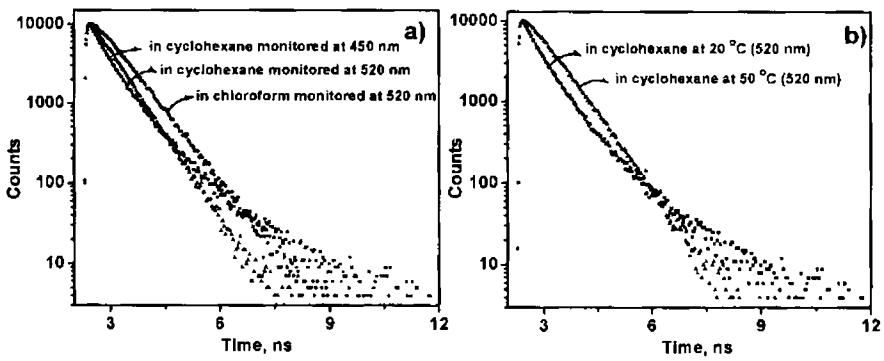

Figure 3.11. a) Normalized fluorescence decay profiles of **BH-OPV1a** in chloroform (20 °C) monitored at 520 nm (•) and in cyclohexane monitored at 450 nm (▲) and at 520 nm (■). b) Fluorescence decay profiles of **BH-OPV1a** in cyclohexane at 20 °C (■) and at 50 °C (▲) when monitored at 520 nm. Excitation wavelength is 418 nm for all the decay profiles.

Stability of the OPV self-assembly under different experimental conditions was established by the plots of the aggregate fraction (α) against temperature which is obtained by monitoring the temperature dependent changes in the UV/Vis absorption spectra at 470 nm (Figure 3.12). As expected for a H-bonded self-assembly, the transition temperatures of **BH-OPV1a** self-assembly increases on changing the solvent from toluene to cyclohexane to dodecane (Figure 3.12a). It is observed that the stability of the self-assembled molecules increases by 10-15 °C, per an order of the increase in concentration (Figure 3.12b). These stability responses obtained from the sigmoidal temperature transition curves of the OPV self-assembly against solvent polarity and concentration is characteristic of the cooperative noncovalent interactions during the self-assembly process. The effect of the alkyl side chains on the stability of the resulting self-assemblies is established from the temperature transition plots of **BH-OPV1a-b** and **BH-OPV1d** in dodecane (1×10^{-5} M) (Figure 3.12c). The transition temperatures of the self-assemblies increase with the increase in alkyl chain length where the maximum stability is noticed for **BH-OPV1a** with hexadecyl chains.

Insight to the effect of structural variation of the OPVs on the self-assembling properties could be obtained by comparing the optical properties of **BM-OPV**, **S-OPV, BH-OPV2** and **BH-OPV3** with those of **BH-OPV1a**. Absorption spectrum of **BM-OPV** in cyclohexane showed only a slight difference from that in chloroform which is relatively weak when compared to the changes for **BH-OPV1a** (Figure 3.13a). However, the absorption spectrum in dodecane showed considerable difference with a maximum at 394 nm ($\varepsilon = 3.53 \times 10^4\ M^{-1}cm^{-1}$), which is blue shifted by 10 nm with a shoulder at 465 nm when compared to that in chloroform (408 nm, $\varepsilon = 4.21 \times 10^4\ M^{-1}cm^{-1}$). In contrast to the observation of **BH-OPV1a** the emission

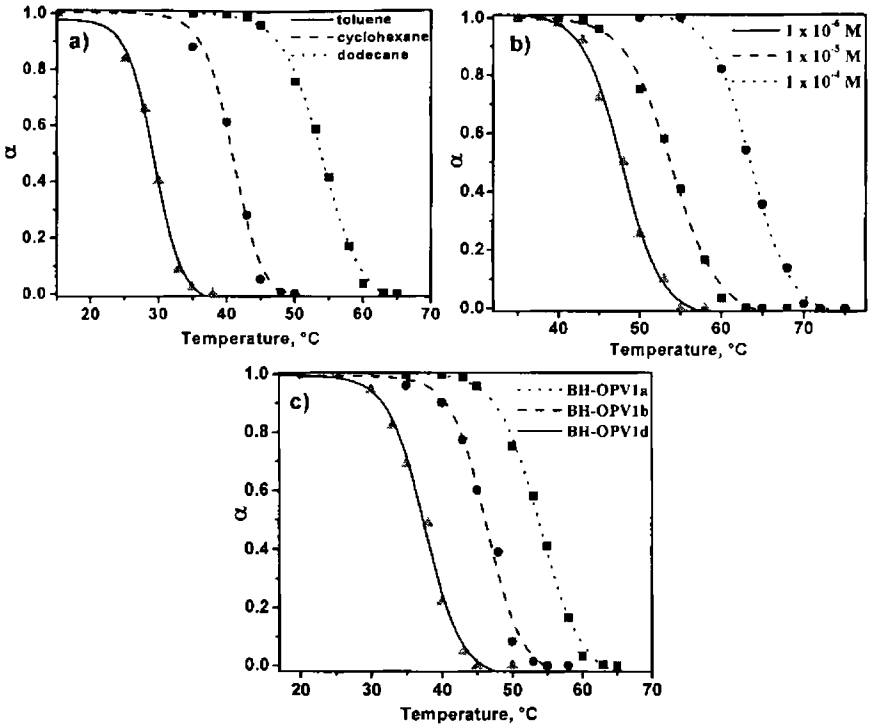

Figure 3.12. Plots of aggregate fraction (α) versus temperature of a) **BH-OPV1a** in different solvents, b) **BH-OPV1a** in different concentrations and c) **BH-OPV1a-b,d** in dodecane (1 x 10^{-5} M) indicating the stability of the OPV self-assemblies. The data points were obtained from the variable temperature absorption spectral changes at 470 nm.

spectra of **BM-OPV** in chloroform and in cyclohexane showed a marginal difference between the two (Figure 3.13b). These observations indicate a weak self-assembly of **BM-OPV** in cyclohexane, which could be due to the lack of H-bonding interactions. However, in dodecane the emission spectrum is completely shifted with two long wavelength maxima at 517 and 552 nm which is an indication of a better self-assembly in this solvent. Temperature dependent absorption and emission changes, shown in the insets of Figures 3.13a and b, respectively revealed a thermoreversible self-assembly for **BM-OPV** in dodecane as in the case of **BH-OPV1a**. The stability of the resulting supramolecular assembly was determined from the plot of the fraction

of the aggregate versus temperature (Figure 3.13c). These plots reveal that the self-assembled stacks of the **BM-OPV** are less stable by 10 °C than **BH-OPV1a** indicating the importance of H-bonding in stabilizing the self-assembly (Figure 3.13d). These data obtained from the photophysical studies are in good agreement with the data obtained from the gel melting studies and DSC analysis of the corresponding organogels (refer Chapter 2).

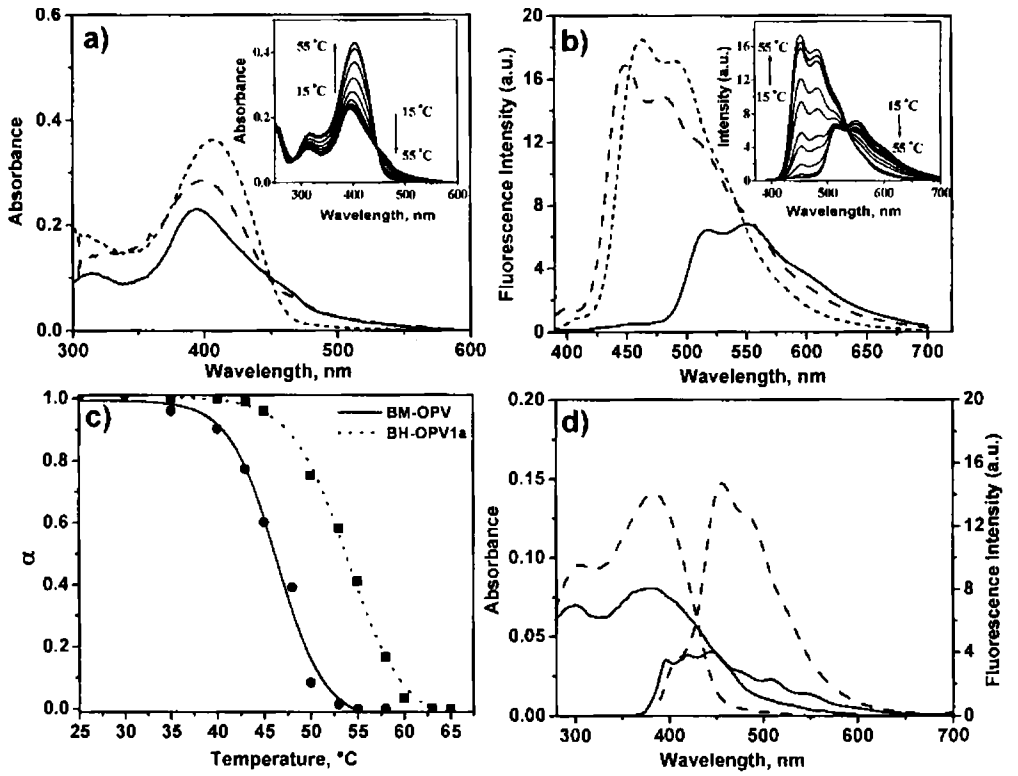

Figure 3.13. a) Absorption and b) emission spectra of **BM-OPV** in dodecane (——), cyclohexane (– – –) and chloroform (------). c) Plots of the aggregate fraction (α) *vs.* temperature of **BH-OPV1a** and **BM-OPV** in dodecane (1 x 10^{-5} M). The data points of the curves were obtained from the variable temperature absorption measurements at 470 nm. d) Absorption and emission spectra of **S-OPV** in dodecane (——) and chloroform (– – –). Insets of Figures 3.13a and 3.13b show the temperature dependent changes in absorption and emission of **BM-OPV** in dodecane, respectively.

The absorption and emission spectral changes of **S-OPV** in chloroform and dodecane are shown in Figure 3.13d. In this case, though the absorption spectrum in dodecane showed a broadening, the emission spectral changes are significantly different from those observed for **BH-OPV1a** and **BM-OPV**. Though the emission is considerably quenched in dodecane, a corresponding growth of the self-assembled species could not be seen. These observations suggest that the nature of the self-assembly in **BH-OPV1a-d**, **BM-OPV** and **S-OPV** have considerable differences. For example, in the case of **BH-OPV1a-d**, the cooperative interactions of H-bonding, π-stacking and van der Waals forces, result in the formation of three-dimensionally extended supramolecular stacks leading to the efficient gelation of the molecules. The observed shifts in the absorption and emission spectra in these cases point towards strong intermolecular electronic interactions within the self-assembly. In the case of **BM-OPV**, due to the absence of H-bonding, the stability of the self-assembly is considerably decreased resulting in relatively weak electronic interaction between molecules in solvents of comparable polarity. However, in the case of **S-OPV**, the self-assembly is restricted to a mere aggregation process, assisted by the weak π-π and van der Waals interactions. These aggregates are not able to form extended assemblies and hence the optical properties are different from those of **BH-OPV1a** and **BM-OPV**. The number and position of the hydrocarbon side chains on the OPV backbone also play considerable role on the optical properties. For example, **BH-OPV2** and **BH-OPV3** having less number of side chains, despite the presence of the H-bonding groups, showed weak self-assembly as evident from the changes in the absorption and emission spectra.

3.2.2. Fluorescence Resonance Energy Transfer (FRET) Studies

For an efficient energy transfer, there should be a good overlap between the emission of the donor with the absorption of the acceptor. It is known that excited OPVs are good donors to acceptors such as Rhodamine B[21b] and porphyrins.[21c] In the present study, as a result of the self-assembly, the emission of OPVs shift towards longer wavelength, which matches with the absorption spectrum of Rhodamine B. Under this situation, self-assembled OPVs are expected to be good FRET donors to Rhodamine B.

Figure 3.14a shows the individual emission spectra of **BH-OPV1a-b, d** and the absorption spectrum of Rhodamine B in dodecane-chloroform (16:1). The overlap between the fluorescence of the OPV derivatives and the absorbance of the Rhodamine B decreases in the order of **BH-OPV1a > BH-OPV1b > BH-OPV1d**. This is consistent with the self-assembling properties of the different OPV derivatives and hence **BH-OPV1d**, carrying the hexyl side chains, has the least overlap integral. **BH-OPV1a** is completely self-assembled in dodecane-chloroform (16:1) and showed a strong fluorescence in the range of 500-650 nm, where Rhodamine B has a strong absorption. The absorption spectrum of a mixture of **BH-OPV1a** (1.01×10^{-5} M) and Rhodamine B (8.38×10^{-5} M) in dodecane-chloroform (16:1) showed the characteristic absorption bands of the individual molecules, revealing the absence of any ground state interaction between the donor and the acceptor molecules.

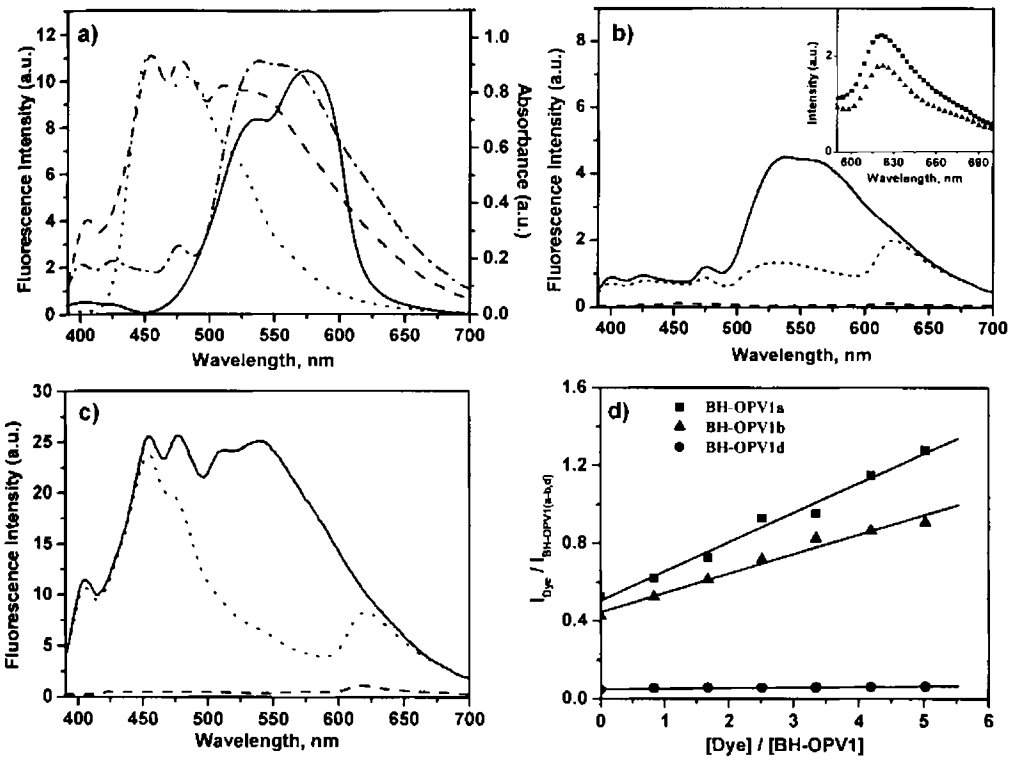

Figure 3.14. a) Emission spectra of **BH-OPV1a** (– · – · –), **BH-OPV1b** (- - -) and **BH-OPV1d** (·····), and the absorption spectrum of Rhodamine B (——). Emission spectra of b) **BH-OPV1a** (1.01 x 10^{-5} M) and c) **BH-OPV1b** (1.01 x 10^{-5} M) in the absence (——) and in the presence (·····) of Rhodamine B (8.38 x 10^{-5} M). Fluorescence of Rhodamine B (- - -) in the absence of OPVs, on excitation at 380 nm is also shown. d) Relative fluorescence intensity I_{Dye} / $I_{BH\text{-}OPV1a\text{-}b,d}$ plotted against the molar ratio **[Dye] / [BH-OPV1a-b,d]**. All spectra were recorded in dodecane-chloroform (16:1) at an excitation wavelength of 380 nm. Inset of Figure 3.14b shows the emission of the dye on indirect excitation at 380 nm (■) and direct excitation at 535 nm (▲).

The fluorescence spectra of **BH-OPV1a** in the absence and in the presence of Rhodamine B in dodecane-chloroform (16:1) when excited at 380 nm are shown in Figure 3.14b. In this solvent mixture, **BH-OPV1a** showed a broad emission with two maxima at 537 and 567 nm, characteristic of the self-assembled OPVs. In the presence of Rhodamine B, the intensity of the emission corresponding to the self-assembled **BH-OPV1a** is decreased while the emission corresponding to Rhodamine B is

appeared at 620 nm. Direct excitation of a blank solution of Rhodamine B (8.38×10^{-5} M) in the absence of OPV donor molecules at 380 nm showed a negligible fluorescence at 620 nm. Therefore, the observed emission at 620 nm is attributed to the FRET from OPV self-assembly to Rhodamine B. The inset of Figure 3.14b shows a comparison of the emission upon direct (λ_{exc} = 535 nm) and indirect excitation (λ_{exc} = 380 nm) of optically matching solutions of Rhodamine B, which indicate an enhanced emission in the latter case, due to an efficient energy transfer from the OPV self-assembly (ca. 72%) to Rhodamine B. The emission spectra of **BH-OPV1b** in the absence and presence of Rhodamine B in dodecane-chloroform (16:1) are shown in Figure 3.14c. In the absence of the acceptor, **BH-OPV1b** shows a broad emission corresponding to both the monomeric and self-assembled OPVs. When excited at 380 nm in the presence of Rhodamine B (8.38×10^{-5} M), selective quenching of the emission (ca. 63%) between 500-650 nm, corresponding to the self-assembled OPV could be seen with the concomitant emission of Rhodamine B at 620 nm. This shows that FRET occurs selectively from the self-assembled OPV molecules to the doped dye molecules. The emission between 400-480 nm of the molecularly dissolved OPVs was virtually unaffected indicating that FRET is not efficient from the unassembled OPVs. The enhanced dye emission on indirect excitation when compared to that of the direct excitation indicates that the fluorescence quenching is not due to a mere radiative energy transfer. In the case of **BH-OPV1d**, FRET was not efficient due to the weak self-assembly. Figure 3.14d shows the relative fluorescence intensity of Rhodamine B and **BH-OPV1a-b,d** ($I_{Dye}/I_{BH\text{-}OPV1a\text{-}b,d}$) when plotted against their molar ratio (**[Dye]/[BH-OPV1**), which is a measure of the efficiency of energy transfer. From the graph, it is clear that the FRET efficiency decreases in the order of

BH-OPV1a>BH-OPV1b>BH-OPV1d, which is in agreement with the self-assembling property of these molecules.

A comparison of the FRET efficiencies of **BM-OPV** and **S-OPV** in dodecane-chloroform (16:1) is shown in Figure 3.15. The emission spectrum of **BM-OPV** shows a good overlap with the absorption of Rhodamine B (Figure 3.15a). A selective quenching of the emission corresponding to the self-assembly is observed when a solution of Rhodamine B is injected into the former (Figure 3.15b). Though the methoxy derivative **BM-OPV** showed considerable energy transfer to the dye molecules in dodecane-chloroform (16:1), the efficiency (ca. 64%) was relatively low when compared to that of the bishydroxy derivative **BH-OPV1a** (Figure 3.15d). This is particularly true when **BM-OPV** was excited in the presence of Rhodamine B in cyclohexane-chloroform (16:1) (Figure 15b, inset). In this case FRET was not feasible since the self-assembly of **BM-OPV** in cyclohexane is very weak. Similarly, the model compound **S-OPV** failed to sensitize the dye emission under the same experimental conditions applied for **BH-OPV1a** and **BM-OPV** (Figure 3.15c). This is attributed to the lack of overlap between the **S-OPV** emission and the dye absorption, due to the poor self-assembling behavior of the former. Plots of the ratios between the intensities of the dye and the OPV emissions against their concentration show a maximum efficiency of FRET for **BH-OPV1a** followed by **BM-OPV** and the least for **S-OPV** (Figure 3.15d). These observations are the indication of the supramolecular control of the OPV self-assembly, and the modulation of the optical properties to facilitate FRET in the presence of an appropriate energy acceptor.

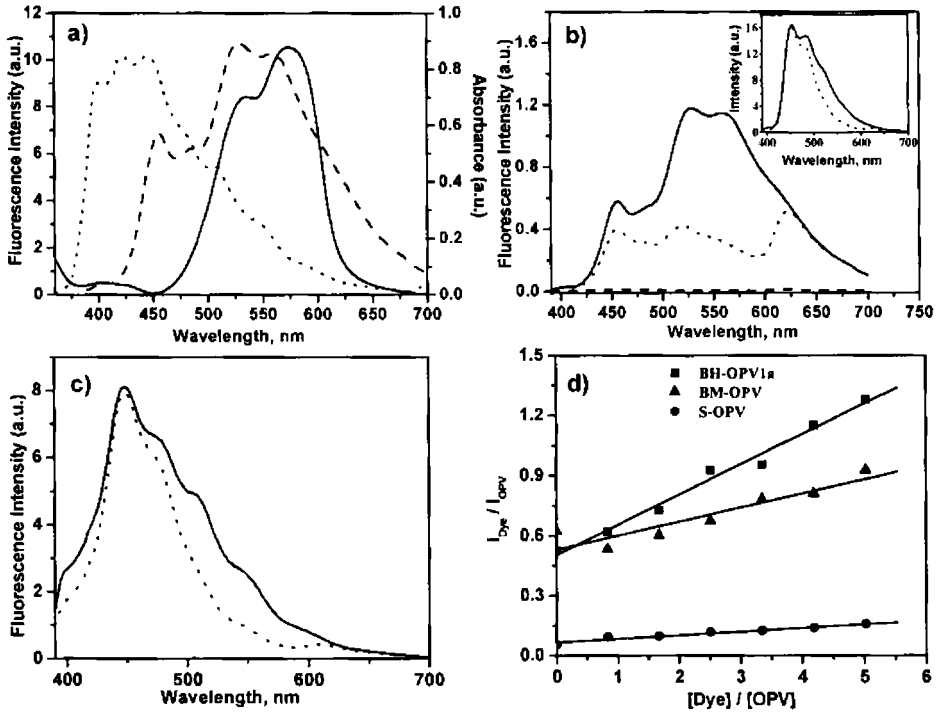

Figure 3.15. a) Emission spectra of **BM-OPV** (- - -) and **S-OPV** (·····), and the absorption spectrum of Rhodamine B (——) in dodecane-chloroform (16:1). b) Emission of **BM-OPV** (1.01 x 10^{-5} M) in the absence (——) and presence (·····) of Rhodamine B. Fluorescence of Rhodamine B (- - -) in the absence of the donor OPVs, on excitation at 380 nm is also shown. Inset shows the emission of **BM-OPV** in cyclohexane-chloroform (16:1) before (——) and after (·····) the addition of Rhodamine B. c) Emission of **S-OPV** in dodecane-chloroform (16:1) (1.01 x 10^{-5} M) in the absence (——) and presence (·····) of Rhodamine B. d) Dependence of relative fluorescence intensity I_{Dye} / I_{OPV} plotted against the molar ratio **[Dye] / [OPV]** (excitation wavelength is 380 nm).

The role of the OPV self-assembly in the selective energy transfer is further established by the solvent and temperature dependent emission studies of **BH-OPV1a**-Rhodamine B system. We have observed that FRET from the self-assembled OPVs to the entrapped Rhodamine B is strongly influenced by the nature of the solvent. This could be due to the fact that the self-assembly of OPVs is sensitive to the solvent, which in turn strongly influences the optical properties. Hence, the spectral overlap between the Rhodamine B absorbance and OPV emission vary with solvents.

For example, the emission spectrum of **BH-OPV1a** in dodecane-chloroform (16:1) is completely shifted towards the long wavelength region corresponding to the self-assembly, whereas in cyclohexane-chloroform (16:1), a broad emission with maxima at 454, 476, 527 and 561 nm was observed, indicating the co-existence of both free and self-assembled OPV chromophores. In the latter case, when excited at 380 nm in the presence of Rhodamine B (8.38×10^{-5} M), selective quenching of the emission (ca. 63%) between 500-650 nm, corresponding to the self-assembled OPV could be seen with the concomitant emission of Rhodamine B at 620 nm (Figure 3.16a). The selective energy transfer from the self-assembled OPVs is more clear when **BH-OPV1a** in cyclohexane-chloroform (16:1) is selectively excited at 470 nm. Figure 3.16b shows the relative fluorescence intensity of Rhodamine B and **BH-OPV1a** ($I_{Dye}/I_{BH\text{-}OPV1a}$) when plotted against their molar ratio (**[Dye]/[BH-OPV1a]**) in dodecane-chloroform and cyclohexane-chloroform, which showed an enhanced efficiency in the former case.

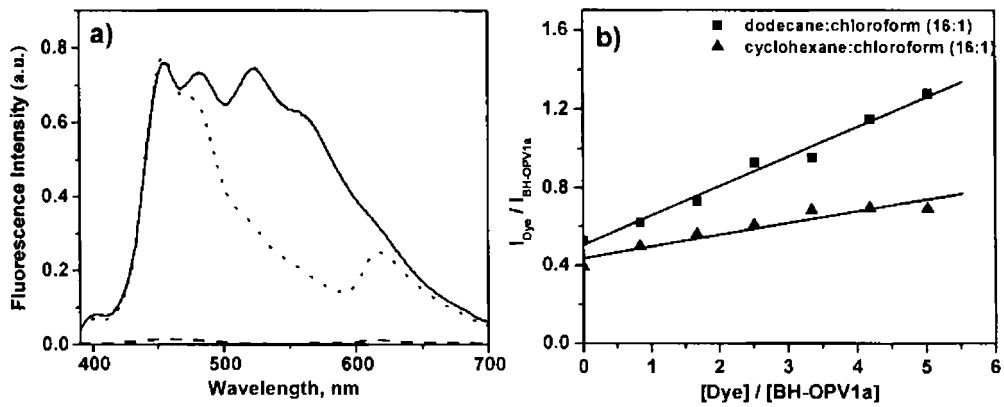

Figure 3.16. a) FRET quenching of the fluorescence of **BH-OPV1a** (1.01×10^{-5} M) in the presence of Rhodamine B (8.38×10^{-5} M) in cyclohexane-chloroform (16:1) solvent mixture. Fluorescence of **BH-OPV1a** (——), fluorescence of **BH-OPV1a** + Rhodamine B (·····) and fluorescence of Rhodamine B (- - -). b) Dependence of relative fluorescence intensity I_{Dye} / $I_{BH\text{-}OVP1a}$ plotted against the molar ratio **[Dye] / [BH-OPV1a]** in various solvents. Excitation wavelength is 380 nm in all cases.

The temperature dependent emission studies of **BH-OPV1a** in the absence and in the presence of Rhodamine B in dodecane-chloroform are shown in Figures 3.17a and 3.17b, respectively. When cooled from 55 °C to 20 °C, the emission corresponding to the monomeric species is significantly quenched with the formation of a red shifted emission corresponding to the self-assembled species (Figure 3.17a). However, when excited at 380 nm, in the presence of Rhodamine B at 20 °C, the emission corresponding to the self-assembled species is quenched and the dye emission is observed at 620 nm (Figure 3.17b). Upon gradual increase of the temperature, the dye emission at 620 nm is gradually decreased with the concomitant increase of the molecularly dissolved OPV emission at 455 nm and 483 nm. Intensities of the dye emission between 600-700 nm at different temperatures are shown in the inset of Figure 3.17b. Increasing the temperature up to 55 °C resulted in the complete disappearance of the dye emission and the complete recovery of the free OPV emission. A comparison of Figures 3.17a and 3.17b, reveals that the absence of the OPV self-assembly emission and the presence of Rhodamine B emission in Figure 3.17b is due to the FRET from the former to the latter. Since the energy transfer between the donor and acceptor usually occurs independent of the temperature, the observed temperature dependent energy transfer is the result of the thermoreversible breaking and forming of the OPV supramolecular self-assembly. This observation highlights the importance of the supramolecular organization of chromophores in facilitating the FRET process.

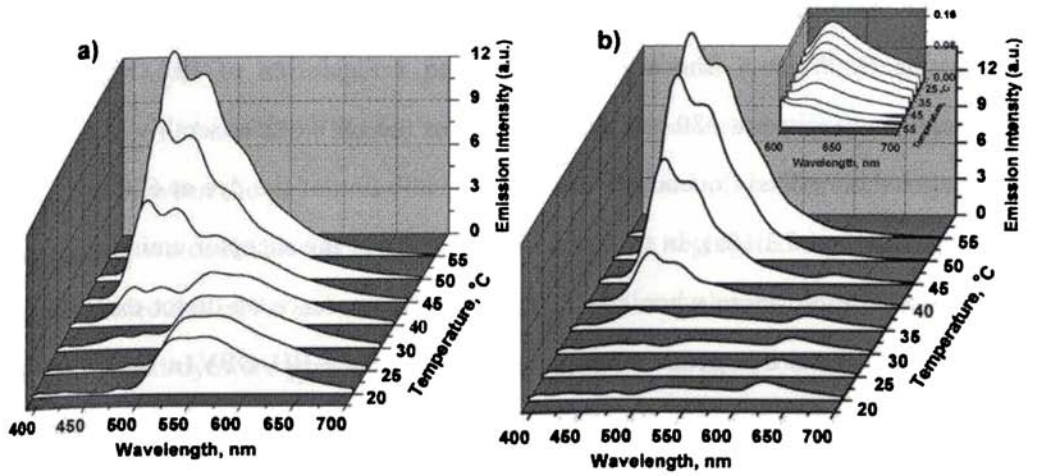

Figure 3.17. Temperature dependent emission spectra of **BH-OPV1a** (1.01 X 10^{-5} M) a) in the absence of Rhodamine B (8.38 x 10^{-5} M) and b) in the presence of Rhodamine B in dodecane-chloroform (16:1) between 20 °C and 55 °C. Inset of Figure 3.17b shows the decrease in Rhodamine B emission on increasing the temperature.

One of the major limitations of the present system, though FRET is specific and efficient from the self-assembled state, is the noncompatibility of the polar cationic Rhodamine B with the OPV self-assembly in nonpolar solvents. Due to this reason, most of the dye injected into the OPV self-assembly may undergo aggregation and phase separation in the solvent and hence only a small amount of the dye may be entrapped into the OPV self-assembly. It must be noted here that the emission quantum yields of Rhodamine B in dodecane and cyclohexane are relatively very weak due to the aggregation of the dye in these solvents. Therefore, the intensity of the FRET emission which occurs from OPV self-assembly to Rhodamine B aggregates in dodecane or cyclohexane is weak. However, this problem could be successfully overcome by performing the FRET experiments in the xerogel films. When a film of **BH-OPV1a** is excited at 380 nm, the emission was completely shifted to the long wavelength region around 530 and 560 nm, corresponding to the self-

assembled species, which completely overlaps with the absorption spectrum of Rhodamine B. When a Rhodamine B dispersed xerogel film of **BH-OPV1a** (1:2 molar ratio) is excited at 380 nm, the emission of the OPV self-assembly at 530-560 nm is almost completely quenched and a strong emission of the dye at 620 nm could be observed (Figure 3.18a). In this case, the intensity of the acceptor emission at 620 nm is almost 6 fold more when compared to the fluorescence on direct excitation at 535 nm even if the dye concentration is only half of the **BH-OPV1a** concentration (Figure 3.18b). Excitation of a Rhodamine B film in the absence of **BH-OPV1a** at 380 nm resulted in a weak emission indicating that the strong emission of Rhodamine B when entrapped in the self-assembled film is due to FRET.

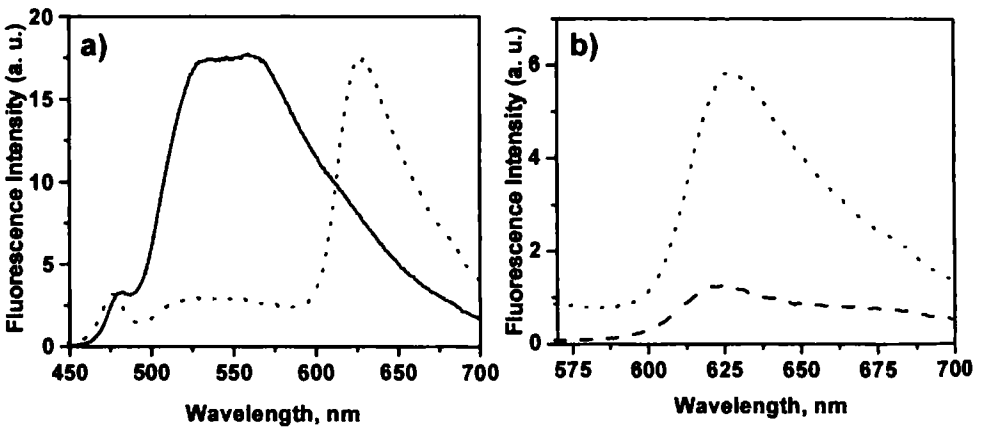

Figure 3.18. a) Normalized emission from the film of **BH-OPV1a** (——) and film of **BH-OPV1a** + Rhodamine B (·····) (2:1 ratio) on excitation at 380 nm. b) Comparison of the FRET emission of Rhodamine B (·····) at 380 nm excitation with the emission on direct excitation at 535 nm (-----).

The physical pictures of the **BH-OPV1a** gel before and after entrapping with Rhodamine B and the corresponding morphologies under AFM and SEM analyses are shown in Figure 3.19. The morphology changes observed after the addition indicate that the aggregated and phase separated dye molecules got entrapped between the

interstitial sites of the fibers. SEM pictures of the dried decane gels before and after loading the dye are shown in Figures 3.19d, 3.19e and 3.19f, respectively. As observed in AFM and SEM studies, most of the dye molecules are aggregated and got deposited between the gel fibers when the solvent is dried off before the analyses. In some cases, we could also observe the presence of the segregated nanoaggregates of the dye molecules in the gel matrix (Figure 3.19f). These pictures reveal that most of the aggregated dyes are present between the entangled fibers. Probably, only a small amount of the dye may be entrapped into the OPV self-assembly. This means that the polar dye molecules prefer to be outside of the nonpolar OPV units. Though the self-assembled OPV fibers are nonpolar, they have polar hydroxymethyl channels and some of the dye aggregates may escape to these polar channels as shown in Figure 3.20. The energy transfer occurs preferably to the entrapped dye aggregates within the polar channels and not to the dye which is present as aggregates outside the fibers. Therefore, an excess of the dye is needed for the better energy transfer in cyclohexane and dodecane. However in the case of the dye doped xerogel film, majority of the dye molecules are in close contact with the self-assembled OPV fibers, which are within the Föster radii. This could be the reason for the enhanced efficiency in FRET even at low dye concentrations.

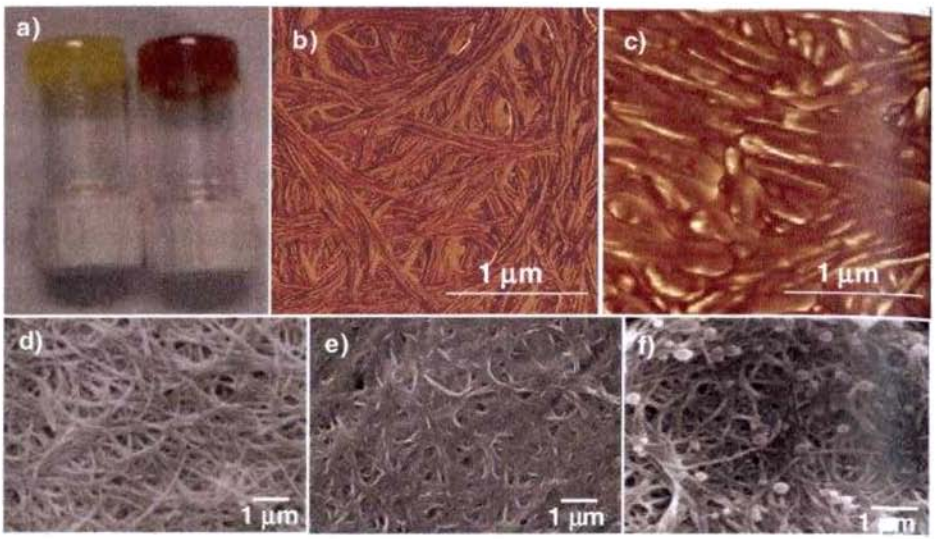

Figure 3.19. a) Photograph of the **BH-OPV1a** gel from decane before and after doping with Rhodamine B. b) and c) are the AFM images of the dried **BH-OPV1a** gel before and after the loading of Rhodamine B, respectively. d) SEM picture before adding the dye. e) and f) SEM pictures after adding the dye.

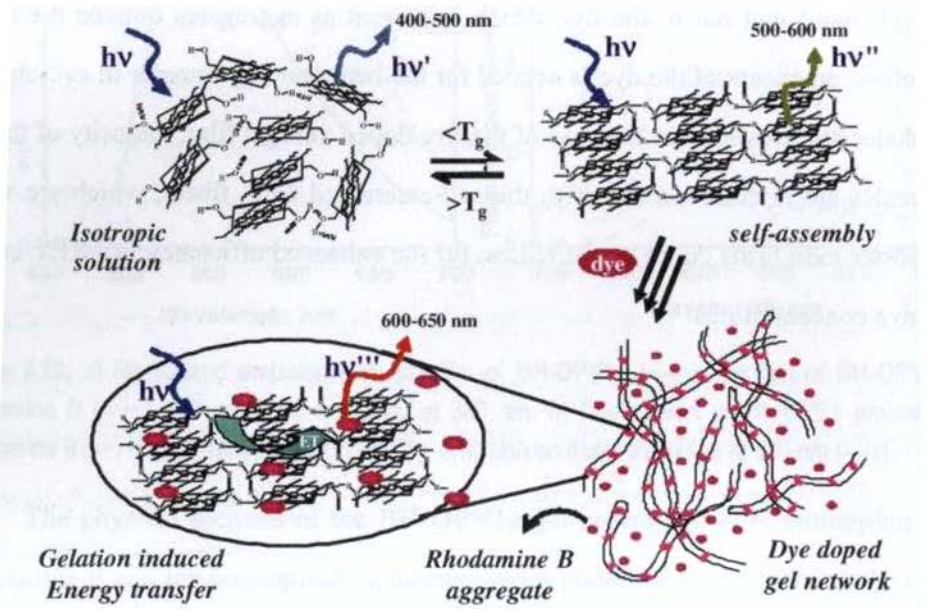

Figure 3.20. Self-assembly induced modulation of OPV emission in the design of a dye entrapped light harvesting gel.

3.3. Conclusions

The unique photophysical properties of phenylenevinylenes, particularly their strong emission characteristics are of great advantage to provide insight into the role of self-assembly in the observed thermoreversible sol-gel phenomena. The absorption and emission properties of OPV organogelators showed dramatic changes upon self-assembly and gelation, indicating the strong intermolecular π-electronic coupling between the OPV chromophores in the self-assembled gel phase. The close resemblance of the self-assembled phase and the solid phase optical properties revealed the nearly identical arrangement of OPV chromophores in both the phases. The structure of the OPVs, solvents and temperature play considerable role in the self-assembly and gelation processes, which in turn strongly influence on their optical properties. From the absorption and emission data, **BH-OPV1a** with hexadecyl side chains showed maximum stability for the self-assembly which decreased in the order **BH-OPV1a** > **BH-OPV1b** > **BH-OPV1c**. Though the methoxy derivative **BM-OPV** forms aggregates in dodecane, it is less stable due to the absence of the directional H-bonding interactions, whereas **S-OPV** with no end functional groups could only form aggregates, which could not gelate any of the solvents. The strong modulation of the emission properties of the OPVs as a result of the self-assembly has been used for the selective energy transfer exclusively from the self-assembly via FRET to entrapped Rhodamine B dyes. Direct energy transfer from isotropic OPV solution was not feasible. FRET is found to be efficient from a xerogel film than from the dodecane or cyclohexane gels of OPVs. More importantly, the energy transfer could be thermally controlled by the reversible self-assembling properties of the OPVs. The results described here show the importance of supramolecular organization of chromophores

in facilitating the energy transfer and is the first example of an organogelator, acting itself as an energy donor in a light harvesting assembly.

3.4. Experimental Section

3.4.1. General Procedure for Energy Transfer Studies

Energy transfer experiments were carried out in cyclohexane-chloroform or dodecane-chloroform solvent mixtures (16:1). The solutions for the optical studies were prepared by adding appropriate concentration of dye in 0.2 mL chloroform to 3 mL cyclohexane or dodecane solution of OPV. For energy transfer studies in the gel state, OPVs were dissolved in cyclohexane or dodecane containing small amount of chloroform (16:1) at their critical gelator concentrations. Rhodamine B in chloroform was injected to this and the solution was kept to allow gelation. Energy transfer in the film form was performed by casting a film of the appropriate OPV containing 10-50 mol% of Rhodamine B from chloroform or toluene. The film was dried before recording the emission spectra.

3.4.2. Description on Experimental Techniques

Optical Measurements. Electronic absorption spectra were recorded on a Shimadzu UV-3101 PC NIR scanning spectrophotometer and the emission spectra were recorded on a SPEX-Fluorolog F112X spectrofluorimeter. Temperature dependent studies were carried out either in a 1 cm or 0.1 cm quartz cuvette with a thermistor directly attached to the wall of the cuvette holder. Fluorescence spectra of optically dilute solutions were recorded from 390-700 nm at the excitation wavelengths of 380 and 470 nm. Fluorescence spectra of the xerogel films were recorded using the front face geometry.

Quantum Yield Measurements. Fluorescence quantum yields of molecularly dissolved OPV molecules upon excitation at 380 nm are reported relative to quinine sulfate (Φ_f = 0.546), whereas the quantum yields of self-assembled molecules are reported relative to Rhodamine 6G (Φ_f = 0.9). The experiments were done using optically matching solutions and the quantum yield is calculated using Equation 1.

$$\Phi_f = \Phi_r (A_r F_s / A_s F_r) (\eta_s^2 / \eta_r^2) \quad \ldots\ldots\ldots\ldots\ldots\ldots \quad (1)$$

where, A_s and A_r are the absorbance of the sample and reference solutions, respectively at the same excitation wavelength, F_s and F_r are the corresponding relative integrated fluorescence intensities and η is the refractive index of the solvent.

Single Photon Counting Experiments. Fluorescence lifetimes were measured using a Tsunami Spectra Physics picosecond single photon counting system. Ti Sapphire laser, having a fundamental wavelength of 934 nm, was used as the excitation source. The average output power is 680 mW with a pump power of 4.5 W. The pulse-width of the laser is <2 ps. Fluorescence lifetimes were determined by deconvoluting the instrumental function with single, bi or triexponential decay and minimizing the χ^2 values of the fit to 1 ± 0.1.

Atomic Force Microscopy. Atomic Force Microscopy images were recorded under ambient conditions using a Digital Instrument Multimode Nanoscope IV operating in the tapping mode regime. Micro-fabricated silicon cantilever tips (NSG01/Pt) with a resonance frequency of approximately 150 kHz and a spring constant of about 5.5 Nm^{-1} were used. The scan rate varied from 0.5 to 1.5 Hz. The set-point amplitude ratio ($r_{sp} = A_{sp}/A_o$, where A_{sp} is the amplitude setpoint, and A_o is the amplitude of the free oscillation) was adjusted to 0.9. All AFM images shown here were subjected to a first-

order plane-fitting procedure to compensate for sample tilt. AFM analysis was done offline. AFM samples were prepared by drop casting the OPV solution before and after adding Rhodamine B on freshly cleaved muscovite mica.

Scanning Electron Microscopy. Gel samples for the SEM analysis were prepared by dissolving the required amount of OPV in decane, cyclohexane or toluene. Into this, the required amount of Rhodamine B in chloroform is injected and the solution was cooled to room temperature. Sheared gels were placed on sample studs and coated with gold by ion sputtering. SEM pictures were obtained either on a JEOL 5600 LV scanning electron microscope with an accelerating voltage of 10 kV, or a Hitachi S 2004 at an accelerating voltage of 15 kV.

3.5. References

1. (a) Tour, J. M. *Chem. Rev.* **1996**, *96*, 537. (b) Müllen, K.; Wegner, G. *Electronic Materials; The Oligomer Approach*; VCH: Weinheim, Germany, 1998. (c) Martin, R. E.; Diederich, F. *Angew. Chem. Int. Ed.* **1999**, *38*, 1350. (d) Watson, M. D.; Fechtenkötter, A.; Müllen, K. *Chem. Rev.* **2001**, *101*, 1267.

2. (a) Yu, G.; Gao, J.; Hummelen, J. C.; Wudl, F.; Heeger, A. J. *Science* **1995**, *270*, 1789. (b) Halls, J. J. M.; Walsh, C. A.; Greenham, N. C.; Marseglia, E. A.; Friend, R. H.; Moratti, S. C.; Holmes, A. B. *Nature* **1995**, *376*, 498. (c) Brabec, C. J.; Sariciftci, N. S.; Hummelen, J. C. *Adv. Funct. Mater.* **2001**, *11*, 15. (d) Ramos, A. M.; Rispens, M. T.; van Duren, J. K. J.; Hummelen, J. C.; Janssen, R. A. J. *J. Am. Chem. Soc.* **2001**, *123*, 6714.

3. (a) Horowitz, G. *Adv. Mater.* **1998**, *10*, 365. (b) Sirringhaus, H.; Brown, P. J.; Friend, R. H.; Nielsen, M. M.; Bechgaard, K.; Langeveld-Voss, B. M. W.; Spiering, A. J. H.; Janssen, R. A. J.; Meijer, E. W.; Herwig, P.; de Leeuw, D. M. *Nature* **1999**, *401*, 685. (c) Cornil, J.; Beljonne, D.; Calbert, J.-P.; Brédas, J.-L. *Adv. Mater.* **2001**, *13*, 1053.

4. (a) Burroughes, J. H.; Bradley, D. D. C.; Brown, A. R.; Marks, R. N.; Mackay, K.; Friend, R. H.; Burns, P. L.; Holmes, A. B. *Nature* **1990**, *347*, 539. (b) Kraft, A.; Grimsdale, A. C.; Holmes, A. B. *Angew. Chem. Int. Ed.* **1998**, *37*, 402. (c) Friend, R. H.; Gymer, R. W.; Holmes, A. B.; Burroughes, J. H.; Marks, R. N.; Taliani, C.; Bradley, D. D. C.; Santos, D. A. D.; Brédas, J. L.; Lögdlund, M.; Salaneck, W. R. *Nature* **1999**, *397*, 121.

5. (a) Tian, B.; Zerbi, G.; Schenk, R.; Müllen, K. *J. Chem. Phys.* **1991**, *95*, 3191. (b) Cornil, J.; Beljonne, D.; Shuia, Z.; Hagler, T. W.; Campbell, I.; Bradley, D. D. C.; Brédas, J. L.; Spangler, C. W.; Müllen, K. *Chem. Phys. Lett.* **1995**, *247*, 425. (c) Barth, S.; Bässler, H.; Wehrmeister, T.; Müllen, K. *J. Chem. Phys.* **1997**, *106*, 321.

6. (a) Peeters, E.; Ramos, A. M.; Meskers, S. C. J.; Janssen, R. A. J. *J. Chem. Phys.* **2000**, *112*, 9445. (b) Peeters, E.; van Hal, P. A.; Knol, J.; Brabec, C. J.; Sacriciftci, N. S.; Hummelen, J. C.; Janssen, R. A. J. *J. Phys. Chem. B* **2000**, *104*, 10174. (c) El-ghayoury, A.; Schenning, A. P. H. J.; van Hal, P. A.; van Duren, J. K. J.; Janssen, R. A. J.; Meijer, E. W. *Angew. Chem. Int. Ed.* **2001**, *40*, 3660.

7. (a) Gaylord, B. S.; Wang, S.; Heeger, A. J.; Bazan, G. C. *J. Am. Chem. Soc.* **2001**, *123*, 6417. (b) Robinson, M. R.; Wang, S.; Heeger, A. J.; Bazan, G. C. *Adv. Funct. Mater.* **2001**, *11*, 413.

8. (a) Stalmach, U.; Kolshorn, H.; Brehm, I.; Meier, H. *Liebigs Ann.* **1996**, 1449. (b) Gebhardt, V.; Bacher, A.; Thelakkar, M.; Stalmach, U.; Meier, H.; Schmidt, H.-W.; Haarer, D. *Adv. Mater.* **1999**, *11*, 119. (c) Meier, H.; Gerold, J.; Kolshorn, H.; Baumann, W.; Bletz, M. *Angew. Chem. Int. Ed.* **2002**, *41*, 292.

9. Self-assembly of π-conjugated oligomers: (a) Nelson, J. C.; Saven, J. G.; Moore, J. S.; Wolynes, P. G. *Science* **1997**, *277*, 1793. (b) Moore, J. S. *Acc. Chem. Res.* **1997**, *30*, 402. (c) Schoonbeek, F. S.; van Esch, J. H.; Wegewijs, B.; Rep, D. B. A.; de Haas, M. P.; Klapwijk, T. M.; Kellogg, R. M.; Feringa, B. L. *Angew. Chem. Int. Ed.* **1999**, *38*,

1393. (d) Brunsveld, L.; Meijer, E. W.; Prince, R. B.; Moore, J. S. *J. Am. Chem. Soc.* **2001**, *123*, 7978.

10. Self-assembly of π-conjugated polymers: (a) McQuade, D. T.; Kim, J.; Swager, T. M. *J. Am. Chem. Soc.* **2000**, *122*, 5885. (b) McQuade, D. T.; Hegedus, A. H.; Swager, T. M. *J. Am. Chem. Soc.* **2000**, *122*, 12389. (c) Bunz, U. H. F. *Chem. Rev.* **2000**, *100*, 1605. (d) Bunz, U. H. F. *Acc. Chem. Res.* **2001**, *34*, 998. (e) Levitus, M.; Schmieder, K.; Ricks, H.; Shimizu, K. D.; Bunz, U. H. F.; Garcia-Garibay, M. A. *J. Am. Chem. Soc.* **2001**, *123*, 4259. (f) Kim, J.; Swager, T. M. *Nature* **2001**, *411*, 1030. (g) Arnt, L.; Tew, G. N. *J. Am. Chem. Soc.* **2002**, *124*, 7664. (h) Breitenkamp, R. B.; Tew, G. N. *Macromolecules* **2004**, *37*, 1163.

11. (a) Schenning, A. P. H. J.; Jonkheijm, P.; Peeters, E.; Meijer, E. W. *J. Am. Chem. Soc.* **2001**, *123*, 409. (b) Schenning, A. P. H. J.; van Herrikhuyzen, J.; Jonkheijm, P.; Chen, Z.; Würthner, F.; Meijer, E. W. *J. Am. Chem. Soc.* **2002**, *124*, 10252. (c) Jonkheijm, P.; Hoeben, F. J. M.; Kleppinger, R.; van Herrikhuyzen, J.; Schenning, A. P. H. J.; Meijer, E. W. *J. Am. Chem. Soc.* **2003**, *125*, 15941.

12. (a) Percec, V.; Glodde, M.; Bera, T. K.; Miura, Y.; Shiyanovskaya, I.; Singer, K. D.; Balagurusamy, V. S. K.; Heiney, P. A.; Schnell, I.; Rapp, A.; Spiess, H.-W.; Hudson, S. D.; Duan, H. *Nature* **2002**, *419*, 384. (b) Meijer, E. W.; Schenning, A. P. H. J. *Nature* **2002**, *419*, 353.

13. (a) Fuhrhop, J.-H.; Demoulin, C.; Boettcher, C.; Koening, J.; Siggel, U. *J. Am. Chem. Soc.* **1992**, *114*, 4159. (b) Biemans, H. A. M.; Rowan, A. E.; Verhoeven, A.; Vanoppen, P.; Latterini, L.; Foekema, J.; Schenning, A. P. H. J.; Meijer, E. W.; De Schryver, F. C.; Nolte, R. J. M. *J. Am. Chem. Soc.* **1998**, *120*, 11054. (c) Würthner, F.; Thalacker, C.; Sautter, A. *Adv. Mater.* **1999**, *11*, 754. (d) Würthner, F.; Thalacker, C.; Sautter, A.; Schärtl, W.; Ibach, W.; Hollricher, O. *Chem. Eur. J.* **2000**, *6*, 3871. (e) Kimura, M.; Muto, T.; Takimoto, H.; Wada, K.; Ohta, K.; Hanabusa, K.; Shirai, H.; Kobayashi, N. *Langmuir* **2000**, *16*, 2078. (f) Sautter, A.; Schmid, D. G.; Jung, G.;

Würthner, F. *J. Am. Chem. Soc.* **2001**, *123*, 5424. (g) Prins, L. J.; Thalacker, C.; Würthner, F.; Timmerman, P.; Reinhoudt, D. N. *Proc. Natl. Acad. Sci. U. S. A.* **2001**, *98*, 10042. (h) Würthner, F.; Sautter, A. *Org. Biomol. Chem.* **2003**, *1*, 240. (i) Yamaguchi, T.; Ishii, N.; Tashiro, K.; Aida, T. *J. Am. Chem. Soc.* **2003**, *125*, 13934. (j) Kimura, M.; Kuroda, T.; Ohta, K.; Hanabusa, K.; Shirai, H.; Kobayashi, N. *Langmuir* **2003**, *19*, 4825.

14. Reviews on H-bonded donor-acceptor systems: (a) Ward, M. D. *Chem. Soc. Rev.* **1997**, *26*, 365. (b) Hunter, C. A.; Hyde, R. K. *Angew. Chem. Int. Ed.* **1996**, *35*, 1936.

15. (a) Devadoss, C.; Bharathi, P.; Moore, J. S. *J. Am. Chem. Soc.* **1996**, *118*, 9635. (b) Wang, P.-W.; Liu, Y.-J.; Devadoss, C.; Bharathi, P.; Moore, J. S. *Adv. Mater.* **1996**, *8*, 237. (c) Stewart, G. M.; Fox, M. A. *J. Am. Chem. Soc.* **1996**, *118*, 4354. (d) Jiang, D.-L.; Aida, T. *Nature* **1997**, *388*, 454. (e) Plevoets, M.; Vögtle, F.; De Cola, L.; Balzani, V. *New J. Chem.* **1999**, *23*, 63. (f) Gilat, S. L.; Adronov, A.; Fréchet, J. M. J. *Angew. Chem. Int. Ed.* **1999**, *38*, 1422. (g) Adronov, A.; Fréchet, J. M. J. *Chem. Commun.* **2000**, 1701. (h) Choi, M.-S.; Aida, T.; Yamazaki, T.; Yamazaki, I. *Angew. Chem. Int. Ed.* **2001**, *40*, 3194.

16. (a) Nowakowska, M.; Foyle, V. P.; Guillet, J. E. *J. Am. Chem. Soc.* **1993**, *115*, 5975. (b) Watkins, D. M.; Fox, M. A. *J. Am. Chem. Soc.* **1994**, *116*, 6441. (c) Schultze, X.; Serin, J.; Adronov, A.; Fréchet, J. M. J. *Chem. Commun.* **2001**, 1160. (d) Kuroda, K.; Swager, T. M. *Macromolecules* **2004**, *37*, 716.

17. Dutton, P. J.; Conte, L. *Langmuir* **1999**, *15*, 613.

18. Chrisstoffels, L. A. J.; Adronov, A.; Fréchet, J. M. J. *Angew. Chem. Int. Ed.* **2000**, *39*, 2163.

19. (a) Armaroli, N.; Barigelletti, F.; Ceroni, P.; Eckert, J.-F.; Nicoud, J.-F.; Nierengarten, J.-F. *Chem. Commun.* **2000**, 599. (b) Eckert, J.-F.; Nicoud, J.-F.; Nierengarten, J.-F.; Liu, S.-G.; Echegoyen, L.; Barigelletti, F.; Armaroli, N.; Ouali, L.; Krasnikov, V.; Hadziioannou, G. *J. Am. Chem. Soc.* **2000**, *122*, 7467. (c) Peeters, E.; van Hal, P. A.;

Knol, J.; Brabec, C. J.; Sariciftci, N. S.; Hummelen, J. C.; Janssen, R. A. J. *J. Phys. Chem. B* **2000**, *122*, 10174. (d) El-ghayoury, A.; Schenning, A. P. H. J.; van Hal, P. A.; van Duren, J. K. J.; Janssen, R. A. J.; Meijer, E. W. *Angew. Chem. Int. Ed.* **2001**, *40*, 3660. (e) Ramos, A. M.; Meskers, S. C. J.; van Hal, P. A.; Knol, J.; Hummelen, J. C.; Janssen, R. A. J. *J. Phys. Chem. A* **2003**, *107*, 9269.

20. Armaroli, N.; Eckert, J.-F.; Nierengarten, J.-F. *J. Chem. Soc., Chem. Commun.* **2000**, 2105.

21. (a) Bolivar, P. H.; Wegmann, G.; Kersting, R.; Deussen, M.; Lemmer, U.; Mahrt, R. F.; Bässler, H.; Göbel, E. O.; Kurz, H. *Chem. Phys. Lett.* **1995**, *245*, 534. (b) Schenning, A. P. H. J.; Peeters, E.; Meijer, E. W. *J. Am. Chem. Soc.* **2000**, *122*, 4489. (c) Morgado, J.; Cacialli, F.; Iqbal, R.; Moratti, S. C.; Holmes, A. B.; Yahioglu, G.; Milgrom, L. R.; Friend, R. H. *J. Mater. Chem.* **2001**, *11*, 278. (d) Brunner, K.; van Haare, J. A. E. H.; Langeveld-Voss, B. M. W.; Schoo, H. F. M.; Hofstraat, J. W.; van Dijken, A. *J. Phys. Chem. B.* **2002**, *106*, 6834.

22. (a) Hoeben, F. J. M.; Herz, L. M.; Daniel, C.; Jonkheijm, P.; Schenning, A. P. H. J.; Silva, C.; Meskers, S.; Beljone, D.; Phillips, R. T.; Friend, R. H.; Meijer, E. W. *Angew. Chem. Int. Ed.* **2004**, *43*, 1976.

23. (a) Nakashima, T.; Kimizuka, N. *Adv. Mater.* **2002**, *14*, 1113. (b) Sagawa, T.; Fukugawa, S.; Yamada, T.; Ihara, H. *Langmuir* **2002**, *18*, 7223. (c) Sugiyasu, K.; Fujita, N.; Takeuchi, M.; Yamada, S.; Shinkai, S. *Org. Biomol. Chem.* **2003**, *1*, 895. (d) Sugiyasu, K.; Fujita, N.; Shinkai, S. *Angew. Chem. Int. Ed.* **2004**, *43*, 1229.

24. The fraction of the aggregated species (α) at each temperatures were calculated on the assumption that in nonpolar solvents such as dodecane, all the OPV molecules are in the self-assembled phase at temperatures less than 15 °C and in the molecularly dissolved phase at temperatures greater than 65 °C.

Chapter 4

Helical Nanostructures of Chiral Oligo(*p*-phenylenevinylene) Derived Organogels

Abstract

Crafting of helical coiled-coil gel nanostructures via the self-assembly of chiral oligo(p-phenylenevinylene)s ***(COPV1-3)*** *having remote chiral handles is described. The chiral side chains account for a bias of helicity by transferring the chiral information to the self-assembled chromophores as evidenced by the exciton coupled CD signal corresponding to the absorption maximum of the chromophore. The hierarchical helical growth of* ***COPV2*** *into coiled-coil gel nanostructures is accompanied by an interesting observation of concentration and temperature dependent helix transition, reminiscent of the multistate folding and unfolding of the helical assemblies of biological macromolecules. Using the 'sergeant and soldiers' experiments with a mixture of chiral* ***(COPV2-3)*** *and achiral* ***(BH-OPV1a-b)*** *OPVs, it was shown that supramolecular chirality and helicity could be induced in the resulting co-assembled gel network. The helical nature of the gel nanostructures are established from the electron microscopic and AFM studies. While the observed helicity and the CD signals account for the formation of left-handed assemblies in the case of the homochiral OPVs, the induced chirality of the co-assemblies showed the opposite screw sense in the CD spectra. However, the SEM images showed the presence of the more stable left-handed helical morphology for higher order assemblies.*

4.1. Introduction

Nature utilizes directional noncovalent supramolecular interactions to create helical and multiple helical complex architectures such as DNA double helix, the collagen triple helix, the α-coiled coil of myosin and the protein coating of tobacco mosaic virus, which are responsible for the control of biological functions. Using nature's self-assembly principles, chemists have been trying to design artificial supramolecular assemblies with definite shape and properties. Use of chiral molecules as building blocks to create helical supramolecular assembly is therefore a topic of considerable interest. The self-assembly of molecules or polymers into overall chiral self-assembled architectures with single handedness is referred as supramolecular chirality. The supramolecular chirality of biomolecules is determined by the configuration of the chiral centers present in their nucleotide or peptide backbone, which can bias the long range overall order to a single handedness in a well-defined self-assembled architecture. This intriguing phenomenon of generation of homochiral supramolecular architectures by nature has fascinated chemists to explore the ability of noncovalent forces such as H-bonding, π-π stacking and van der Waals interactions in chiral molecules to form a variety of aesthetically appealing helical supramolecular assemblies.[1-9]

Peripheral chiral centers present in the side chains attached to synthetic molecules are known to express chirality at the supramolecular level. The resultant chiral induction could be monitored via CD spectroscopy and electron microscopy. An isolated UV/Vis-active chromophore provided with a chiral side chain does not feature a Cotton effect, as the remote chiral center cannot influence the absorption of the two helical components of light by the chromophore. However, when the molecules self-assemble into an organized supramolecular architecture, the chiral side

chains can induce a bias of one of the supramolecular diastereomers thereby expressing chirality in the chromophore stack in a helical sense that will eventually lead to a Cotton effect.

The groups of Moore and Meijer have made significant contributions to the helical self-assembly of π-conjugated oligomers derived from phenyleneethynylenes[10] and phenylenevinylenes,[11] respectively where the chirality of the attached side chains are expressed to the conjugated oligomer backbone at a supramolecular level. A series of *m*-phenyleneethynylene oligomers containing either chiral polar (2*S*)-methyl-3,6,9-trioxadecyloxy side chains (**1**) or chiral apolar (*S*)-3,7-dimethyl-1-octyloxy side chains (**2**) have been synthesized and studied in detail by Moore *et al.* The oligomers are present in a random coil conformation in chloroform. However, under solvophobically driven conditions, they fold in a stepwise process via helical conformations into chiral helices, which will further undergo intermolecular stacking resulting in helical columns (Figure 4.1a). Meijer and coworkers have studied in detail the hierarchical self-organization of uriedo-*s*-triazine substituted OPVs (**3**) into helical stacks as a cooperative effect of π-π interactions and quadruple H-bonding interactions (Figure 4.1b).[11a]

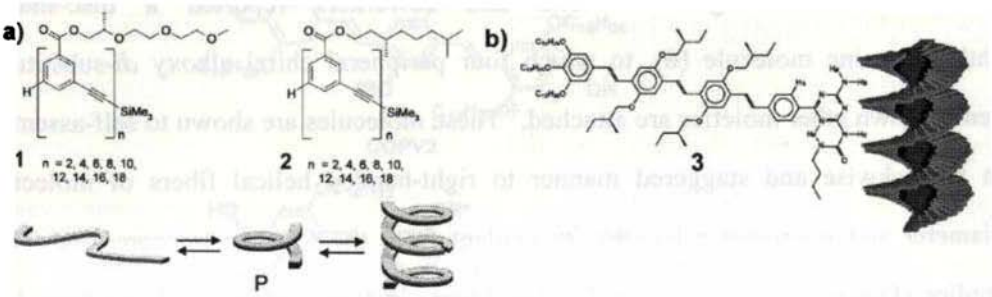

Figure 4.1. Schematic representations of the a) solvophobically induced stacking of *m*-phenyleneethynylene oligomers and b) H-bond and π-stack directed self-assembly of phenylenevinylene oligomers.

A variety of helical gels based on chiral self-assembling cores such as cholesterol,[12] and chiral hydrogen bond donor/acceptor groups such as urea,[13] amide,[14] and carbohydrates[15] have been reported. In an interesting report, Oda *et al.* describe the evolution of helical gel nanostructures of a gemini surfactant (**4**) based helical gel nanostructures, the helicity of which can be tuned by the introduction of opposite handed chiral counter anions such as tartrates (**5**) (Figure 4.2).[7,16]

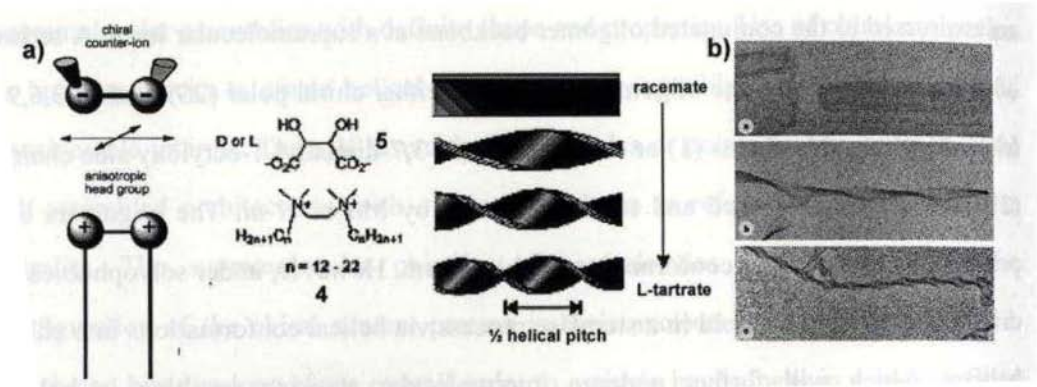

Figure 4.2. a) Schematic representation and b) TEM images of the tuning of helical ribbons in gemini surfactant (**4**) derived organogels, by the addition of chiral counter anions (**5**).

There are several examples where supramolecular chirality is elegantly expressed to create helical and multiple helical nanostructures derived from chromophore based gels.[4,17] Nolte and coworkers reported a disc-shaped phthalocyanine molecule (**6**), to which four peripheral chiral alkoxy *di*-substituted benzo crown ether moieties are attached.[4] These molecules are shown to self-assemble in a clockwise and staggered manner to right-handed helical fibers of molecular diameter and micrometer lengths, as evident from the CD spectroscopy and TEM studies (Figure 4.3). These right-handed fibers, in turn, self-assemble to form left-handed coiled-coil helices, the helicity of which could be controlled by complexing the peripheral crown ether groups with K^+ ions.

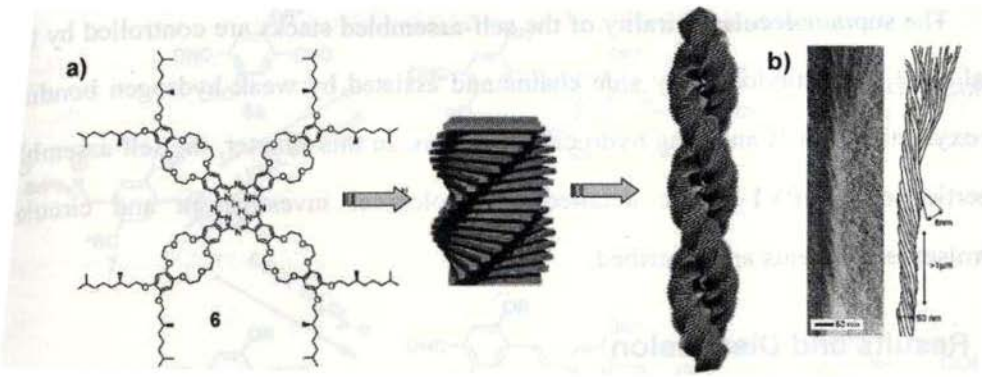

Figure 4.3. a) Hierarchical self-assembly of phthalocyanine disc-shaped molecules to coiled-coil helical nanostructures and b) TEM images of the coiled-coil fiber bundles.

In the light of the microscopic data obtained for the OPV gels, which showed the presence of randomly twisted nanostructures with no helical sense, we got interested to the design and properties of OPV based helical gels. For this purpose, chiral OPV derivatives **COPV1-3** (Chart 4.1) are synthesized and characterized by spectral analysis.

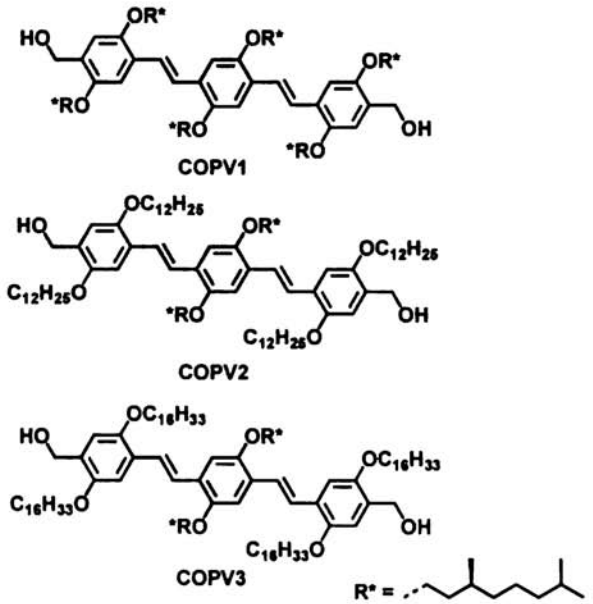

Chart 4.1

The supramolecular chirality of the self-assembled stacks are controlled by the chiral (*S*)-3,7-dimethyloctyloxy side chains and assisted by weak hydrogen bonding hydroxymethyl motifs and long hydrocarbon chains. In this chapter, the self-assembly properties of **COPV1-3**, the detailed morphological investigation and circular dichroism experiments are described.

4.2. Results and Discussion

4.2.1. Synthesis and Characterization of Chiral OPVs

The chiral OPV derivatives **COPV1-3** were synthesized as shown in Scheme 4.1. The chiral handles were obtained from (*S*)-citronellol, which was first catalytically hydrogenated and then brominated giving rise to (*S*)-(+)-1-bromo-3,7-dimethyloctane.[5a] The chiral bistriphenyl phosphonium bromide **7** and the bisaldehydes **8a-c** were prepared using standard procedures.[18] Controlled Wittig reaction between chiral wittig salt **7** and the appropriate bisaldehydes **8a-c**, in a 1:1 stoichiometry provided the chiral bisaldehydes **9a-c** in 60% yields.[18] These compounds on subsequent reduction with $NaBH_4$, provided the corresponding bisalcohols **COPV1-3** in 95% yields. All the new chiral OPV derivatives were characterized with IR, ^1H NMR, ^{13}C NMR and MALDI-TOF mass spectra.

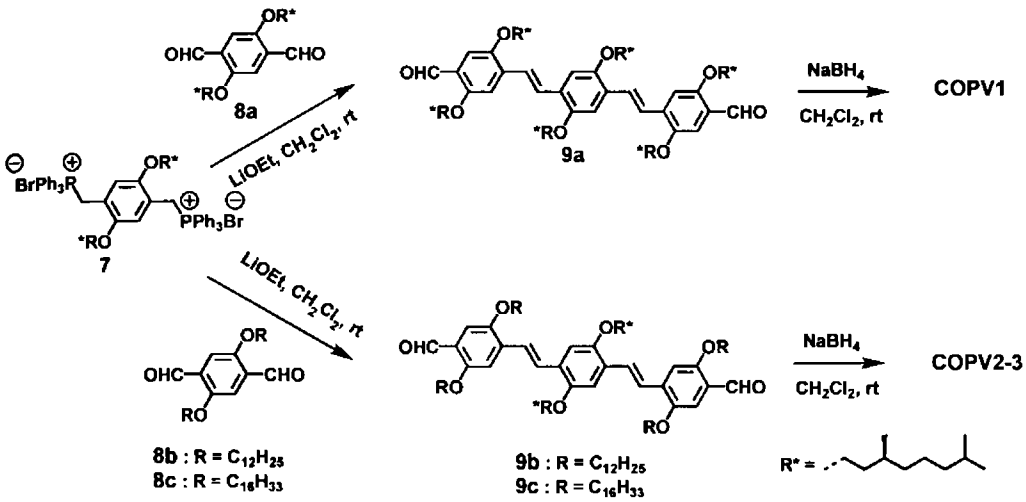

Scheme 4.1

4.2.2. Gelation Studies

Gelation behavior of the chiral OPV derivatives **COPV1-3** was examined in a range of nonpolar organic solvents and the results are summarized in Table 4.1. Among the three chiral OPVs, **COPV2**, with dodecyl side chains, was found to be the better gelator to form yellow fluorescent gels in dodecane, heptane and cyclohexane. The critical gelator concentration of **COPV2** in dodecane is high (6.5 mM) when compared to the gelation abilities of achiral OPVs, which could form gels even at a concentration of 1 mM (see Chapter 2). Though, **COPV3** with hexadecyl side chain forms self-assembled aggregates in nonpolar solvents (as evidenced from the optical properties which will be discussed in section 4.2.3) they could not trap organic solvents inside their self-assembled network and hence phase separated from the solvent. However **COPV1**, which is substituted with six chiral side chains failed to form gels in any of the solvents investigated, and resulted a homogeneous solution due to its high solubility imparted by six branched chiral side chains.

Table 4.1. Critical gelator concentration (CGC) (mM) of chiral OPVs[a]

Compound	Dodecane	Heptane	Cyclohexane	Hexane	Chloroform
COPV1	P	PG	PG	P	S
COPV2	6.5	7.0	7.2	S	S
COPV3	S	S	S	S	S

[a]Souble (S), precipitation (P) and partial gelation (PG).

4.2.3. Optical and Chiroptical Properties of Chiral OPVs

The absorption and emission spectra of **COPV1-3** in chloroform and dodecane are shown in Figure 4.4. In the case of **COPV1**, the absorption spectra did not show much change in the two solvents (Figure 4.4a). However, in dodecane **COPV2** developed an additional shoulder band at 470 nm (Figure 4.4c), whereas in the case of **COPV3** in dodecane, the spectrum is broadened towards the long wavelength region and the shoulder band at 472 nm is predominant even at low concentration (Figure 4.4e). The emission spectra of **COPV1** in chloroform and dodecane showed two maxima around 455 and 484 nm with a shoulder around 525 nm (Figure 4.4b). The spectrum in dodecane is slightly blue shifted (ca. 5 nm) without changing the intensities of the various emission bands. In the case of **COPV2** and **COPV3**, considerable differences could be observed for the emission spectra in chloroform and dodecane. For example, for **COPV2** in dodecane, the emission spectrum showed four major bands at 450, 480, 525 and 570 nm in which the intensities of the long wavelength emitting bands are relatively strong when compared to those in chloroform (Figure 4.4d). Interestingly, for **COPV3** in dodecane, the emission spectrum is significantly shifted towards the long wavelength region where the bands

at 528 and 571 nm are predominant (Figure 4.4f). The change in the absorption and emission spectra of **COPV2** and **COPV3** in dodecane relative to chloroform indicates the self-assembly of the molecules in dodecane, which is strong for **COPV3**. Interestingly, despite the strong aggregation of **COPV3** in dodecane, it is surprising to note that this molecule showed very weak gelation. This could probably be due to the bias of the delicate balance between the crystallization and precipitation of the molecule in favor of latter, which plays a critical role in gelation.

Temperature dependent UV/Vis and emission spectra of **COPV2** and **COPV3** in dodecane showed a transition from the self-assembled species to the molecularly dissolved species as the temperature is increased. In the case of **COPV2**, on increasing the temperature, the intensity of the absorption maximum at 406 nm was increased with a concomitant decrease in the intensity of the shoulder band at 470 nm through an isosbestic point at 433 nm (Figure 4.5a). Similarly in the fluorescence spectra (λ_{ex} = 380 nm), the intensity of the long wavelength maximum at 525 nm decreases with the simultaneous increase in the intensity of the emission bands at 450 nm and 480 nm (Figure 4.5b). Similar observations were made with the variable temperature UV/Vis and fluorescence measurements of **COPV3** in dodecane, even though much higher temperatures were needed for the complete breaking of the self-assembly to molecularly dissolved phase (Figures 4.6a and b).

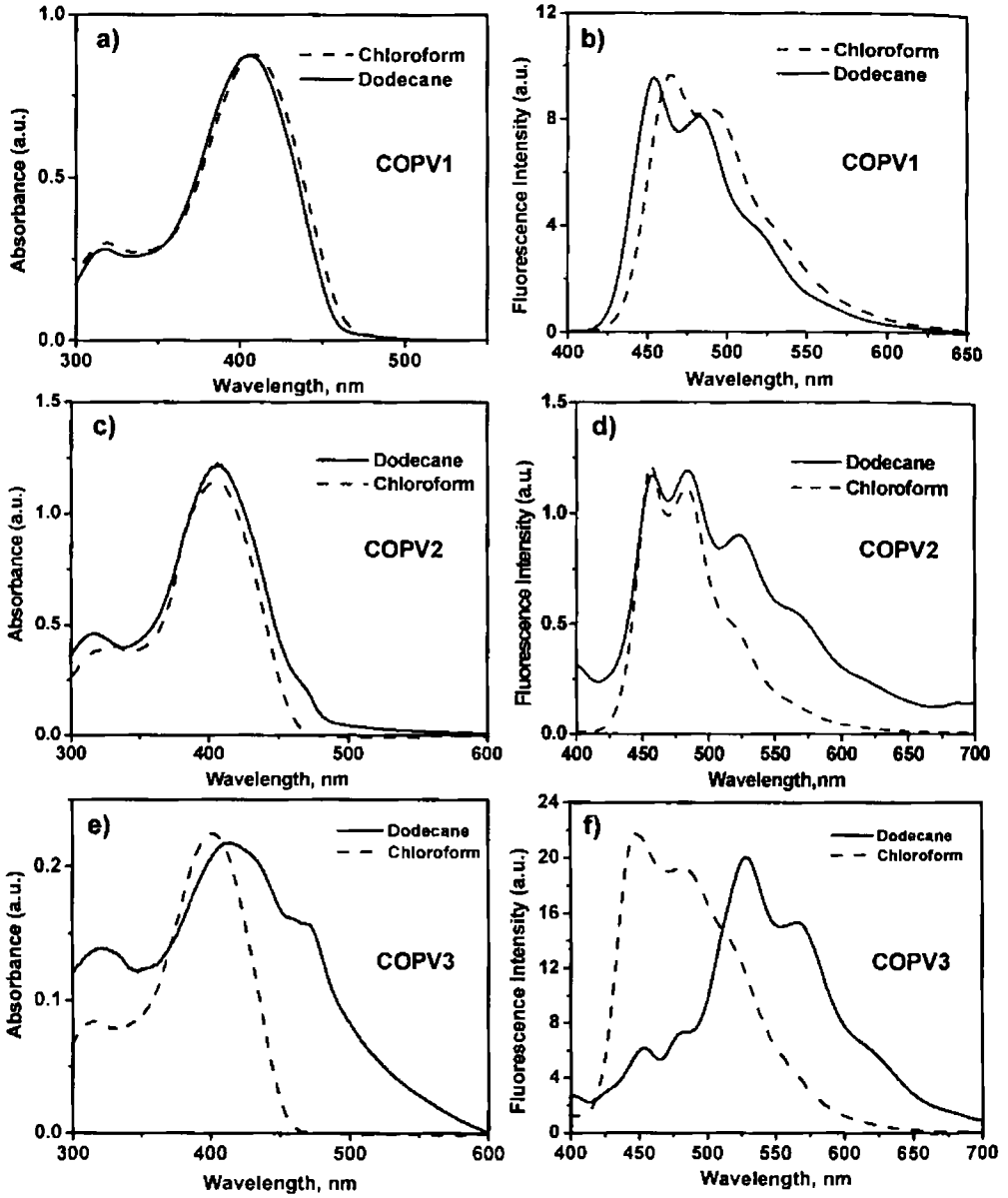

Figure 4.4. Normalized a) UV/Vis and b) fluorescence spectra of **COPV1-3** in dodecane and chloroform.

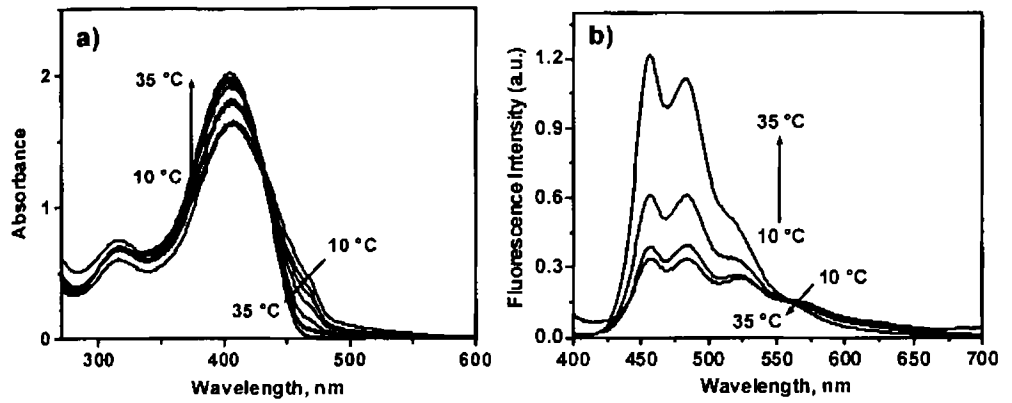

Figure 4.5. Temperature dependent a) UV/Vis and b) fluorescence spectra (excitation at 380 nm) of **COPV2** in dodecane (c = 5.3 x 10^{-4} M, l = 1 mm).

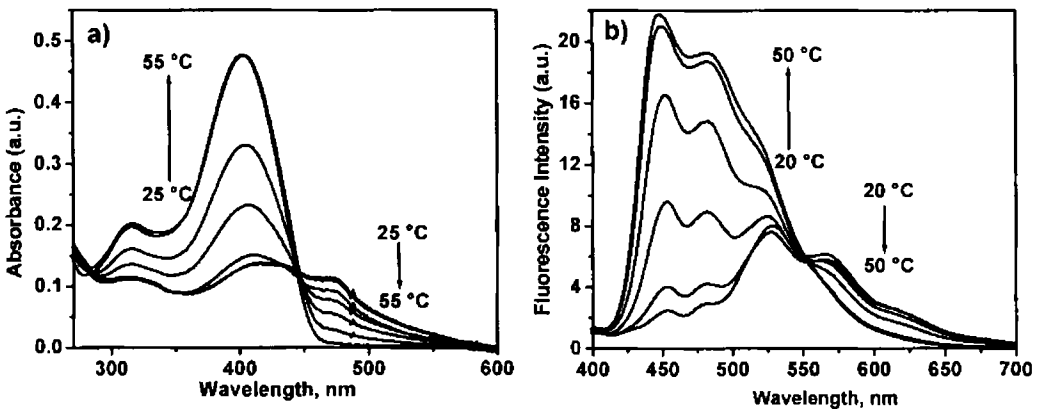

Figure 4.6. Temperature dependent a) UV/Vis and b) fluorescence spectra (excitation at 380 nm) of **COPV3** in dodecane (c = 1.24 x 10^{-5} M, l = 1 cm).

Detailed circular dichroism experiments of **COPV1-3** have been carried out in order to get better understanding on the nature of the self-assemblies. As expected, no Cotton effects were observed for **COPV1-3** in chloroform solution, reiterating the molecularly dissolved state of the OPVs. Furthermore, **COPV1** does not feature any Cotton effect in dodecane, as they are not aggregated even in nonpolar solvents. However, the presence of self-assembled molecules of **COPV2** in dodecane (5.3×10^{-4} M) at room temperature was clear from the CD experiments, which showed

a strong bisignated Cotton effect at the position of the π-π* band, with a zero crossing close to the absorption maximum (400 nm) (Figure 4.7). The exciton coupled bisignated negative couplet in the CD spectrum is a signature of the left-handed helical assembly of OPVs.

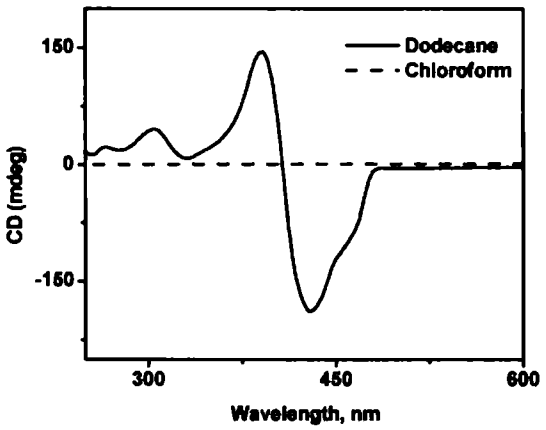

Figure 4.7. CD spectra of **COPV2** in dodecane and chloroform (c = 5.3 x 10^{-4} M. l = 1 mm).

Detailed concentration and temperature dependent CD measurements of **COPV2** in dodecane provided insight into the hierarchical helical self-assembly and the gelation of the molecules. The CD spectral changes between 8.8 x 10^{-5} M - 5.3 x 10^{-4} M concentration range at 20 °C is shown in Figure 4.8a (with chiral anisotropic factor at 381 nm, g_{381nm} = 6.8 x 10^{-4} - 5.2 x 10^{-3}).[19] Up to a concentration of 2.7 x 10^{-4} M, **COPV2** in dodecane showed a bisignated CD signal with a negative first Cotton effect followed by a second positive Cotton effect with a zero crossing around 440 nm, which is not on the absorption maximum of the chromophore. During this concentration range, a linear increase is observed, on plotting the intensity of the CD signal at 391 nm against the concentration (Figure 4.8b). Surprisingly, above 3.5 x 10^{-4} M concentration, a sharp transition of the CD signal could be seen. The zero crossing of the new CD signal is now exactly at the absorption maximum (400 nm), indicating a true exciton coupled spectrum. The transition of the CD signal is

accompanied by a strong amplification of the chirality as evident from the deviation of the Cotton effects from linearity (Figure 4.8b), indicating that the observed transition is a highly cooperative process. Temperature dependent study at a concentration of 5.3 x 10^{-4} M in dodecane showed a decrease in the CD signal up to a temperature of 24 °C along the zero crossing point (Figures 4.8c and d). However at 26 °C, a sharp transition of the intense exciton coupled CD signal to a weak bisignated signal with a shift of the zero crossing from 400 nm to 440 nm was noted, which continued to decrease till it reached the baseline at 35 °C.

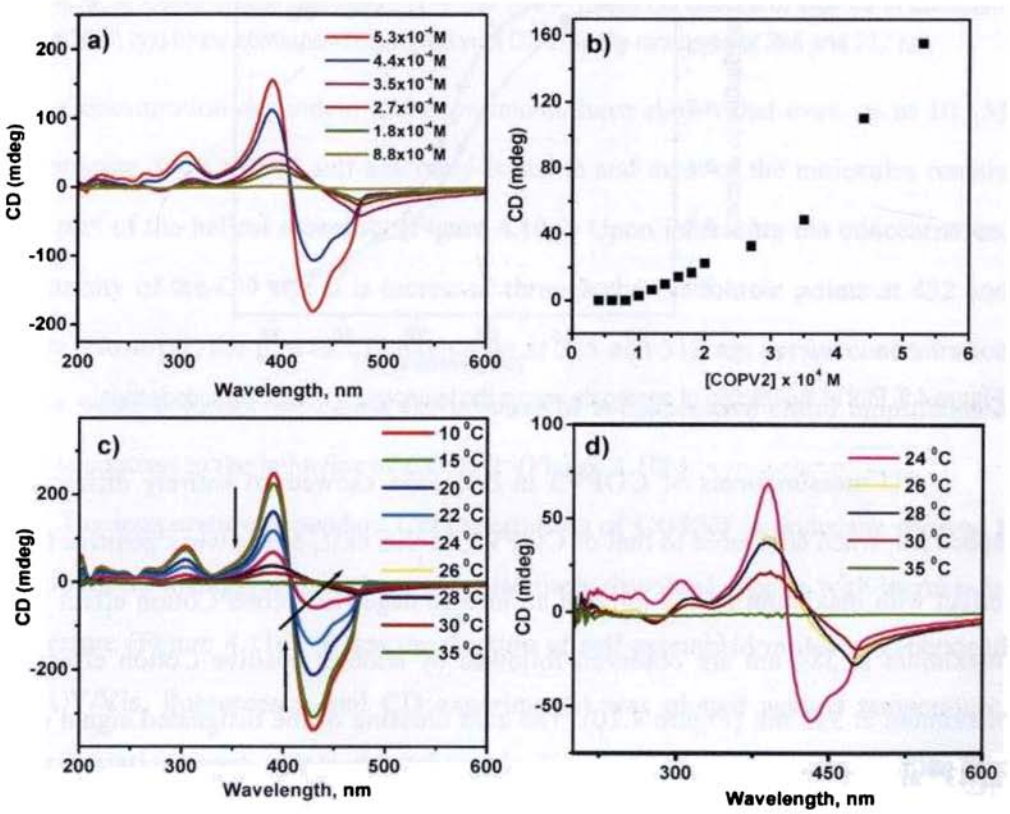

Figure 4.8. a) Concentration dependent (T = 293 K, l = 1 mm) CD spectra of **COPV2** in dodecane and b) the corresponding transition of CD intensity monitored at 391 nm. c) Temperature dependent (c = 5.3 x 10^{-4} M, l = 1 mm) CD spectra of **COPV2** in dodecane and d) is the zoomed portion of the temperature dependent CD spectra of **COPV2** between 24-35 °C.

Moreover the melting transition curves obtained by plotting the fraction of aggregate molecules versus temperature, as inferred from the temperature dependent CD and UV/Vis studies clearly showed two transitions during the temperature dependent denaturation of the helical assembly (Figure 4.9). It is interesting to note that both concentration and temperature dependent transition of the CD signals are complementary to each other, which indicate a similar pathway involving same chiral intermediate during the formation and breaking of the supramolecular assembly.

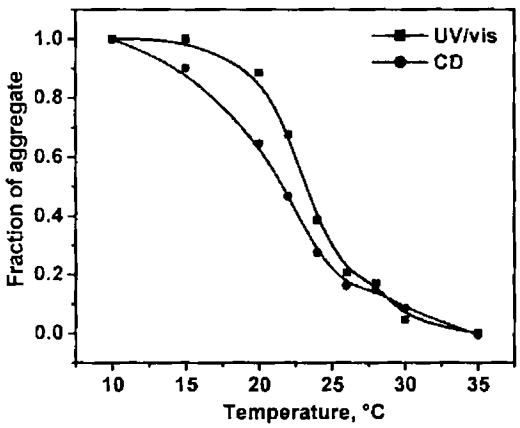

Figure 4.9. Plot of the fraction of aggregate versus the temperature of **COPV2** in dodecane.

CD measurements of **COPV3** in dodecane showed an entirely different CD spectrum, when compared to that of **COPV2**. In this case, a first weak positive Cotton effect with maximum at 474 nm and an intense negative second Cotton effect with a maximum at 384 nm are observed followed by another positive Cotton effect with maximum at 313 nm (Figure 4.10). The zero crossing of the bisignated signal occurs at 432 and 343 nm. Even though the CD spectrum is consistent with an exciton model, in which the OPV molecules aggregate in a chiral supramolecular stack, the complex nature of the CD signal with double pseudo bisignated curves makes the prediction of the helical bias of the aggregate difficult.

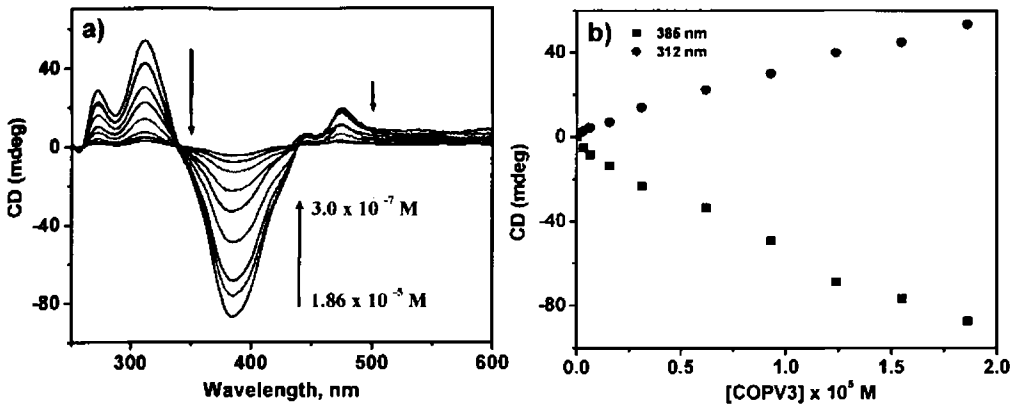

Figure 4.10. a) Concentration dependent (T = 293 K, l = 1 mm) CD spectra of **COPV3** in dodecane (1.25 x 10^{-5} M) and b) the corresponding transition of CD intensity monitored at 385 and 312 nm.

Concentration dependent CD experiments have shown that even up to 10^{-7} M concentration, the **COPV3** self-assembly is stable and most of the molecules remain as the part of the helical assembly (Figure 4.10a). Upon increasing the concentration, the intensity of the CD signal is increased through the isodichroic points at 432 and 343 nm. However, the plot of CD intensities at 385 and 312 nm versus concentration show a linear behavior indicating the absence of a cooperative chiral amplification which is contrast to the behavior of **COPV2** (Figure 4.10b).

The temperature dependent CD experiments of **COPV3** in dodecane showed a transition from the aggregated phase to molecularly dissolved species with increase in temperature (Figure 4.11a). When the fraction of self-assembled molecules (obtained from UV/Vis, fluorescence and CD experiments) was plotted against temperature, good correlations were obtained as shown in Figure 4.11b. In all cases, similar first order transitions were found. The transition temperature of the **COPV3** self-assembly is found to be 42 °C, which is 16 °C higher when compared to that of **COPV2** (26 °C) assemblies.

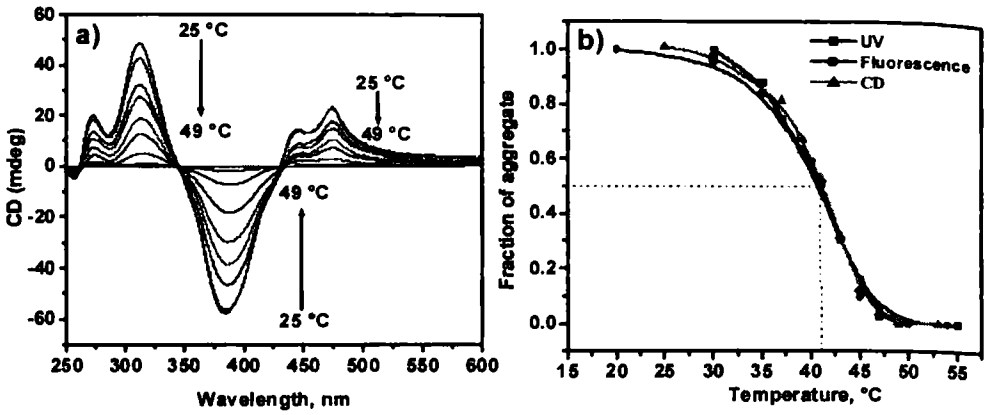

Figure 4.11. a) Temperature dependent CD spectra of **COPV3** (1 x 24 10^{-5} M) and b) the plots of the fraction of aggregate against temperature of **COPV3** in dodecane.

4.2.4. Optical Polarizing Microscopic (OPM) Studies

OPM studies of the neat **COPV2-3** showed the formation of spherulite like textures. When **COPV3** is cooled at a rate of 20 °Cmin^{-1} from the isotropic melt, spherulite textures appeared at 67 °C, which was stable up to room temperature (Figure 4.12a). It is interesting to note that, the structurally related achiral **BH-OPV1** derivatives described in Chapter 2 showed long fibers when cooled from the isotropic melt and hence the spherulite textures obtained for **COPV3** could be attributed to the chirality of the molecule. Similar observation was made with neat **COPV2** (Figure 4.12b). Interestingly, when **COPV2** and **COPV3** were rapidly cooled from isotropic melt, by quenching with ice, transparent organic glasses were formed, showing birefringent textures (Figures 4.12c-d). OPM studies of the dodecane gels of **COPV2** revealed birefringent four-arm brush textures emanating from several nucleation centers, when cooled from the isotropic solution at a rate of 5 °Cmin^{-1} (Figure 4.13). From the OPM studies it can be concluded that, the spherulite and four-arm brush textures of chiral OPVs in their neat and gel phases, could be the indication of the

helical ordering of the molecules. In order to confirm this speculation detailed microscopic investigation of the gel samples were performed.

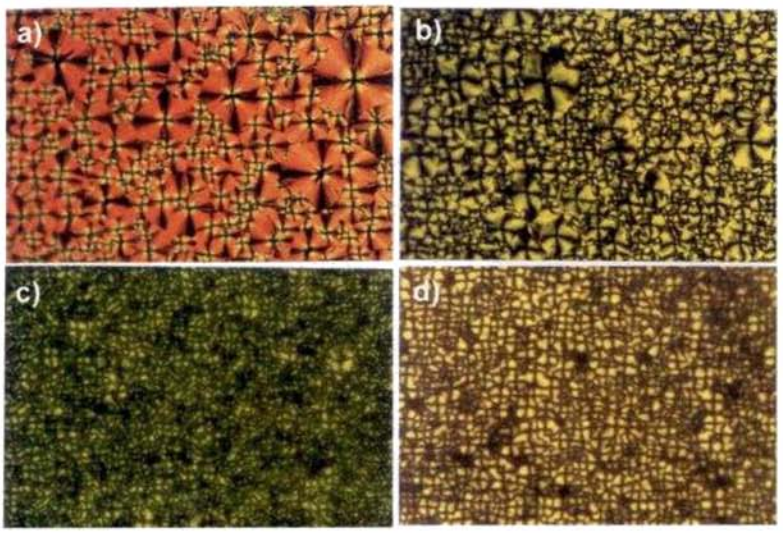

Figure 4.12. Optical polarizing microscopic pictures of a) spherulite crystalline textures of **COPV3** and b) **COPV2**, c) organic glasses formed by **COPV3** and d) **COPV2**.

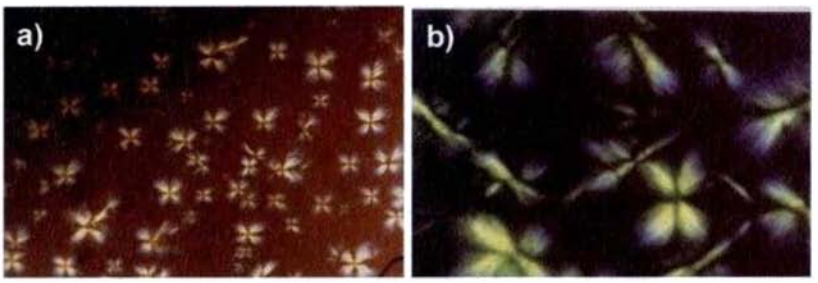

Figure 4.13. Optical polarizing microscopic pictures of dodecane gels of **COPV2** (c = 9 mg/mL). magnification is a) 100x and b) 400x.

4.2.5. Morphological Characterization of Chiral OPV Nanostructures

Field emission scanning electron microscope (FE-SEM) images of **COPV2** from a dilute solution in dodecane (9×10^{-5} M) showed left-handed helical fibers of 20-50 nm in diameter and a few micrometers in length with a uniform helical pitch of

approximately 200 nm (Figures 4.14a and b). This is in agreement with the CD studies, in which a negative exciton coupled CD signal indicated a left-handed organization of the chromophores. However, the FE-SEM image of **COPV2** (partially gelled) from a more concentrated solution in dodecane (5 x 10^{-4} M) showed the formation of left-handed coiled-coil rope-like structures of 50-100 nm in diameter with an average pitch of 330 nm. These rope-like structures are formed by the twisting together of several helical fibers (Figure 4.14c).

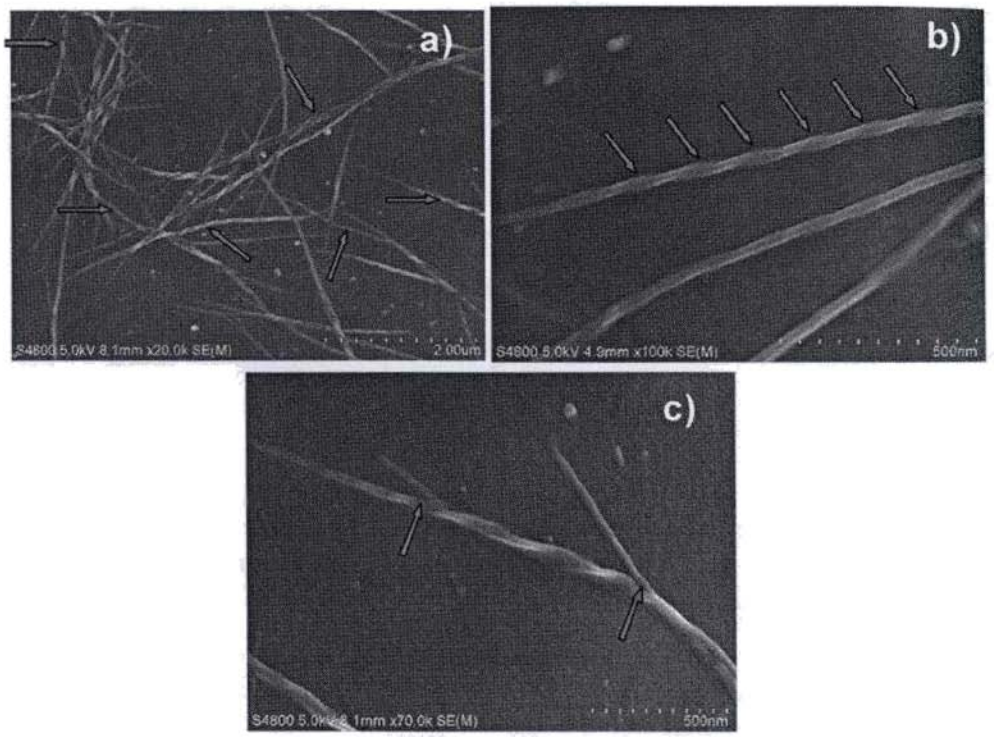

Figure 4.14. Helical morphology of **COPV2** self-assembly from a dodecane solution: FE-SEM images of a) left-handed helical fibers, b) isolated single helical fibers and c) formation of coiled-coil ropes (5 x 10^{-4} M).

AFM analysis of the **COPV2** gel from dodecane (6.5 x 10^{-3} M) indicates the formation of entangled left-handed helical coiled-coil fibers of 50-100 nm in diameter

(Figures 4.15a and b). Careful analysis of a single fiber showed the morphology of a left-handed coiled-coil rope of approximately 90 nm in width and 11 nm in height in which the pitch of each helix has an angle of about 40° with respect to the main fiber axis (Figure 4.15c). These observations point towards a hierarchical self-organization of **COPV2** into coiled-coil gel nanostructures.

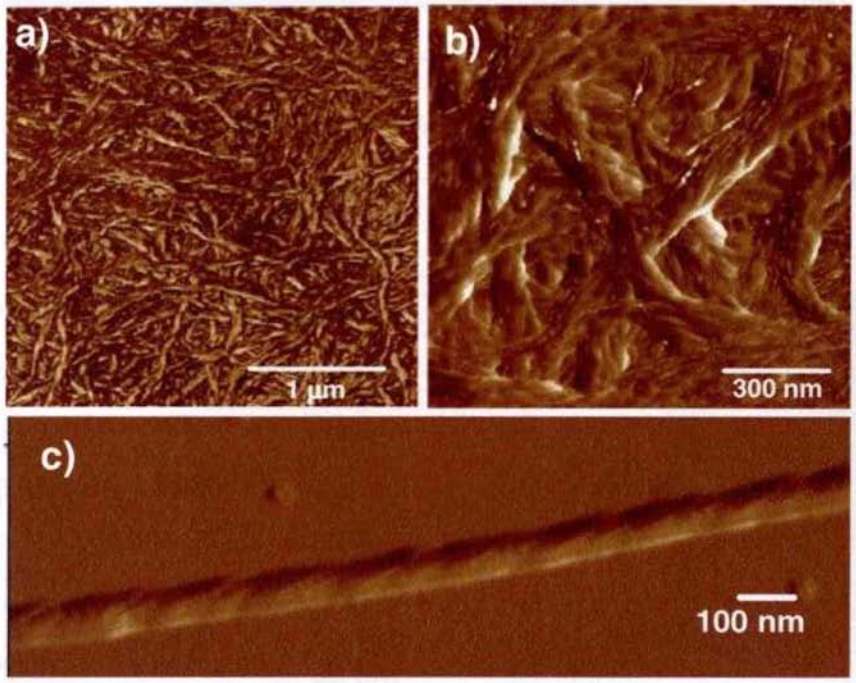

Figure 4.15. a) and b) AFM images of the dense coiled network of **COPV2** gel fibers (6 x 10^{-3} M) and c) AFM image of a single left-handed coiled-coil rope.

SEM pictures of a drop casted dodecane solution of **COPV3** (3 x 10^{-5} M) showed, bundles of 'leaf-like' structures emanating from several randomly arranged nucleation points (Figure 4.16a) which are entirely different from the morphology of **COPV2**. Each bundle is composed of several leaves having diameter ca. 1-2 µm and length around 15-20 µm (Figure 4.16b) with relatively low aspect ratio when compared to that of **COPV2** structures.

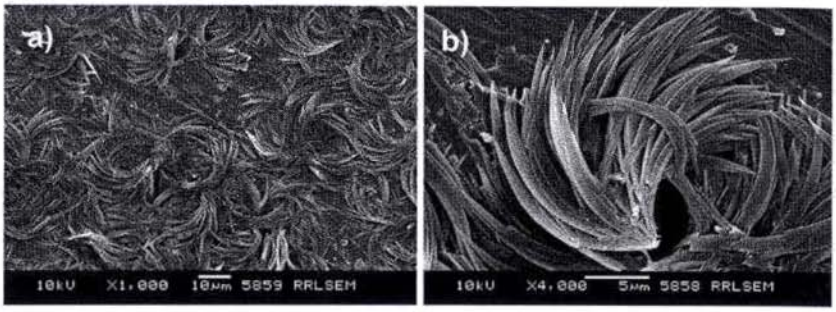

Figure 4.16. a) and b) SEM images of the **COPV3** aggregates form dodecane solution (3 x 10^{-5} M).

4.3. Gelation Induced Hierarchical Growth of Helical Coiled-Coil Gel Nanostructures

The concentration and temperature dependent CD signal transition of **COPV2** is a unique observation associated with the gelation of chiral OPVs. During the gelation of **COPV2**, several hierarchical levels of supramolecular assemblies could be possible. In the initial levels, the molecules organize to form left-handed chiral aggregates, which are helical as indicated by the weak bisignated CD signal. At higher concentrations, these initial chiral assemblies grow further into helical fibers and coiled-coil ropes, thus resulting in a strong exciton coupled CD signal. It is interesting to note that the CD transition and the chiral amplification are accompanied by the gelation. A plausible helical packing of **COPV2** to form the left-handed coiled-coil rope, is represented along with the observed AFM image in Figure 4.17. As we have postulated earlier in the case of the molecular packing of the achiral OPVs, the cooperative interaction of H-bonding and π-stacking facilitate the lamellar organization of the chromophores to form a supramolecular tape-like morphology. The remote chiral handles present in the molecules will induce a long range twisting of the tapes, thereby forming twisted tapes as evidenced by the FE-SEM analysis. In the next level of assembly, several of the twisted tapes will join together to evolve

coiled-coil rope-like structures of an average of 90-100 nm in width and several micrometers in length as evidenced by the AFM image shown in Figure 4.17b. Interestingly, when the results of the CD and microscopic analyses are considered together, it is evident that the coiled-coil structures evolve through two distinct chiral assemblies. At higher temperatures, denaturing of the coiled-coil gel assemblies occurs via intermediate chiral states, and the helical self-assembly ultimately collapses into isotropic single molecules for which no CD signals are observed.

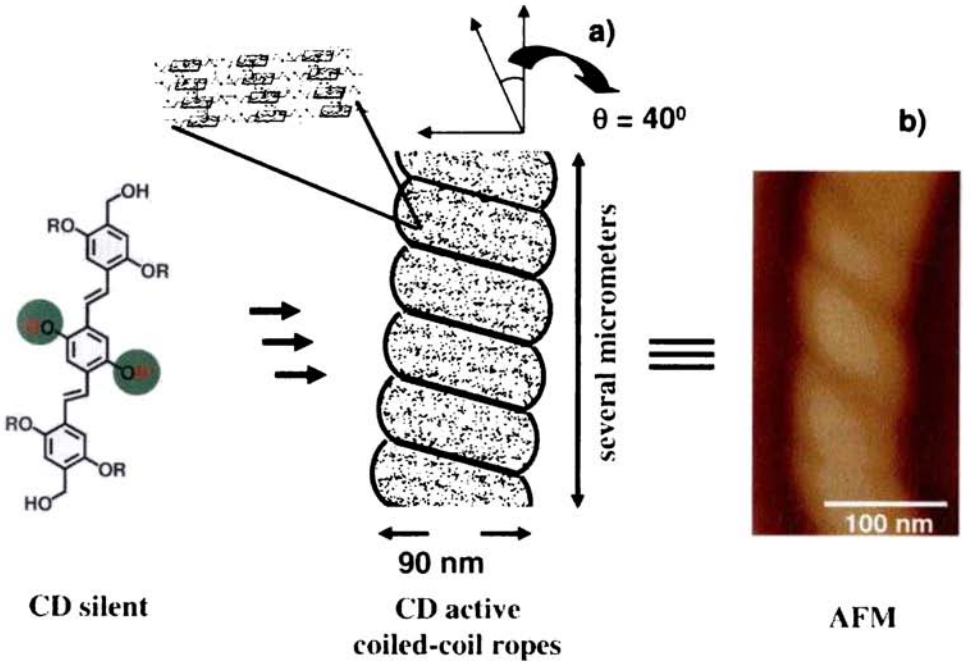

Figure 4.17. Schematic representation of the hierarchical self-assembly of **COPV2** into helical coiled-coil gel nanostructures. A magnified AFM picture of the coiled-coil rope is shown on the right hand side.

4.4. 'Sergeants and Soldiers' Approach to Supramolecular Chirality Amplification

Green and coworkers have introduced the idea of 'Sergeant and Soldiers' principle and 'Majority Rules' to induce helicity in poly(isocyanate)s with the help of

a chiral guest.[20] These rules illustrate that, to favor one of the helical conformations, either P or M of poly(*n*-alkylisocyanate)s, it is only required to add a small portion of the chiral monomer units (sergeants) to the achiral monomers (soldiers) or have a slight majority of 'R' over 'S' (Majority Rule). The ability of poly(isocyanate)s to bias the helicity is explained on the basis of its highly cooperative helical folding. Recently, Meijer and coworkers have successfully applied the 'sergeant and soldiers' principle in a variety of supramolecular discotic systems.[5] The co-assembly of C_3-symmetric discotic chiral and achiral molecules results in the amplification of chirality, with one chiral molecule capable of organizing as much as 80 achiral ones in either a right- or a left-handed helical stack.[5a] Except in discotic systems, chiral amplification via the 'sergeants and soldiers' approach to form helical supramolecular architectures remains elusive and challenging. This is particularly true in the case of rigid π-conjugated molecules which self-organize via supramolecular lamellar fashion. This has prompted us to explore the possibilities of chiral induction and amplification of a helical bias using co-assembly behavior of the chiral OPVs (**COPV1-3**) with the achiral OPVs, **BH-OPV1a** and **BH-OPV1b** (Chart 4.2).

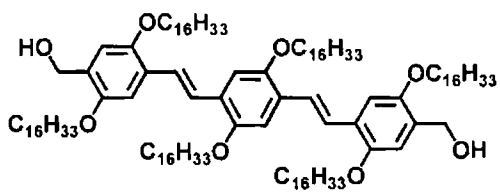

BH-OPV1a

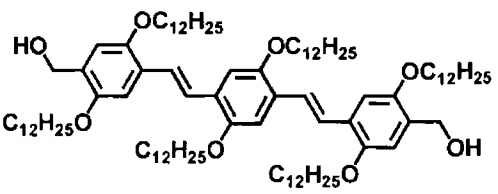

BH-OPV1b

Chart 4.2

A series of co-assembled OPV gels of the achiral OPV derivatives **BH-OPV1b**, carrying dodecyl side chains, with varying amounts of structurally related chiral **COPV2** (0-50%) were prepared in dodecane, by heating the mixed OPV

solution to 90 °C and the subsequent cooling to 5 °C at a cooling rate of 20 °Cmin^{-1}. In all cases stable, transparent and fluorescent gels were obtained indicating the co-assembly of both achiral and chiral OPVs. The 'sergeant and soldiers' experiment of **BH-OPV1b/ COPV2** dodecane gels were conducted at 5 °C by monitoring the CD spectra as a function of the mol% of **COPV2** (sergeant) (Figure 4.18a). As expected, the dodecane gel of pure **BH-OPV1b** does not show any Cotton effect. However, the **BH-OPV1b/ COPV2** dodecane gels showed pseudo-bisignated Cotton effects at the OPV absorption, the intensity of which increases with the mole fraction of the **COPV2**. Up to 25% of **COPV2**, the co-assembled OPV gel showed a weak pseudo-bisignated CD signal with the negative maxima at 456, 380 and 317 nm and the positive maximum at 406 nm, whose intensity increases linearly with **COPV2** concentration. This is further evident from the plot of the CD intensity at 406 and 317 nm, versus the percentage of **COPV2** in the co-assembled gels as shown in Figure 4.18b. However, when the percentage of the **COPV2** is increased beyond 25%, a strong amplification of chirality is observed, which is clear from the deviation of the plot of the CD intensity from linearity. The CD signals grow in intensity through the isodichroic points at 436 nm and 388 nm. Even though, the strong pseudo-bisignated Cotton effect with positive maximum at 406 nm and the negative maximum at 380 nm with a zero crossing at 388 nm obtained with 50% **COPV2** co-assembled gels can be attributed to a helical arrangement of the OPV chromophores, the appearance of an additional negative Cotton effect at 460 nm, makes it difficult to assign the exact handedness from the CD signal.

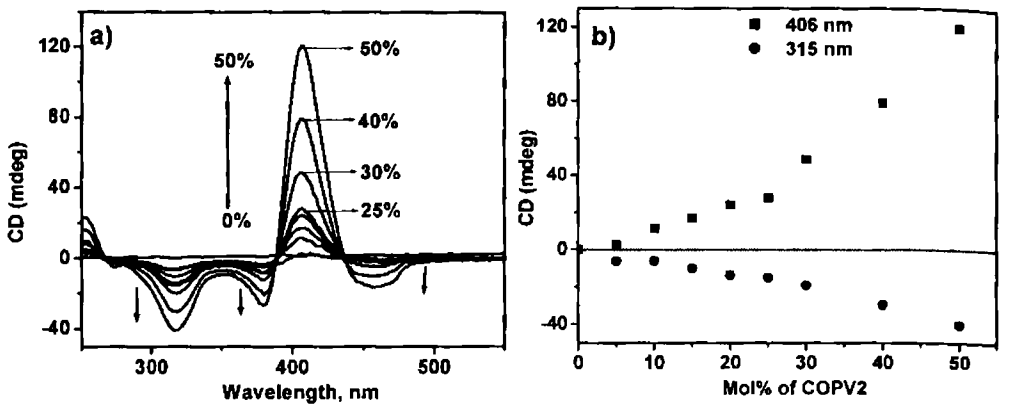

Figure 4.18. a) CD spectra of **BH-OPV1b/COPV2** co-assembled dodecane gels (T = 278 K, l = 1 mm, cooled from the isotropic solution at a rate of 20 °C/min) and b) the corresponding changes in the CD intensity monitored at 406 and 315 nm, as a function of the concentration of **COPV2** in the co-assembled gels.

Interestingly, when a pre-heated dodecane solution of **BH-OPV1b** containing 50% **COPV2**, is allowed to gel by slow cooling at room temperature, a strong amplification of chirality is observed, resulting in an intense exciton coupled bisignated CD signal with a first positive Cotton effect having a maximum at 415 nm and a second negative Cotton effect with a maximum at 380 nm, through a zero crossing at 392 nm (Figure 4.19a). This CD signal is nearly three times more intense than that of the fast cooled gel. However, the slow cooled **BH-OPV1b/COPV2** dodecane gel showed the opposite sign of Cotton effect when compared to the CD signal of the pure **COPV2** dodecane gel (5.3×10^{-4} M) (Figure 4.19b). Although, the two CD spectra are not the exact mirror images, the inversion of Cotton effect indicates that, the OPV chromophores in the **BH-OPV1b/COPV2** dodecane gels are arranged in a different helical sense in the co-aggregate, when compared to that of the pure **COPV2** assembly.

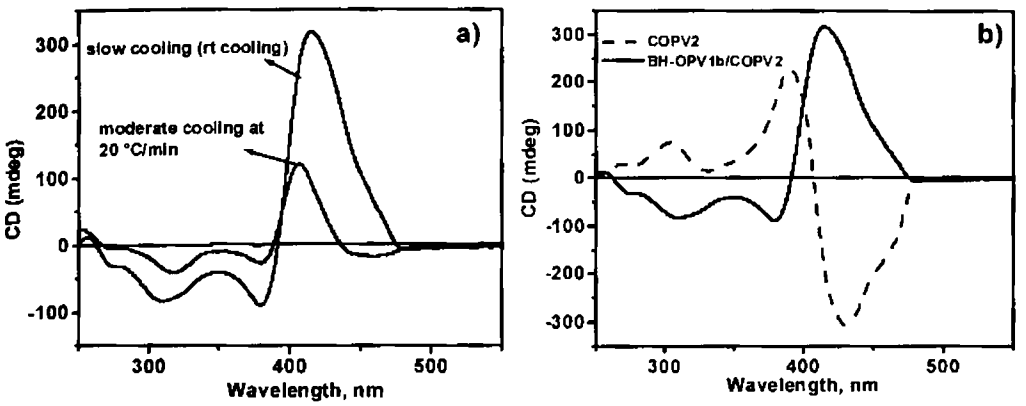

Figure 4.19. a) CD spectra of the fast cooled (20 °C/min) and slow cooled (room temperature cooling) **BH-OPV1b/COPV2** co-assembled dodecane gels (T = 278 K, l = 1 mm) containing 50% of **COPV2** and b) comparison of the slow cooled **BH-OPV1b/COPV2** co-assembled dodecane gels with the CD spectrum of pure **COPV2** dodecane gels (5.3×10^{-4} M).

Figure 4.20 shows the plots of the CD signal intensities of the **BH-OPV1b**, **COPV2** and the **BH-OPV1b/COPV2** co-assembled dodecane gels. It is interesting to note that at same concentrations of **COPV2**, the CD signal intensity of the co-assembled gels of **BH-OPV1b/COPV2** is larger than that of **COPV2** dodecane gel which is a clear indication of the 'sergeants and soldiers' effect in chirality amplification. In the co-assembled gel state, the chiral OPV molecules can efficiently bias the packing of the achiral OPV molecules resulting in the amplification of chirality, indicating the cooperative nature of the self-assembly.

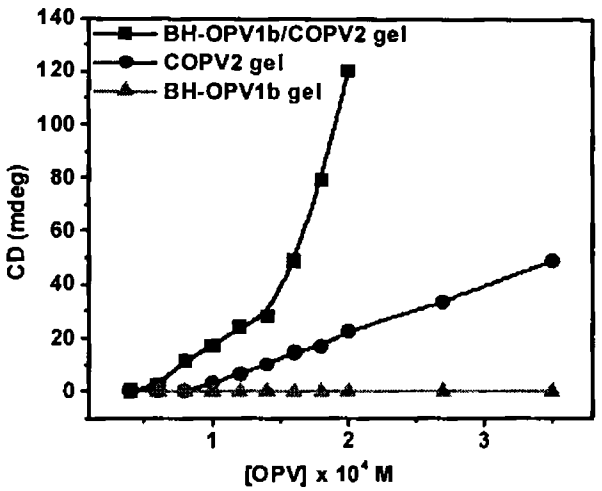

Figure 4.20. Plots of the concentration dependent CD intensity at 391 nm of the pure **COPV2**, co-assembled **BH-OPV1b/COPV2** and pure **BH-OPV1b** dodecane gels.

The temperature dependence of the Cotton effect of the co-assembled **BH-OPV1b/COPV2** gels has been investigated to get insight into the cooperativity of the self-assembly process. Figure 4.21 shows the temperature dependent CD spectra of the slow cooled dodecane **BH-OPV1b/COPV2** gel doped with 50% **COPV2.** The inset of the Figure 4.21 shows the corresponding self-assembly transition curve obtained by plotting the fraction of the aggregates versus temperature. From the temperature dependent CD curves, it is evident that the co-aggregated OPV helices have intense CD signal up to 50 °C, and the denaturation of the helix took place over a small temperature range, as is indicated by the complete loss of the CD signal at 63 °C. The lack of isodichroic point during the temperature dependent breaking of the helical OPV stacks supports the involvement of intermediate chiral states during the hierarchical evolution of the helical assembly. The difference in the CD spectrum of the fast cooled co-assembled gels can be attributed to that of a kinetically controlled assembly, whereas a thermodynamically more stable self-assembly is resulted upon slow cooling, as evident from the appearance of the intense exciton coupled CD

signal. It is interesting to note that the stability of the chiral OPV gels have been considerably increased, by co-assembling with achiral OPVs. The pure **COPV2** (5.3 x 10^{-4} M) gels are stable only up to 30 °C, while the co-assembled **BH-OPV1b/COPV2** gel containing 2 x 10^{-4} M of **COPV2** is stable up to 63 °C as observed from the temperature dependent studies.

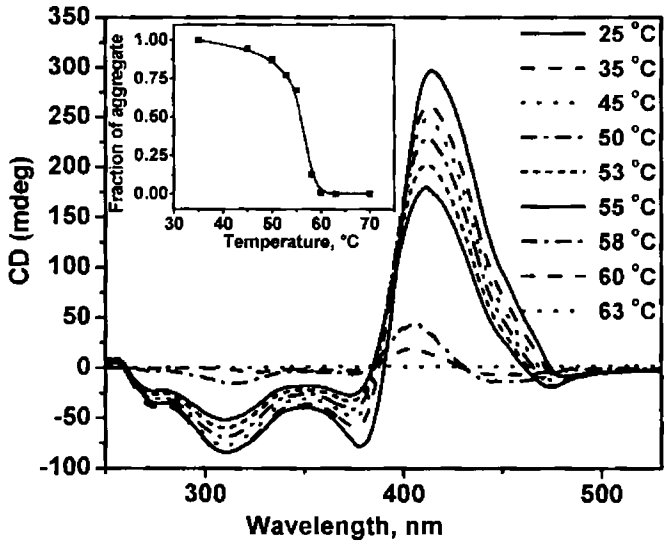

Figure 4.21. Temperature dependent CD spectra of slow cooled dodecane **BH-OPV1b/COPV2** gel doped with 50% **COPV2**. The inset shows the aggregate stability curve obtained by plotting the fraction of self-assembled molecules versus temperature.

Results of the CD spectral studies of the co-assembly between the achiral **BH-OPV1a** and the chiral **COPV3** are shown in Figure 4.22. Even though, **COPV3** could not form gels despite its strong aggregation ability, co-assembly of **COPV3** with **BH-OPV1a** in dodecane resulted in the formation of stable gels. When **BH-OPV1a** is doped with different concentrations of **COPV3,** rapid formation of stable and transparent co-assembled gels could be observed.

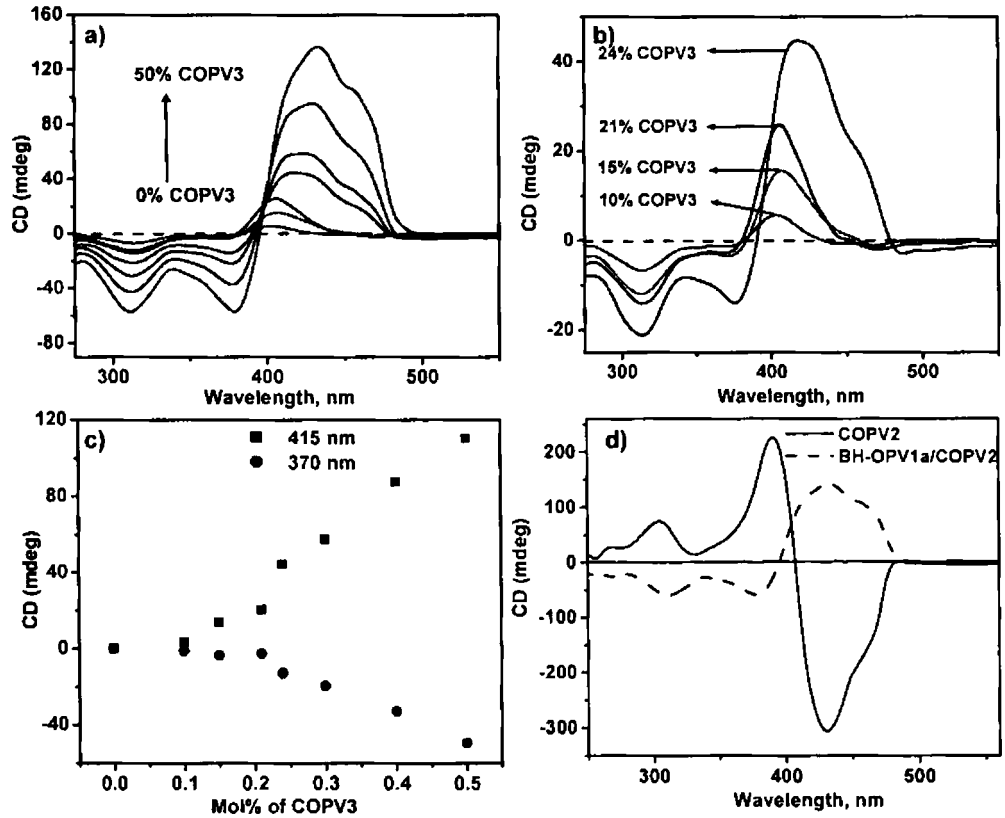

Figure 4.22. a) and b) CD spectra of **BH-OPV1a/COPV3** co-assembled dodecane gels (T = 278 K, l = 1 mm) at various mol% of **COPV3** and c) the corresponding changes in the CD intensity monitored at 415 and 370 nm, as a function of the concentration of **COPV3** in the co-assembled gels. d) Comparison of the CD spectra of **BH-OPV1a/COPV3** co-assembled dodecane gels with that of pure **COPV2** dodecane gels (5.3×10^{-4} M).

Up to 25% of **COPV3**, the co-assembled OPV gels showed a weak exciton coupled CD signal with a positive maximum at 406 nm and negative maximum at 314 nm through a zero crossing at 380 nm (Figure 4.22a). At a concentration of 24% of **COPV3**, a sudden transition to a new exciton coupled bisignated signal with positive and negative maxima at 433 and 378 nm, respectively was observed, which is accompanied by a shift in the zero crossing to 390 nm (Figure 4.22b). The observed shift in the CD signal accompanied by the significant increase in the intensity is an

indication of the reorganization of the initial co-assembly to a more stable packing of the chromophores. The plot of CD signal intensities at 415 nm and 370 nm, against the mol% of **COPV3** showed a sharp increase above 20 mol% indicating a strong chiral induction from **COPV3** to **BH-OPV1a** in the co-assembly (Figure 4.22c). Comparison of the CD signals of pure **COPV2** with **BH-OPV1a/COPV3** co-assembly showed a near mirror image relationship indicating apposite helical sense between the two supramolecular assemblies (Figure 4.22d).

The presence of the intermediate chiral states is further evident from the temperature dependent CD studies of the **BH-OPV1a/COPV3** dodecane gels. When the temperature was increased up to 55 °C, a sudden transition of the strongly exciton coupled CD signal to a weak CD signal was observed, which is similar in shape to the one observed during the initial stages of the growth of the co-assembled gels (Figure 4.23a). This could be easily observed in the corresponding stability curve (Figure 4.23b). The intensity of the CD signal continued to decrease with increase in temperature until it reached the baseline at 70 °C.

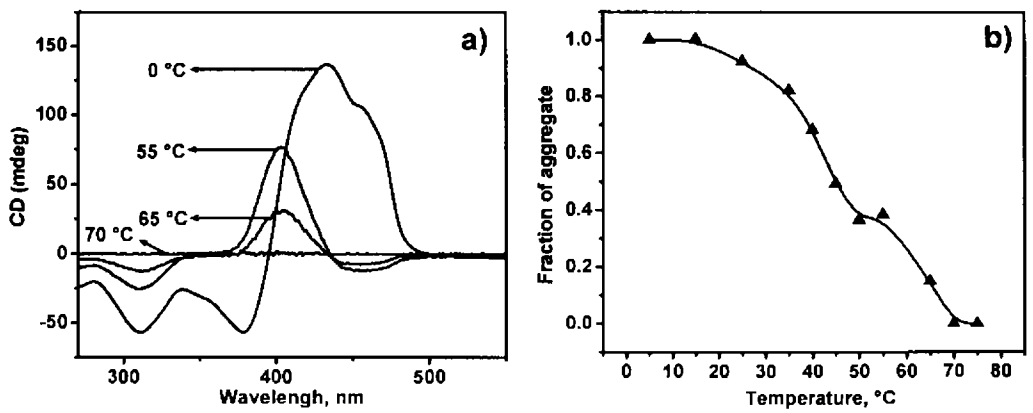

Figure 4.23. a) Temperature dependent CD spectra of the dodecane **BH-OPV1a/COPV3** gel doped with 50% **COPV3** and b) the corresponding melting transition plot obtained by plotting the fraction of self-assembled molecules versus temperature.

From the detailed CD studies, it is clear that supramolecular chirality can be induced into achiral OPV gels by co-assembling with structurally related chiral self-assembling OPV derivatives. However, in the present case for the efficient induction of the supramolecular chirality more than 25% of the chiral oligomers are needed. This is in contrast to the amplification of chirality observed for the helical columnar discotic molecules, for which even 2.5% of chiral 'sergeant' molecules are sufficient for a full bias of the helicity.[5a] This may be due to the difference in the stacking interaction of the OPV chromophores in a lamellar assembly leading to a three-dimensional supramolecular structure in contrast to the one-dimensional columnar stacks of the discotic molecules. In such situations, the chirality of the 'sergeant' molecules would not be strongly recognized by the achiral 'soldiers'. However, to the best of our knowledge, this induction of chirality using 'sergeant and soldiers' principles in achiral OPV gels by co-assembling with chiral OPVs, furnishes the first example of its kind for the design of helical OPV nanostructures. The most remarkable observation during the chiral induction experiments is the unusual bias of the supramolecular chirality towards right-handedness in the co-assembly. The '*S*'-chiral center present in the side chains of chiral OPVs are expected to direct the self-assembly of achiral OPVs in a left-handed direction, as observed in the case of pure chiral **COPV2** gels. Recently, Jonkheim *et al.* have also observed such an inversion of supramolecular chirality during the helical rosette formation of homochiral triazine substituted OPVs.[11c] Detailed studies have shown that, the right-handed OPV rosette helical assembly is only a kinetically controlled metastable state, which changed into the thermodynamically favored left-handed helical assembly very quickly with first-order kinetics. However, in the present co-assembled gel systems, the induced right-handed helicity is preserved even after two weeks. These results indicate that, the

intact arrangement of the OPV chromophores in the co-assembled network enabled the locking of the induced right-handed supramolecular chirality and to memorize it for several weeks.

We have carried out detailed optical polarizing and scanning electron microscopic studies in order to confirm the induction of chirality in the co-assembled OPV gels. The optical polarizing microscopic studies of the co-assembled dodecane gels of **BH-OPV1b/COPV2** showed considerable differences from that of the individual chiral and achiral OPVs. For example, the achiral OPV gels have long birefringent fibrous textures (Figure 4.24a), whereas the chiral OPV gels (Figure 4.24b) exhibit four-arm brush textures characteristic of the helical packing of the molecules. Interestingly, when the co-assembled **BH-OPV1b/COPV2** dodecane gels are cooled from the isotropic solution, a texture which is different from the individual molecules could be observed (Figure 4.24c). This observation is an indication of the co-assembly of **COPV2** with **BH-OPV1b** which is responsible for the supramolecular chirality and the helical bias.

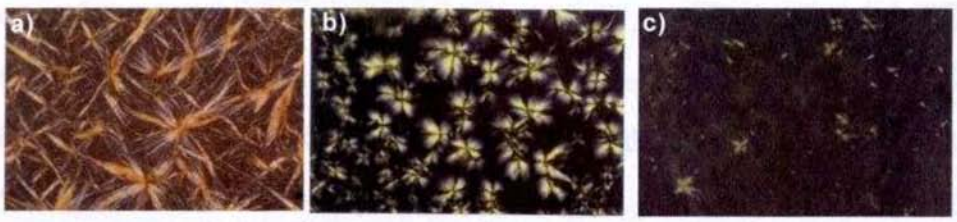

Figure 4.24. Optical polarizing micrographs of a) **BH-OPV1b**, b) **COPV2** and c) co-assembled **BH-OPV1b/COPV2** dodecane gels (magnification is 100x).

Scanning electron micrographs of **BH-OPV1b/COPV2** co-assembly showed the presence of long entangled twisted tapes of 50-200 nm diameters and several micrometers length (Figure 4.25). Careful analysis revealed that all fibers have left-

handed twist. However, the positive bisignated CD signal of co-assembled gels suggest a right-handed helical arrangement of the OPV chromophores. These observations point towards the possibility of having several hierarchical structures of organization in the co-assembled OPV gels. At the primary level, the OPV chromophores are directed to assemble in a right-handed helical manner by the remote chiral side chains, which is responsible for the positive bisignated CD signal. However, at the secondary level of the self-assembly, the right-handed primary structures organize into left-handed tape-like assemblies, as observed through SEM images.

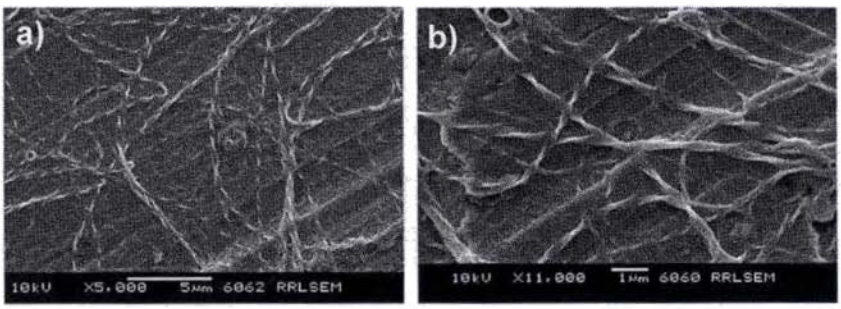

Figure 4.25. Scanning electron microscopic pictures of **BH-OPV1b/COPV2** dodecane gels.

4.5. Conclusions

Three different oligo(*p*-phenylenevinylene)s, **COPV1-3** having remote chiral handles have been designed and synthesized. Among the three derivatives, only **C-OPV2** forms gel in apolar hydrocarbon solvents, which indicates that the nature of the side chain is crucial in the gelation of chiral OPVs. While **COPV1** failed to form gel, **COPV2** provided stable gel in dodecane whereas **COPV3** forms strong aggregates with weak gelation property. Optical polarizing microscopy showed birefringent fibrous four-arm brushes revealing strong molecular anisotropy. FE-SEM pictures of

COPV2 revealed concentration dependent hierarchical self-assembly leading to the formation of left-handed helical fibers of 20-50 nm and coiled-coil ropes of ca. 150 nm in width. AFM analysis of the gel fibers showed the characteristics of left-handed coiled-coil ropes. Concentration and temperature dependent CD spectral studies of **COPV2** revealed a helix transition during the hierarchical growth of the self-assembly indicating the presence of different chiral intermediates. Helical bias through an amplified chiral induction could be achieved to achiral OPV gels by co-assembling with the chiral OPVs which showed a right-handed supramolecular chirality in the initial levels of the co-assembly and a left-handed helicity at the higher levels of the co-assembly as evidenced from the SEM images. This is the first report of a gelation assisted chiral amplification and helical bias in the supramolecular co-assembly of extended π-conjugated system.

4.6. Experimental Section

4.6.1. Synthesis and Characterization of COPV1-3

Solvents and the reagents used were purified and dried by usual methods. All starting materials were obtained from commercial suppliers and used as received. All melting points were determined with a Mel-Temp-II melting point apparatus and are uncorrected. ^{1}H and ^{13}C NMR were measured on a 300 MHz Bruker Avance DPX spectrometer or on a Varian Gemini 300 MHz spectrophotometer. IR spectra were recorded on a Nicolet Impact 400D Infrared spectrophotometer. Matrix assisted laser desorption ionization time of flight (MALDI-TOF) mass spectrometry was conducted on a perspective Biosystems Voyager DE-Pro MALDI-TOF mass spectrometer. Chiral side chains were prepared according to previous report.[5a] The compounds

COPV1-3 were synthesized using similar procedures used for the synthesis of corresponding achiral derivatives (see Chapter 2 for details).

COPV1. Yield 95%. mp 75-76 °C. FT-IR (KBr) ν_{max} = 865, 912, 1051, 1124, 1201, 1253, 1382, 1418, 1470, 1506, 2918, 2955, 3348 cm^{-1}. ^1H NMR (300 MHz, $CDCl_3$, TMS) δ 0.75-1.8 (m, 114H, $-CH_3$ and $-CH_2$), 3.95-4.03 (m, 12H, $-OCH_2$), 4.6-4.62 (d, 4H, $-CH_2OH$), 6.8 (s, 2H, aromatic), 7.06 (s, 2H, aromatic), 7.08 (s, 4H, aromatic), 7.38 (s, 4H, vinylic) ppm. ^{13}C NMR (300 MHz, $CDCl_3$, TMS) δ 14.09, 22.64, 25.93, 29.34, 29.68, 31.37, 62.30, 69.52, 69.73, 108.49, 114.26, 115.91, 126.76, 128.47, 128.60, 129.73, 151.12, 151.51 ppm. MALDI-TOF MS (MW = 1280.02): *m/z* = 1279.64 $[M]^+$.

COPV2. Yield 94%. mp 83-84 °C. FT-IR (KBr) ν_{max} = 865, 968, 1046, 1206, 1258, 1387, 1424, 1465, 1506, 2846, 2924, 3348 cm^{-1}. ^1H NMR (300 MHz, $CDCl_3$, TMS) δ 0.75-1.8 (m, 130H, $-CH_3$ and $-CH_2$), 4.02-4.16 (m, 12H, $-OCH_2$), 4.72-4.74 (d, 4H, $-CH_2OH$), 6.92 (s, 2H, aromatic), 7.17 (s, 2H, aromatic), 7.21(s, 4H, aromatic), 7.51(s, 4H, vinylic) ppm. ^{13}C NMR (300 MHz, $CDCl_3$, TMS) δ 14.04, 19.25, 24.45, 25.62, 27.60, 28.70, 28.93, 29.37, 29.19, 29.80, 31.68, 62.43, 68.21, 69.10, 69.51, 110.54, 114.12, 123.56, 126.76, 127.21, 127.76, 129.46, 150.67, 151.07 ppm. MALDI-TOF MS (MW = 1391.2): *m/z* = 1392.15 $[M]^+$.

COPV3. Yield 96%. mp 90-91 °C. FT-IR (KBr) ν_{max} = 725, 860, 979, 1046, 1124, 1253, 1346, 1418, 1470, 1506, 2851, 2918, 3327 cm^{-1}. ^1H NMR (300 MHz, $CDCl_3$, TMS) δ 0.75-1.76 (m, 162H, $-CH_3$ and $-CH_2$), 3.91-4.01 (m, 12H, $-OCH_2$), 4.61-4.62 (d, 4H, $-CH_2OH$), 6.79 (s, 2H, aromatic), 7.05 (s, 2H, aromatic), 7.08 (s, 4H, aromatic), 7.38(s, 4H, vinylic) ppm. ^{13}C NMR (300 MHz, $CDCl_3$, TMS) δ 14.54,

19.34, 22.34, 24.40, 25.56, 27.69, 28.45, 28.90, 29.23, 29.45, 29.75, 31.61, 62.45, 68.34, 69.15, 69.54, 110.43, 114.01, 123.43, 126.65, 127.21, 127.45, 129.73, 150.97, 151.14.

4.6.2. General Procedure for Gelation Studies

A weighed amount of the compound in an appropriate solvent (6-8 mM) was placed in a glass vial, which was sealed and heated until the compound was dissolved. The solution was allowed to cool to room temperature and the gel formation was confirmed by the failure of the gel mixture to flow by inverting the glass vial. The thermo reversibility of the gelation was confirmed by repeated heating and cooling.

4.6.3. General Procedure for 'Sergeant and Soldiers' Experiments

The co-assembled OPV dodecane gels of the achiral **BH-OPV1a/b**, and chiral **COPV2/3 OPV** derivatives were prepared by heating the mixed OPV solution to 90 °C and the subsequent cooling either at a cooling rate of 20 °Cmin^{-1} or by slow cooling at room temperature. In all cases stable, transparent and fluorescent gels were obtained indicating the co-assembly of both achiral and chiral OPVs and the measurements were carried out 5 °C, in a 1 mm cuvette.

4.6.4. Description on Experimental Techniques

Optical Polarizing Microscopy. The gel texture was observed on a polarizing light microscope (Nikon HFX 35 A Optiphot equipped with a Linkan THMS 600 heating and freezing stage connected to Linkan TP 92 temperature programmer).

Atomic Force Microscopy. Atomic Force Microscopy images were recorded under ambient conditions using a Digital Instrument Multimode Nanoscope IV operating in the tapping mode regime. Micro-fabricated silicon cantilever tips (NSG01/Pt) with a

resonance frequency of approximately 150 kHz and a spring constant of about 5.5 Nm^{-1} were used. The scan rate varied from 0.5 to 1.5 Hz. The set-point amplitude ratio ($r_{sp} = A_{sp}/A_o$, where A_{sp} is the amplitude setpoint, and A_o is the amplitude of the free oscillation) was adjusted to 0.9. All AFM images shown here were subjected to a first-order plane-fitting procedure to compensate for sample tilt. AFM analysis was done offline. AFM samples were prepared by drop casting the **OPV** solution on freshly cleaved muscovite mica.

Field-Emission Scanning Electron Microscopy. FE-SEM studies were carried out on a CARL Zeiss LEO GEMINI 1550. The SEM samples were prepared by transferring the dodecane solution of **COPV1** onto a 400 mesh carbon-coated Formvar copper grid. The samples were allowed to dry and then coated with platinum prior to imaging.

Optical and Chiroptical Measurements. Electronic absorption spectra were recorded on a Shimadzu UV-3101 PC NIR scanning spectrophotometer and the emission spectra were recorded on a SPEX-Fluorolog F112X spectrofluorimeter. Temperature dependent studies were carried out either in a 0.1cm or 1 cm quartz cuvette with a thermistor directly attached to the wall of the cuvette holder. CD spectra were recorded either on JASCO-J-600 or JASCO-J-810 spectropolarimeters equipped with a JASCO PTC-348WI or JASCO PTC-423S Peltier type temperature control system.

4.7. References

1. Recent reviews on helical supramolecular architectures: (a) Rowan, A. E.; Nolte, R. J. M. *Angew. Chem. Int. Ed.* **1998**, *37*, 63. (b) Schmuck, C. *Angew. Chem. Int. Ed.* **2003**, *42*, 2448.

2. Nelson, J. C.; Saven, J. G.; Moore, J. S.; Wolynes, P. G. *Science* **1997**, *277*, 1793.

3. Berl, V.; Huc, I.; Khoury, R. G.; Krische, M. J.; Lehn, J.-M. *Nature* **2000**, *407*, 720.

4. Engelkamp, H.; Middelbeek, S.; Nolte, R. J. M. *Science* **1999**, *284*, 785.

5. (a) Palmans, A. R. A.; Vekemans, J. A. J. M.; Havinga, E. E.; Meijer, E. W. *Angew. Chem. Int. Ed.* **1997**, *36*, 2648. (b) Brunsveld, L.; Zhang, H.; Glasbeek, M.; Vekemans, J. A. J. M.; Meijer, E. W. *J. Am. Chem. Soc.* **2000**, *122*, 6175. (c) Palmans, A. R. A.; Vekemans, J. A. J. M.; Fischer, H.; Hikmet, R. A.; Meijer, E. W. *Chem. Eur. J.* **1997**, *3*, 300. (d) van Gorp, J. J.; Vekemans, J. A. J. M.; Meijer, E. W. *J. Am. Chem. Soc.* **2002**, *124*, 14759.

6. Hirschberg, J. H. K. K.; Brunsveld, L.; Ramzi, A.; Vekemans, J. A. J. M.; Sijbesma, R. P.; Meijer, E. W. *Nature* **2000**, *407*, 167.

7. Oda, R.; Schmutz, M.; Candau, S. J.; MacKintosh, F. C. *Nature* **1999**, *399*, 566.

8. (a) Zubarev, E. R.; Pralle, M. U.; Sone, E. D.; Stupp, S. I. *J. Am. Chem. Soc.* **2001**, *123*, 4105. (b) Sone, E. D.; Zubarev, E. R.; Stupp, S. I. *Angew. Chem. Int. Ed.* **2002**, *41*, 1706.

9. Fenniri, H.; Deng, B.-L.; Ribbe, A. E. *J. Am. Chem. Soc.* **2002**, *124*, 11064.

10. Brunsveld, L.; Meijer, E. W.; Prince, R. B.; Moore, J. S. *J. Am. Chem. Soc.* **2001**, *123*, 7978.

11. (a) Schenning, A. P. H. J.; Jonkheijm, P.; Peeters, E.; Meijer, E. W. *J. Am. Chem. Soc.* **2001**, *123*, 409. (b) Jonkheijm, P.; Hoeben, F. J. M.; Kleppinger, R.; Herrikhuyzen, J. V.; Schenning, A. P. H. J.; Meijer, E. W. *J. Am. Chem. Soc.* **2003**, *125*, 15941. (c) Jonkheijm, P.; Miura, A.; Zdanowska, M.; Hoeben, F. J. M.; De Feyter, S.; Schenning, A. P. H. J.; De Schryer, F. C.; Meijer, E. W. *Angew. Chem. Int. Ed.* **2004**, *43*, 74.

12. (a) Lin, Y.-C.; Kachar, B.; Weiss, R. G. *J. Am. Chem. Soc.* **1989**, *111*, 5542. (b) Murata, K.; Aoki, M.; Suzuki, T.; Harada, T.; Kawabata, H.; Komori, T.; Ohseto, F.; Ueda, K.; Shinkai, S. *J. Am. Chem. Soc.* **1994**, *116*, 6664. (c) Jung, J. H.; Ono, Y.;

Shinkai, S. *Angew. Chem. Int. Ed.* **2000**, *39*, 1862. (d) Wang, R.; Geiger, C.; Chen, L.; Swanson, B.; Whitten, D. G. *J. Am. Chem. Soc.* **2000**, *122*, 2399. (e) Jung, H. J.; Kobayashi, H.; Masuda, M.; Shimizu, T.; Shinkai, S. *J. Am. Chem. Soc.* **2001**, *123*, 8785.

13. van Esch, J.; Schoonbeek, F. S.; de Loos, M.; Kooijman, H.; Kellogg, R. M.; Feringa, B. L. *Chem. Eur. J.* **1999**, *5*, 937.

14. (a) Hanabusa, K.; Yamada, M.; Kimura, M.; Shirai, H. *Angew. Chem. Int. Ed.* **1996**, *35*, 1949. (b) de Jong, J. P. D.; Lucas, L. N.; Kellog, R. M.; van Esch, J. H.; Feringa, B. L. *Science* **2004**, *304*, 278.

15. (a) Hafkamp, R. H.; Feiters, M. C.; Nolte, R. J. M. *J. Org. Chem.* **1999**, *64*, 412. (b) Jung, J. H.; John, G.; Masuda, M.; Yoshida, K.; Shinkai, S.; Shimizu, T. *Langmuir* **2001**, *17*, 7229. (c) Friggeri, A.; Gronwald, O.; van Bommel, K. J. C.; Shinkai, S.; Reinhoudt, D. N. *J. Am. Chem. Soc.* **2002**, *124*, 10754. (d) Kawano, S.; Tamaru, S.; Fujita, N.; Shinkai, S. *Chem. Eur. J.* **2004**, *10*, 343.

16. Oda, R.; Hue, I.; Candau, S. J. *Angew. Chem. Int. Ed.* **1998**, *37*, 2689.

17. Maitra, U.; Potluri, V. K.; Sangeetha, N. M.; Babu, P; Raju, A. R. *Tetrahedron: Asymmetry* **2001**, *12*, 477.

18. Wang, B.; Wasielewski, M. R. *J. Am. Chem. Soc.* **1997**, *119*, 12.

19. A measure of for the induced chirality is given by the chiral anisotropy factor 'g'. $g = \Delta\varepsilon/\varepsilon$, in which $\Delta\varepsilon$ can be calculated as follows: $\Delta\varepsilon$ = CD-effect/(32980cl), where 'CD-effect' is the intensity of Cotton effect in mdeg, 'c' is the molar concentration and 'l' is the path length in cm.

20. Green, M. M.; Peterson, N. C.; Sato, T.; Teramoto, A.; Cook, R.; Lifson, S. *Science* **1995**, *268*, 1860.

List of Publications

1. First Phenylenevinylene Based Organogels. Self-Assembled Nanostructures via Cooperative Hydrogen Bonding and π-Stacking

   Ajayaghosh, A.; **George, S. J.** *J. Am. Chem. Soc.* **2001**, *121*, 5148.

2. Gelation Assisted Light Harvesting via Selective Energy Transfer from Oligo(*p*-phenylenevinylene) Based Self-assembly to an Organic Dye

   Ajayaghosh, A.; **George, S. J.**; Praveen, V. K. *Angew. Chem. Int. Ed.* **2003**, *42*, 332.

3. Coiled-Coil Gel Nanostructures of Oligo(*p*-phenylenevinylene)s: Gelation Induced Helix Transition in a Higher Order Supramolecular Assembly of a Rigid π-Conjugated System

   George, S. J.; Ajayaghosh, A.; Jonkheijm, P.; Schenning, A. P. H. J.; Meijer, E. W. *Angew. Chem. Int. Ed.* **2004**, *43*, 3421.

4. Anion Induced Modulation of Self-Assembly and Optical Properties in Urea End-capped Oligo(*p*-phenylenevinylene)s

   Varghese, R.; **George, S. J.**; Ajayaghosh, A. (Submitted)

5. π-Conjugated Organogels: A Novel Class of Supramolecular Materials Derived from Self-Assembled Oligo(*p*-phenylenevinylene)s

   George, S. J.; Ajayaghosh, A. (To be submitted)

6. Optical Properties as a Tool to Probe the Sol-Gel Process of π-Conjugated Organogels

   George, S. J.; Ajayaghosh, A. (To be submitted)

7. π-Conjugated Organogels as Supramolecular Energy Donor Scaffolds: Selective Fluorescence Resonance Energy Transfer from Self-Assembled Donors to Entrapped Acceptor

   George, S. J.; Praveen, V. K.; Ajayaghosh, A. (To be submitted)

Posters Presented at Conferences

1. New Light Emitting Oligomers Derived from Alternate Pyrrolenevinylene and Phenylenevinylene Moieties

   Subi J. George and A. Ajayaghosh, Symposium on Recent Trends in Photochemical Sciences, RRL, Trivandrum, India, January 8-10, 2001.

2. Oligo(*p*-phenylenevinylene) Derived Organogels: A Novel Class of Self-Assembled Nanostructures via Noncovalent Interactions

   Subi J. George, V. K. Praveen and A. Ajayaghosh, 4th National Symposium in Chemistry, NCL, Pune, February 1-3, 2002 **(Best Poster Award).**

3. Oligo(phenylenevinylene)s: A Novel Class of Light Harvesting Gels

   Subi J. George and A. Ajayaghosh, Recent Advances in Chemical Sciences (RACS 2002), M. G. University, Kottayam, December 18-21, 2002.

4. Energy Harvesting Organogels: Selective Energy Transfer from OPV Based Self-Assembly to Rhodamine B

   Subi J. George, V. K. Praveen and A. Ajayaghosh, 5th National Symposium in Chemistry, CLRI, Chennai, February 7-9, 2003.

5. Novel Organogelators Derived from Oligo(*p*-phenylenevinylene) Self-Assembly

   Subi J. George, V. K. Praveen and A. Ajayaghosh, 3rd Trivandrum International Symposium on Recent Trends in Photochemical Sciences, RRL, Trivandrum, India, January 5-7, 2004.

6. H-Bond and π-Stack Induced Self-assembly and Gelation of Oligo(phenyleneethynylene)s

   Reji Varghese, **Subi J. George** and A. Ajayaghosh, 3rd Trivandrum International Symposium on Recent Trends in Photochemical Sciences, RRL, Trivandrum, India, January 5-7, 2004.

7. Organogels Derived From Helical Self-Assembly of Cholesterol-Appended Oligo(phenylenevinylene)s

   Chakkooth Vijayakumar, **Subi J. George** and A. Ajayaghosh, 3rd Trivandrum International Symposium on Recent Trends in Photochemical Sciences, RRL, Trivandrum, India, January 5-7, 2004.

8. Helical Gel Nanostructures of Chiral Oligo(phenylenevinylene)s: Expression of Helicity in a Secondary Level Supramolecular Self-Assembly

   Subi J. George and A. Ajayaghosh, 6th National Symposium in Chemistry, IIT, Kanpur, India, February 6-8, 2004 (**Best Poster Award**).

9. Fluorescent Oligo(*p*-phenylenevinylene) Gels via Cooperative Dipolar and π-Stacking Interactions

   V. K. Praveen, **Subi J. George** and A. Ajayaghosh, 6th National Symposium in Chemistry, IIT, Kanpur, India, February 6-8, 2004.